THE UNIVERSITY OF MANITOBA

INFLUENCE OF TUBE INCLINATION ON THE FLOW-REGIME BOUNDARIES OF CONDENSING FLOWS: EXPERIMENTAL AND ANALYTICAL STUDIES

By
Thambiayah Nitheanandan

A Thesis
Submitted to the Faculty of Graduate Studies
in partial fulfillment of the requirements for the degree of
Doctor of Philosophy

Department of Mechanical and Industrial Engineering
Winnipeg, Manitoba

1993

ISBN 0-315-85955-5

Name

Dissertation Abstracts International is arranged by broad, general subject categories. Please select the one subject which most nearly describes the content of your dissertation. Enter the corresponding four-digit code in the spaces provided.

MECHANICAL | 0 5 4 8 | U·M·I

SUBJECT TERM | SUBJECT CODE

Subject Categories

THE HUMANITIES AND SOCIAL SCIENCES

COMMUNICATIONS AND THE ARTS
Architecture 0729
Art History 0377
Cinema 0900
Dance 0378
Fine Arts 0357
Information Science 0723
Journalism 0391
Library Science 0399
Mass Communications 0708
Music 0413
Speech Communication 0459
Theater 0465

EDUCATION
General 0515
Administration 0514
Adult and Continuing 0516
Agricultural 0517
Art 0273
Bilingual and Multicultural 0282
Business 0688
Community College 0275
Curriculum and Instruction 0727
Early Childhood 0518
Elementary 0524
Finance 0277
Guidance and Counseling 0519
Health 0680
Higher 0745
History of 0520
Home Economics 0278
Industrial 0521
Language and Literature 0279
Mathematics 0280
Music 0522
Philosophy of 0998
Physical 0523
Psychology 0525
Reading 0535
Religious 0527
Sciences 0714
Secondary 0533
Social Sciences 0534
Sociology of 0340
Special 0529
Teacher Training 0530
Technology 0710
Tests and Measurements 0288
Vocational 0747

LANGUAGE, LITERATURE AND LINGUISTICS
Language
- General 0679
- Ancient 0289
- Linguistics 0290
- Modern 0291

Literature
- General 0401
- Classical 0294
- Comparative 0295
- Medieval 0297
- Modern 0298
- African 0316
- American 0591
- Asian 0305
- Canadian (English) 0352
- Canadian (French) 0355
- English 0593
- Germanic 0311
- Latin American 0312
- Middle Eastern 0315
- Romance 0313
- Slavic and East European 0314

PHILOSOPHY, RELIGION AND THEOLOGY
Philosophy 0422
Religion
- General 0318
- Biblical Studies 0321
- Clergy 0319
- History of 0320
- Philosophy of 0322

Theology 0469

SOCIAL SCIENCES
American Studies 0323
Anthropology
- Archaeology 0324
- Cultural 0326
- Physical 0327

Business Administration
- General 0310
- Accounting 0272
- Banking 0770
- Management 0454
- Marketing 0338

Canadian Studies 0385
Economics
- General 0501
- Agricultural 0503
- Commerce-Business 0505
- Finance 0508
- History 0509
- Labor 0510
- Theory 0511

Folklore 0358
Geography 0366
Gerontology 0351
History
- General 0578
- Ancient 0579
- Medieval 0581
- Modern 0582
- Black 0328
- African 0331
- Asia, Australia and Oceania 0332
- Canadian 0334
- European 0335
- Latin American 0336
- Middle Eastern 0333
- United States 0337

History of Science 0585
Law 0398
Political Science
- General 0615
- International Law and Relations 0616
- Public Administration 0617

Recreation 0814
Social Work 0452
Sociology
- General 0626
- Criminology and Penology 0627
- Demography 0938
- Ethnic and Racial Studies 0631
- Individual and Family Studies 0628
- Industrial and Labor Relations 0629
- Public and Social Welfare 0630
- Social Structure and Development 0700
- Theory and Methods 0344

Transportation 0709
Urban and Regional Planning 0999
Women's Studies 0453

THE SCIENCES AND ENGINEERING

BIOLOGICAL SCIENCES
Agriculture
- General 0473
- Agronomy 0285
- Animal Culture and Nutrition 0475
- Animal Pathology 0476
- Food Science and Technology 0359
- Forestry and Wildlife 0478
- Plant Culture 0479
- Plant Pathology 0480
- Plant Physiology 0817
- Range Management 0777
- Wood Technology 0746

Biology
- General 0306
- Anatomy 0287
- Biostatistics 0308
- Botany 0309
- Cell 0379
- Ecology 0329
- Entomology 0353
- Genetics 0369
- Limnology 0793
- Microbiology 0410
- Molecular 0307
- Neuroscience 0317
- Oceanography 0416
- Physiology 0433
- Radiation 0821
- Veterinary Science 0778
- Zoology 0472

Biophysics
- General 0786
- Medical 0760

EARTH SCIENCES
Biogeochemistry 0425
Geochemistry 0996
Geodesy 0370
Geology 0372
Geophysics 0373
Hydrology 0388
Mineralogy 0411
Paleobotany 0345
Paleoecology 0426
Paleontology 0418
Paleozoology 0985
Palynology 0427
Physical Geography 0368
Physical Oceanography 0415

HEALTH AND ENVIRONMENTAL SCIENCES
Environmental Sciences 0768
Health Sciences
- General 0566
- Audiology 0300
- Chemotherapy 0992
- Dentistry 0567
- Education 0350
- Hospital Management 0769
- Human Development 0758
- Immunology 0982
- Medicine and Surgery 0564
- Mental Health 0347
- Nursing 0569
- Nutrition 0570
- Obstetrics and Gynecology 0380
- Occupational Health and Therapy 0354
- Ophthalmology 0381
- Pathology 0571
- Pharmacology 0419
- Pharmacy 0572
- Physical Therapy 0382
- Public Health 0573
- Radiology 0574
- Recreation 0575
- Speech Pathology 0460
- Toxicology 0383

Home Economics 0386

PHYSICAL SCIENCES

Pure Sciences
Chemistry
- General 0485
- Agricultural 0749
- Analytical 0486
- Biochemistry 0487
- Inorganic 0488
- Nuclear 0738
- Organic 0490
- Pharmaceutical 0491
- Physical 0494
- Polymer 0495
- Radiation 0754

Mathematics 0405
Physics
- General 0605
- Acoustics 0986
- Astronomy and Astrophysics 0606
- Atmospheric Science 0608
- Atomic 0748
- Electronics and Electricity 0607
- Elementary Particles and High Energy 0798
- Fluid and Plasma 0759
- Molecular 0609
- Nuclear 0610
- Optics 0752
- Radiation 0756
- Solid State 0611

Statistics 0463

Applied Sciences
Applied Mechanics 0346
Computer Science 0984
Engineering
- General 0537
- Aerospace 0538
- Agricultural 0539
- Automotive 0540
- Biomedical 0541
- Chemical 0542
- Civil 0543
- Electronics and Electrical 0544
- Heat and Thermodynamics 0348
- Hydraulic 0545
- Industrial 0546
- Marine 0547
- Materials Science 0794
- Mechanical 0548
- Metallurgy 0743
- Mining 0551
- Nuclear 0552
- Packaging 0549
- Petroleum 0765
- Sanitary and Municipal 0554
- System Science 0790

Geotechnology 0428
Operations Research 0796
Plastics Technology 0795
Textile Technology 0994

PSYCHOLOGY
General 0621
Behavioral 0384
Clinical 0622
Developmental 0620
Experimental 0623
Industrial 0624
Personality 0625
Physiological 0989
Psychobiology 0349
Psychometrics 0632
Social 0451

INFLUENCE OF TUBE INCLINATION ON THE FLOW-REGIME BOUNDARIES OF CONDENSING FLOWS: EXPERIMENTAL AND ANALYTICAL STUDIES

BY

THAMBLAYAH NITHEANANDAN

A Thesis submitted to the Faculty of Graduate Studies of the University of Manitoba in partial fulfillment of the requirements for the degree of

DOCTOR OF PHILOSOPHY

ABSTRACT

Flow-regime data of condensing steam inside an inclined 13.4-mm I.D. tube are presented. The effect of upward and downward inclinations within $\pm 10^\circ$ on the different transition lines is discussed. In all test runs, complete condensation was achieved inside the condenser, with or without a full-tube condition at the exit depending on the total mass flow rate and the inclination angle. It is shown that the zones occupied by the wavy and slug regimes experience significant shifts, whereas the effect on the annular-flow boundary appears to be insignificant at the present small inclination angles. The present data sets are compared with adiabatic gas-liquid flow-regime maps developed analytically and experimentally for horizontal and inclined tubes. Deviations due to the condensation process are observed; however, consistent trends are identified among the two types of flow. For small inclinations the trend shown by condensing flow in the horizontal position is similar to the trend shown by gas-liquid flow with a slight upward inclination. The occurrence of slugging in the horizontal condenser was found to be coincident with the condition of tube running full at the exit. When the tube was not running full at the exit, slugging was not observed. A simple correlation was developed for the upper bound on slugging. This correlation agreed well with the experimental data.

A mechanistic model was developed for determining the stratified boundary for condensing flows in horizontal and slightly inclined tubes based on mass, momentum and energy conservation laws. Two formulations, namely a complete and a simplified version are considered for the equilibrium liquid level. Good agreement is found between the two formulations and generalized results were derived from the simplified version of the model. From these results, the effect of condensation is shown to be equivalent to adding a small upward inclination in adiabatic gas-liquid flow. The predicted transition line is compared with flow-regime data of different fluid properties, tube diameters, and inclinations. The predictions showed good agreement with horizontal and inclined flow data of different fluids and tube diameters.

ACKNOWLEDGEMENT

The author wishes to express his deepest gratitude to Dr. H. M. Soliman for suggesting this topic and for his continuing interest, encouragement and guidance, without which this thesis would have been impossible. Special thanks are due to Dr. G. E. Sims and Dr. J. Townsend for their encouragement and helpful suggestions.

Thanks are also due to Mr. M. Kapitoler for his help during the construction of the experimental test facility. The author also wishes to thank the other technicians in the Department of Mechanical and Industrial Engineering who have helped him by providing services.

The financial assistance provided by the following agencies is gratefully acknowledged: Faculty of Graduate Studies through the University of Manitoba Graduate Fellowship; the Natural Sciences and Engineering Research Council of Canada through the research grant of Dr. H. M. Soliman; and the Department of Mechanical and Industrial Engineering through Teaching Assistantships.

Finally, the author wishes to thank his parents, wife and sons for their sincere support and encouragement.

TABLE OF CONTENTS

LIST OF FIGURES

LIST OF TABLES

NOMENCLATURE

A = cross-sectional area of the tube, m^2

$\bar{A}$ = dimensionless tube cross-sectional area

A_G = cross-sectional area occupied by the vapor phase, m^2

$\bar{A}_G$ = dimensionless vapor cross-sectional area

A'_G = vapor cross-sectional area above the wave crest, m^2

A_L = liquid cross-sectional area, m^2

$\bar{A}_L$ = dimensionless liquid cross-sectional area

C_{Gf} = coefficient given in Equation (5.11b)

C_{Lf} = coefficient given in Equation (5.11a)

C_{pL} = liquid specific heat, J/kg.K

C_{3G} = distribution parameter of the vapor defined in Equation (5.5a)

C_{3L} = distribution parameter of the liquid defined in Equation (5.5b)

D = tube diameter, m

D_G = vapor hydraulic diameter, m

$\bar{D}_G$ = dimensionless vapor hydraulic diameter

D_L = liquid hydraulic diameter, m

$\bar{D}_L$ = dimensionless liquid hydraulic diameter

E = parameter defined by Equation (5.18)

F = modified Froude number defined in Equation (5.30)

F_B = Bernoulli force per unit surface area, N/m^2

F_g = gravitational force per unit surface area, N/m^2

F_V = reaction force per unit surface area due to momentum change during condensation, N/m^2

f_G = vapor friction factor defined by Equation (5.11b)

f_L = liquid friction factor defined by Equation (5.11a)

G = total mass flux, $kg/m^2.s$

G_L = liquid mass flux, $kg/m^2.s$

G_G = vapor mass flux, $kg/m^2.s$

g = gravitational acceleration, m/s^2

G_N = mass flux entering the liquid due to condensation, $kg/m^2.s$

H = dimensionless condensation heat-transfer parameter defined by Equation (5.15g)

h_G = vapor height, m

h'_G = vapor height above the wave crest, m

h_L = liquid height, m

$\bar{h}_L$ = dimensionless equilibrium liquid height

h_{av} = average heat-transfer coefficient, $W/m^2.K$

h_{fg} = latent heat of vaporization, J/kg

h'_{fg} = modified latent heat defined in Equation (5.17), J/kg

j_G^* = dimensionless vapor velocity defined by Equation (4.4)

j_L^* = dimensionless liquid velocity defined by Equation (4.5)

k_L = liquid thermal conductivity, W/m.K

m = coefficient in Equation (5.11b)

$\mathring{m}$ = mass flow rate, kg/h

n = coefficient in Equation (5.11a)

P = local static pressure, N/m^2

P_{av} = mean saturation pressure, N/m^2

$(\Delta p)_N$ = pressure change due to mass transfer, N/m^2

q'' = average heat flux, W/m^2

Re_{GS} = vapor superficial Reynolds number defined by Equation (2.2c)

Re_{LS} = liquid superficial Reynolds number defined by Equation (2.2b)

R_{SM} = minimal liquid hold up within a liquid slug

S_G = vapor perimeter, m

$\bar{S}_G$ = dimensionless vapor perimeter

S_i = interfacial perimeter, m

$\bar{S}_i$ = dimensionless interfacial perimeter

S_L = liquid perimeter, m

$\bar{S}_L$ = dimensionless liquid perimeter

T_s = local saturation temperature, °C

$T_{s, av}$ = mean saturation temperature, °C

ΔT = saturation to wall temperature, °C

u_G = local vapor velocity, m/s

$\langle u_G \rangle_G$ = vapor velocity averaged over the vapor phase, m/s

u_i = mean interfacial velocity, m/s

u_L = local liquid velocity, m/s

$<u_L>_L$ = liquid velocity averaged over the liquid phase, m/s

V_{GS} = superficial vapor velocity, m/s

V_{LS} = superficial liquid velocity, m/s

v_{GN} = mean vapor velocity normal to the interface, m/s

v_{LN} = mean liquid velocity normal to the interface, m/s

$\mathring{W}_i$ = mass flow rate crossing the interface per unit volume, kg/m^3.s

X = Lockhart-Martinelli parameter defined in Equation (5.15e)

x = vapor quality

Y = dimensionless inclination parameter defined by Equation (5.15f)

Z = axial coordinate along the tube axis, m

$\bar{Z}$ = dimensionless axial coordinate along the tube axis

Greek letters

α = local void fraction

β = parameter defined by Equation (5.15b)

β' = parameter defined by Equation (5.20a)

γ = parameter defined by Equation (5.15c)

γ' = parameter defined by Equation (5.20b)

ε = parameter defined by Equation (5.15a)

ζ = parameter defined by Equation (5.15d)

η = interfacial momentum transfer parameter

θ = tube inclination from horizontal

μ_L = liquid dynamic viscosity, $N.s/m^2$

ν_G = vapor kinematic viscosity, m^2/s

ν_L = liquid kinematic viscosity, m^2/s

ρ_G = vapor density, kg/m^3

ρ_L = liquid density, kg/m^3

τ_i = average interfacial shear stress, N/m^2

σ = surface tension, N/m

τ_{WG} = average wall shear stress on gas phase, N/m^2

τ_{WL} = average wall shear stress on liquid phase, N/m^2

Chapter 1

INTRODUCTION

The flow of condensing fluids inside tubes occurs in a wide range of engineering applications. Numerous examples of these applications can be found in the power generation, refrigeration, process, air-conditioning and spacecraft industries. In the power-generation industry, condensers play an important role in providing the low-temperature heat sink required in the operation of power cycles. During postulated Loss of Coolant Accidents in pressurized-water nuclear power plants, reflux condensation provides an important heat removal mechanism in vertical inverted U-tube steam generators. In the refrigeration and air-conditioning industry, the heat absorbed from a low-temperature heat reservoir is rejected through air- or water-cooled condensing units into a high-temperature heat reservoir. In spacecrafts, where high-capacity thermal transport is required at low mass flow rates, thermal load is regulated by two-phase systems [utilizing the latent heat] operating under microgravity conditions. In chemical process industries condensing units are extensively used for fractional distillation of substances.

Such large and important uses in industry requires that condensers are designed effectively and appropriately. For an effective design of condensers, the heat, mass and momentum transport mechanisms must be properly understood. In condensers the void fraction continuously decreases until complete condensation is achieved, and the flow never fully develops as it progresses along the condensation path. As the liquid and vapor fractions change gradually along the flow direction, the forces acting on the flow also change. A shift in the dominant forces acting on the flow is accompanied by a change in the flow regime. Consequently, the mass, momentum and heat transport mechanisms change, from one flow regime to another along the condensation path. The changing and non-developing nature of condensing flows brings about a complex interaction between the thermal and hydrodynamic characteristics of the flow. The dependence of design parameters such as the friction factor and Nusselt number on the flow regimes of condensing flows has been illustrated [Bell *et al.*, 1970; Sardesai *et al.*, 1981; Nitheanandan *et al.*, 1990]. Therefore, flow-regime prediction has been identified as an essential part of the design process in condensing flows.

A hydrodynamically coupled transport mechanism motivated several studies of flow-regime transition in adiabatic and diabatic flows [Soliman, 1986; Barnea and Taitel, 1986]. The adiabatic gas-liquid flow studies covered, to some degree, the effects of tube diameter, fluid properties and tube inclination. The diabatic studies involving condensation, however, are only confined to a variety of tube diameters, fluid properties and flow rates in the horizontal position.

One interesting aspect of the studies on condensing vapor flows is that there is consistent disagreement between adiabatic flow-regime maps and the location of visually observed flow regimes during condensation, especially in the slug and wavy regimes. The continuously changing void fraction, liquid level and flow velocities have been attributed to this disagreement [Rashwan and Soliman, 1987; Rahman *et al.*, 1985]. The disagreement between the adiabatic gas-liquid flow maps and the flow-regime data of condensing flows prompted the development of flow-regime maps exclusively for condensing vapor flows [e.g., Brebar *et al.*, 1980; Soliman, 1986; Gupta *et al.*, 1986]. All these flow-regime maps dealt only with the horizontal orientation of the tube.

Rahman *et al.* (1985) postulated that the increasing liquid depth in a horizontal condenser is similar to an adiabatic gas-liquid flow provided a small upward inclination is given to the tube. This similarity between slightly inclined adiabatic gas-liquid flow maps and the horizontal condensing flow regime data, at least in trend, was demonstrated by Rahman *et al.* (1985).

This thesis is motivated by the need for extending the state of knowledge [both experimentally and theoretically] to the effect of tube inclination on the flow regime transitions during condensation. In doing so, it will be possible to explain the discrepancy between the results from adiabatic flow and those from condensing flow. In more explicit terms, the objectives of the present study are:

(a) to develop new experimental data on the flow regimes of condensing steam inside a tube with different angles of upward and downward inclinations, including the horizontal orientation [no similar data is available yet in the literature],

(b) to determine the effect of inclination on the flow regime boundaries of condensing flows,

(c) to compare the new data with the existing correlations for gas-liquid flows in order to obtain improved understanding of the possible relationships [in magnitude and trend] between the regime boundaries of the two types of flow,

(d) to develop a generalized theoretical model for the transition boundary between the stratified and nonstratified flows during condensation inside horizontal and slightly inclined tubes, and

(e) to compare the new model with data of different tube diameters, fluid properties, and tube inclinations in order to demonstrate the capability of the model.

Chapter 2

LITERATURE REVIEW

Two-phase flow occurring inside tubes is generally classified based on the presence [diabatic flow] or absence [adiabatic flow] of heat transfer through the tube wall. Adiabatic gas-liquid flows occurring in horizontal, vertical and inclined tubes have been subjected to several experimental and analytical studies. The primary objective of the experimental studies was to observe and map-out the flow regimes for different cross-sectional geometries, fluid properties, and inclinations. Based on the broad base of experimental data, analytical and empirical flow-regime transition correlations have been formulated. The empirical correlations are limited to the range of experimental conditions on which the correlations were based. On the contrary, the analytical correlations may be extrapolated [with caution] to conditions where no data are available. By contrast, the data base for condensing flow regimes does not include any information about the effects of tube inclination.

In this chapter the existing condensing flow-regime data and the flow-regime maps [analytical and empirical] are discussed. This discussion is followed by a review of pertinent adiabatic gas-liquid maps developed for horizontal and inclined tubes.

2.1 Condensing Flow-Regime Data

A number of studies have been directed towards experimentally generating data on the condensing flow-regime transitions. A major portion of these data were reported by Soliman and Azer (1971, 1974), Traviss and Rohsenow (1973), Fuji *et al.* (1976), Tandon *et al.* (1983), Rahman *et al.* (1985), and Rashwan (1987). These data sets cover a tube inside-diameter range of 4.8 to 37.6 mm and five working fluids [R-11, R-12, R-22, R-113 and steam]. The test condensers used in these studies were double pipe heat exchangers where the condensing fluid flowed through the inner tube while the coolant [water was used in all experiments as the coolant] flowed through the outer jacket. Short visual observation sections were installed at a number of locations along the test condenser to enable visual observation of the flow regimes. The thermodynamic quality existing at each of the visual sections was calculated based on a heat balance application. All these data correspond to horizontal flow.

The flow-regime classification used by investigators in the condensing-flow studies were generally consistent. Seven major flow regimes and three transitional flow regimes were identified. The sequential development of these flow regimes in a condenser from the inlet to the outlet is shown in Figure 2.1. The seven major flow regimes are mist flow, annular flow, semiannular flow, wavy flow, slug flow, stratified flow and plug flow. The three transitional flow regimes are mist-annular flow, annular-wavy flow and semiannular-wavy flow. Visual classification of the transitional flow regimes were often difficult and subjective. Therefore, special techniques, such as the use of a stroboscope, were required to slow the flow down to make objective identification of these flow regimes. The descriptions used by investigators to classify the major and the transitional flow regimes are [see Figure 2.2]:

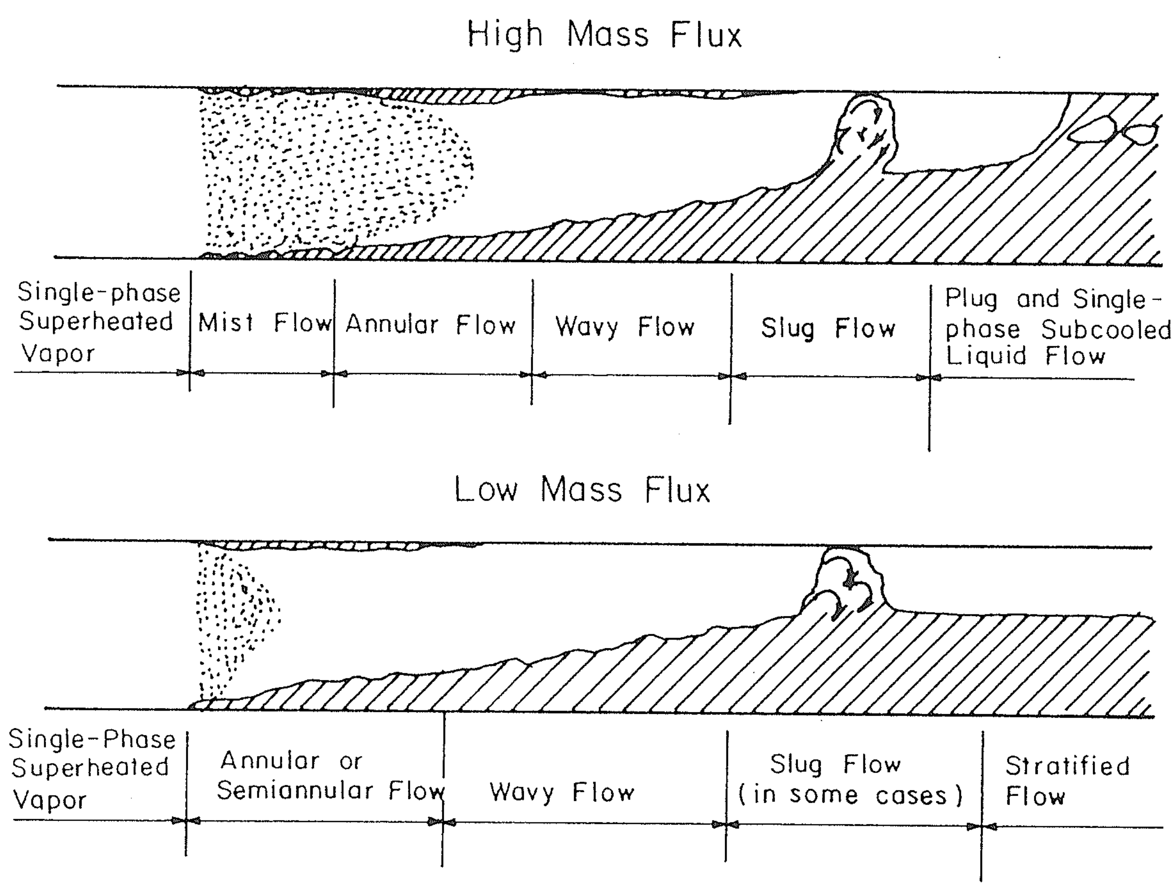

Figure 2.1 Development of flow regimes in the direction of flow during condensation

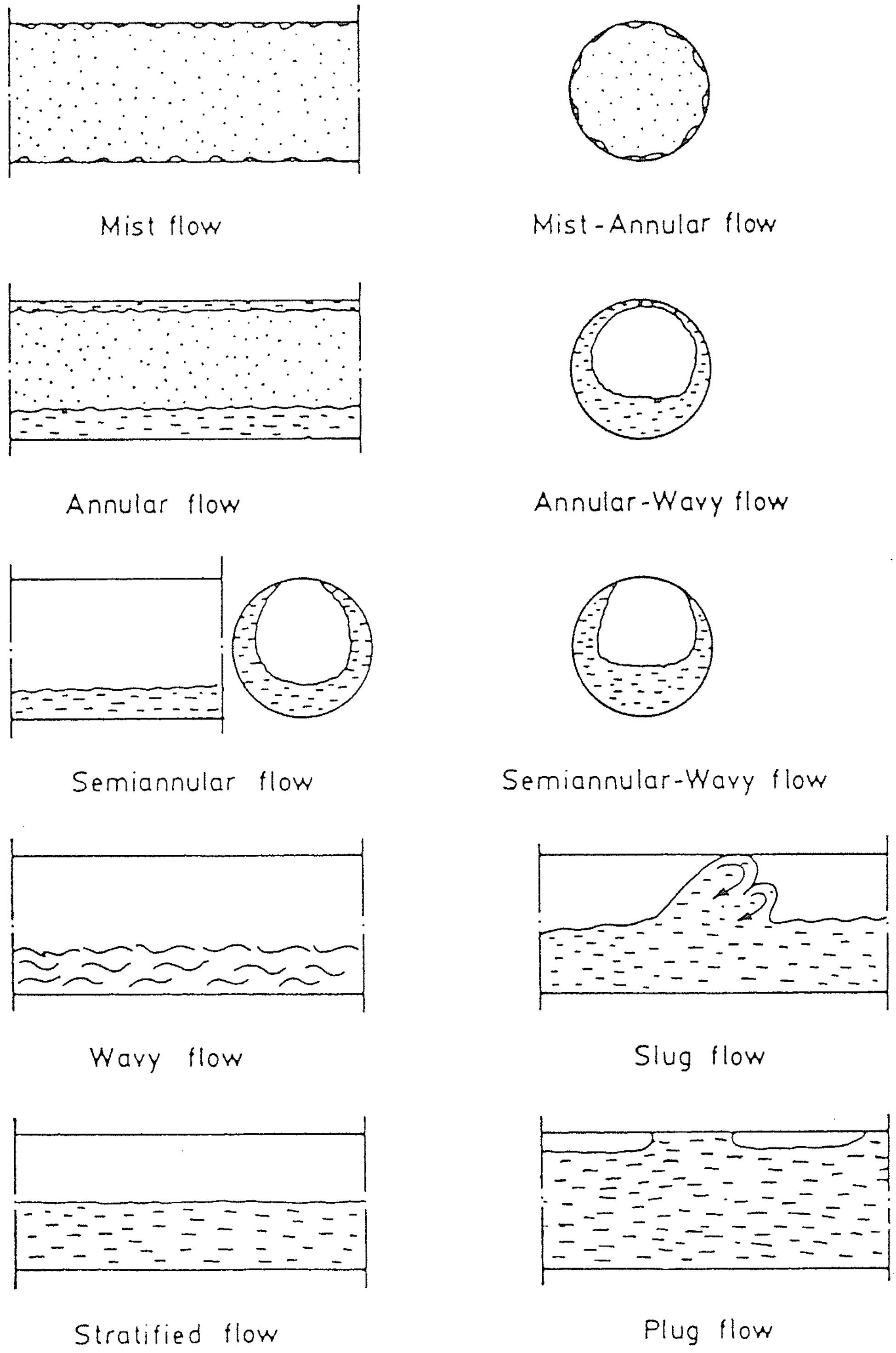

Figure 2.2 Schematic of individual flow regimes during condensation

Mist flow: No stable liquid film was apparent. Most of the liquid phase was entrained by the vapor in the form of a mist.

Annular flow: A stable liquid film covered the entire tube wall, while the vapor flowed in the core. Part of the liquid phase was entrained by the vapor. Asymmetry was apparent in the liquid film with the maximum thickness being at the bottom of the tube.

Semiannular flow: The flow had an appearance similar to the annular flow, except that the stable film did not cover the entire wall periphery. A small portion of the upper half of the tube appeared dry, while the liquid film thickness increased to a maximum at the bottom.

Wavy flow: The two phases were separated, with the liquid flowing at the bottom of the tube. The velocity difference between the vapor and liquid caused the liquid surface to be wavy. The wavelength increased with the decrease in quality. A draining thin film may appear on the upper half of the wall periphery.

Slug flow: The flow was basically wavy; however, surface waves grew frequently forming slugs wetting the upper tube wall. The slugs travelled at high speeds and the frequency of their occurrence depended on the flow conditions.

Stratified flow: Liquid flowed at the bottom of the tube and vapor at the top with a smooth interface. This flow regime existed mainly near the exit of the condenser in cases where the mass flux was small.

Plug flow: The flow appeared as a single-phase liquid flow with the intermittent appearance of large vapor plugs at the upper tube wall. Vapor plugs were irregular in shape, different in size and appeared to be flowing at the same velocity of the liquid.

Mist-annular flow: Intermittent liquid films appeared but were swept away after their appearance to become part of the mist.

Annular-wavy flow: The flow had the annular appearance but the thickness of liquid increased at the bottom forming a thick stratum.

Semiannular-wavy flow: The flow had the semiannular appearance but with a thick stratum flowing at the bottom of the tube. A fraction of the upper half of the tube was still covered by a stable liquid film.

2.2 Condensing Flow-Regime-Transition Correlations

2.2.1 Flow-regime maps

A number of flow-regime maps were developed for horizontal condensers. Among them, Soliman and Azer (1974) proposed two different maps; one of them used the vapor mass flux, G_G, and the ratio of liquid and vapor mass fluxes, G_L/G_G, as coordinates. The second map proposed by the above authors used the average velocity of the liquid phase, $\langle u_L \rangle_L$, and $[(1 - \alpha)/\alpha]$ as coordinates. The third map, suggested by Breber *et al.* (1980), used the nondimensional vapor velocity, j_G^*, and the Lockhart-Martinelli parameter, X, as coordinates. A fourth map, suggested by Tandon *et al.* (1983) used j_G^* and $[(1 - \alpha)/\alpha]$ as coordinates.

The generality of the full-map approach in predicting all flow regime transitions in a condenser is not currently accepted. It was recognized that every flow regime is uniquely dominated by a single dominant force. A shift in the dominant force results in a change in flow regime. Therefore, attempting to define transition boundaries in maps based on two fixed coordinate axes tend to predict one or more transitions relevant to these axes adequately while showing highly unacceptable performance in other transitions. More recent studies [Fathi, 1980; Rahman, 1983; Rahman *et al.*, 1985; Soliman, 1986] compared the available flow-regime data with the existing condensing flow-regime maps and found the full-map approach to be inadequate in defining all the transitions occurring in a condenser. Consequently, attempts were made to correlate each transition boundary individually.

2.2.2 Individual Analytical Correlations

Three analytical correlations for flow-regime transition in horizontal condensers were reported by Soliman (1982 and 1983) and Rashwan and Soliman (1987). These three correlations are for the annular-to-wavy, mist-to-annular, and wavy-to-slug transitions, respectively. The first two correlations were compared with the existing flow-regime data by Rahman *et al.* (1985) and Rashwan (1987). The wavy-to-slug transition correlation was compared with the available data by Rashwan and Soliman (1987). Satisfactory results were obtained in all comparisons.

(a) The Mist-to-Annular Transition

Soliman (1983) developed a correlation for the mist-to-annular transition based on a force balance between the dominant destructive force and the stabilizing forces. The inertia force of the vapor was assumed to be the dominant destructive force acting on the liquid film, while the surface tension and liquid viscous forces were the major stabilizing forces. A modified Weber number was formulated based on a balance between the vapor inertia, liquid viscosity, and surface tension forces. Based on comparisons with the experimental data, it was concluded that the mist-annular transition can be characterized by the modified Weber number for different fluid properties and tube diameters. Annular flow corresponded to Weber numbers below 20 and mist flow corresponded to Weber numbers greater than 30.

(b) The Annular-to-Wavy Transition

This transition line, developed by Soliman (1982), marks the shift from vapor-shear-controlled flow into gravity-controlled flow. The hypothesis adopted in that analysis was that the annular-wavy transition occurs when the Froude number, which is a measure of the ratio of inertia to gravitational forces, reached a certain value. The resulting formulation for Froude number was compared with ten data sets and it was found that the annular-wavy transition coincided with a constant value of Froude number of about seven.

(c) The Wavy-to-Slug Transition

Rashwan and Soliman (1987) developed a theoretical model for the wavy-to-slug transition in condensing fluids inside horizontal tubes. The authors observed that the surface waves seemed to be travelling upstream and downstream when the tube was running full at the exit, in the horizontal tube. The interaction between the upstream-travelling and the downstream-travelling waves resulted in a hydraulic jump. In the absence of a full tube at the exit the surface waves appeared to be travelling downstream only and as a result no slugging was observed. Based on these observations they characterized the flow upstream of the slugging location as supercritical and the downstream flow as subcritical. The slugging location was determined analytically when the flow transits from supercritical flow to subcritical flow. The model showed good agreement with the available horizontal tube data.

2.3 Adiabatic Flow-Regime-Transition Correlations (Empirical)

2.3.1 Horizontal Flow

Among the most popular flow-regime maps used in horizontal gas-liquid flows are those suggested by Baker (1954) and Mandhane *et al.* (1974). Both maps used dimensional coordinates: Baker(1954) used G_G and G_L/G_G as coordinates with correction factors for physical properties, while Mandhane *et al.* (1974) used the gas superficial velocity V_{GS}, and the liquid superficial velocity, V_{LS}, as coordinates. Based on a total of 5,935 observations, a map was proposed by Mandhane *et al.* (1974) which was shown to be an average of the flow regime maps proposed by Hoogendoorn(1959), Baker (1954), and Govier and Omar (1962). Mandhane *et al.* (1974) proposed correction factors to account for the effects of fluid properties on the transition boundaries.

2.3.2 Inclined Flow

Several experimental studies have been reported with gas-liquid flows inside inclined tubes. Based on these experimental studies, a number of flow-regime maps have been developed. The gas-liquid flow regimes in horizontal and downward inclined tubes [0°, -1°, -5°, -10°, -30°, -50°, -70°, -80°, and -90°] were experimentally studied by Barnea *et al.* (1982) using 2.55-cm and 5.1-cm I. D. pipes. The flow regimes were determined by visual observation and by conductivity probes. The experimental data were compared with the theoretical model suggested by Taitel and Dukler (1976). The theoretical prediction of the intermittent-to-annular transition agreed with the data for up to about 10°. Within this range of inclination, Barnea *et al.* (1982) found that the intermittent-to-annular transition is best described by $h_L/D = 0.35$, rather than $h_L/D = 0.5$ as suggested by Taitel and Dukler (1976). The model of Taitel and Dukler (1976), however, predicted the stratified-to-nonstratified transition in the whole range, i.e. 0° to -90°, of downward inclination satisfactorily.

Experimental data in 2.5-cm and 3.8-cm I. D. tubes with a two-phase mixture of refrigerant 113 as the test fluid were obtained by Crawford *et al.* (1985). An adiabatic test section was used in this experiment. Flow regimes were visually observed at downward angles of -90°, -60°, -45°, -30°, and -15° with the 2.5-cm tube, whereas only the -90° downward angle was tested with the 3.8-cm tube. The horizontal flow-regime transition conditions developed by Weisman et al. (1979) and Weisman and Kang (1981) were compared with the experimental data. Based on the comparisons, the annular and dispersed flow conditions for horizontal flow predicted the regime transition in downward inclinations satisfactorily. In the bubble-to-intermittent and separated-to-intermittent transitions, however, small modifications were applied to the horizontal correlations for satisfactory predictions.

Flow-regime data for upward inclined tubes [at 0, +0.25°, +2°, +10°, +20°, +50°, +70°, and +90°] were reported by Barnea *et al.* (1985). Experiments were conducted in 2.5-cm and 5.1-cm I.D. tubes. The data were compared with the horizontal and slightly inclined flow correlation [Taitel and Dukler, 1976] and the vertical upward flow correlation [Taitel *et al.*, 1980]. They hypothesized that the transition mechanisms in the whole range of inclinations from -90° to +90° change gradually as the angle of inclination is changed gradually. For small inclinations, the Taitel and Dukler (1976) model adequately predicted the transition boundary, however, at large inclinations modifications were applied. When the inclinations were large, certain transition mechanisms became inoperative. For example, they observed that the bubbly flow regime did not occur for angles below 60°. Hence, a model to predict the limiting condition for the existence of bubbly flow became important. Small upward inclinations had a major effect on the transition from stratified-to-intermittent flow and on the transition from stratified-to-annular flow. Even for small angles [less than 1°], the stratified boundary shrank to a small bell-shaped region and the intermittent flow occupied the region previously occupied by stratified flow.

Mukherjee and Brill (1985) developed empirical transition correlations to predict the flow regimes in pipes at all possible inclinations. Experimental data were obtained using kerosene and lubricating oil as test fluids in a U-shaped, 3.81-cm I.D. steel pipe. Their empirical regime-transition correlations were obtained from a nonlinear regression analysis conducted on the test data.

The experimental trends observed by Mukherjee and Brill (1985) agreed with the observations made by Barnea *et al.* (1982 and 1985). For example, the stratified flow envelope increased as the downward inclination was increased from horizontal to -30°. In the downward flow, slug flow was observed only at high gas flow rates, whereas in the upward flow, slug flow expanded towards low liquid flow rates at the expense of stratified flow. The inclination angle had insignificant influence on the annular-mist boundary.

Kokal and Stanislav (1989) conducted flow-regime, liquid-holdup and pressure-drop studies in 25-m long test sections with 25.8-mm, 51.2-mm, and 76.3-mm I. D. tubes. The experimental set up was able to incline the test section within $\pm 10^{\circ}$ from the horizontal. The flow regimes were observed visually and using volume sensor traces. The regime transitions were modelled and compared with the data. A dimensionless momentum equation developed by Taitel and Dukler (1976) was modified by using the friction-factor correlation given by Chen (1984). Taitel and Dukler (1976) used Blasius' equation to calculate the friction factors and assumed the interfacial friction factor was approximately equal to the gas friction factor. Kokal and Stanislav (1989) calculated the interfacial friction factor using the Ellis and Gay (1959) correlation. With these modifications, the stratified-nonstratified transition was derived analytically.

2.4 Adiabatic Flow-Regime-Transition Correlations (Theoretical)

A generalized analytical model based on physical mechanisms was proposed by Taitel and Dukler (1976) for predicting all flow regime transitions in horizontal and near-horizontal gas-liquid flows. The model defined specific physical mechanisms responsible for a given flow regime to exist. From these mechanisms analytical expressions were developed to define the transition boundaries.

Five basic regimes were considered important: stratified smooth, stratified wavy, intermittent [slug and elongated bubble], annular and dispersed bubble. Starting from a stratified equilibrium flow, a dimensionless momentum equation was derived. This equation determined the equilibrium liquid level as a function of two dimensionless groups.

The stratified flow was assumed to be a basic flow configuration. When a given condition is satisfied, the flow changes from stratified to another regime. The mechanisms which cause these changes were expressed in terms of four dimensionless groups. Therefore, in order to locate a flow regime, only two dimensionless parameters are required for any given inclination. The model incorporated the effects of gas and liquid flow rates, physical properties of the fluids, pipe diameter and the angle of inclination on the transition boundaries.

Barnea (1986) suggested a unified model for all angles of inclination that can successfully predict the annular-to-intermittent flow transition in gas-liquid flow. Two mechanisms were considered in deriving this unified model; first the instability of the liquid film due to liquid drainage near the wall blocking the entrance, and the second, the blockage of the gas core due to a large supply of liquid in the film. Both of these mechanisms are applicable only outside the range of stable stratified flow.

Transition mechanisms for each individual flow regime boundary for the whole range of pipe inclinations were presented by Barnea (1987). This comprehensive model incorporated the models suggested by Taitel and Dukler (1976) and Barnea *et al.* (1982 and 1985). The authors demonstrated reasonable success against experimental data.

One of the most important transitions for the present investigation is the transition from stratified [or wavy] to nonstratified [annular, slug and bubble] flow. The stratified-nonstratified correlations of Barnea (1987), Mukherjee and Brill (1985), and Kokal and Stanislav (1989) are compared at -5°, -1°, 0° and +1° inclinations in Figures 2.3, 2.4, 2.5,

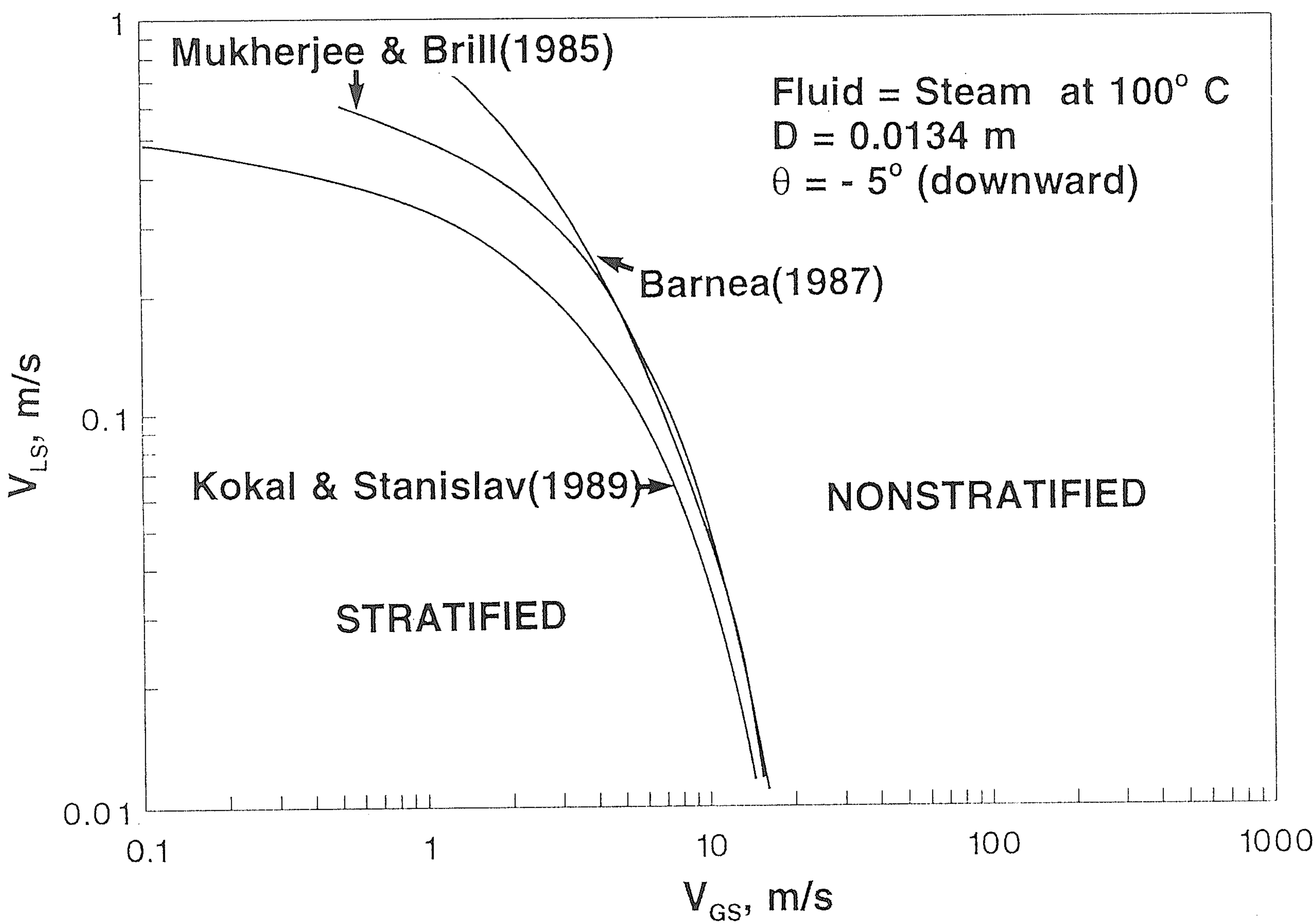

Figure 2.3 Predictions of the stratified-nonstratified adiabatic correlations at -5° [downward] inclination.

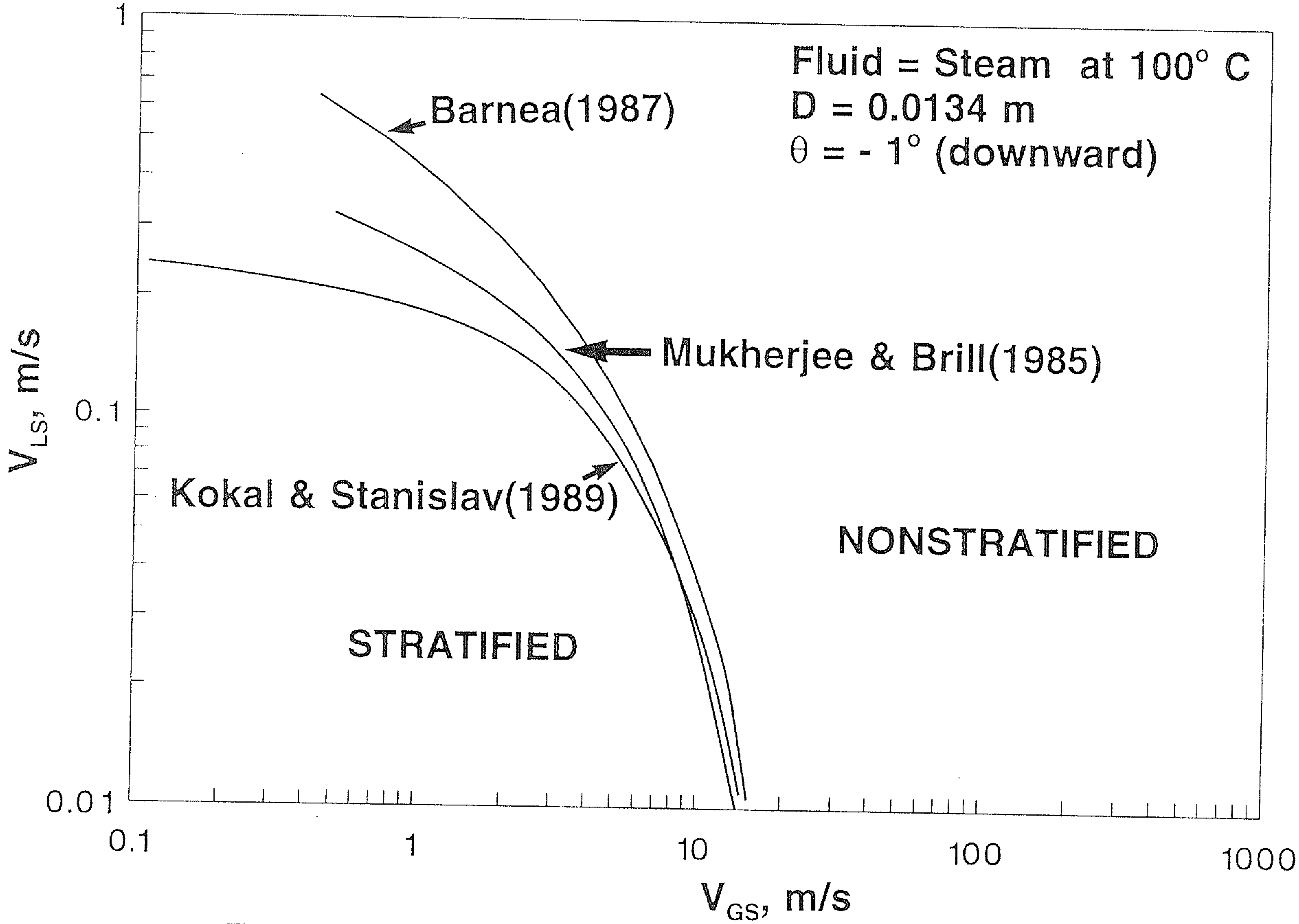

Figure 2.4 Predictions of the stratified-nonstratified adiabatic correlations at −1° [downward] inclination.

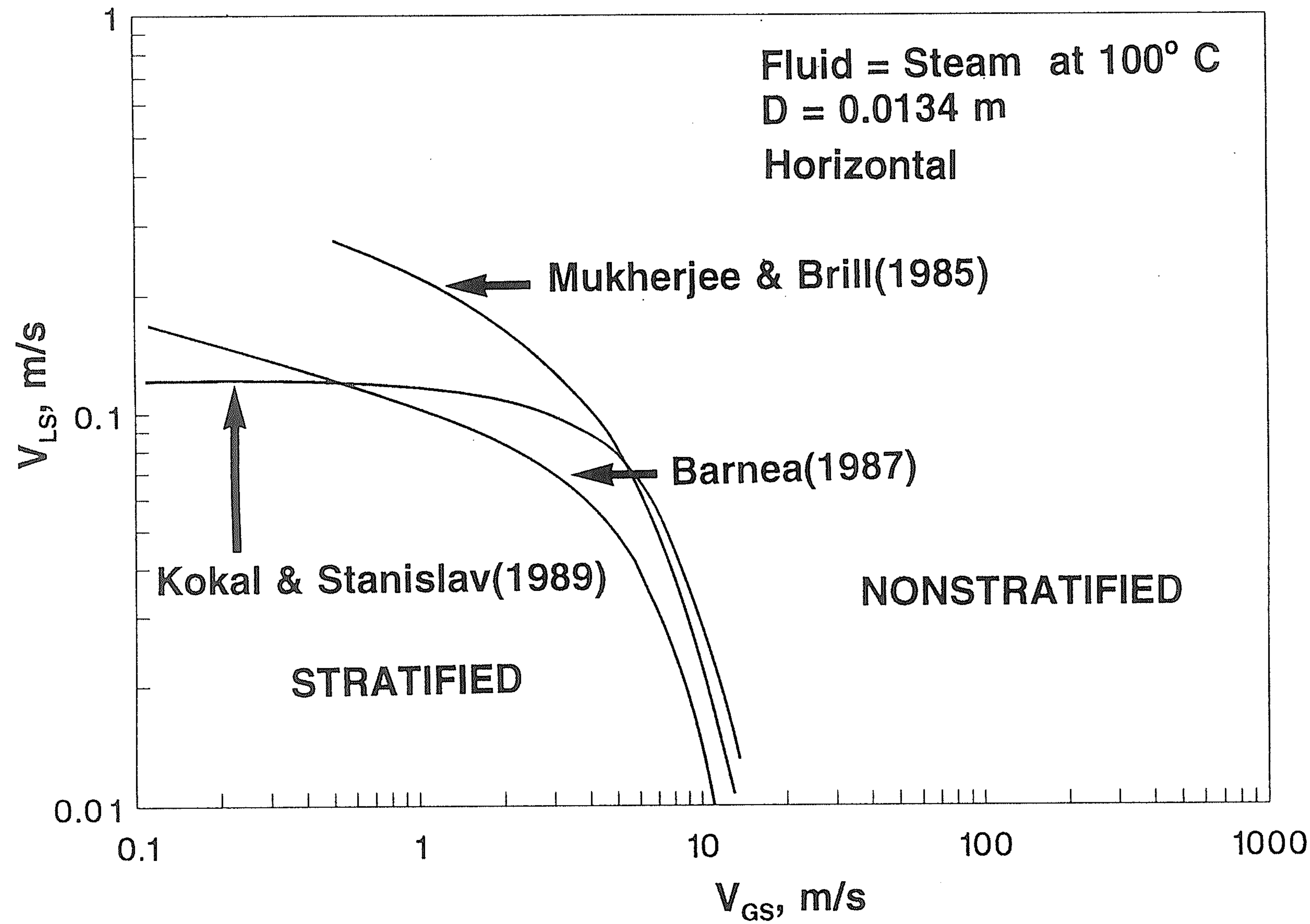

Figure 2.5 Predictions of the stratified-nonstratified adiabatic correlations in the horizontal position.

and 2.6, respectively. All three correlations predict a shrinking stratified region as the inclination increases from -10°. This trend agrees well with the trend observed in the experiments. The agreement among correlations in predicting the transition boundary is very good at low liquid superficial velocities, however, slight differences appear as the liquid superficial velocity increases beyond 0.1 m/s.

This review of existing adiabatic gas-liquid correlations and the experimental observations provide an insight into the different mechanisms that were assumed to be important in flow regime transitions. These physical mechanisms were based on experimental observation of the flow. Experimental methods have also shown that the flow regime is a function of several variables, such as fluid properties, flow rates, tube orientation, and tube size. Although several flow-regime-transition models have been proposed for the whole range of inclinations in the adiabatic gas-liquid flows, there are no studies [analytical or empirical] available that have investigated the effect of inclination on condensing flows. The condensing flow data that are available in the published literature deal only with the horizontal orientation. Therefore, the effect of inclination on condensing flow-regime transitions has been identified as the major objective of the present study.

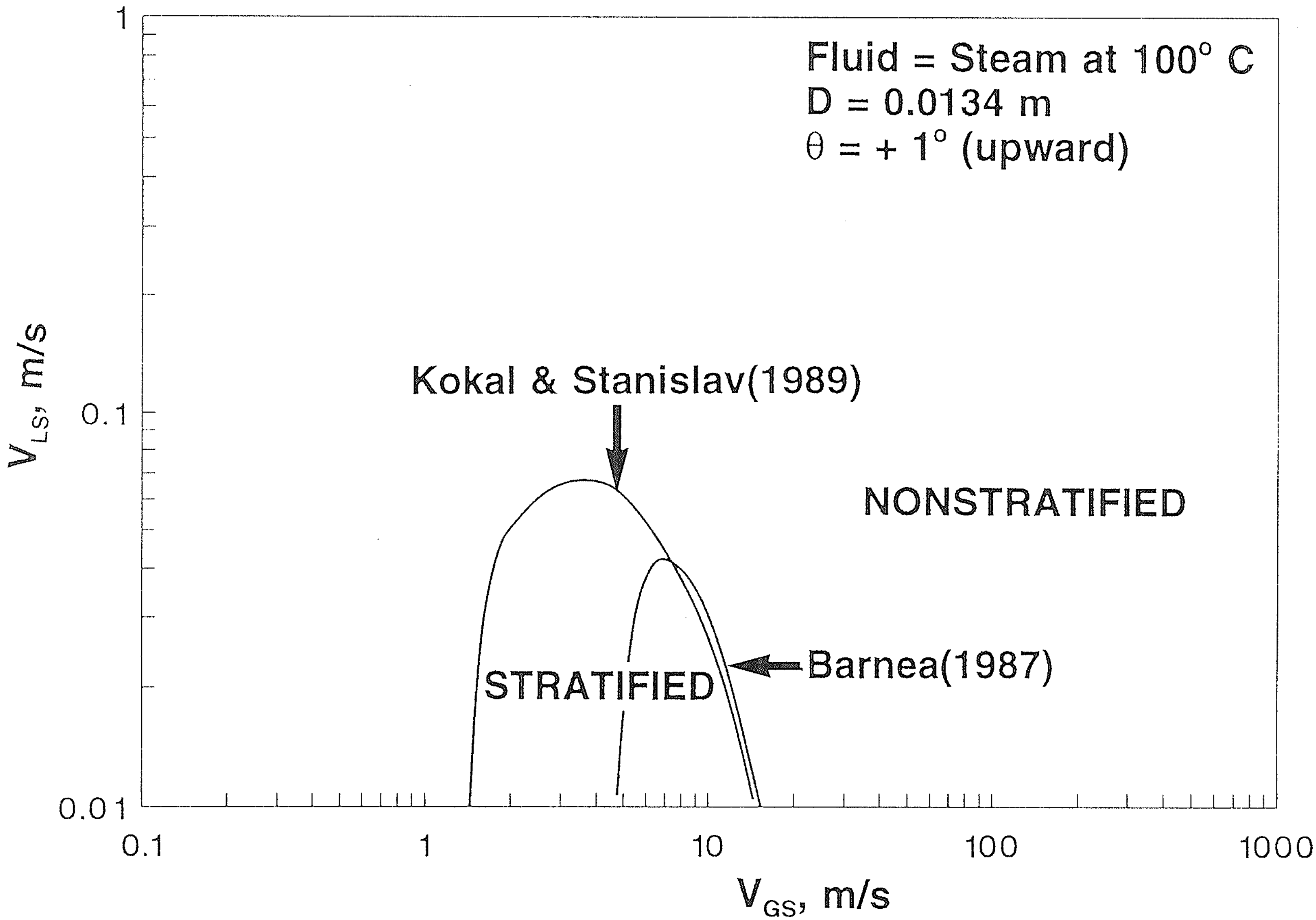

Figure 2.6 Predictions of the stratified-nonstratified adiabatic correlations at +1° [upward] inclination.

Chapter 3

EXPERIMENTAL TEST FACILITY AND PROCEDURE

An experimental investigation was conducted to generate condensing flow-regime data in inclined tubes. As part of this experimental investigation, a test facility was designed and constructed. The experiment was conducted in a 13.4-mm I. D. tube with steam as the test fluid. Seven data sets were generated; three data sets each in the upward and downward inclinations, and one data set in the horizontal position. The objectives of the experimental investigation were:

1. To obtain new flow-regime data in the upward [+1°, +5°, and +10°], downward [-1°, -5°, and -10°], and in the horizontal positions. Attention is directed towards studying the effect of tube inclination on the flow-regime transitions during condensation.
2. To observe and record the sequence of flow-regime development under a range of mass flow rates inside the tube. The principal aim will be to locate the boundaries between the different flow regimes occurring in each inclination.
3. To investigate the upper bound for the slugging phenomenon during condensation.

3.1 The Steam Circuit

The test facility, shown schematically in Figure 3.1, is a closed-loop circuit on the test fluid [steam] side. A heat-exchanger-type boiler produced controllable amounts of steam from distilled water using a regulated supply [at a pressure of about 780 kPa] of building steam as a heat source. The degree of superheat in the steam entering the test section was controlled by a superheater installed downstream from the boiler. The superheater is basically a double-pipe heat exchanger [3-m long] with the test fluid flowing inside the inner tube and the building steam flowing countercurrently inside the outer jacket. Type K copper tubing with 37.6-mm I.D. and 41.3-mm O.D. was used for the inner pipe, and 49.8-mm I.D. and 54.0-mm O.D. tubing was used for the outer pipe. The superheater was insulated with a 40-mm thick fiberglass insulation. The flow of building steam into the superheater was regulated by a needle valve. This provided some control over the degree of superheat of the test fluid.

Following the superheater, the flow was directed to a precondenser. This component was found to be necessary in previous investigations where large-diameter test condensers were used and it was desirable to achieve complete condensation within the test condenser. However, the precondenser was never engaged in the present experiment and the flow was channelled directly from the superheater to the test condenser.

A detailed description of the condenser is provided in a later section. The pressure at the test-condenser inlet was measured by a calibrated "USG" Bourdon-tube pressure gauge and the temperature was measured by a 20-gauge copper-constantan

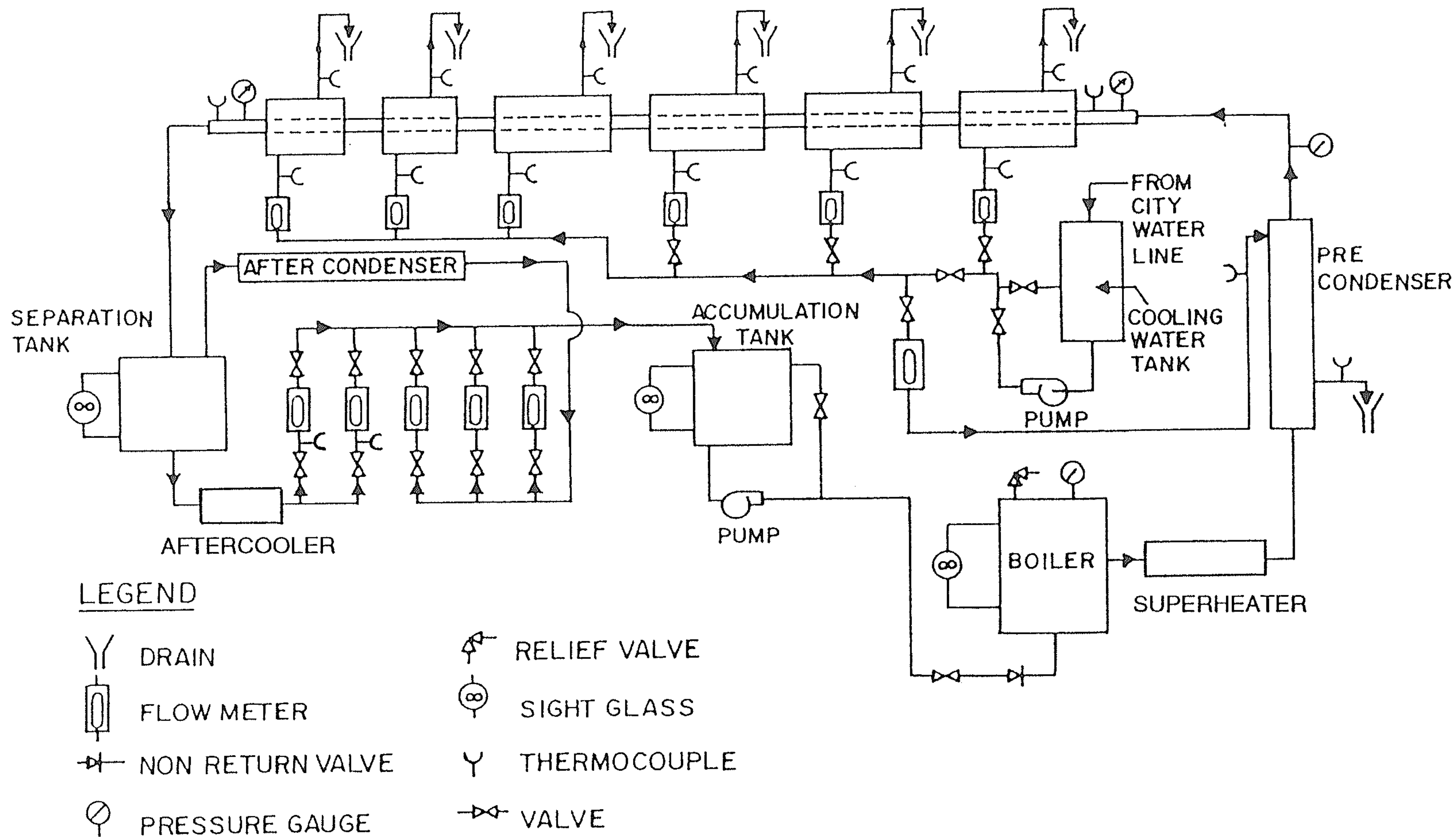

Figure 3.1 Experimental test facility.

thermocouple. The steam at the inlet of the test condenser was always in the superheated region. The pressure and temperature at the outlet of the test condenser were measured using a calibrated "Ashcroft" Bourdon-tube pressure gauge and a 20-gauge copper-constantan thermocouple, respectively. Complete condensation was always achieved in the test condenser during this experiment.

Downstream of the test condenser, a vapor-liquid separator was installed to receive the condensate. This component was found to be necessary in previous investigations in order to separate the vapor and liquid when complete condensation was not achieved in the test condenser. In this experiment, the separator was used as a liquid accumulator. It was basically a 42.4-L copper tank with a 309-mm long sight glass to indicate the height of the liquid inside, and covered on the outside by 63.5-mm thick fiberglass insulation. The outflow of liquid from the separator was controlled by a valve, and hence by adjusting the opening of this valve a steady liquid level can be achieved in which case the liquid flow rates into and out of the separator would be equal. Thus, measuring the rate of flow leaving the separator would give the total steam mass flow rate through the test condenser. This was done by two calibrated "Fischer and Porter" variable-area-type flowmeters with maximum capacities of 30.3 and 157 cm^3/s. Either one of these flowmeters was used in any particular test run. An aftercooler was installed in the line between the separator and the liquid flowmeters. This insured liquid subcooling and avoided any possible flashing in the flowmeters. Each flowmeter was provided with a copper-constantan thermocouple immediately upstream. This allowed the measurement of condensate temperature for the purpose of evaluating the density at the flowmeters.

After measuring the flow rate, the condensate was discharged into a liquid receiver. The liquid receiver was 48.8 L in capacity provided with a sight glass to monitor the liquid level. The main purpose of the receiver was to insure a steady liquid supply to the circulating pump. The circulating pump is a single-speed, 0.56 kW centrifugal pump with a by-pass line used for returning the condensate back to the boiler.

The steam circuit described above was tested against leaks using compressed air. It proved to be leakproof up to a pressure of 400 kPa. Before the start of the experiments, the system was evacuated, then charged with steam and then re-evacuated. This was necessary to insure the absence of air or any noncondensable gases in the circuit during tests.

3.2 Test Condenser

The test section, shown in Figure 3.2 consisted of six copper, double-pipe heat exchangers, each followed by a visual section. The first four heat exchangers [labelled A, B, C, and D] were 0.61-m long, whereas the last two [labelled E and F] were 0.46-m long. The steam flowed in the inner pipe and the cooling water flowed countercurrently in the outer jacket. For all units, the inner pipe was type-K copper tubing, 13.4-mm I.D. and 15.9-mm O.D. The outer pipe was 18.9-mm I.D. and 22.2-mm O.D. All heat exchangers were covered by a layer of insulation in order to minimize heat losses to the surroundings.

Each visual section contained a 15-cm length of standard clear-glass tubing. The construction details of a typical visual observation section are shown in Figure 3.3. The

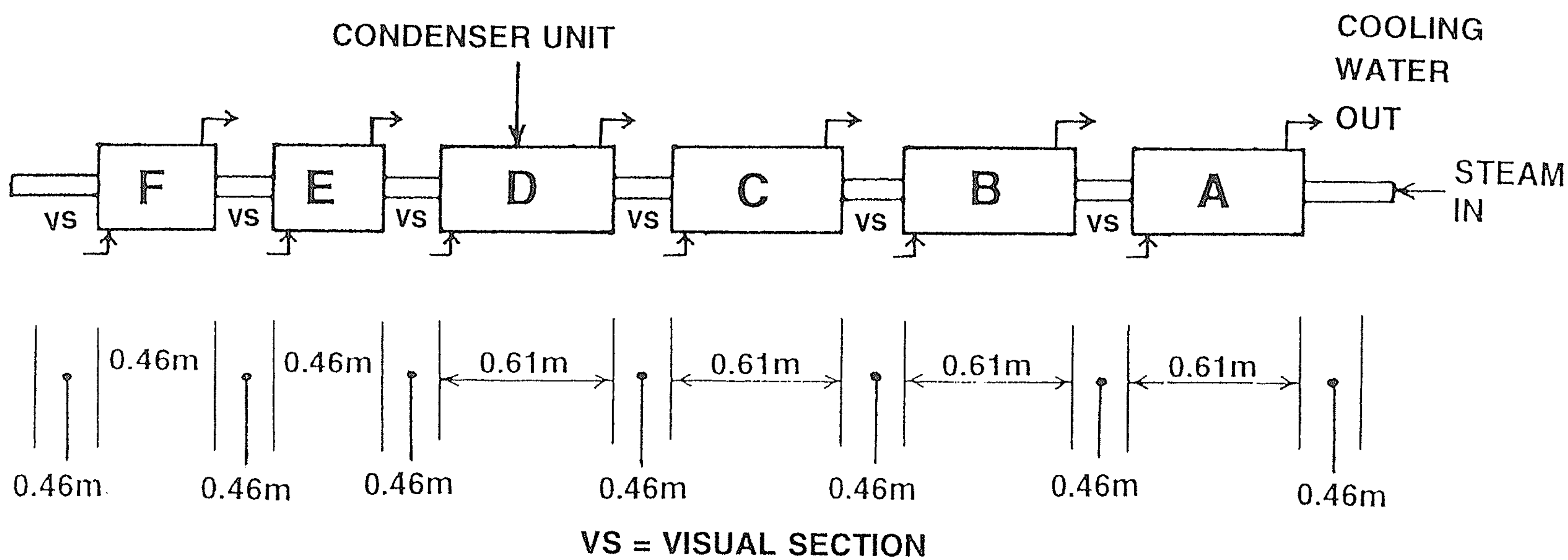

Figure 3.2 Schematic of the 13.4-mm I.D. test section.

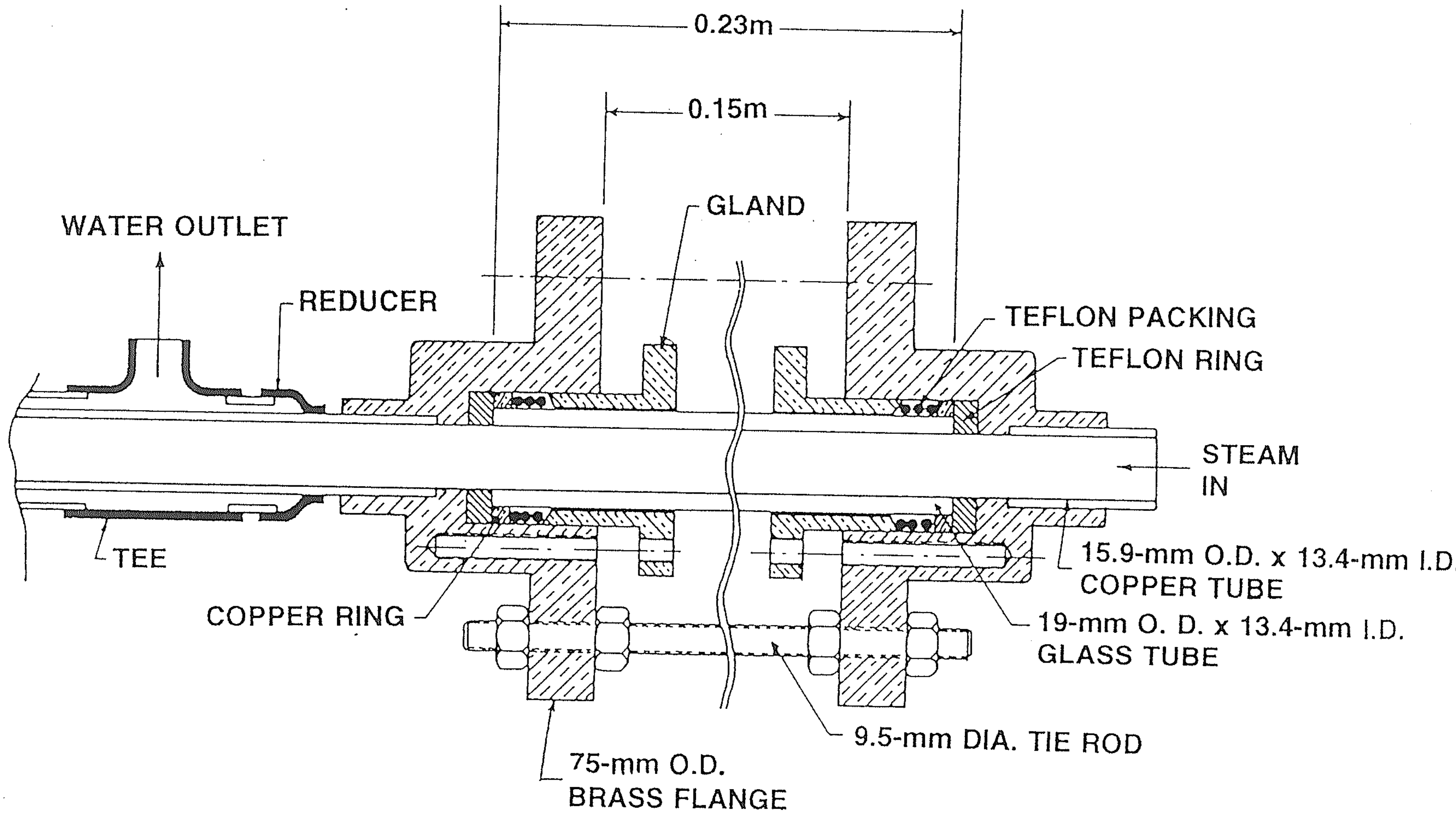

Figure 3.3 Construction details of a visual section.

visual sections consisted of high pressure glass tubes supported on both ends by a stuffing box to prevent leakage. Throughout the test section [heat exchangers and visual sections], the inside diameter was maintained uniform at 13.4 mm. Care was exercised in ensuring reasonable concentricity and coaxiality of the test section segments [heat exchangers and visual sections]. An insulated, straight length of 30 diameters was provided at the inlet and outlet sides of the test condenser in order to minimize end effects.

3.3 Measurement of Inclination Angle

The test section was mounted on a beam truss, shown schematically in Figure 3.4. Each test-section segment was clamped to the beam truss with two adjustable fixtures [Figure 3.5]. These adjustable fixtures provided sufficient flexibility for any level adjustments required between the beam truss and the test section. The beam truss was pivoted at the centre and was constructed with sufficient rigidity for minimum deflection at the two free ends. At the centre of the truss, a 13-mm thick [26.6-cm x 30-cm] steel plate was bolted. Two journal bearings were fixed to this steel plate, as shown in Figure 3.6. A 43-mm diameter steel shaft was passed through the journal bearings to provide rotational flexibility about the axis of the shaft. Slippage between the shaft and the journal bearings was prevented by a key inserted between them. The shaft was supported at both ends by self-aligning end bearings mounted on a pair of columns. The entire weight of the test section, visual section, adjustable fixtures and the steel truss was supported by these two vertical columns. On one end of the two supporting columns the shaft was

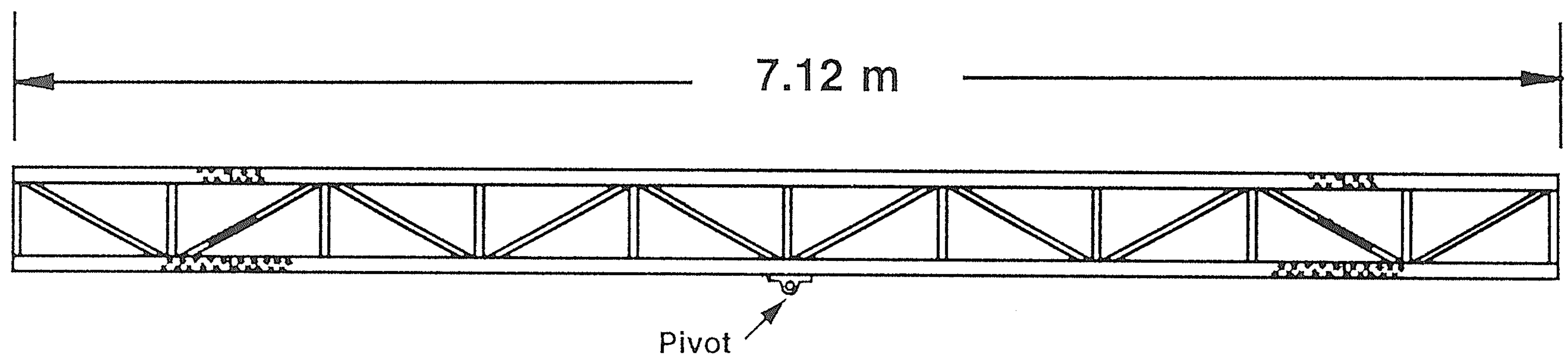

Figure 3.4 Schematic diagram of the truss beam.

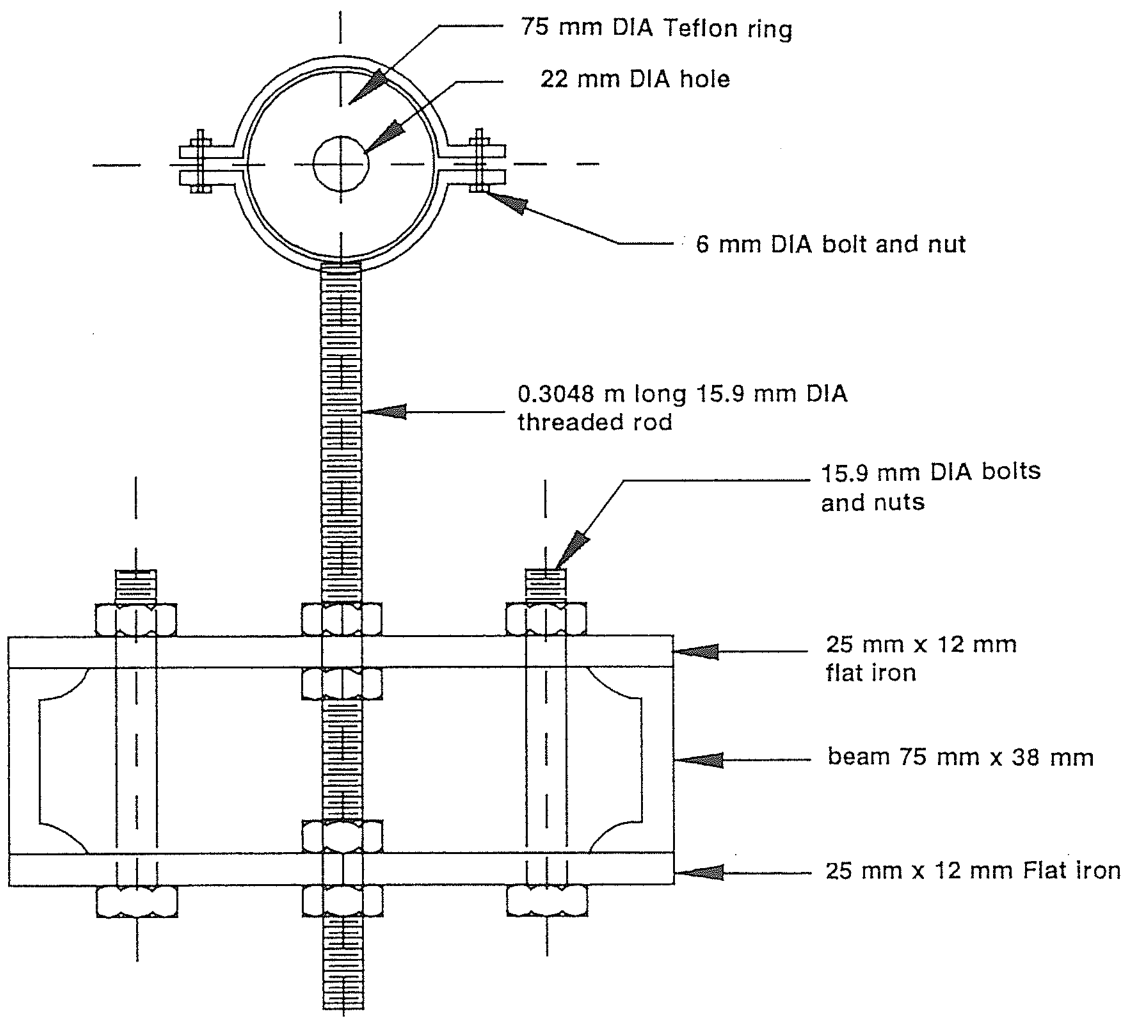

Figure 3.5 Construction details of the adjustable fixtures.

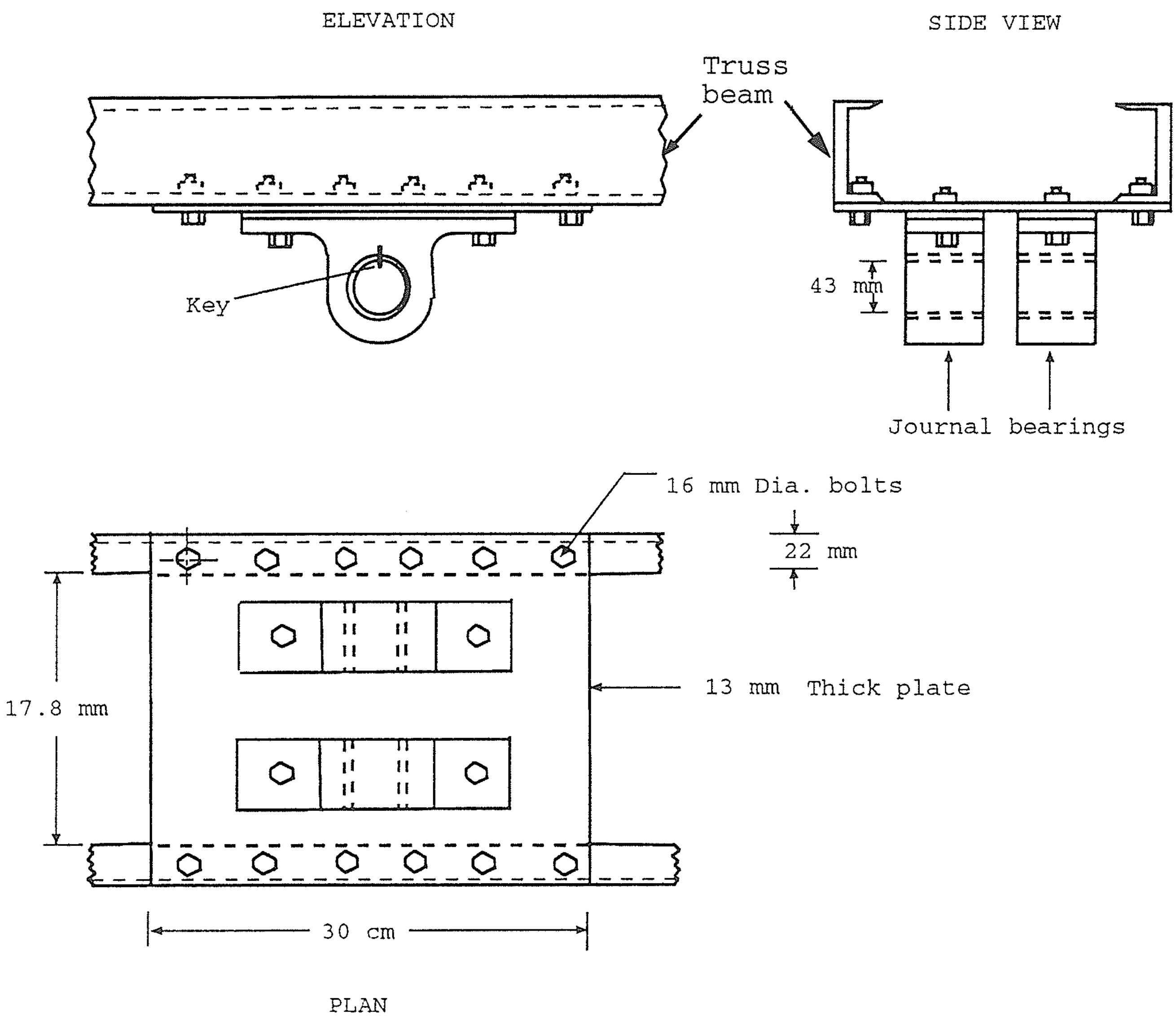

Figure 3.6 Construction details at the centre of the truss beam.

extended to protrude by 75 mm, where an adjustable "platform mount", shown in Figure 3.7, was securely bolted. This piece was necessary in order to support a surveying level. The "platform mount" and the shaft were bolted such that both of them rotated without any slippage. A surveying level was bolted to the "platform mount", as shown in Figure 3.8. A graduated surveyor's staff rod was placed at a distance [B] from the axis of the shaft, as shown in Figure 3.9 . The smallest graduation available on the staff rod is 1 mm. Therefore, the uncertainty in measuring the elevation of the test section can be assumed to be ± 1 mm. With the surveying level, a datum height was obtained when the test section, the beam truss, the "platform mount" and the surveying level were placed in the horizontal position.The axis of the shaft and the line of sight of the surveying level were ensured to lie in the same plane. Any inclination introduced to the test section rotates the surveying level about the axis of the shaft. As a result, the line of sight in the surveying level rotates about the axis of the shaft, as shown in Figure 3.9, by an angle equal to the inclination of the test section, thereby giving a new elevation reading on the staff rod. The difference between the current staff rod reading and the datum [value obtained in the horizontal position] gives the vertical height [A]. The angle of inclination of the test section was obtained by $\theta = \tan^{-1}$ (A/B).

3.4 The Cooling Water Circuit

A separate loop was used to supply cooling water to the test section and aftercooler. This circuit was designed to permit complete control on the flow rate of coolant to the aftercooler and each condensing unit. City water was used as the coolant

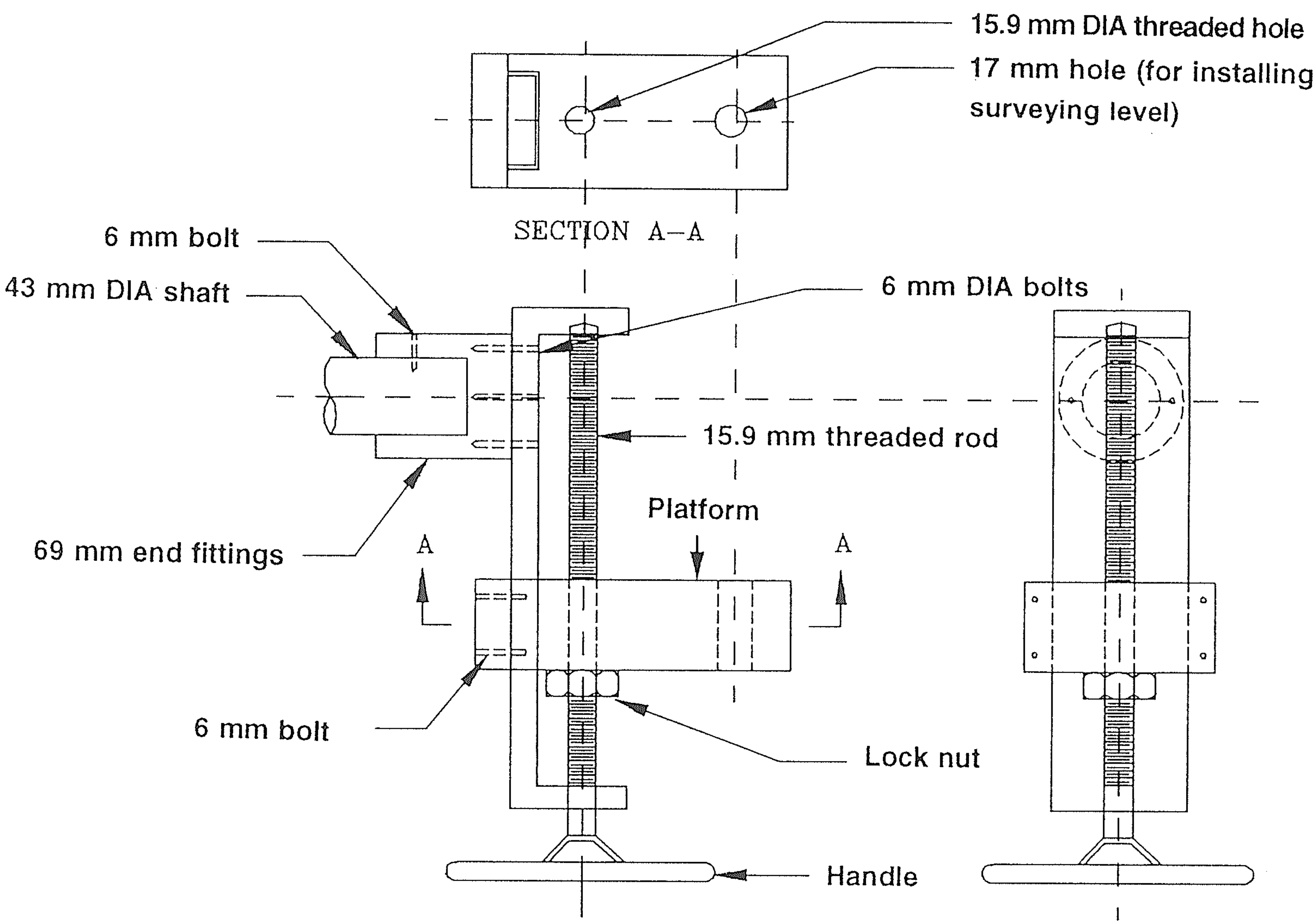

Figure 3.7 Construction details of the "Platform mount".

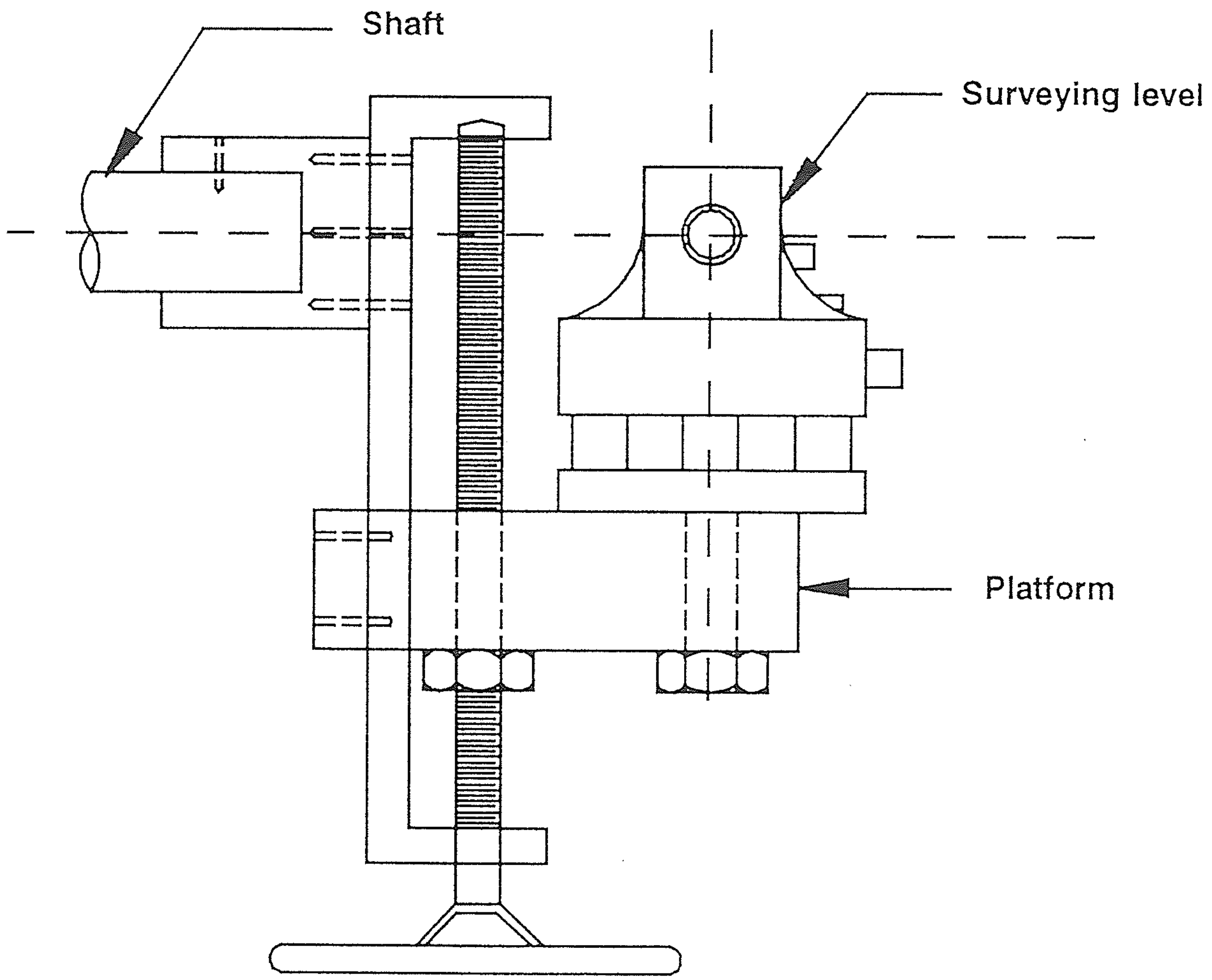

Figure 3.8 Alignment of the axis of the shaft with the line of sight of the surveying level.

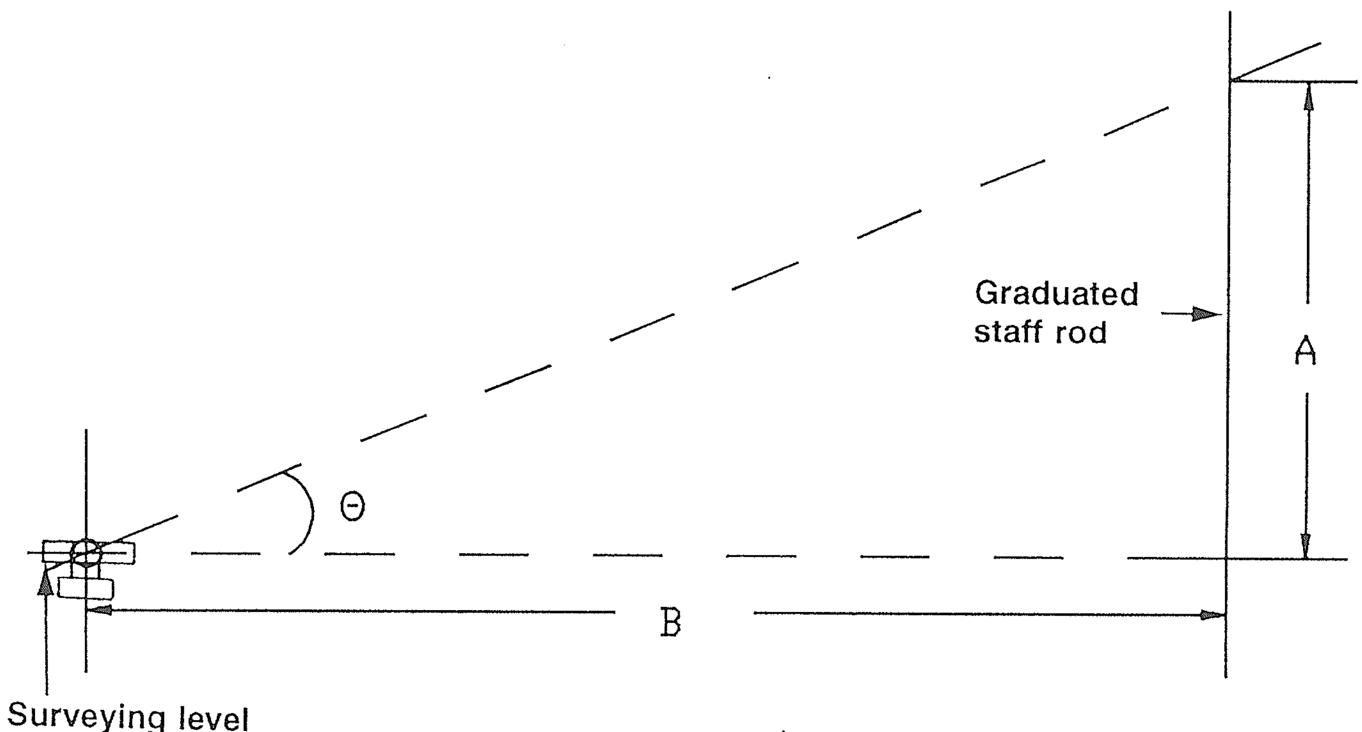

$$\Theta = \tan^{-1}(A/B)$$

Figure 3.9 Measurement of the angle of inclination of the test section.

for this experiment in an open-circuit arrangement.

The circuit starts at a 190-litre surge tank provided with an overflow line to avoid any possible flooding. The water was circulated through the circuit by a 7.457-kW turbine pump with a maximum head of 155 m of water and a maximum discharge of 142 L/min. Downstream from the pump, a by-pass line was used to adjust the total rate of water supply to the cooling system. Parallel feed lines were installed to supply water to each condensing unit and the aftercooler. Each of these lines was provided with a check valve to avoid back-flow. The water leaving the condensing units and aftercooler was allowed to discharge into a common drain.

To control the cooling water flow rate to each unit of the test condenser and the aftercooler, a valve was installed in each of the upstream and downstream lines of these heat exchangers. The upstream valves were all kept wide open, and the flow rate was controlled by adjusting the downstream valves. This resulted in higher pressure in the cooling water and consequently prevented any possible boiling. The following instrumentation was provided to record the mass flow rate and the temperature rise across each heat exchanger. The first three condensers [A, B, and C] used "Fisher and Porter" variable-area type flowmeters. The maximum capacities of these flowmeters were 26.2 L/min, 25.7 L/min, and 16 L/min, respectively. The next two condensing units [D and E] used "Brooks" variable-area type flowmeters having a maximum capacity of 15.5 L/min. The last condensing unit F used a "Fisher and Porter" variable-area flowmeter with a maximum capacity of 9.8 L/min. All these flowmeters were calibrated before their use. The temperature at the inlet and outlet of each condensing unit was measured by 20-

gauge, copper-constantan thermocouples. A "Leeds and Northrup" digital potentiometer [model 914] was used to measure the outputs of these thermocouples.

3.5 Experimental Procedure

For every data set representing a specific tube inclination, a number of test runs were conducted and the main variable changed from one test to the other was the mass flow rate of the test fluid. The flow regime was observed at each visual section in all test runs. Another important variable was the mass flow rate of cooling water flowing into the individual condenser units. By adjusting the cooling water flow rates it was possible to change the qualities, and possibly the flow regimes, at the different visual sections while keeping the steam flow rate approximately constant. The pressure in the test condenser depended on the flow rates of steam and coolant, hence it was not an independent variable. In order to calculate the inlet enthalpy of the steam it was necessary to maintain superheated conditions at the inlet end of the test condenser; however this superheat was not considered an experimental variable. In each data set, experimentation commenced from the lowest possible mass flow rate of steam through the test section and continued until the maximum possible steam flow was achieved while ensuring enough data were collected so that the transition lines between different flow regimes were established with reasonable confidence.

3.5.1 The Start-up Procedure

The following procedure was followed to prepare the experimental set-up for any particular test run:

1. The digital potentiometer was switched on.
2. The cooling water surge tank was filled to the overflow level.
3. The cooling water circulating pump was turned on with its by-pass valve fully open.
4. The valves upstream and downstream of each condensing unit were turned to the wide open position.
5. The by-pass valve of the cooling water circulating pump was partially closed to force the water to flow into the test condenser and aftercooler.
6. The downstream valves on the drain line of each condensing unit as well as the aftercooler were adjusted to establish the desirable flow rate and pressure of the cooling water.
7. The building steam, after regulating its pressure, was allowed to flow through a valve into the boiler coil.
8. The valves downstream of the separator [condensate line] were all closed.
9. When steam started flowing into the test condenser, the bleeding valve on top of the separator was gradually opened allowing air and noncondensable gases to ventilate out of the system. This valve was then closed.
10. When the liquid in the separator reached half level, the downstream valves [condensate line] were partially opened to allow the

condensate to flow into the appropriate flowmeter.

11. When the separator became half full, the condensate circulating pump was turned on with its by-pass valve continuously adjusted to maintain a constant liquid level in the liquid receiver and the boiler.

12. The flow rate of building steam into the boiler coil and superheater, cooling water flow rates, condensate flow rate out of the separator and rate of condensate flow back to the boiler were all adjusted continuously until steady-state conditions were achieved.

3.5.2 Steady-State Conditions

Before assuming that steady-state conditions were achieved in any test run, the following readings must have remained unchanged for at least ½ hour:

1. Liquid levels in the separator, liquid receiver and the boiler.
2. Pressure in the boiler.
3. Pressures at inlet and outlet of the test condenser.
4. Temperatures at condenser inlet, in the separator, and inlet and outlet [cooling water] of each condensing unit.
5. Flow rate of cooling water to each condensing unit.
6. Flow rate of condensate out of the separator.
7. Observed flow regime at each visual observation section.

Typically, the system required at least 2½ hours before steady state conditions could be reached.

3.5.3 Recording of Data

After steady-state conditions were established the following readings [taken in British units and later converted to SI units] were recorded in order:

1. The boiler pressure in psig.
2. The building steam pressure in psig.
3. Test condenser inlet and outlet pressures in psig.
4. Test condenser inlet temperature in °F.
5. Condensate temperature in the separator in °F.
6. Condensate temperature upstream of the flowmeter in °F.
7. Cooling water flow rates to each unit of the test condenser in either L/min or percentage of maximum reading.
8. Cooling water temperatures upstream and downstream of the condensing units in °F.
9. Condensate flow rate in percentage of maximum reading.

In addition to the above readings, the flow regime at each visual observation section was identified and recorded by a sketch and a detailed written description. The flow regime development from the inlet to the outlet of the test condenser was sketched separately for each test run.

3.5.4 The Shut-Down Procedure

In order to shut-down the experimental facility after recording of data and flow regime observations, the following procedure was followed:

1. Building steam to the boiler and superheater was shut down.

2. When the boiler pressure dropped to near atmospheric, the flow of steam to the test condenser was stopped.

3. The condensate circulating pump was turned off.

4. The by-pass valve of the cooling-water circulating pump was turned wide open, then the pump was switched off.

3.6 Data Reduction

The data recorded during the experiments of the present investigation were reduced on a Personal Computer using FORTRAN 77 language. The computer first calculated the rates of heat gained by the cooling water and the heat lost by the steam in the test condenser. Knowing the thermodynamic state [pressure and temperature] at the inlet and outlet of the test condenser, the flow rate of the test fluid, as well as the flow rate and temperature rise of the cooling water in each heat exchanger, it was possible to perform an overall energy balance on the whole condenser. Based on these values, the percentage heat balance error was evaluated as { rate of heat lost by steam - rate of heat gained by cooling water } / { rate of heat lost by steam } x 100. Only test runs with a heat balance error within ±10% were accepted. The operating pressure in the test condenser, P_{av}, was calculated as the average of the inlet and outlet pressures. The average saturation temperature, $T_{s,av}$, was evaluated corresponding to the operating pressure, P_{av} . The operating conditions and heat balance errors for all the accepted runs are tabulated in Appendix A.

With the rate of heat transfer determined for each of the condenser units, it was possible to calculate the quality of the test steam at each of the visual sections from simple heat balances following the procedure described by Fathi (1980). Once the quality was determined, the superficial liquid and vapor velocities were calculated at each visual section. All fluid properties needed in these calculations were determined at the operating pressure P_{av}. A list of the observed flow regimes, as well as the corresponding qualities, mass fluxes, and mean saturation temperatures is given in Appendix B.

Chapter 4

EXPERIMENTAL RESULTS AND DISCUSSION

4.1 Test Range and Experimental Uncertainty

The range of operating conditions for each of the seven data sets is given in Table 4.1. An attempt was made to keep the number of flow-regime classifications to a minimum. Four flow regimes were identified in this study. The descriptions used in classifying these regimes [listed below for completeness] are consistent with previous gas-liquid and condensation studies [see Figure 2.2].

Annular Flow: A stable liquid film covered the entire tube wall, while the vapor flowed in the core. Part of the liquid phase was entrained by the vapor. Asymmetry was apparent in the liquid film with the maximum thickness being at the bottom of the tube.

Annular-Wavy Flow: The flow had annular appearance with a thin continuous film covering the top part of the tube; however, the thickness of liquid film increased at the bottom forming a thick stratum. A crucial feature of this classification is that the liquid height at the bottom had to exceed one quarter of the tube radius.

Wavy Flow: The two phases were separated with the liquid flowing at the bottom of the tube. Waves of different length and amplitude appeared at the vapor-liquid interface.

Slug Flow: The flow is basically wavy; however, surface waves grew frequently forming slugs wetting the upper tube wall. These slugs were pushed downstream by the vapor at a velocity much higher than the mean velocity of the remaining liquid. Frequency

Table 4.1 Range of operating conditions

Data Set	Inclination Angle	Mass Flux, G ($kg/m^2.s$)	System Pressure, P_{av} (kPa)	Saturation Temp., $T_{s,av}$ (°C)	Superficial Vapor Velocity, V_{GS} (m/s)	Superficial Liquid Velocity, V_{LS} (m/s)
1	0 (horizontal)	21.9 - 273	99.9 - 182	99.6 - 117	0.10 - 200	0.018 - 0.29
2	1°(upward)	25.4 - 240	102 - 160	100 - 113	0.60 - 178	0.02 - 0.25
3	5°	22.4 - 277	102 - 165	100 - 114	0.17 - 200	0.02 - 0.28
4	10°	47.1 - 262	106 - 168	101 - 115	0.37 - 184	0.02 - 0.27
5	- 1°(downward)	32.9 - 223	102 - 154	100 - 112	0.10 - 185	0.02 - 0.23
6	- 5°	39.2 - 242	103 - 156	100 - 113	0.29 - 185	0.02 - 0.25
7	-10°	32.5 - 207	108 - 154	102 - 112	0.70 - 160	0.02 - 0.21

of formation for these slugs depended on flow conditions.

In the present study, flow-regime identification was mostly based on visual observations using the above descriptions. The distinguishing features among the annular, wavy, and slug flow regimes are so clearly identifiable that objective classification was possible without difficulty. On the other hand, the distinction between annular and annular-wavy was often hard to make with just visual observation. In these cases, an electronic stroboscope was used to visually slow down the flow and allow for a more confident classification. Visual observation is the most commonly used method of flow-regime identification [e.g., Traviss and Rohsenow, 1973; Barnea et al., 1982; Tandon et al., 1983; Crawford et al., 1985; Barnea et al., 1985; Mukherjee and Brill, 1985].

A total of 395 test runs were performed in this investigation, out of which 90% of the test runs had heat balance errors within ±5% and the remaining 10% of the test runs had heat balance errors within ±8%. The flow regime data [total of 1139 points] obtained in this investigation will be presented in the form of flow regime maps using the superficial velocities V_{LS} and V_{GS} as coordinates. The superficial velocities were calculated using,

$$V_{LS} = G(1 - x)/\rho_L , \tag{4.1}$$

and

$$V_{GS} = Gx/\rho_G . \tag{4.2}$$

Uncertainty estimates in the calculated values of V_{LS} and V_{GS} were determined for all data points using the method described by Moffat (1988) based on 95% confidence levels, or 20/1 odds. For all data points, the uncertainty in V_{LS} was estimated to lie within ±5.3%. A major portion of the data [855 points, or 75.1%] corresponds to $V_{GS} \geq 20$ m/s. Out of this portion, 66.2% of the data points have uncertainties in V_{GS} within ±5% and 32.2% have uncertainties in V_{GS} outside ±5% but within ±10%. For the remaining data [284 points, or 24.9%] corresponding to the low velocity range $V_{GS} < 20$ m/s, uncertainty in V_{GS} is generally outside ±10%. However, the magnitudes of estimated errors in V_{GS} have an average value of ±2.1 m/s and never exceed ±2.8 m/s. The details of the uncertainty estimates are given in Appendix C. The inclination angle of the test section was measured as described in Chapter 3 using a surveying level. The uncertainty in measuring this angle is estimated to be within ±0.03°.

4.2 Flow Condition at the Condenser Exit

Complete condensation was always achieved in the test section before discharging the flow into the separation tank where liquid and vapor existed with a stable interface. For the horizontal orientation and the three upward inclinations of +1°, +5°, and +10°, the condenser tube was always running full at the end of the condensation path. On the other hand, the full-tube condition was achieved only beyond certain flow rates with the downward inclinations even though complete condensation was achieved at all flow rates. For example, at 1° downward inclination [Figure 4.1], the discharging flow was stratified for all mass fluxes G < 58 kg/m^2 . s [corresponding to terminal velocities at the end of the condensation path of $V_{LS} < 0.052$ m/s], and the tube ran full only for G > 58 kg/m^2. s. In

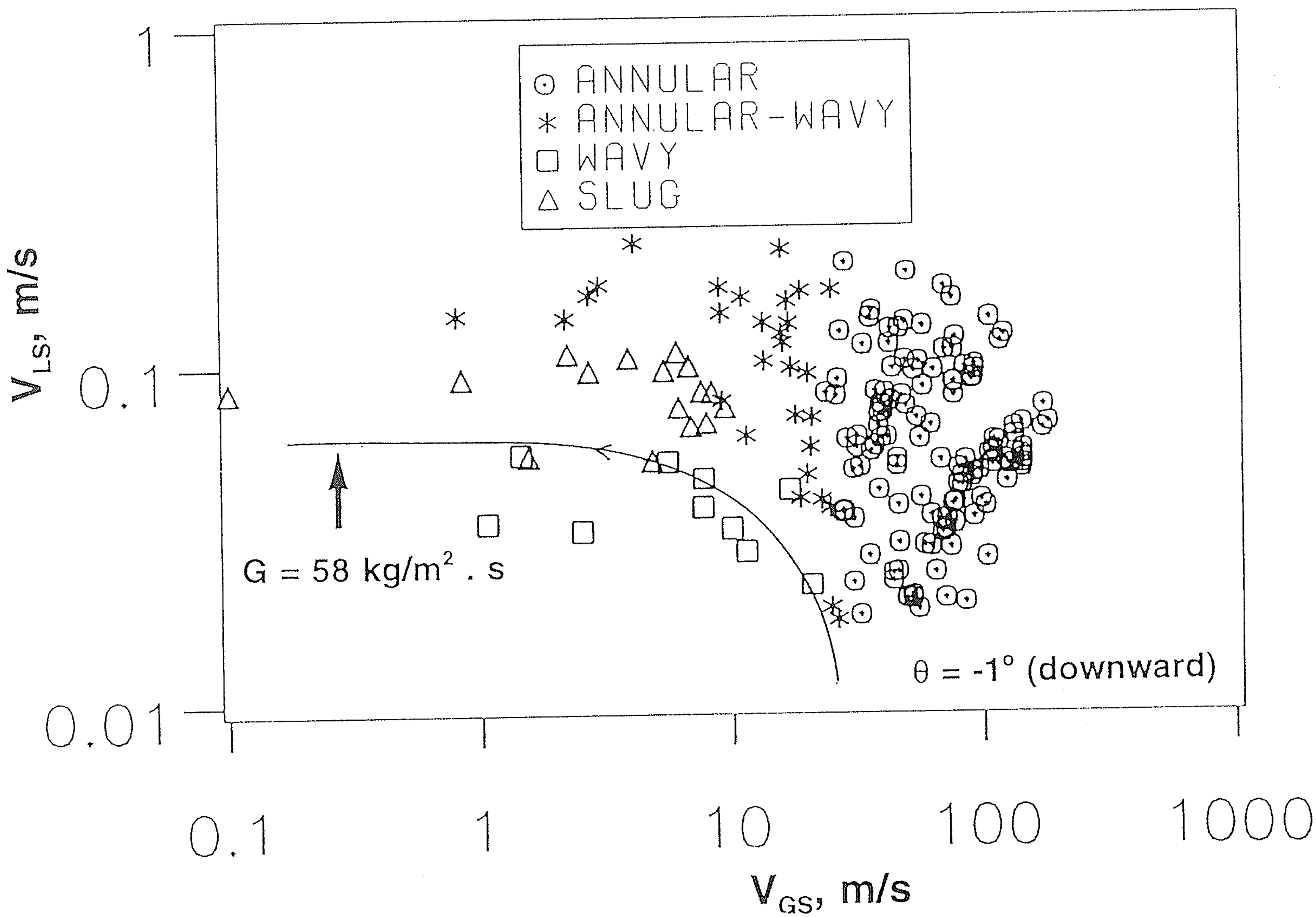

Figure 4.1 The stratified/full tube boundary for $\theta = -1°$ [downward] inclination.

the present experiment, the exit condition of stratified or full-tube was found to be independent of the rate of cooling and dependent only on the discharge flow rate [Wallis et al., 1977]. The boundary between stratified and full-tube condition shifted to higher mass flow rates as the inclination angle increased; in -5° [downward] inclination the stratified boundary coincides approximately with G = 128 kg/m^2. s, whereas in -10° [downward] inclination the stratified boundary shifts to approximately G = 151 kg/m^2. s. The tube condition at exit was found to be a major factor in determining whether or not slugging would occur, as discussed in the following section.

4.3 Effect of Inclination on the Flow-Regime Boundaries

The present results for the seven data sets are shown in Figures 4.2 - 4.8. For the horizontal orientation, Figure 4.2 shows that the wavy flow regime is limited to a small bell-shaped area. For small mass fluxes of $G < 65$ kg/m^2. s [corresponding to terminal velocities at the end of the condensation path of $V_{LS} < 0.058$ m/s], the flow regime progresses from annular to annular-wavy to wavy to slug before complete condensation with a full tube is achieved. With intermediate mass fluxes within $65 < G < 157$ kg/m^2. s [corresponding to terminal velocities within $0.058 < V_{LS} < 0.14$ m/s], wavy flow was not observed and the flow regime progressed from annular to annular-wavy to slug followed by complete condensation. Interestingly, slug flow was not observed in test runs with high mass flow rates corresponding to terminal velocities $V_{LS} > 0.14$ m/s. Consistent with the observation by Rashwan and Soliman (1987), the occurrence of slugging in the present experiment always coincided with the full-tube condition at the end of the condensation

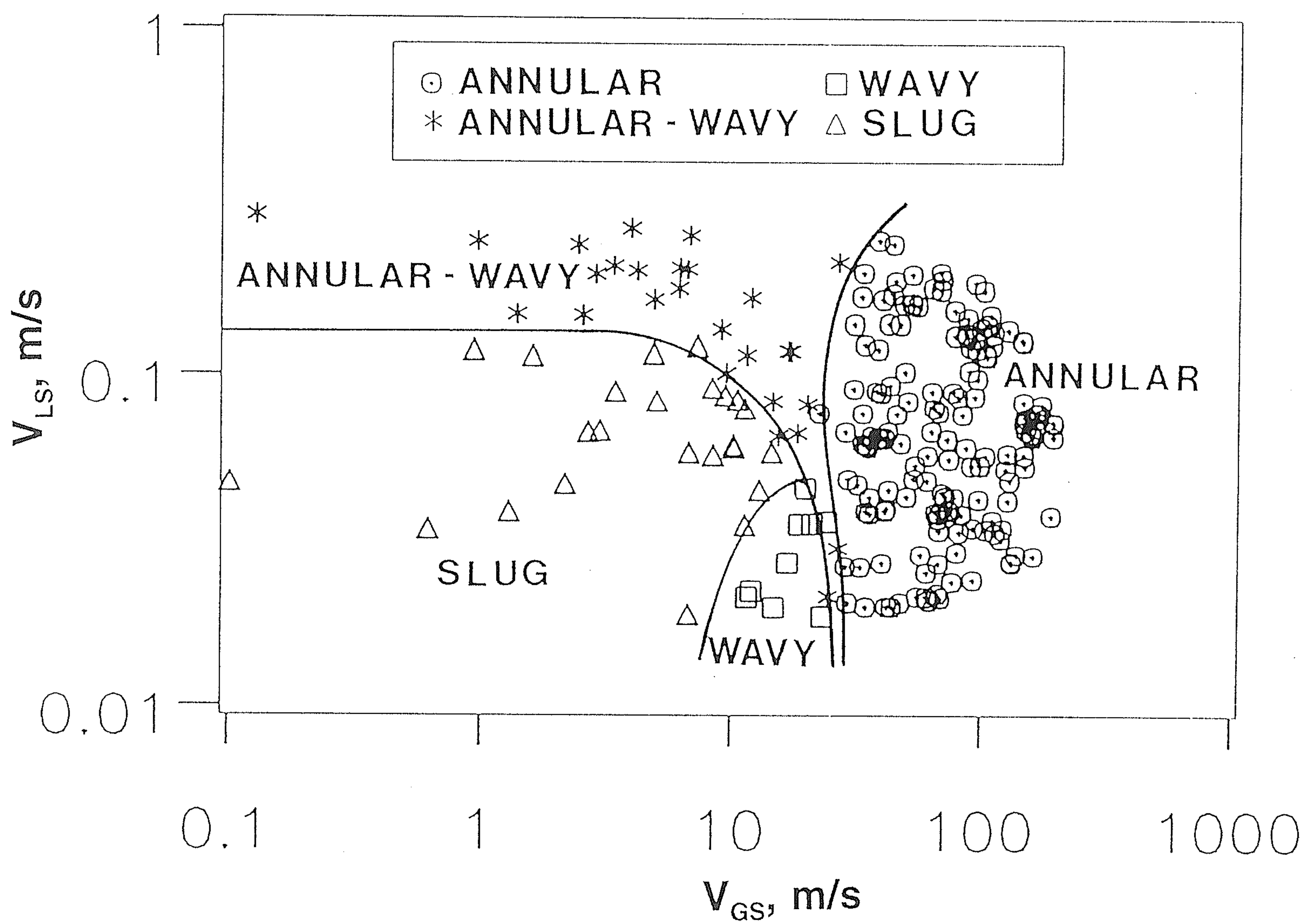

Figure 4.2 Flow regime data for the horizontal orientation.

path. The upper limit [$V_{LS} \approx 0.14$ m/s] for slug initiation will be considered analytically in a later section.

The most significant effect of inclination observed during this experiment was on the wavy and slug flow regime boundaries. The bell-shaped wavy flow region, observed in the horizontal position [Figure 4.2], disappears completely in the 1° upward inclination [Figure 4.3]. Higher angles of inclination [5° and 10°] produced small changes in the transition lines, as shown in Figures 4.4 and 4.5. The tube was always running full at the end of the condensation path for all test runs with upward inclination of 1° or higher. This coincided with the occurrence of slugging in all test runs with terminal velocities below the upper limit of $V_{LS} \approx 0.14$ m/s. It is interesting to note that this upper limit for slug initiation appears to be independent of inclination for angles below 10°.

In downward inclination, however, the area occupied by wavy flow expands at the expense of the slug flow area. Figure 4.6 shows the results for -1° [downward] inclination. In this case, the tube was running full at the end of the condensation path only for test runs corresponding to terminal velocities $V_{LS} > 0.052$ m/s. The slug flow for this inclination appears to be limited to flow rates with terminal velocities within the range $0.052 < V_{LS} < 0.14$ m/s. For $V_{LS} < 0.052$ m/s, the tube did not run full at exit and the condensation path terminated with wavy [or stratified] flow. With further increase in downward inclination to 5° and 10°, Figures 4.7 and 4.8, respectively, show that slug flow disappears completely and its zone is now occupied by wavy flow. At these inclinations, the tube started running full at exit only with flow rates corresponding to terminal velocities $V_{LS} > 0.14$ m/s. Figures 4.7 and 4.8 also show that the shift in the transition lines is

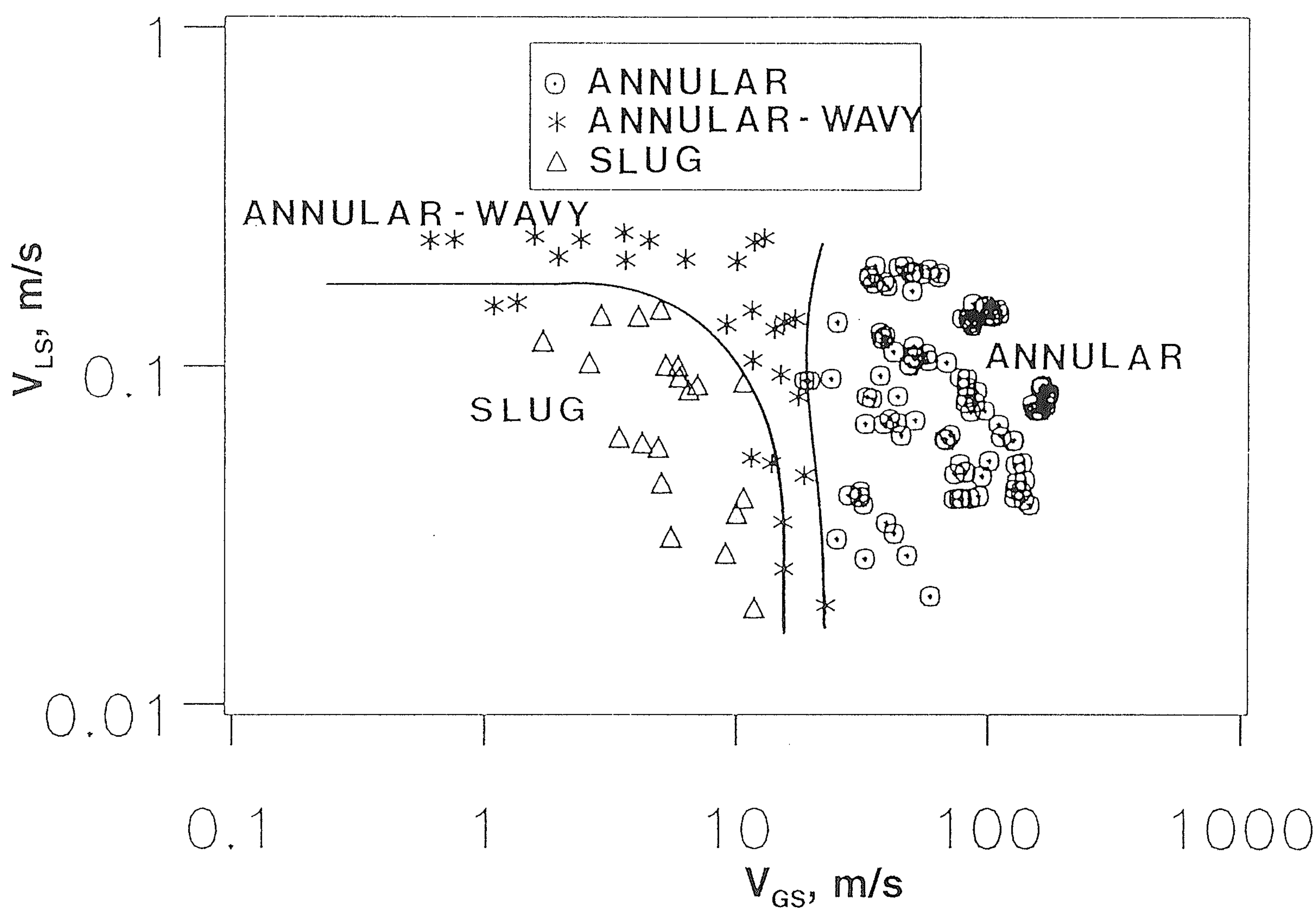

Figure 4.3 Flow regime data for +1° [upward] inclination.

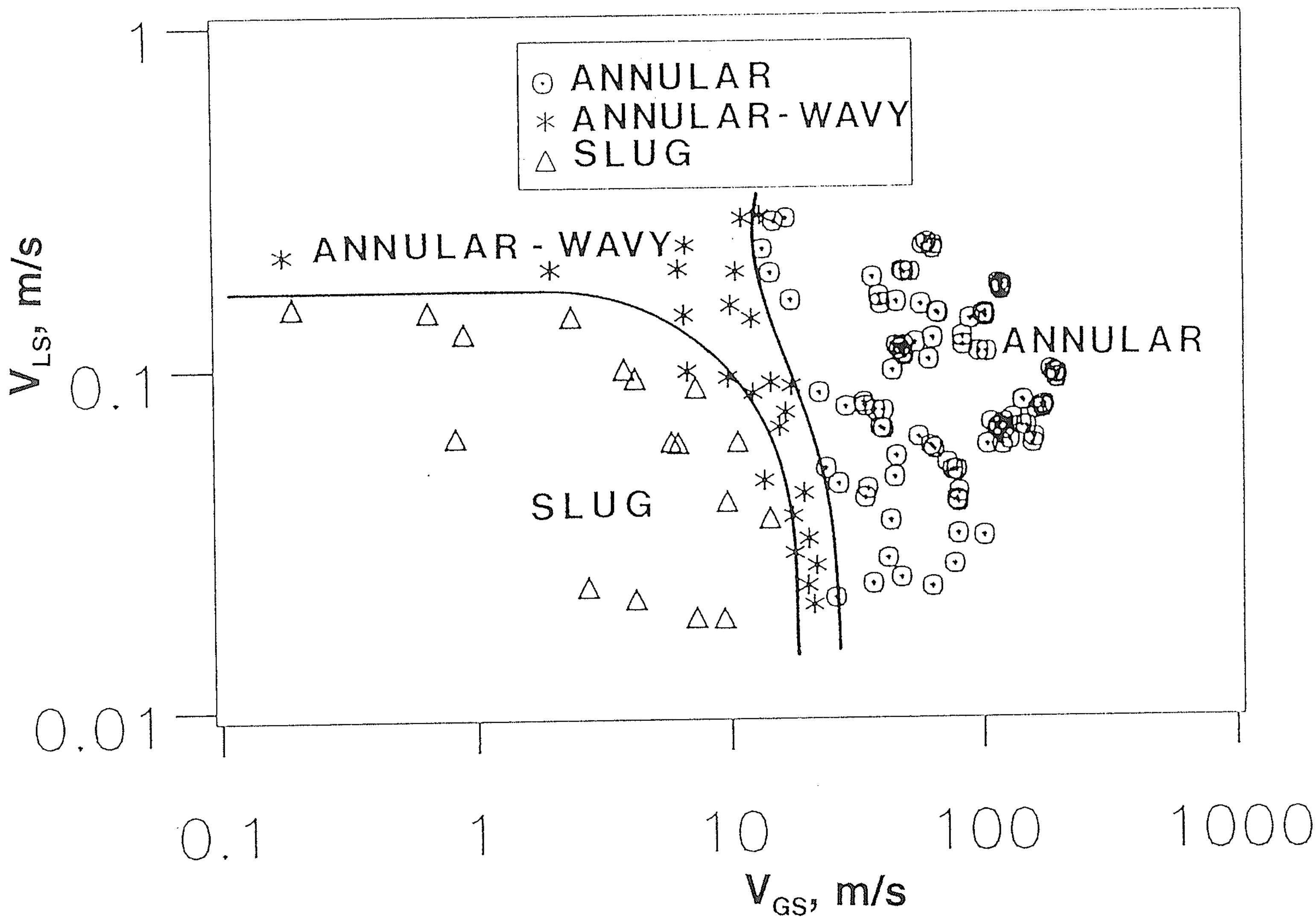

Figure 4.4 Flow regime data for +5° [upward] inclination.

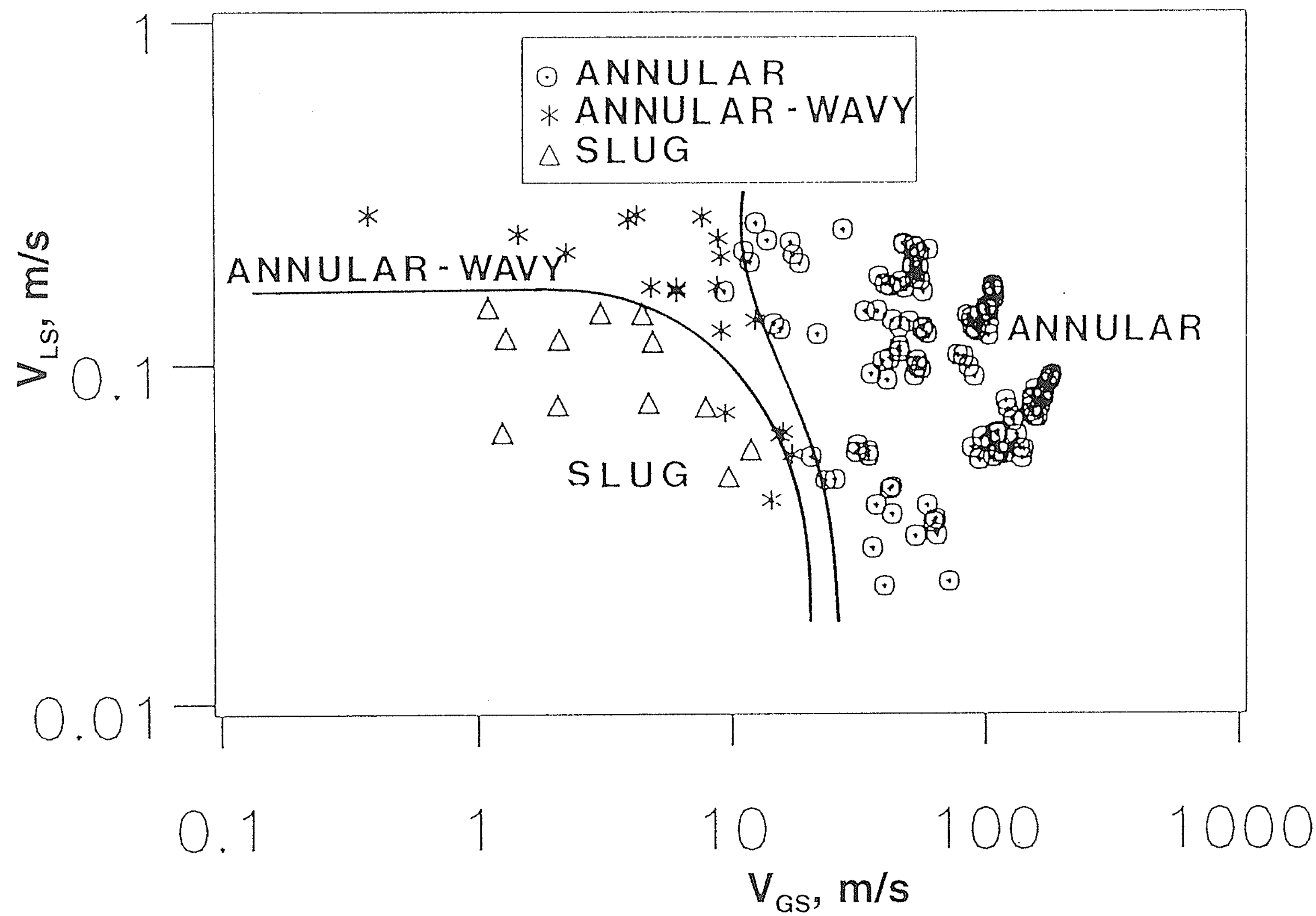

Figure 4.5 Flow regime data for +10° [upward] inclination.

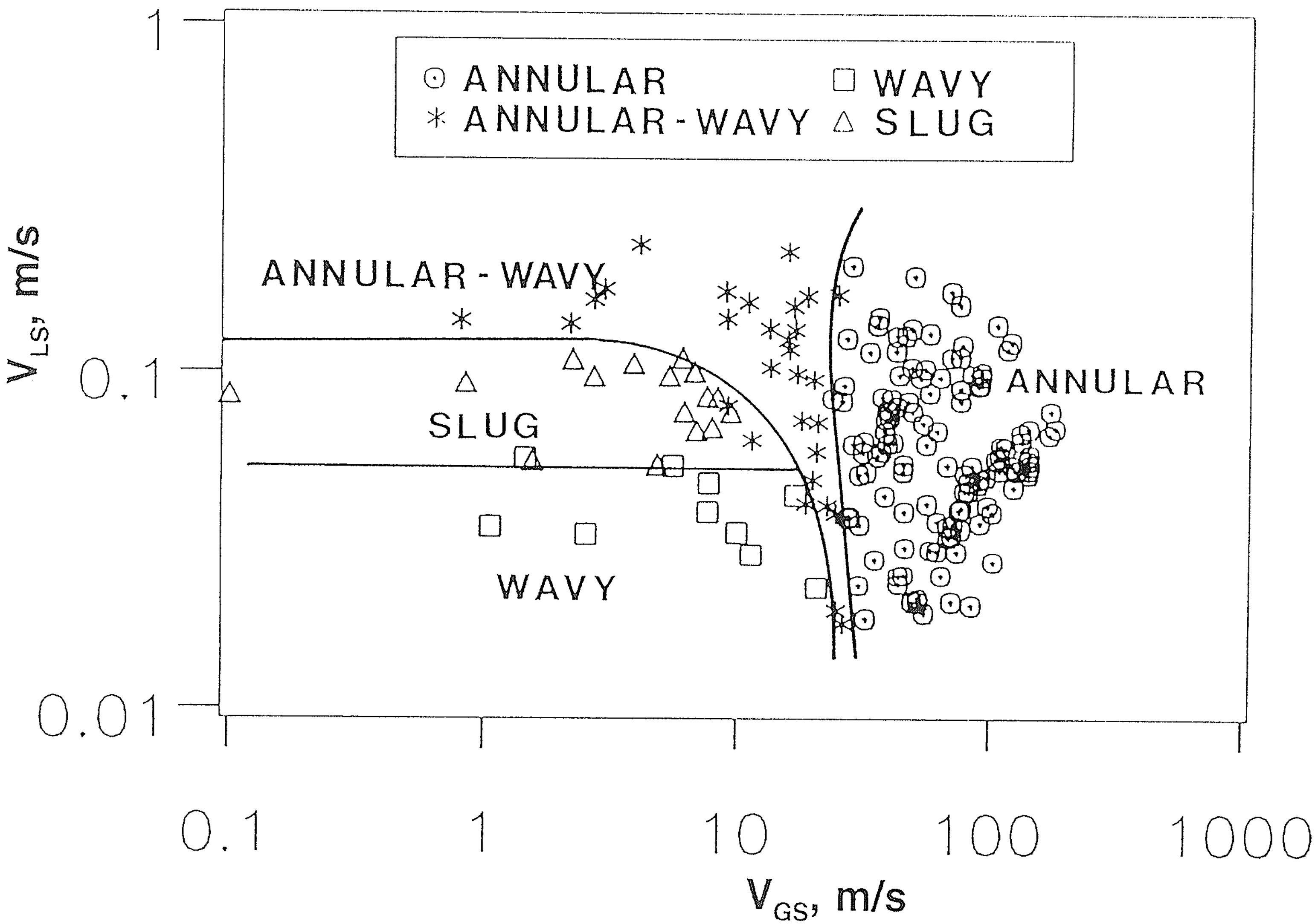

Figure 4.6 Flow regime data for −1° [downward] inclination.

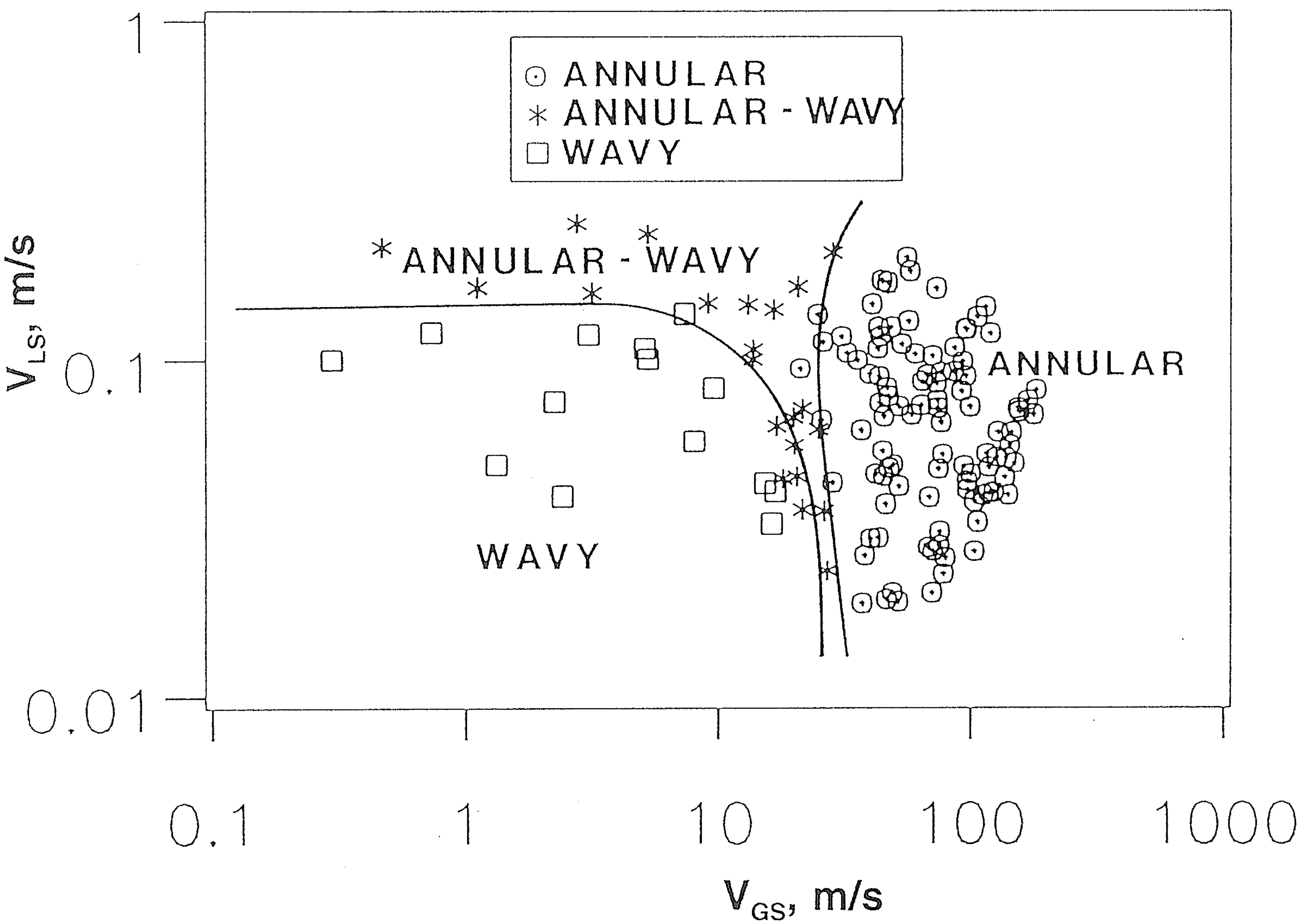

Figure 4.7 Flow regime data for –5° [downward] inclination.

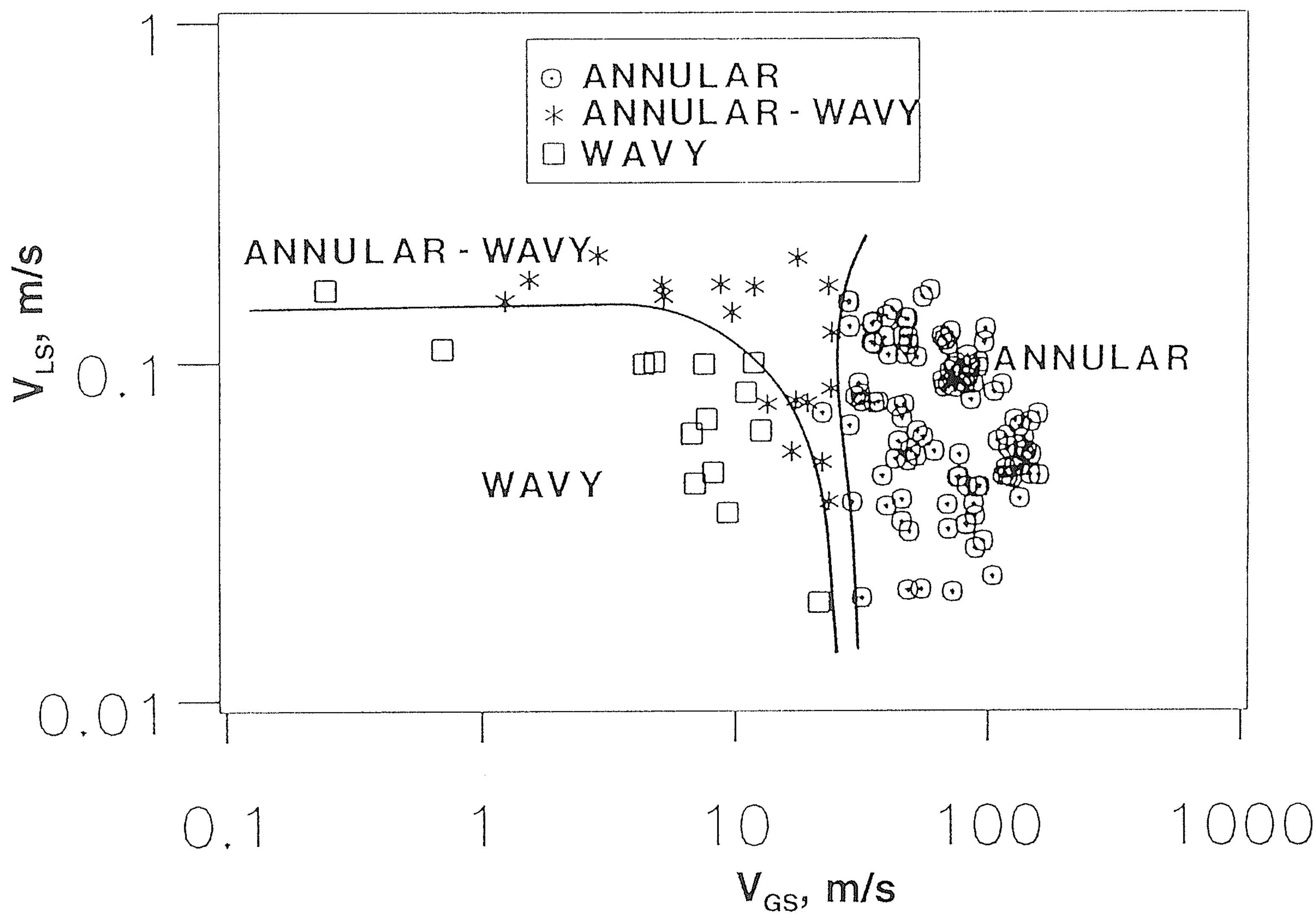

Figure 4.8 Flow regime data for –10° [downward] inclination.

insignificant as the downward inclination angle changes from 5° to 10°.

The influence of inclination [within ±10°] on the annular flow regime boundary is much less pronounced than the influence on the wavy and slug areas. The three downward inclinations considered in this investigation produced insignificant effects on this boundary [Figure 4.9]. For upward inclinations, there appears to be a slight shift in the annular flow boundary towards lower vapor velocities, particularly in the region of high liquid velocities [Figure 4.10].

Another interesting feature of the results in Figures 4.2 - 4.8 is that for $V_{LS} > 0.14$ m/s; i.e., high total mass flow rates, the flow regime is annular-wavy near the end of the condensation path and this regime exists down to V_{GS} of about 1 m/s. By contrast, significantly higher values of V_{GS} are normally required in gas-liquid flows in order to support a liquid film at the wall. Two observations can be made in order to explain this difference between the two flow situations. First, in condensing flows, liquid is naturally formed on the tube wall which is not the case in adiabatic gas-liquid flows. Secondly, at the high flow rates corresponding to $V_{LS} > 0.14$ m/s, the heat-transfer coefficient and the rate of condensation are high, thus contributing to an increased rate of liquid formation on the tube wall and a stable annular-wavy flow regime.

4.4 Estimate of the Upper Bound for the Slug Region

A flow mechanism has been developed by Rashwan and Soliman (1987) for the onset of slugging in horizontal condensers. As illustrated in Figure 4.11, slugging was proposed to be initiated by a hydraulic jump as the two-phase mixture changes from

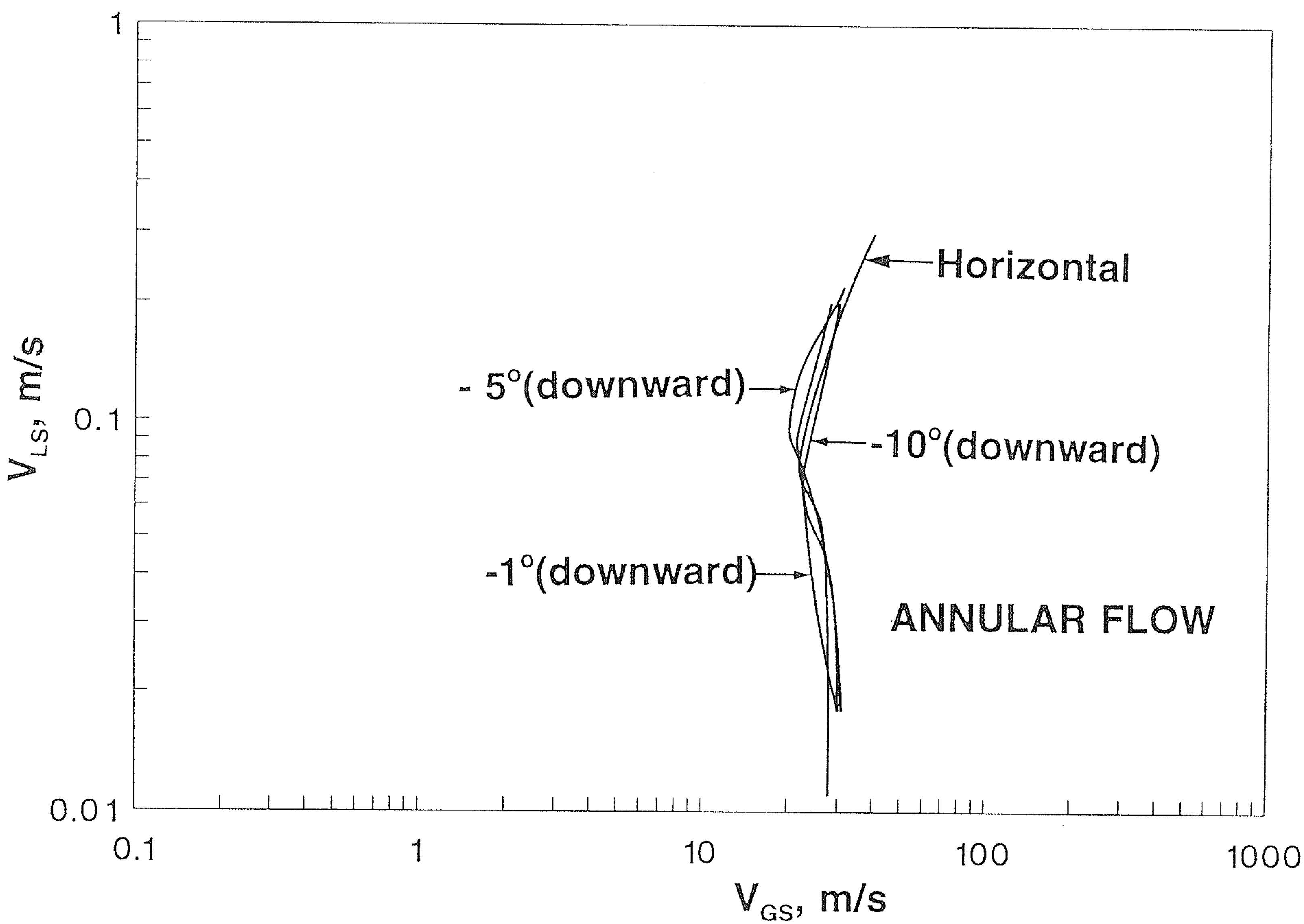

Figure 4.9 Effect of the downward inclination on the annular flow boundary.

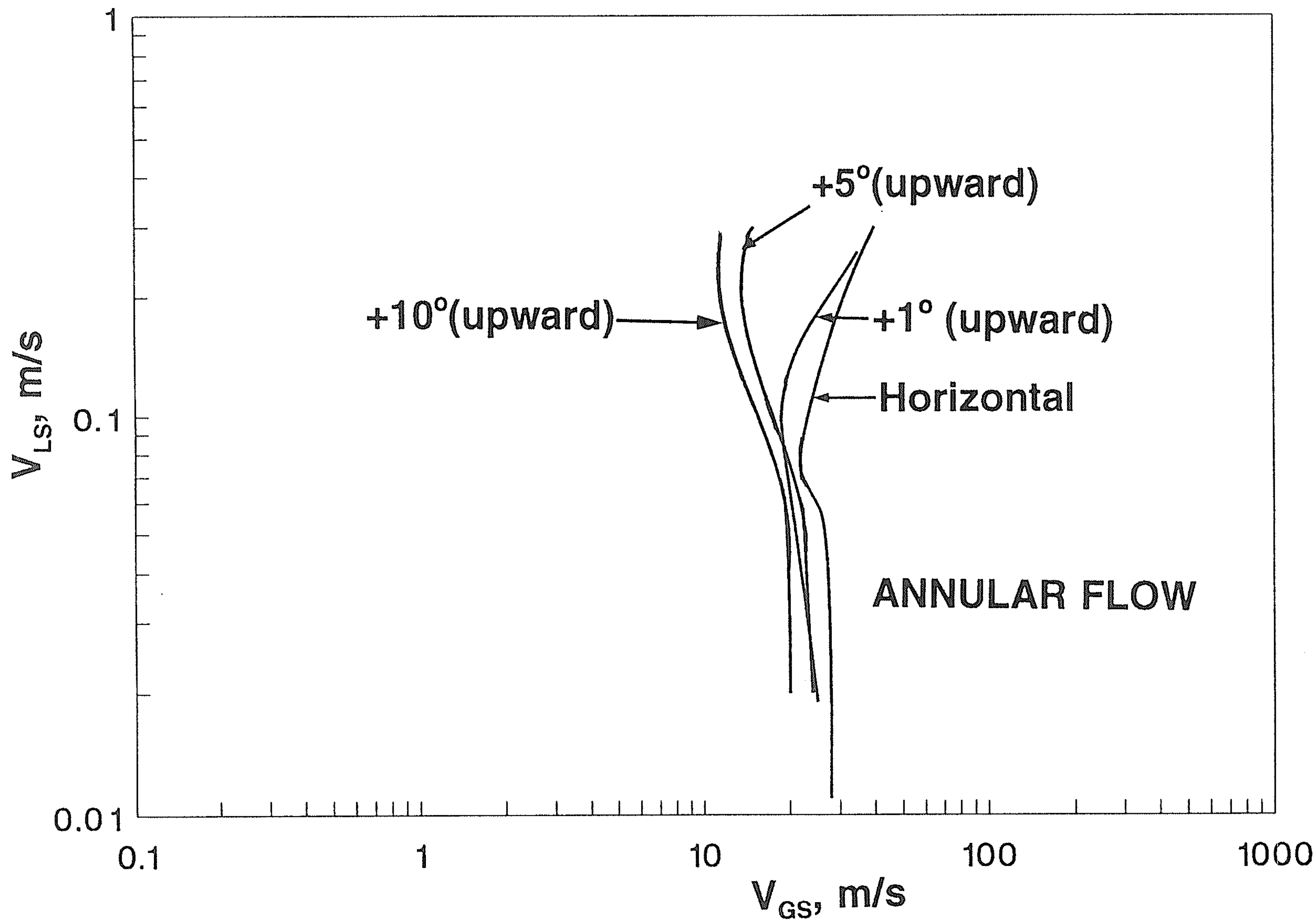

Figure 4.10 Effect of upward inclination on the annular flow boundary.

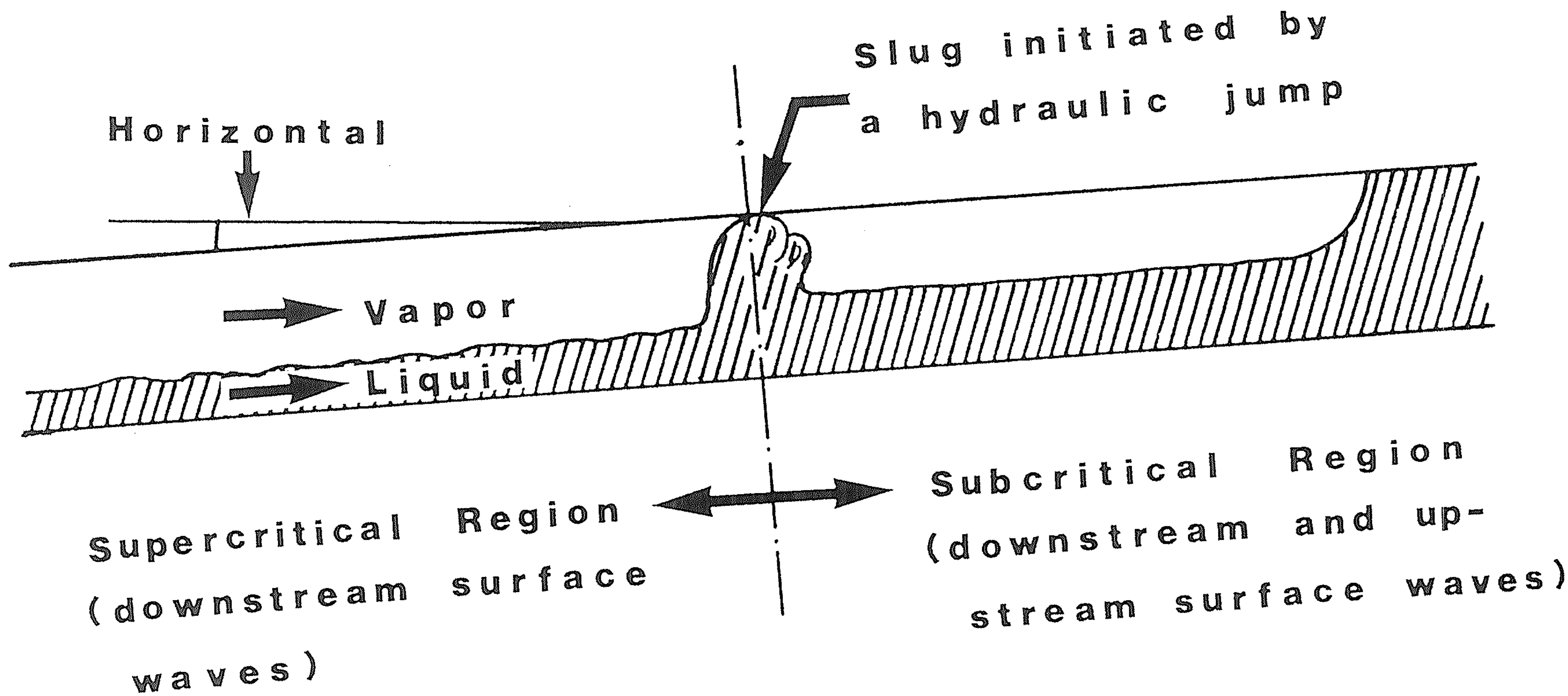

Figure 4.11 Slug initiation in an upwardly inclined condenser tube.

supercritical to subcritical flow due to condensation. A mathematical model based on this criterion for slug initiation succeeded in predicting the wavy-slug transition for a large segment of the available data.

Starting from the above criterion by Rashwan and Soliman (1987), the objective here is to develop a simple analytical correlation for the upper bound of the slug flow region during condensation. It is proposed that this upper bound coincides with the condition where the flow rate is high enough to prevent the transition into subcritical flow. Therefore, at this bound, the two-phase flow would be supercritical throughout the condenser and it only becomes critical at the end of the condensation path. The criticality criterion, which is also the condition for no upstream propagation of surface waves, has been commonly developed as [e.g., Wallis, 1969]

$$\frac{j_G^{*2}}{\alpha^3} + \frac{j_L^{*2}}{(1-\alpha)^3} = 1 \tag{4.3}$$

where,

$$j_G^* = V_{GS}\,[\rho_G/\{gD\,(\rho_L - \rho_G)\}]^{0.5}\ , \tag{4.4}$$

$$j_L^* = V_{LS}\,[\rho_L/\{gD\,(\rho_L - \rho_G)\}]^{0.5}\ , \tag{4.5}$$

and α is the void fraction.

At the end of the condensation path, the liquid is flowing under a stagnant vapor bubble and therefore, $V_{GS} = j^*_G = 0$. Substituting into Equation (4.3) results in

$$V_{LS} = [gD\,(1-\alpha)^3(1-\rho_G/\rho_L)]^{0.5} \tag{4.6}$$

The motion of large bubbles through stationary liquids in horizontal ducts has been investigated by Benjamin (1968) assuming negligible viscous and surface tension effects. For the two-dimensional case of flow between two parallel plates, Benjamin (1968) predicted $\alpha = 0.5$ far downstream of the bubble nose for the flow to be steady and free from energy dissipation. For the three-dimensional problem of liquid emptying from a horizontal tube, Benjamin (1968) obtained $\alpha = 0.42$. There are obvious similarities between the flow at the end of the condensation path, where liquid is flowing under a stationary bubble, and Benjamin's problem, where bubbles were flowing through a stationary liquid. As well, the liquid height in horizontal and slightly inclined tubes necessary for the slug formation was discussed by Taitel and Dukler (1976). They argued that slug flow will develop only when the liquid level is at or above the pipe centreline; i.e., $\alpha \leq 0.5$ and they used a constant value of $\alpha = 0.5$ at the annular-slug boundary.

It seems from the above discussion that a reasonable estimate of α in Equation (4.6) is somewhere between 0.42 and 0.5. Using these limits with steam-water at an average saturation temperature of 100°C [$\rho_G = 0.82$ kg/m^3 and $\rho_L = 951$ kg/m^3] and the present tube diameter D = 0.0134 m, Equation (4.6) produces $V_{LS} = 0.128$ m/s at $\alpha = 0.5$ and $V_{LS} = 0.16$ m/s at $\alpha = 0.42$. These values form a narrow band around $V_{LS} = 0.14$ m/s, which was obtained experimentally at this flow-regime boundary.

4.5 Comparisons with Gas-Liquid Correlations

Many of the trends discussed above for condensing flows, such as the prominence of slug flow in upward inclinations, the prominence of wavy flow in downward inclinations and the relative insensitivity of the annular flow boundary to small inclinations, are consistent with the trends reported for adiabatic gas-liquid flows. The objective of this section is to perform quantitative comparisons between the present data and some of the available gas-liquid flow regime maps [empirical and theoretical]. Perfect agreements should not be expected from these comparisons. However, this effort can illustrate the relationship, if any, between the flow-regime boundaries of the two types of flow, which may guide future studies in this area.

A comparison between the present data for horizontal flow and the horizontal, adiabatic, gas-liquid flow-regime map proposed by Mandhane et al. (1974) is shown in Figure 4.12. The necessary property corrections, as recommended by Mandhane et al., were applied to the boundaries. Reasonable agreement can be seen in the annular flow region. However, an obvious discrepancy appears in the slug flow region where the majority of these data points fall in the stratified and wavy areas of the map.

The varying liquid height along a horizontal condenser can influence the onset of slugging in ways similar to providing a very small upward inclination to a tube carrying a gas-liquid mixture. In order to test this hypothesis, the horizontal flow data are compared in Figure 4.13 with the theoretical map for a tube with +1° [upward] inclination proposed by Taitel and Dukler (1976). The theoretical boundaries shown in Figure 4.13 correspond to fluid properties of a saturated steam-water mixture at 110°C and a tube diameter of 13.4 mm. Even though the present data do not fall exactly in the same areas predicted by Taitel and Dukler (1976), the similarity in trend is obvious with the wavy flow limited to a small, bell-shaped area and the prominence of slug flow at low superficial vapor

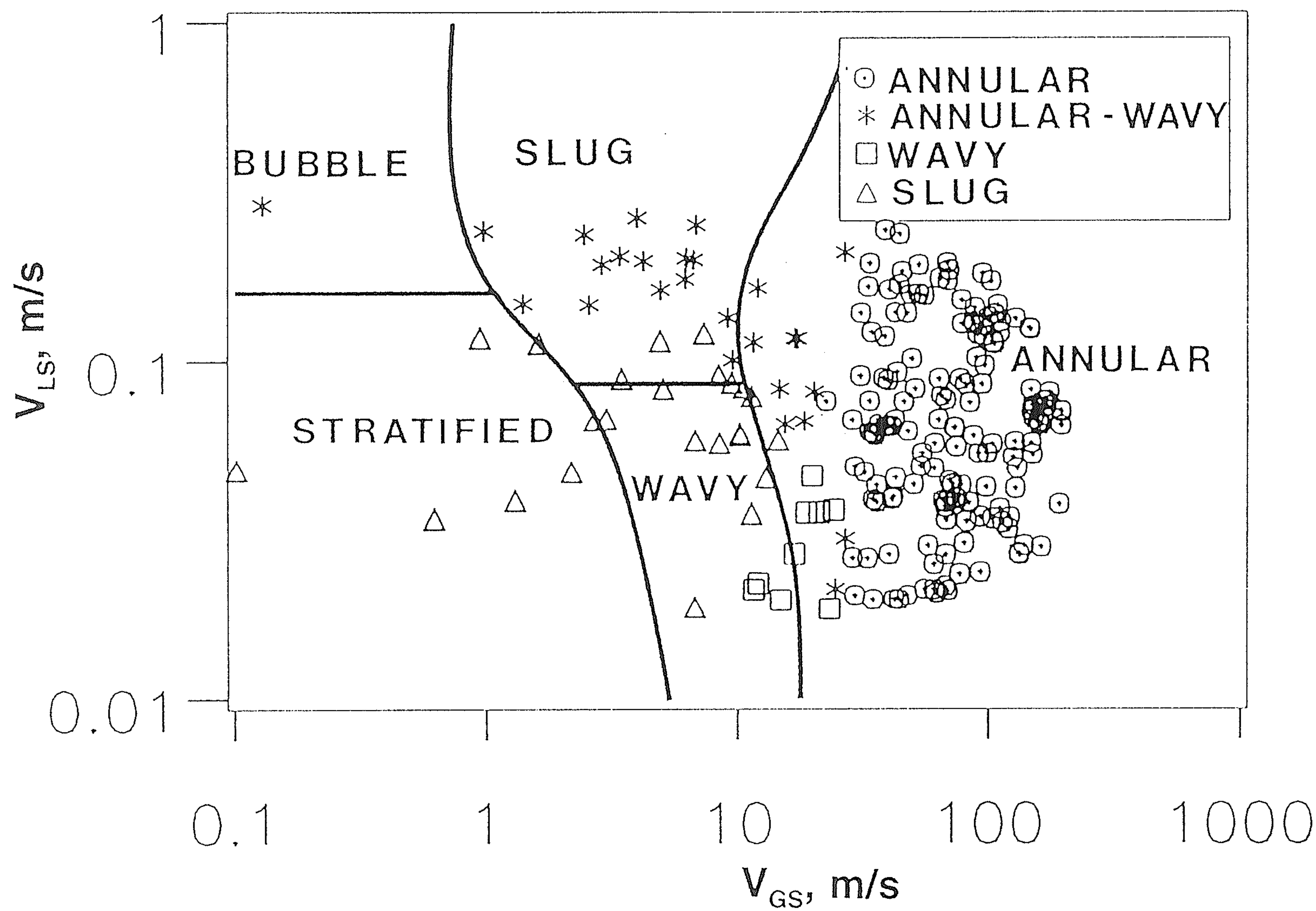

Figure 4.12 Comparison between the present data for horizontal flow and the map of Mandhane *et al.* (1974).

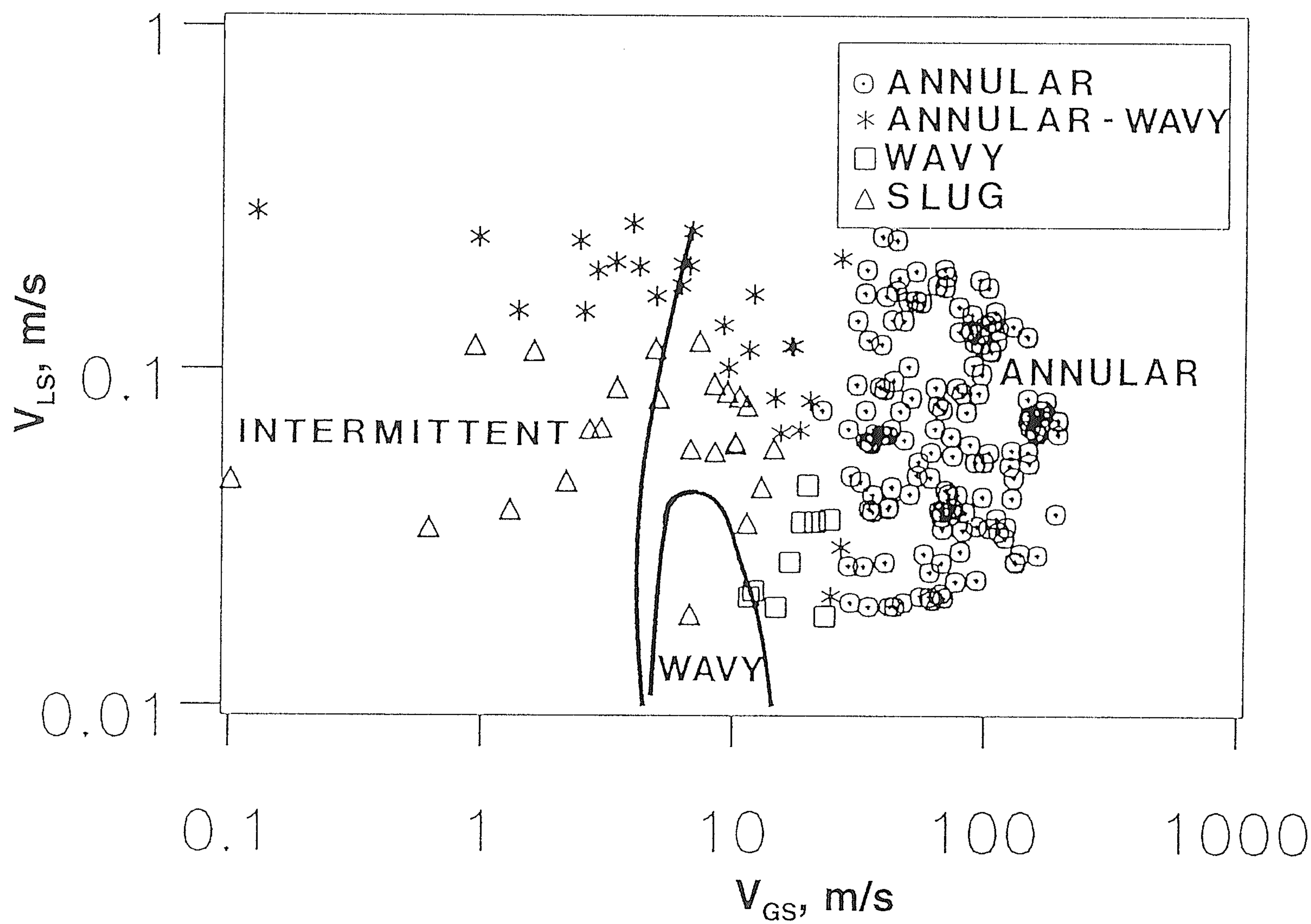

Figure 4.13 Comparison between the present data for horizontal flow and the map of Taitel and Dukler (1976) for +1° [upward] inclination.

velocities. As a further test of this hypothesis, a comparison was made between the present data of -1° [downward] inclination and the empirical map of Mandhane et al. (1974) for horizontal, gas-liquid flow. This comparison, given in Figure 4.14, shows a much better fit in the wavy and slug regions than the one seen earlier in Figure 4.12. The slug flow data in Figure 4.14 fall above the wavy flow data, as the map stipulates, although the exact transition between the two regimes is not exactly predicted. A closer agreement may be possible with data corresponding to a slightly higher downward inclination.

For the larger inclinations of ±5° and ±10°, comparisons are made in Figure 4.15 for upward flow and Figure 4.16 for downward flow between the present data and the predictions of Taitel and Dukler (1976). The transition lines in Figures 4.15 and 4.16 correspond to steam-water flow at 110°C in a 13.4 mm tube. According to the present data, the annular to slug transition in upward flows and the annular-to-wavy transition in downward flows do not shift significantly as the inclination angle changes from 5° to 10°. The predictions by Taitel and Dukler (1976), plotted for both angles in Figures 4.15 and 4.16, also show small shifts in both boundaries. As well, good agreement between data and predictions can be seen in both figures suggesting that gas-liquid correlations may apply satisfactorily for condensation with larger inclinations such as 5° and 10°. However, according to the previous comparisons, care must be exercised for smaller inclinations where, there appears to be a need for theoretical flow-regime correlations specific to condensing flows.

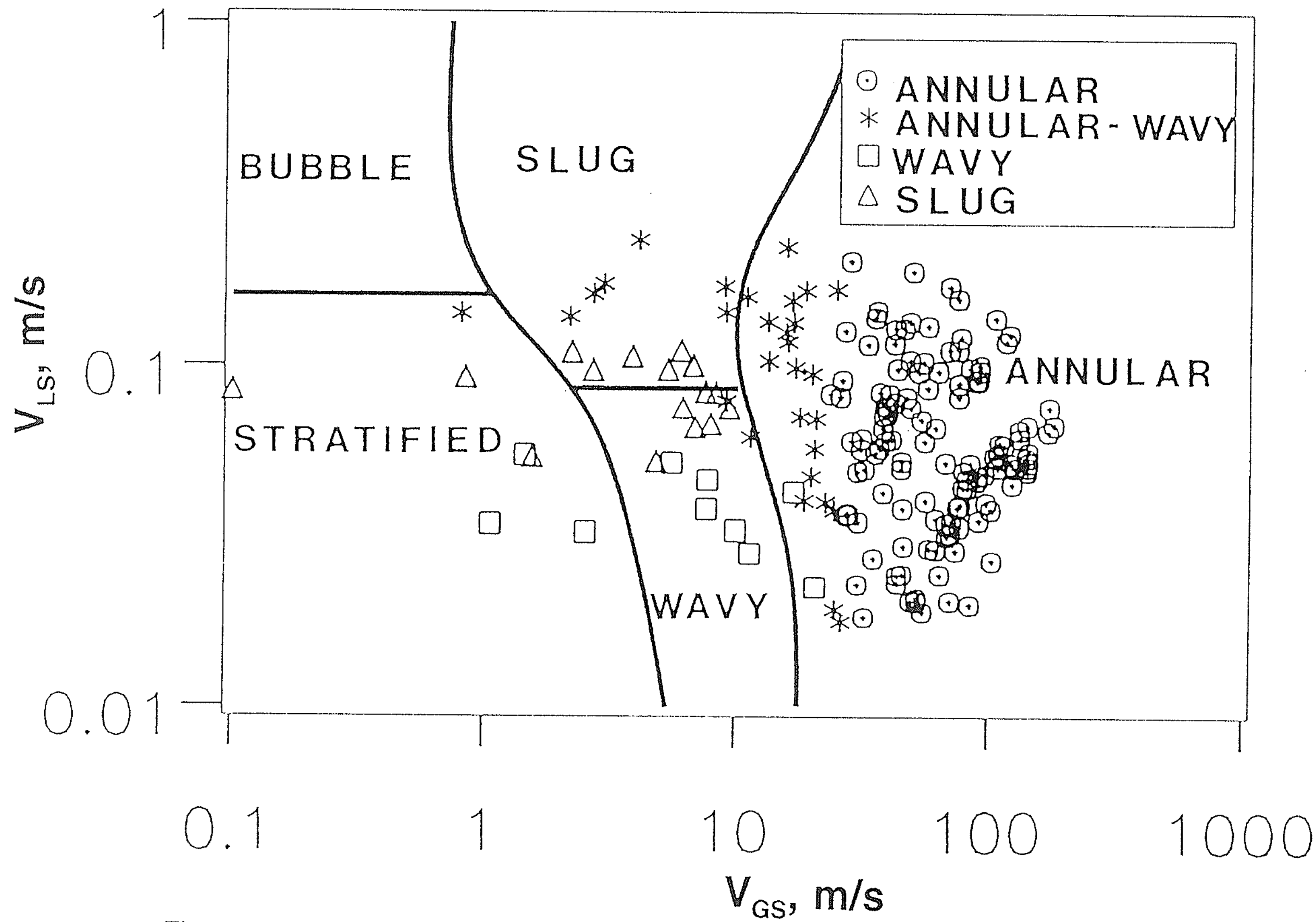

Figure 4.14 Comparison between the present data for −1° [downward] inclination and the map of Mandhane *et al.* (1976).

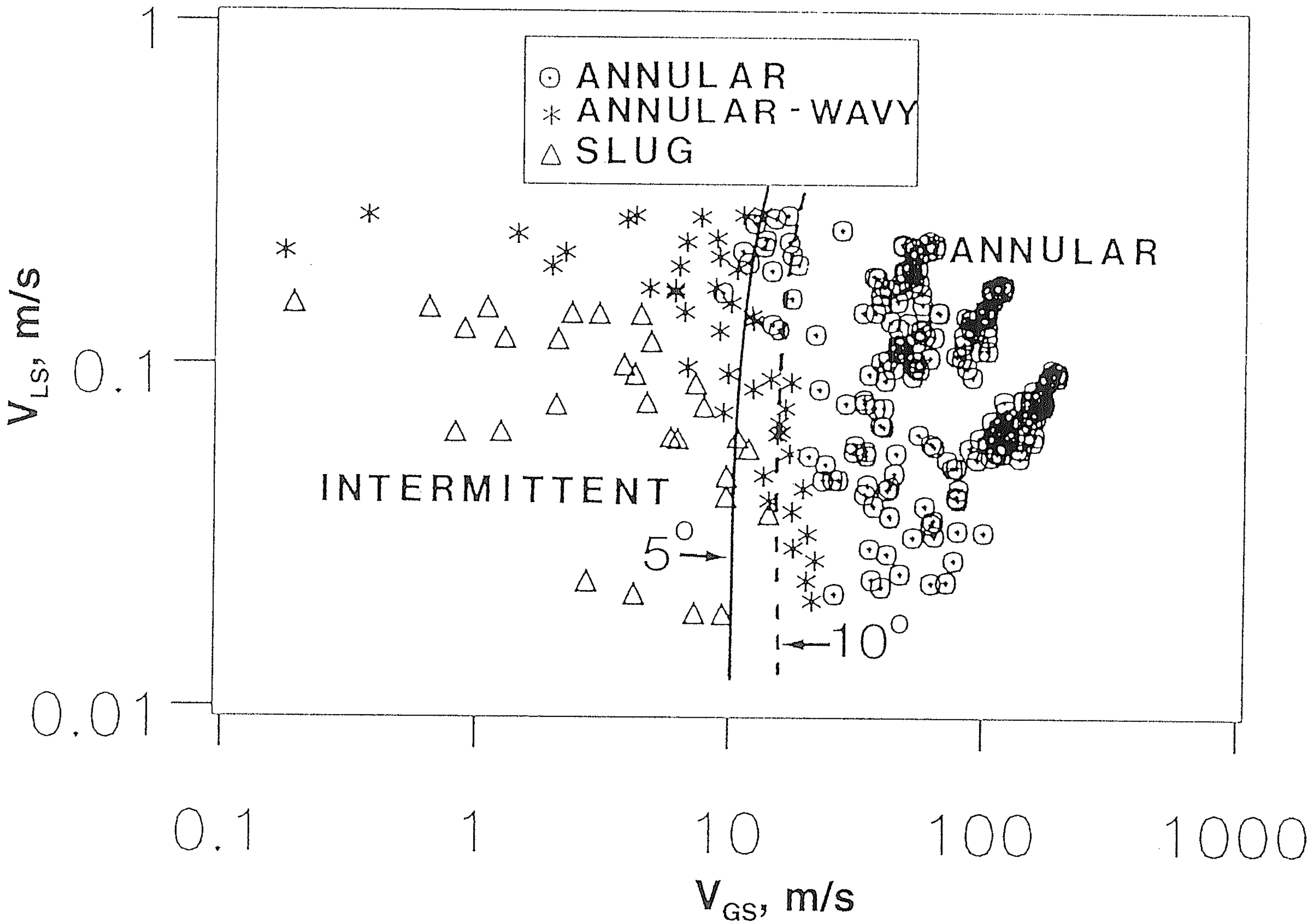

Figure 4.15 Comparison between the present data for +5° and +10° [upward] inclination with the map of Taitel and Dukler (1976).

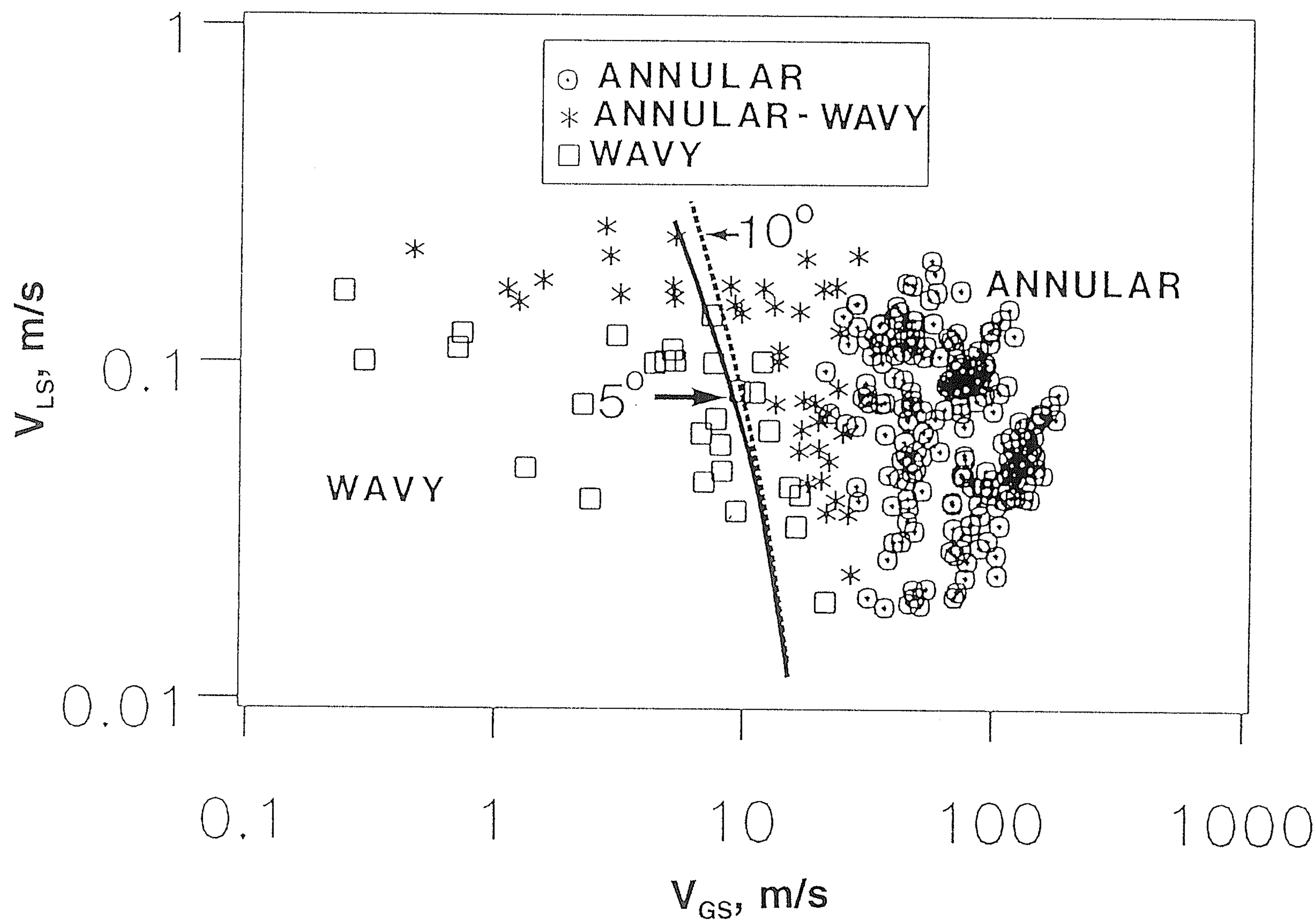

Figure 4.16 Comparison between the present data for $-5°$ and $-10°$ [downward] inclination with the map of Taitel and Dukler(1976).

Chapter 5

THEORETICAL ANALYSIS OF THE STRATIFIED-NONSTRATIFIED TRANSITIONAL BOUNDARY

The objective of this theoretical analysis is to develop a physically-based, generalized, theoretical model for the transition boundary between the stratified and nonstratified flows during condensation inside horizontal and slightly inclined tubes. Attention is focused on this boundary since the present data suggest that the most significant deviation between adiabatic and condensing flows correspond to this boundary at small inclinations. Comparisons are made in the next chapter between the present analysis and data of different tube diameters, fluid properties, and tube inclinations in order to demonstrate the capability of the model.

The presence of heat transfer along the condensation path results in a continuously varying liquid height. Therefore, the flow never becomes fully developed, contrary to the case of adiabatic, gas-liquid flow. Influences of heat transfer and flow development are considered in the present analysis.

The stratified-nonstratified boundary can be analyzed through two different approaches. The traditional approach is through the application of the classical inviscid Kelvin-Helmholtz theory to explore the departure from a stratified configuration. This approach was followed by Taitel and Dukler (1976) in their analysis of the stratified-nonstratified transition during adiabatic gas-liquid flow inside horizontal and near horizontal tubes. The second approach involves analyzing the stability of flow on the basis of wave theory. Wallis (1969) has shown that the condition for marginal stability of a flow phenomenon is obtained when the kinematic and dynamic wave velocities become equal. Recently Brauner and Maron (1991) proposed that, in addition to the above criteria, the stability problem may also be analyzed using the well-posedness of the hyperbolic transient equations that govern the stratified flow. They have shown that the boundary of the stratified configuration can be represented by a buffer zone confined between a lower bound given by the stability of flow and an upper bound given by the well-posedness of the transient equation.

Two different approaches were attempted in the present analysis. These are the Kelvin-Helmholtz approach, later followed by Taitel and Dukler (1976), and the mathematical approach proposed by Brauner and Maron (1991). The results from both approaches were compared and found to be very close for all inclinations. Therefore, it was decided to include all derivations and results obtained from extending the approach of Brauner and Maron (1991) to condensing flows in Appendix D.

The modelling approach followed in the remaining part of this chapter, and the results presented in the following chapter, are based on extending the well-known work of Taitel and Dukler (1976) to condensing flows. First, a stratified flow condition is assumed and the equilibrium liquid level is determined from application of the appropriate conservation laws. The boundary of stratified flow is then determined by considering the mechanism by which transition from the stratified condition is expected to take place.

5.1 Equilibrium Liquid Level [Complete Formulation]

The one dimensional, co-current stratified flow in an inclined condenser tube is shown schematically in Figure 5.1. The flow of liquid and vapor is at equilibrium under the influences of wall and interfacial drag, gravity, acceleration, momentum transfer and pressure gradient. The flow is assumed to be steady and both phases are in thermodynamic equilibrium with constant properties. The tube has a uniform cross section along the flow direction.

An equation for the equilibrium liquid level can be derived by performing mass and momentum balances on the differential control volume shown in Figure 5.1. Considering the liquid and vapor phases separately, conservation of mass results in the following relations, respectively:

$$\rho_L \frac{\partial}{\partial Z}\left[\langle u_L (1 - \alpha)\rangle \right] = \dot{W}_i , \tag{5.1}$$

and

$$\rho_G \frac{\partial}{\partial Z}\left[\langle u_G\, \alpha\rangle \right] = - \dot{W}_i , \tag{5.2}$$

where Z is the axial coordinate along the tube axis, u_L is the local liquid velocity, u_G is the local vapor velocity, α is the local void fraction, and $\dot{W}_i$ is the mass flow rate crossing the interface per unit volume. The angle brackets [< >] used in the present formulation indicate averaging over the entire cross-sectional area of the tube. After reduction, the

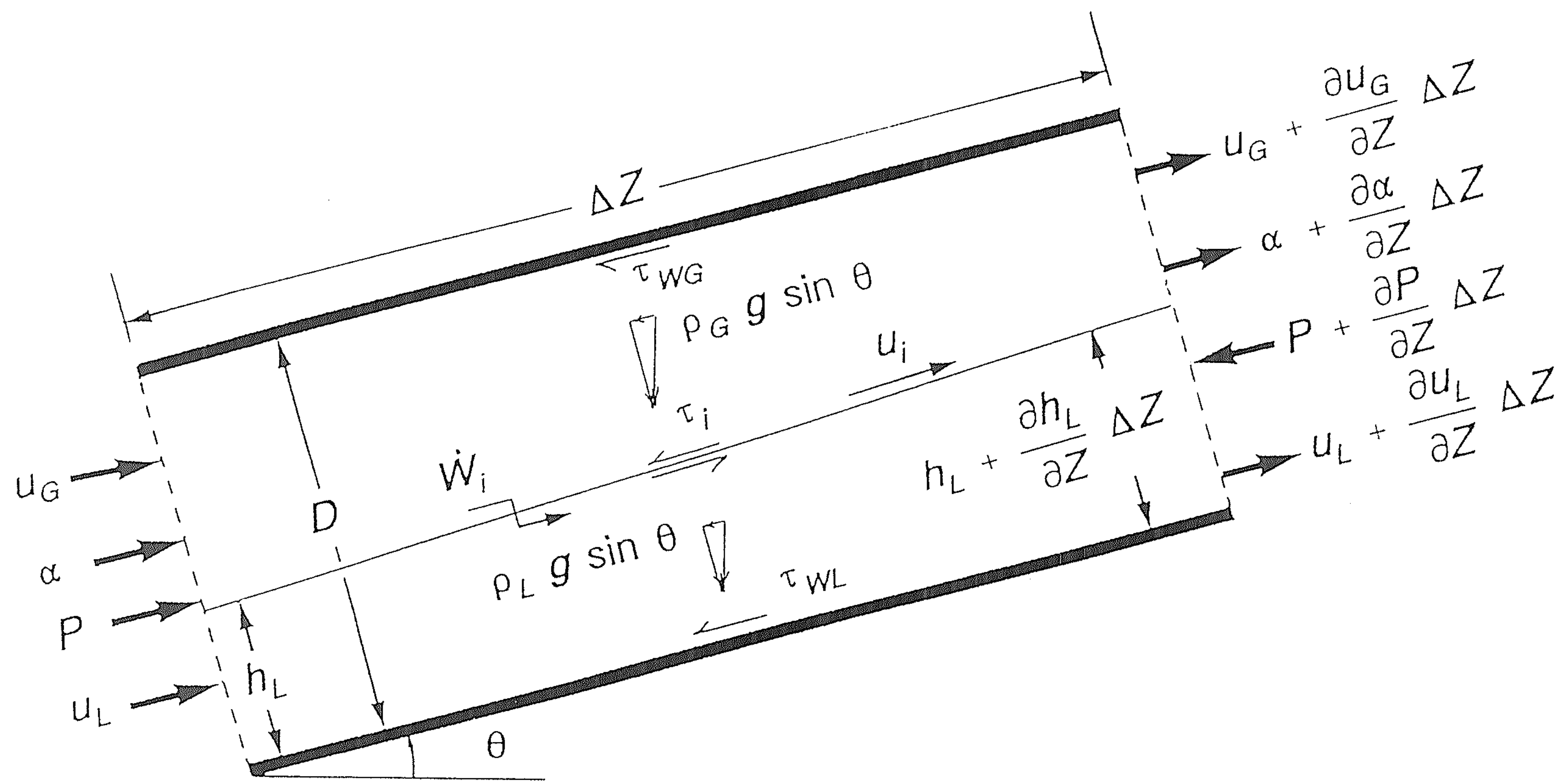

Figure 5.1 Stratified flow situation.

momentum balances applied to the liquid and vapor phases produce, respectively,

$$\frac{\partial P}{\partial Z} + g\,\rho_L \sin\theta + g\,\rho_L \cos\theta\,\frac{\partial h_L}{\partial Z} + \frac{\tau_{WL}\,S_L}{A\,<1-\alpha>} - \frac{\tau_i\,S_i}{A\,<1-\alpha>}$$

$$-\left[\frac{(1-\eta)<u_G\,\alpha>}{<1-\alpha><\alpha>} - \frac{(C_{3L}-\eta)<u_L(1-\alpha)>}{(<1-\alpha>)^2}\right]\frac{\partial}{\partial Z}\left[\rho_L <u_L(1-\alpha)>\right]$$

$$+ C_{3L}\,\rho_L\,\frac{<u_L(1-\alpha)>}{<1-\alpha>}\,\frac{\partial}{\partial Z}\left[\frac{<u_L(1-\alpha)>}{<1-\alpha>}\right] = 0\,, \qquad (5.3)$$

and

$$\frac{\partial P}{\partial Z} + g\,\rho_G \sin\theta + \frac{\tau_{WG}\,S_G}{A<\alpha>} + \frac{\tau_i\,S_i}{A<\alpha>}$$

$$-\left[(1-\eta-C_{3G})\frac{<u_G\,\alpha>}{(<\alpha>)^2} + \frac{\eta<u_L(1-\alpha)>}{<1-\alpha><\alpha>}\right]\frac{\partial}{\partial Z}\left[\rho_G <u_G\,\alpha>\right]$$

$$+ C_{3G}\,\rho_G\,\frac{<u_G\,\alpha>}{<\alpha>}\,\frac{\partial}{\partial Z}\left[\frac{<u_G\,\alpha>}{<\alpha>}\right] = 0\,, \qquad (5.4)$$

where P is the static pressure, θ is the tube inclination, h_L is the liquid height, A is the cross-sectional area of the tube, τ_{WL} is the average wall shear stress on the liquid phase, τ_{WG} is the average wall shear stress on the vapor phase, and τ_i is the average interfacial shear stress. Definitions of S_G, S_L, and S_i are given in Figure 5.2. The coefficients C_{3G} and C_{3L} are distribution parameters commonly defined by [e.g., Hancox and Nicoll, 1971]

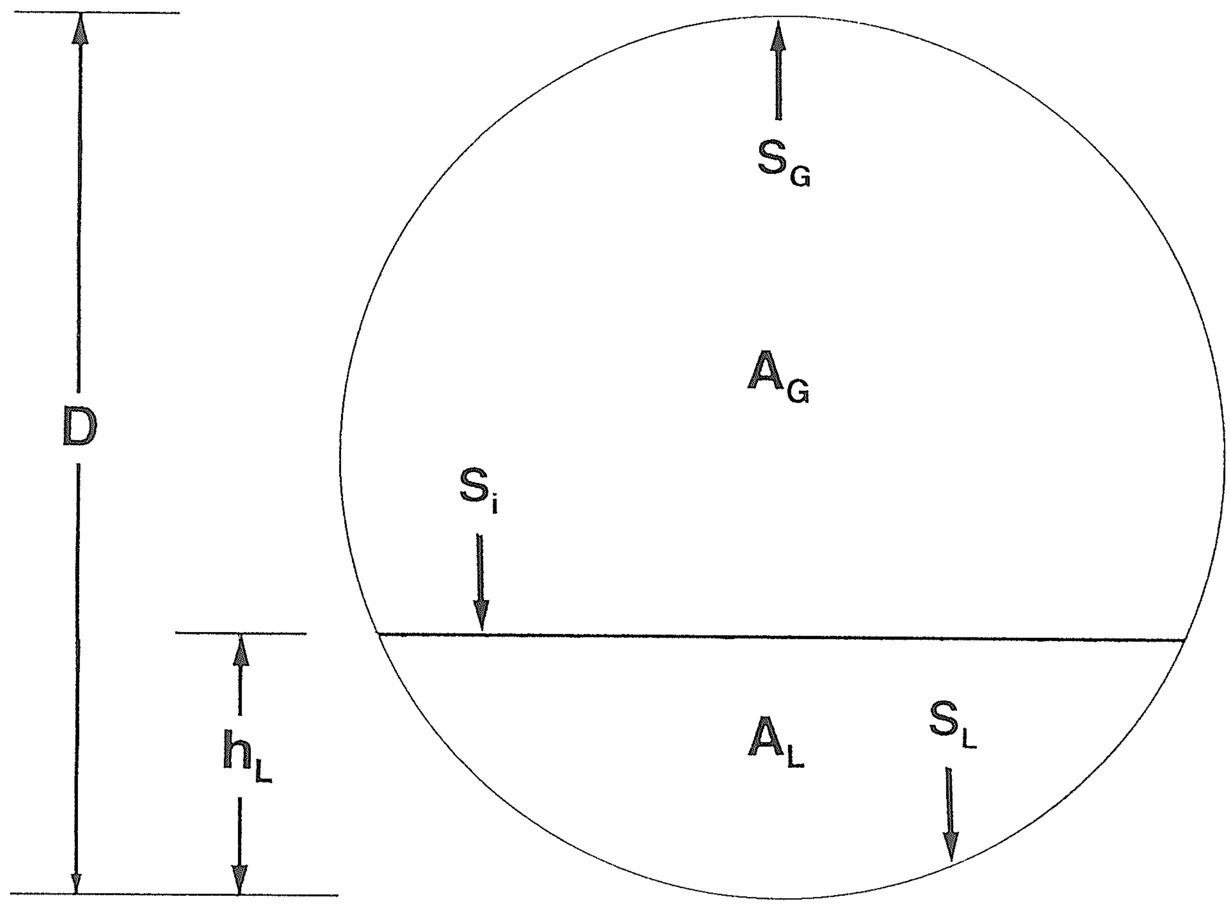

Figure 5.2 Definition of cross-sectional parameters.

$$C_{3G} = \frac{<\alpha\ u_G^2>}{<\alpha>\ (\ <u_G>_G\ )^2}\ , \tag{5.5a}$$

and

$$C_{3L} = \frac{<(\ 1\ -\ \alpha\ )\ u_L^2>}{<1\ -\ \alpha>\ (\ <u_L>_L\ )^2}\ , \tag{5.5b}$$

where the symbols [$< \ >_G$] and [$< \ >_L$] indicate averaging over the vapor and liquid flow areas, respectively. In deriving Equations (5.3) and (5.4), the interfacial momentum transfer was formulated using the interfacial rate of mass transfer $\mathring{W}_i$ and the mean interfacial velocity u_i, which was related to the averaged phase velocities by the relation [Yadigaroglu and Lahey, 1976]

$$u_i = \eta\ <u_L>_L + (\ 1\ -\ \eta\ )\ <u_G>_G\ \ . \tag{5.6}$$

The rate of condensation can be evaluated from a simple heat balance as follows:

$$\dot{W}_i\ =\ \frac{4\ q''}{D\ h_{fg}}\ , \tag{5.7}$$

where q" is the average heat flux based on the whole pipe perimeter and h_{fg} is the latent heat of vaporization. Equation (5.7) was substituted in Equations (5.1) and (5.2) and the pressure-gradient term was eliminated between Equations (5.3) and (5.4) using Equations (5.1) and (5.2) in the reduction. Thus, after algebraic manipulation, a momentum equation for the mixture was produced

$$\frac{\tau_{WL}\, S_L}{A_L} - \frac{\tau_{WG}\, S_G}{A_G} - \tau_I\, S_I \left[\frac{1}{A_G} + \frac{1}{A_L} \right] + (\rho_L - \rho_G)\, g \sin\theta$$

$$+ \frac{\pi\, D\, q''}{A\, h_{fg}} \left\{ \frac{<u_L (1 - \alpha)>}{<1 - \alpha>} \left[\frac{2\, C_{3L} - \eta}{<1 - \alpha>} - \frac{\eta}{<\alpha>} \right] \right\}$$

$$+ \frac{\pi\, D\, q''}{A\, h_{fg}} \left\{ \frac{<u_G\, \alpha>}{<\alpha>} \left[\frac{2\, C_{3G} + \eta - 1}{<\alpha>} + \frac{\eta - 1}{<1 - \alpha>} \right] \right\}$$

$$- \left[C_{3L}\, \rho_L \frac{(<u_L (1 - \alpha)>)^2}{(<1 - \alpha>)^3\, A} + C_{3G}\, \rho_G \frac{(<u_G\, \alpha>)^2}{(<\alpha>)^3\, A} \right] \left(\frac{dA_L}{dh_L} \frac{\partial h_L}{\partial Z} \right)$$

$$+ \rho_L\, g \cos\theta \left(\frac{\partial h_L}{\partial Z} \right) = 0 \,, \tag{5.8}$$

where

$$A_G = A <\alpha> \,, \tag{5.9a}$$

and

$$A_L = A <1 - \alpha> \,. \tag{5.9b}$$

The shear stresses appearing in Equation (5.8) were formulated using these conventional expressions [Taitel and Dukler, 1976]

$$\tau_{WL} = f_L \frac{\rho_L (<u_L>_L)^2}{2} \,, \tag{5.10a}$$

$$\tau_{WG} = f_G \frac{\rho_G (<u_G>_G)^2}{2} , \tag{5.10b}$$

and

$$\tau_I = f_G \frac{\rho_G [<u_G>_G - <u_L>_L]^2}{2} , \tag{5.10c}$$

where the friction coefficients are given by

$$f_L = C_{Lf} \left(\frac{D_L <u_L>_L}{\nu_L} \right)^{-n} , \tag{5.11a}$$

and

$$f_G = C_{Gf} \left(\frac{D_G <u_G>_G}{\nu_G} \right)^{-m} , \tag{5.11b}$$

while the liquid and vapor hydraulic diameters are given by

$$D_L = \frac{4 A_L}{S_L} , \tag{5.12a}$$

and

$$D_G = \frac{4 A_G}{S_G + S_I} . \tag{5.12b}$$

The coefficients appearing in Equations (5.11a) and (5.11b) were set as $C_{Lf} = C_{Gf} = 0.046$ and n = m = 0.2 for turbulent flow, and $C_{Lf} = C_{Gf} = 16$ and n = m = 1 for laminar flow. The actual Reynolds numbers [based on the phasic flow areas] were used in determining the transition between laminar and turbulent flow.

Equations (5.10) to (5.12) were substituted into Equation (5.8), and the mixture momentum equation was further reduced using the following identities:

$$V_{LS} = <u_L>_L <1 - \alpha> = <u_L (1 - \alpha)>, \tag{5.13a}$$

and

$$V_{GS} = \langle u_G \rangle_G \langle \alpha \rangle = \langle u_G \, \alpha \rangle, \tag{5.13b}$$

where V_{LS} and V_{GS} are the superficial liquid and vapor velocities, respectively. In final dimensionless form, the mixture momentum equation can be written as

$$\epsilon \, X^2 - \beta - 4 \, Y + \gamma \, H = \zeta \, \frac{\partial \bar{h}_L}{\partial \bar{Z}} \, , \tag{5.14}$$

where

$$\epsilon = \left(\bar{D}_L \frac{\bar{A}}{\bar{A}_L} \right)^{-n} \left(\frac{\bar{A}}{\bar{A}_L} \right)^2 \frac{\bar{S}_L}{\bar{A}_L} \, , \tag{5.15a}$$

$$\beta = \left(\bar{D}_G \frac{\bar{A}}{\bar{A}_G} \right)^{-m} \left(\frac{\bar{A}}{\bar{A}_G} \right)^2 \left\{ \frac{\bar{S}_G}{\bar{A}_G} + \left[\frac{\bar{S}_i}{\bar{A}_L} + \frac{\bar{S}_i}{\bar{A}_G} \right] \left[1 - \left(\frac{V_{LS}}{V_{GS}} \right) \frac{\bar{A}_G}{\bar{A}_L} \right]^2 \right\} , \tag{5.15b}$$

$$\gamma = \pi \left(\frac{V_{LS}}{V_{GS}} \right) \frac{\bar{A}}{(\bar{A}_L)^2} \left[2 \, C_{3L} - \eta \left(1 + \frac{\bar{A}_L}{\bar{A}_G} \right) \right]$$
$$+ \, \pi \frac{\bar{A}}{(\bar{A}_G)^2} \left[2 \, C_{3G} - (1 - \eta) \left(1 + \frac{\bar{A}_G}{\bar{A}_L} \right) \right] , \tag{5.15c}$$

$$\zeta = \left[\frac{2 \left(\frac{\rho_L}{\rho_G} \right)}{C_{Gf} \left(\frac{V_{GS} \, D}{\nu_G} \right)^{-m}} \right] \left[\frac{1}{\bar{A}} \left\{ C_{3L} \left(\frac{V_{LS}}{V_{GS}} \right)^2 \left(\frac{\bar{A}}{\bar{A}_L} \right)^3 + C_{3G} \left(\frac{\rho_G}{\rho_L} \right) \left(\frac{\bar{A}}{\bar{A}_G} \right)^3 \right\} \frac{d\bar{A}_L}{d\bar{h}_L} - \frac{g \, D \cos \theta}{(V_{GS})^2} \right] , \tag{5.15d}$$

$$X^2 = \frac{\dfrac{4\, C_{Lf}}{D}\left(\dfrac{V_{LS}\, D}{\nu_L}\right)^{-n} \dfrac{\rho_L\, V_{LS}^2}{2}}{\dfrac{4\, C_{Gf}}{D}\left(\dfrac{V_{GS}\, D}{\nu_G}\right)^{-m} \dfrac{\rho_G\, V_{GS}^2}{2}} , \qquad \textbf{(5.15e)}$$

$$Y = \frac{-\,(\rho_L - \rho_G)\, g \sin\theta}{\dfrac{4\, C_{Gf}}{D}\left(\dfrac{V_{GS}\, D}{\nu_G}\right)^{-m} \dfrac{\rho_G\, V_{GS}^2}{2}} , \qquad \textbf{(5.15f)}$$

and

$$H = \frac{2\, q''}{h_{fg}\, \rho_G\, V_{GS}\, C_{Gf}\left(\dfrac{V_{GS}\, D}{\nu_G}\right)^{-m}} . \qquad \textbf{(5.15g)}$$

All parameters with a bar superscript in Equations (5.14) and (5.15) are nondimensionalized using the reference variables D for length, D^2 for area, and the superficial velocities V_{LS} and V_{GS} for the mean liquid and vapor velocities, respectively. Equation (5.14) reduces to the Taitel and Dukler (1976) model when H = 0 [i.e., no heat transfer] and $\partial \bar{h}_L / \partial \bar{Z} = 0$ [i.e., fully -developed conditions with constant liquid height].

The term q" in Equation (5.15g) was evaluated by using an appropriate correlation that can give the condensing heat-transfer coefficient at the tube wall. In this study, a correlation by Collier (1981) was used. During stratified flow in a condenser tube, the flow experiences an adverse pressure gradient while there is considerable shear force on the liquid due to vapor flow. Collier (1981) modified Nusselt's theory by including the effect of vapor shear on the cross-sectional average heat-transfer coefficient. His modified correlation is given by

$$h_{av} = \frac{q''}{\Delta T} = E \left[\frac{\rho_L (\rho_L - \rho_G) \, g \, h'_{fg} \, k_L^3}{D \, \mu_L \, \Delta T} \right]^{0.25} , \tag{5.16}$$

where

$$h'_{fg} = h_{fg} + 0.68 \left(C_{P_L} \, \Delta T \right) , \tag{5.17}$$

k_L is the liquid thermal conductivity, μ_L is the liquid viscosity, C_{pL} is the liquid specific heat, and ΔT is the saturation-to-wall temperature difference. The parameter E is a correction factor given by Collier (1981) in table form and is closely represented by the following polynomial:

$$E = \langle\alpha\rangle \left[2.04 - 4.30 \langle\alpha\rangle + 4.45 (\langle\alpha\rangle)^2 - 1.46 (\langle\alpha\rangle)^3 \right] \tag{5.18}$$

5.2 Equilibrium Liquid Level [Simplified Formulation]

The presence of the term $\partial \overline{h}_L / \partial \overline{Z}$ in Equation (5.14) reflects the reality of the developing nature of the flow. However, starting from an initial condition at Z = 0, a numerical procedure is necessary in order to progress the solution along the condensation path. A simplified approach was considered whereby the term $\partial \overline{h}_L / \partial \overline{Z}$ in Equation (5.14) was dropped and the ratio $[V_{LS} / V_{GS}]$ was assumed negligible in Equations (5.15b), (5.15c), and (5.15d). Thus, the model reduces to

$$\epsilon X^2 - \beta' - 4 Y + \gamma' H = 0 , \tag{5.19}$$

where

$$\beta' = \left(\bar{D}_G \frac{\bar{A}}{\bar{A}_G} \right)^{-m} \left(\frac{\bar{A}}{\bar{A}_G} \right)^2 \left\{ \frac{\bar{S}_G}{\bar{A}_G} + \frac{\bar{S}_i}{\bar{A}_L} + \frac{\bar{S}_i}{\bar{A}_G} \right\} , \tag{5.20a}$$

$$\gamma' = \pi \frac{\bar{A}}{(\bar{A}_G)^2} \left[2\, C_{3G} - (1 - \eta) \left(1 + \frac{\bar{A}_G}{\bar{A}_L} \right) \right] , \tag{5.20b}$$

and ε is given by Equation (5.15a). In this formulation, ε, β', and γ' are unique functions of $\bar{h}_L$. Therefore, for given values of X, Y, and H, Equation (5.19) can be solved algebraicly for the corresponding value(s) of $\bar{h}_L$. A quantitative assessment of this approach is given in the following chapter.

Of course, this approach may be considered meaningful only if it produces results close enough to those of Equation (5.14). Any deviation between the two sets of results would be due to the effect of the gradient of the interface on the equilibrium liquid level. This simplified approach, if successful, can produce generalized results of $\bar{h}_L$ as a function of X, Y, and H. A quantitative assessment of this approach is given in the following chapter.

5.3 Transition Criterion

A finite amplitude disturbance on the smooth interface between the two phases is shown in Figure 5.3. Taitel and Dukler (1976) developed [for adiabatic gas-liquid flow] a criterion for the condition where a finite wave amplitude would grow based on Kelvin-Helmholtz theory. The wave amplitude would grow when the gas flow rate is large

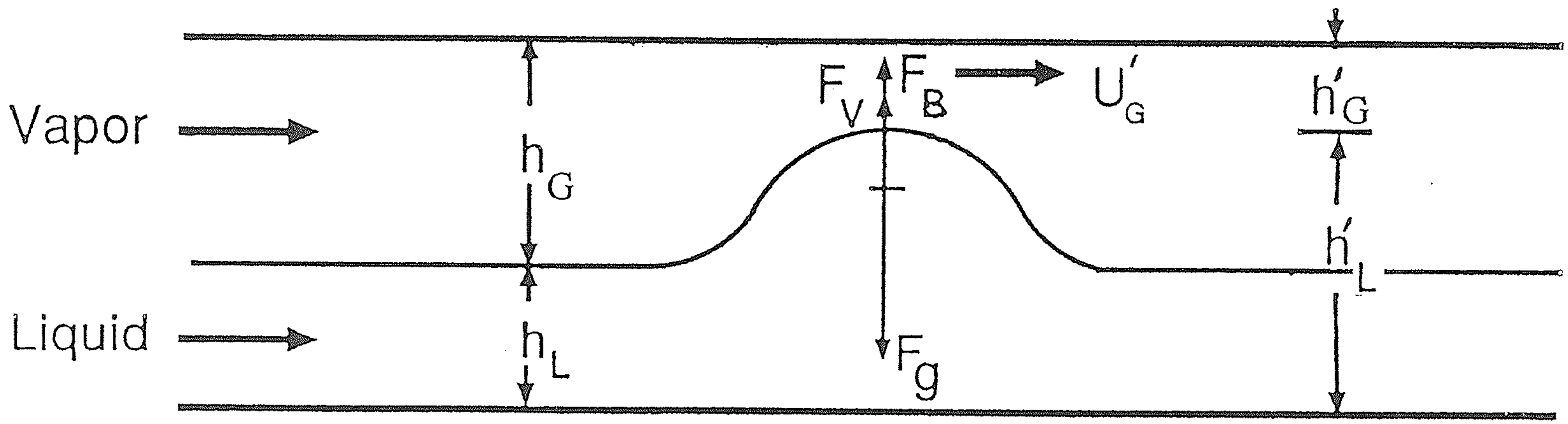

Figure 5.3 Stability of a wave crest.

enough over the wave crest to cause a lift force [Bernoulli effect]. Dukler (1978) proposed a transition criterion for boiling flows based on this mechanistic approach. This approach is extended to condensing flows in this study.

In condensing flows, in addition to the lift force from the vapor flow, a destabilizing effect is created by the reaction force to vapor molecules condensing on the vapor-liquid interface. The condition for the finite amplitude wave to grow is assumed to take the form

$$F_B \geq F_g - F_V \,, \tag{5.21}$$

where F_V is the reaction force due to momentum change during condensation per unit surface area, F_B is the Bernoulli force due to the accelerating vapor above the wave per unit surface area, and F_g is the gravitational force per unit surface area. The gravitational force is given by

$$F_g \; = \; (\, h_G - h'_G \,) \, (\, \rho_L - \rho_G \,) \, g \cos \theta \,, \tag{5.22}$$

where h_G and h'_G are the distances above the interface to the top surface, as shown in Figure 5.3.

The Bernoulli force can be formulated as

$$F_B = \frac{1}{2} \, \rho_G \, (< u_G >_G)^2 \left[\left(\frac{A_G}{A'_G} \right)^2 - 1 \right] , \tag{5.23}$$

where A_G and A'_G are the flow cross-sectional areas of the vapor phase where the vapor heights are h_G and h'_G, respectively.

The force due to the momentum change during condensation can be obtained through the Reynolds flux concept given by Wallis (1969). From mass continuity across the interface, we get

$$\rho_G \, v_{GN} = \rho_L \, v_{LN} = G_N \quad , \tag{5.24}$$

where v_{GN} and v_{LN} are the mean velocity components normal to the interface acting towards the liquid surface, and G_N is the mass flux entering the liquid due to condensation. It can be shown that the pressure drop $(\Delta p)_N$ associated with this mass transfer is

$$(\Delta p)_N = G_N \, (v_{GN} - v_{LN}) = \left(\frac{G_N}{\rho_G} \right)^2 \left[\rho_G - \frac{\rho_G^2}{\rho_L} \right] . \tag{5.25}$$

Since $\rho_L >> \rho_G$, the last term within the parenthesis in Equation (5.25) can be ignored. From a simple heat balance, G_N can be estimated. The reaction force due to condensation can finally be written as

$$F_V = (\Delta p)_N = \left[\frac{\pi \, D \, q''}{h_{fg} \, S_i} \right]^2 \frac{1}{\rho_G} \quad . \tag{5.26}$$

Equations (5.22), (5.23) and (5.26) were substituted into Equation (5.21) using definition (5.15g) for the relationship between q" and H. Thus, the following formulation for the transition criterion was obtained:

$$(<u_G>_G)^2 \geq \left\{ \frac{(\rho_L - \rho_G) \, g \cos \theta}{\rho_G} (h_G - h'_G) - \left[\frac{\pi \, D \, H \, V_{GS}}{2 \, S_i} \, C_{Gf} \left(\frac{V_{GS} \, D}{\nu_G} \right)^{-m} \right]^2 \right\} \times$$

$$\left[\frac{2 \, A'^2_G}{A_G^2 - A'^2_G} \right] \tag{5.27}$$

For small finite disturbances, A'_G can be expanded in a Taylor series around A_G keeping only the first term of the series and ignoring the higher-order terms. Thus,

$$(<u_G>_G)^2 \geq \left\{ \frac{(\rho_L - \rho_G)\, g\, A_G \cos\theta}{\rho_G \dfrac{dA_L}{dh_L}} - \left(\frac{D}{h_L}\right) \left[\left(\frac{\pi\, D\, V_{GS}\, H}{2\, S_i} \right) C_{Gf} \left(\frac{V_{GS}\, D}{\nu_G} \right)^{-m} \right]^2 \right\} \times$$

$$\left\{ \frac{2 \left(\dfrac{A'_G}{A_G} \right)^2}{1 + \dfrac{A'_G}{A_G}} \right\} \qquad \textbf{(5.28)}$$

Following Taitel and Dukler (1976), the first quantity between brackets on the right hand side of Equation (5.28) was approximated by $(1 - h_L / D)^2$. Introducing this approximation and simplifying using Equation (5.13b), we get this final form for the transition criterion

$$F^2 \left(\frac{d\bar{A}_L / d\bar{h}_L}{\bar{A}_G} \right) \left(\frac{(\bar{A} / \bar{A}_G)^2}{(1 - \bar{h}_L)^2} + \frac{1}{\bar{h}_L} \left[\frac{\pi\, H}{2\, \bar{S}_i} C_{Gf} \left(\frac{V_{GS}\, D}{\nu_G} \right)^{-m} \right]^2 \right) \geq 1 \;, \qquad \textbf{(5.29)}$$

where,

$$F^2 = \frac{V_{GS}^2}{D\, g \cos\theta} \, \frac{\rho_G}{\rho_L - \rho_G} \;, \qquad \textbf{(5.30)}$$

and the term $d\bar{A}_L/d\bar{h}_L$ is determined from simple geometric considerations [Taitel and Dukler, 1976] as,

$$\frac{d\bar{A}_L}{d\bar{h}_L} = \sqrt{1 - (2\bar{h}_L - 1)^2}\,. \qquad (5.31)$$

Computed results from the two formulations; the approximate [given by Equation (5.19)] and the complete [given by Equation (5.14)], will be compared in the following chapter. Based on the comparisons, one of the methods will be adopted to obtain the equilibrium liquid levels for condensing flows in inclined tubes. The predictions of the equilibrium liquid level will then be applied to the transition criterion. From this transition criterion, the stratified-nonstratified transition boundary will be determined for different fluid properties and tube diameters. These analytical boundaries will then be compared with the experimental data.

Chapter 6

THEORETICAL RESULTS AND COMPARISONS

The boundary between stratified and nonstratified flow during condensation in horizontal and slightly inclined tubes is given by Equation (5.29). Application of this equation requires knowledge of the dimensionless liquid height $\bar{h}_L$. A mechanistic model has been developed for the evaluation of $\bar{h}_L$ with two possible formulations; a complete formulation given by Equations (5.14) and (5.15), and a simplified formulation given by Equations (5.19) and (5.20). In order to solve either formulation, suitable values for the coefficients C_{3G}, C_{3L}, and η are required. Hancox and Nicoll (1971) recommended a value between 1.0 and 1.2 for the distribution coefficients C_{3G} and C_{3L}, depending on the flow regime. All results in this study were obtained with a value of 1.0 for the distribution parameters. This choice makes the present results for the special case of adiabatic flow identical to those of Taitel and Dukler (1976). A number of suggestions have been made for the momentum transfer parameter η ranging from 0.5 to 1.0 [Wallis, 1969; Yadigaroglu and Lahey, 1976]. The interfacial velocity is influenced by the relative magnitudes of the average phase velocities and the liquid height. For small liquid heights, the interfacial velocity would be more influenced by the average velocity of the liquid because of the proximity of the wall to the interface. Similarly, near the end of the condensation path, the interfacial velocity is more likely to be closer to the average vapor velocity. Therefore, an appropriate estimate of η must take into consideration the changes in the liquid height along the flow. A simple relationship, $\eta = 1 - h_L/D$, was used in generating the present results.

In the following sections, a comparison is made between the results of the complete and the simplified formulations of the equilibrium-liquid-level model, followed by a presentation of the $\bar{h}_L$-results, and finally the predictions of the stratified-nonstratified transition criterion are presented and compared with experimental flow-regime data.

6.1 Comparison Between the Complete and Simplified Formulations

The development of h_L/D along the condensation path was obtained for the case of condensing steam at a saturation temperature of 100°C inside a tube with D = 13.4 mm for a saturation-to-wall temperature difference of 10°C. These results are presented sequentially from Figure 6.1 for $\theta = +10°$ [upward] to Figure 6.7 for $\theta = -10°$ [downward]. The curves corresponding to the complete and simplified formulations are marked [CF] and [SF], respectively, in Figures 6.1 to 6.7. For all inclinations except the horizontal, the results cover the range of total mass flow rates $21.6 \leq \dot{m} \leq 144$ kg/h, which coincides with the mass-flow range tested in the experimental investigation [Chapter 4]. In the horizontal position the maximum value of mass flow rate tested was 1080 kg/h. This higher value of mass flow rate was used to illustrate that the CF and SF formulations are capable of providing very close results when the mass flow rates are sufficiently high.

In executing the complete formulation, it was assumed that the region $\bar{Z} \leq 0$ is adiabatic with a very small liquid height $(h_L/D)_o = 0.005$ and that condensation starts at $\bar{Z} = 0$. Therefore, an initial solution [at $\bar{Z} = 0$] was established by solving Equations (5.14) and (5.15) iteratively for the adiabatic condition [$H = \partial \bar{h}_L / \partial \bar{Z} = 0$], thus yielding

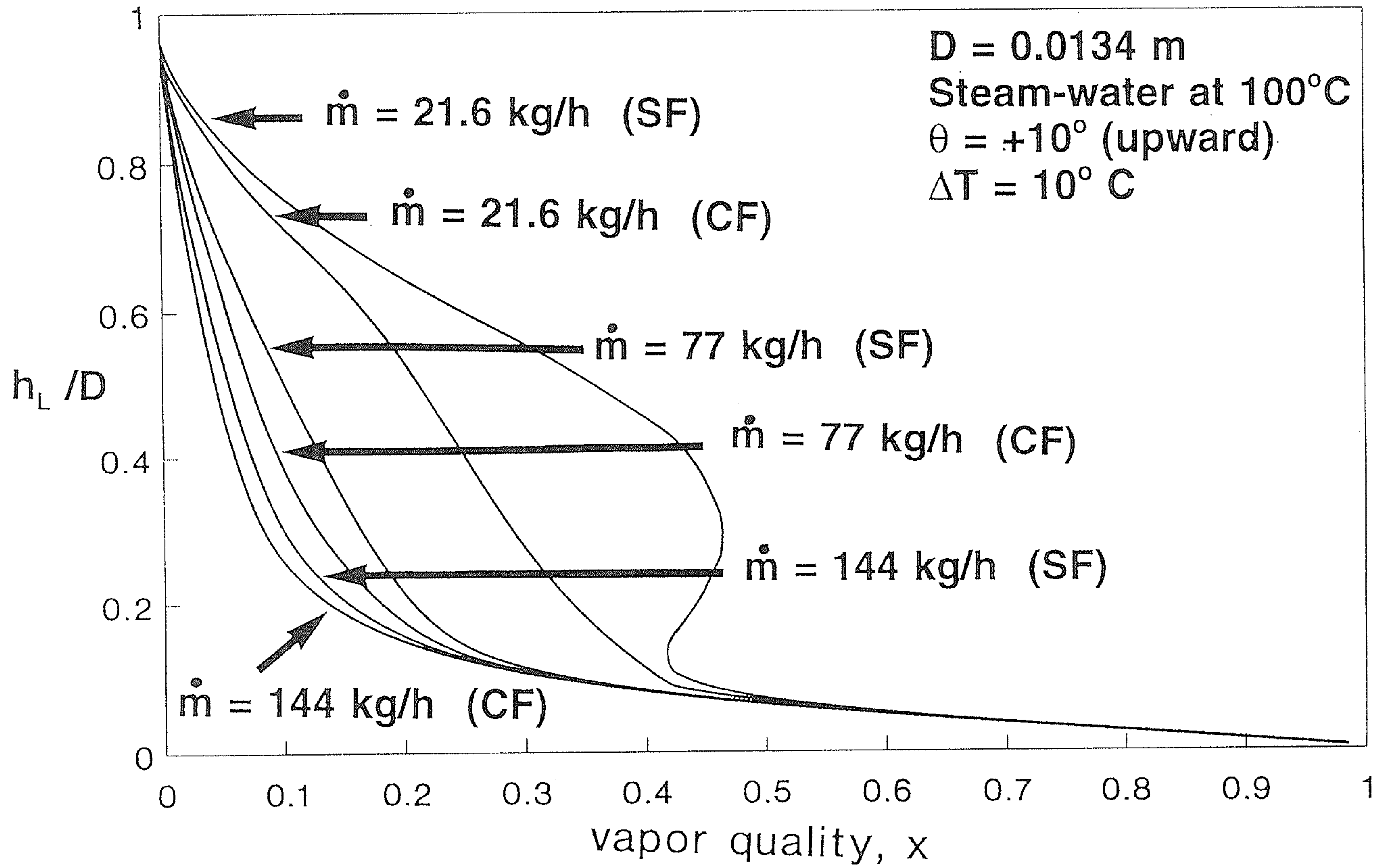

Figure 6.1 Comparison between the complete and simplified formulations for $\theta = +10°$ [upward].

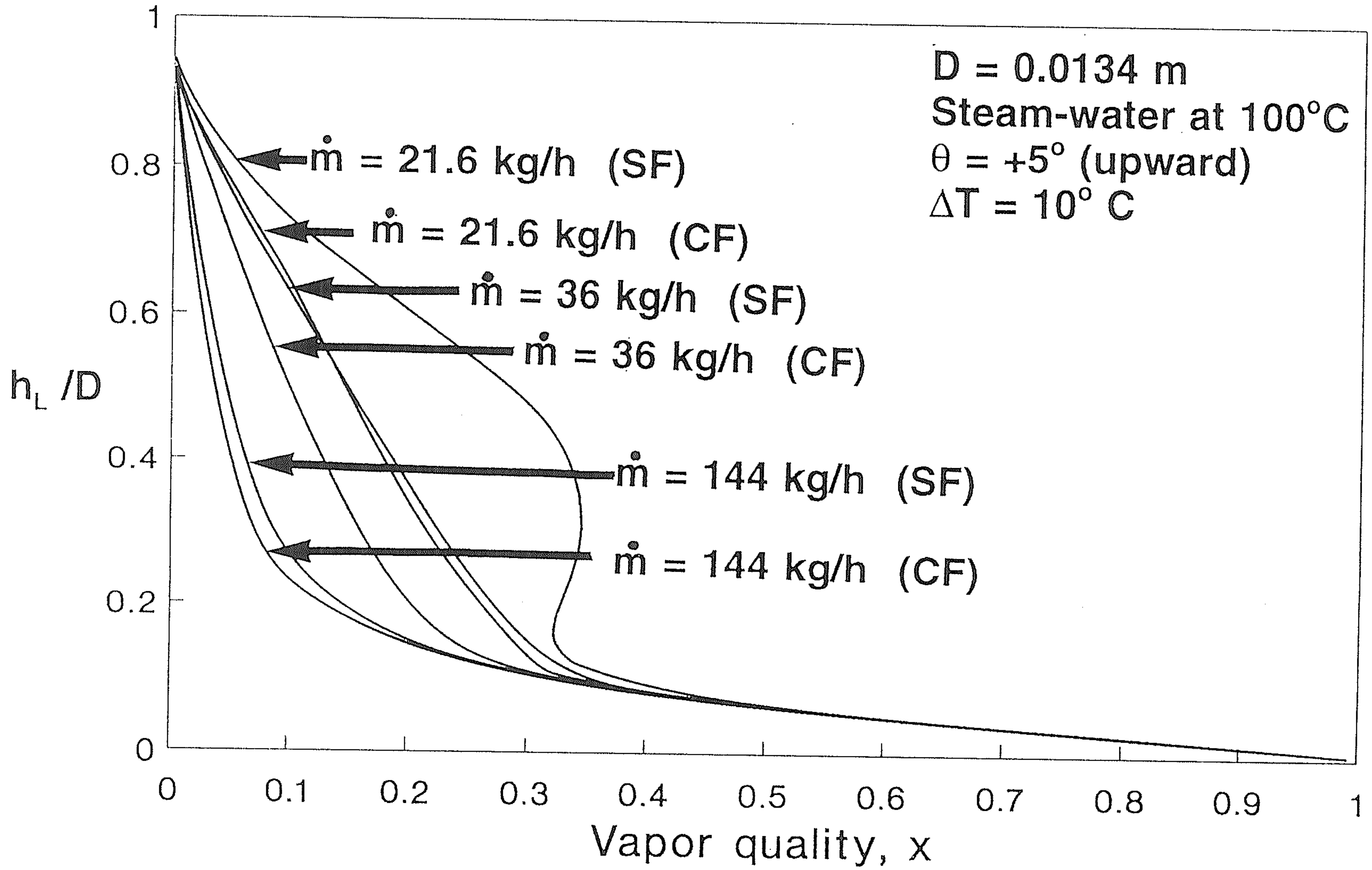

Figure 6.2 Comparison between the complete and simplified formulations for $\theta = +5°$ [upward].

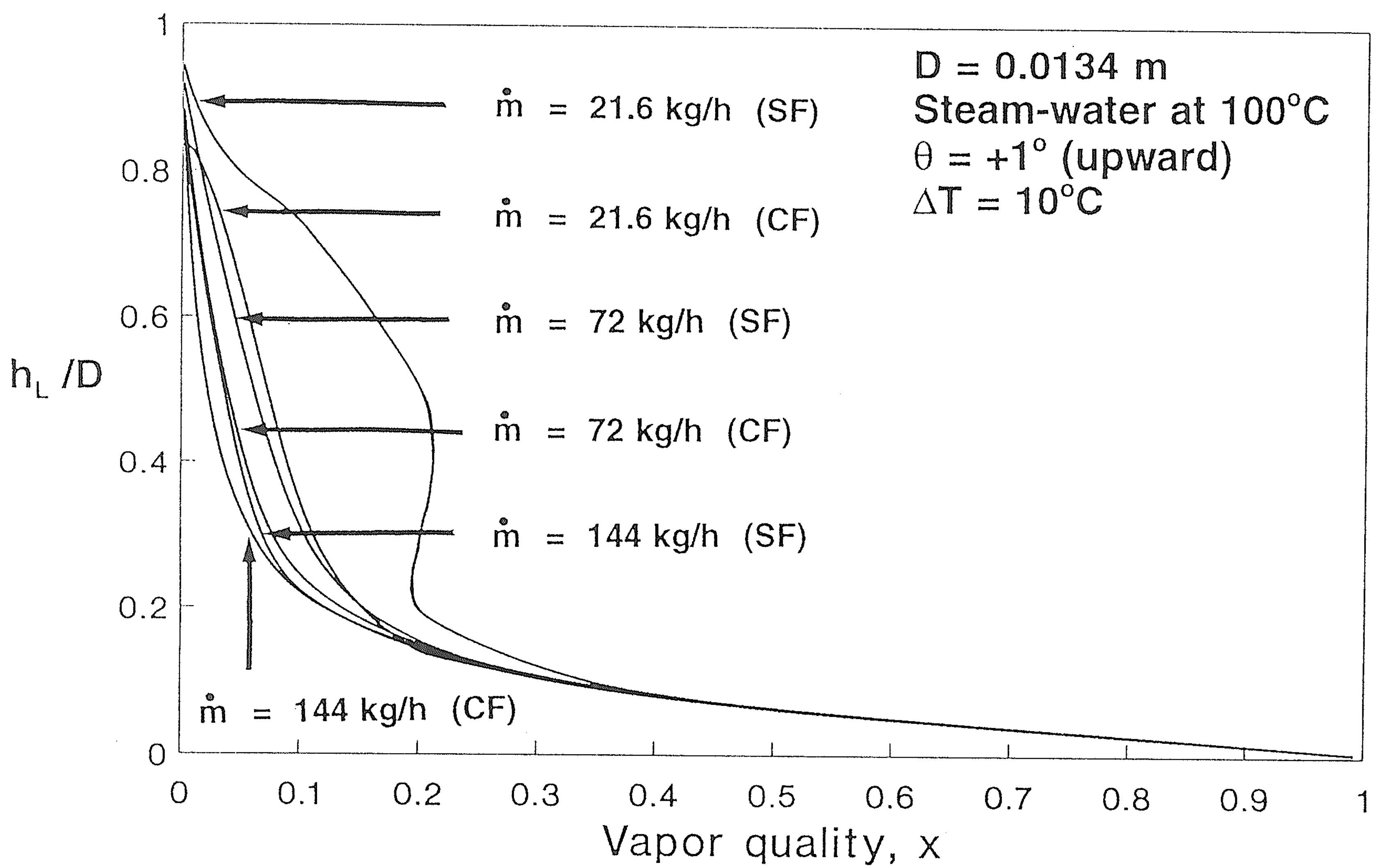

Figure 6.3 Comparison between the complete and simplified formulations for $\theta = +1°$ [upward].

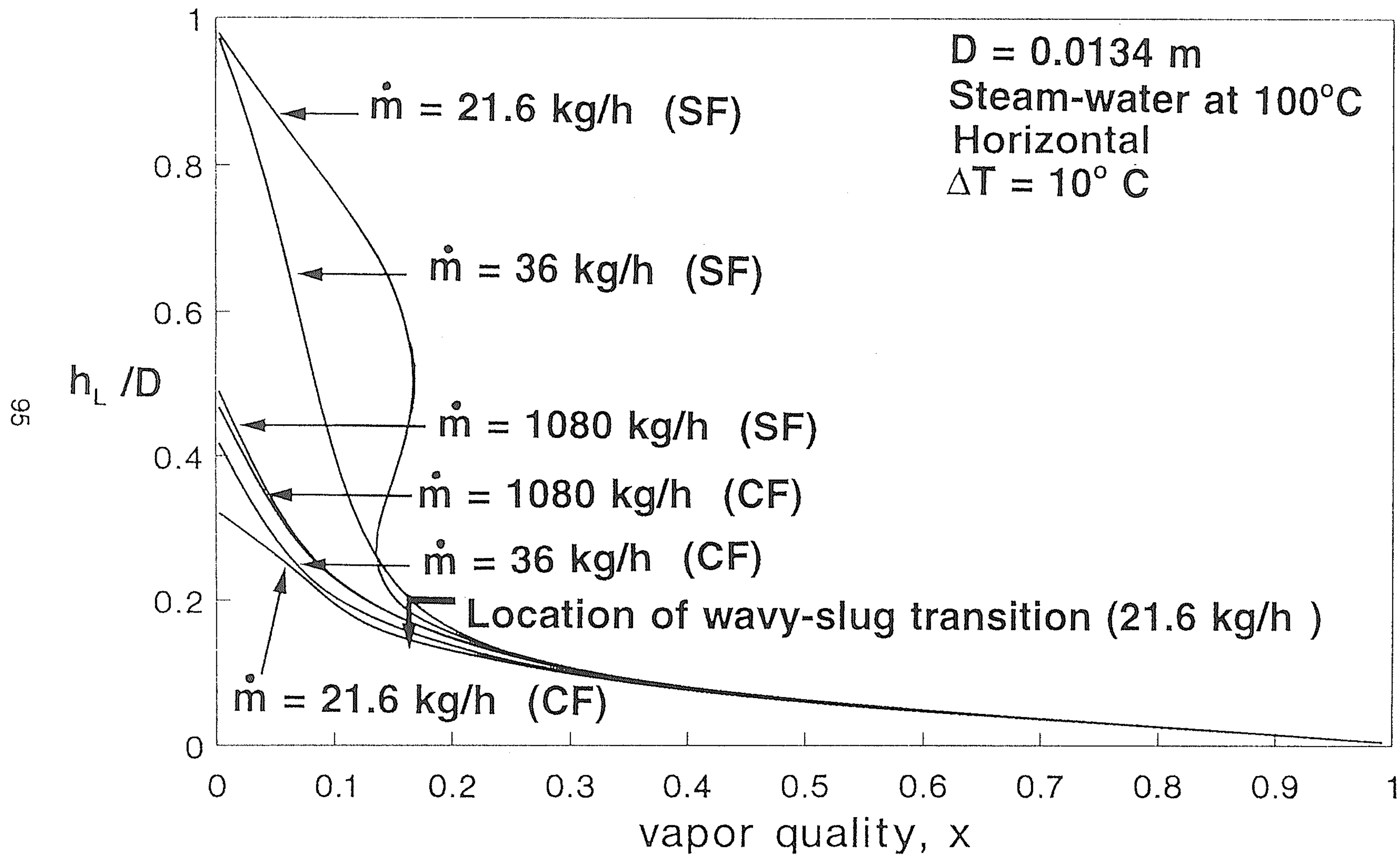

Figure 6.4 Comparison between the complete and simplified formulations for horizontal position.

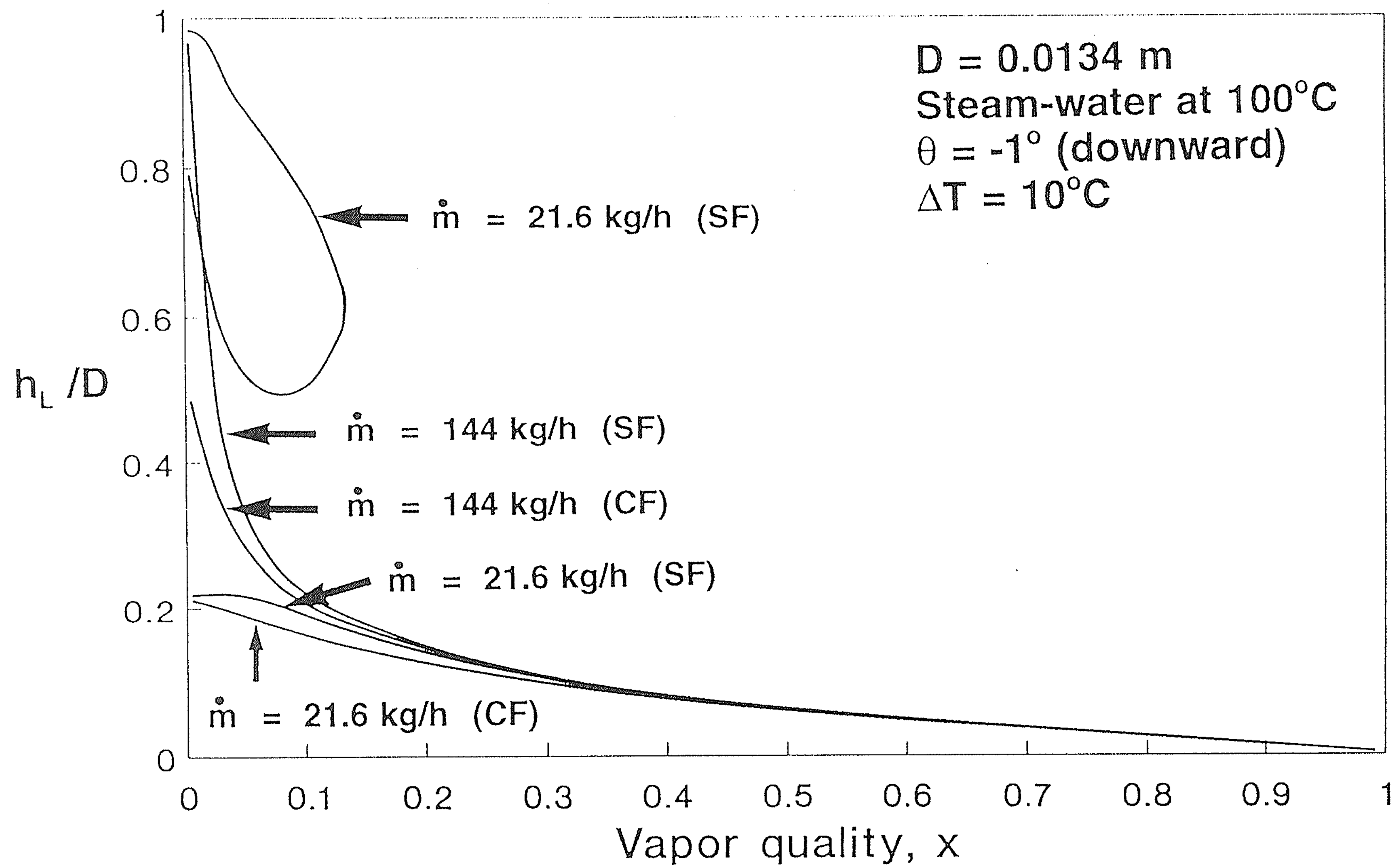

Figure 6.5 Comparison between the complete and simplified formulations for $\theta = -1°$ [downward].

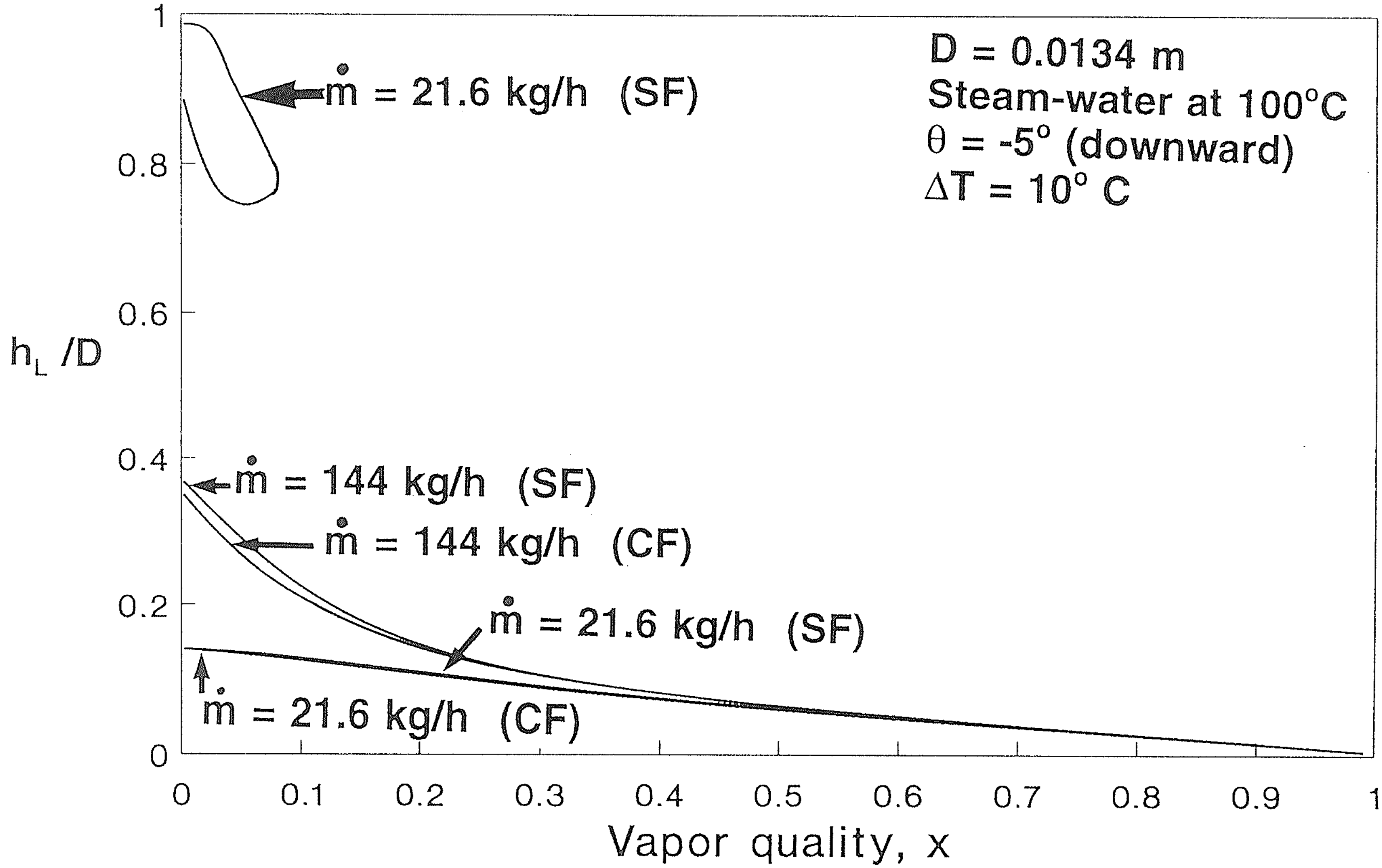

Figure 6.6 Comparison between the complete and simplified formulations for $\theta = -5°$ [downward].

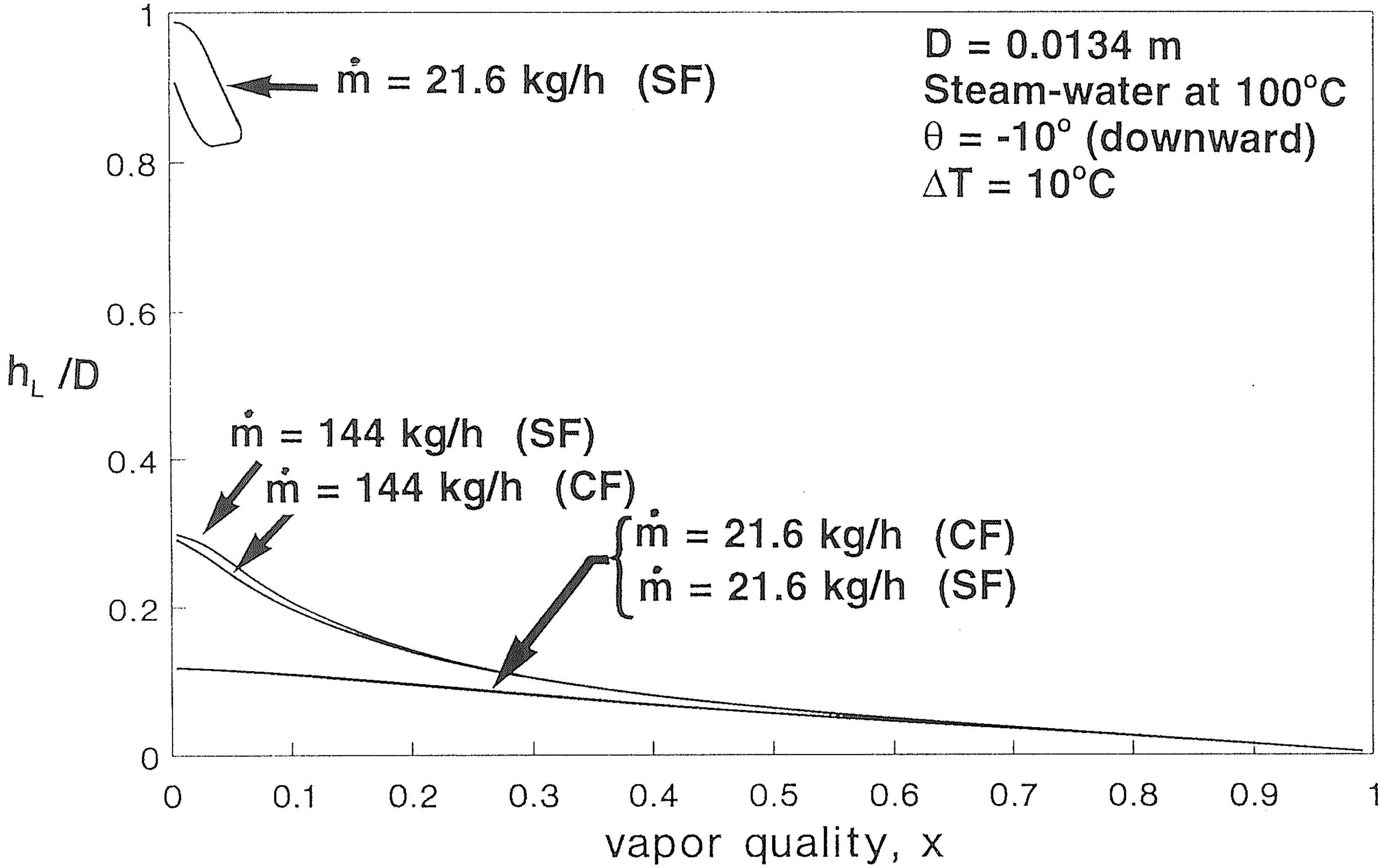

Figure 6.7 Comparison between the complete and simplified formulations for $\theta = -10°$ [downward].

the corresponding initial quality x_o. The solution was then advanced along the condenser using an explicit finite-difference scheme. After numerical experimentation, it was found that the results become grid-independent with a grid size of about $\Delta \bar{Z} = 0.001$. Numerical experiments were also conducted in order to study the effect of the initial value $(h_L/D)_o$ and it was found that starting from values lower than 0.005 had insignificant effect on the rest of the solution domain. For each value of $\dot{m}$, the solution was then advanced using Equations (5.14) and (5.15) and values of h_L/D and x were determined at each axial station $\bar{Z}$.

Results were also obtained from the simplified formulation using Equations (5.19) and (5.20) at the same conditions applied to the complete formulation. At each axial station, the value of x was matched for the two formulations and the value of h_L/D for the simplified formulation was determined.

Figures 6.1 to 6.7 show generally good agreement between the two solutions, particularly for $x \geq 0.2$ and larger values of $\dot{m}$. The simplified formulation produced multiple solutions of h_L/D for the same x at low values of $\dot{m}$ and x. The existence of multiple solutions for this type of formulation was discussed in a recent paper by Landman (1991), who argued that the lowest value of h_L/D at a given x is the most stable solution. Keeping that in mind, it may be concluded from Figures 6.1 to 6.7, that the simplified formulation is reasonably accurate for the present application. In most instances, the stratified-nonstratified transition was found to occur at condenser locations where the deviation between the two solutions is practically indistinguishable [Figure 6.4].

6.2 Equilibrium Liquid Level

The simplified formulation was solved for a wide range of parameters and the results are shown in Figures 6.8 - 6.13. Figure 6.8 corresponds to H = 0, and it is identical to the results of Taitel and Dukler (1976). Multiple solutions are predicted for the upward inclinations corresponding to $Y < -4$ over a range of X. With condensation, as shown in Figure 6.9 - 6.13, the influence on the results is very small for large Y-values. However, significant changes in h_L/D occur for small values of Y with multiple solutions possible for even downward inclinations. The influence of H on the results of h_L/D is consistent in trend with the introduction of an additional upward inclination on the adiabatic solution. This is further illustrated in Figure 6.14 for the horizontal orientation Y = 0. It can be seen from Figures 6.8 and 6.14 that increasing H for Y = 0 produces trends in the h_L/D-values similar to decreasing Y [or increasing upward inclination] for H = 0.

Examining the results in Figures 6.8 - 6.13, we note that the multiple roots for the equilibrium liquid level occur at lower values of Y as H increases. For example, multiple roots are shown for Y = -4 when H = 0 [Figure 6.8], whereas, at H = 1, multiple roots appear at Y = -3 [Figure 6.9]. This trend is seen for all values of H tested. The region of X where multiple roots appear corresponds to low qualities, as demonstrated earlier in Figures 6.1 - 6.7.

In the region of X where the equilibrium liquid level is multivalued, a maximum of three roots are possible. As H is increased, the roots with a value of $h_L/D < 0.5$ tend to decrease in value whereas the roots with a value of $h_L/D > 0.5$ tend to increase in value.

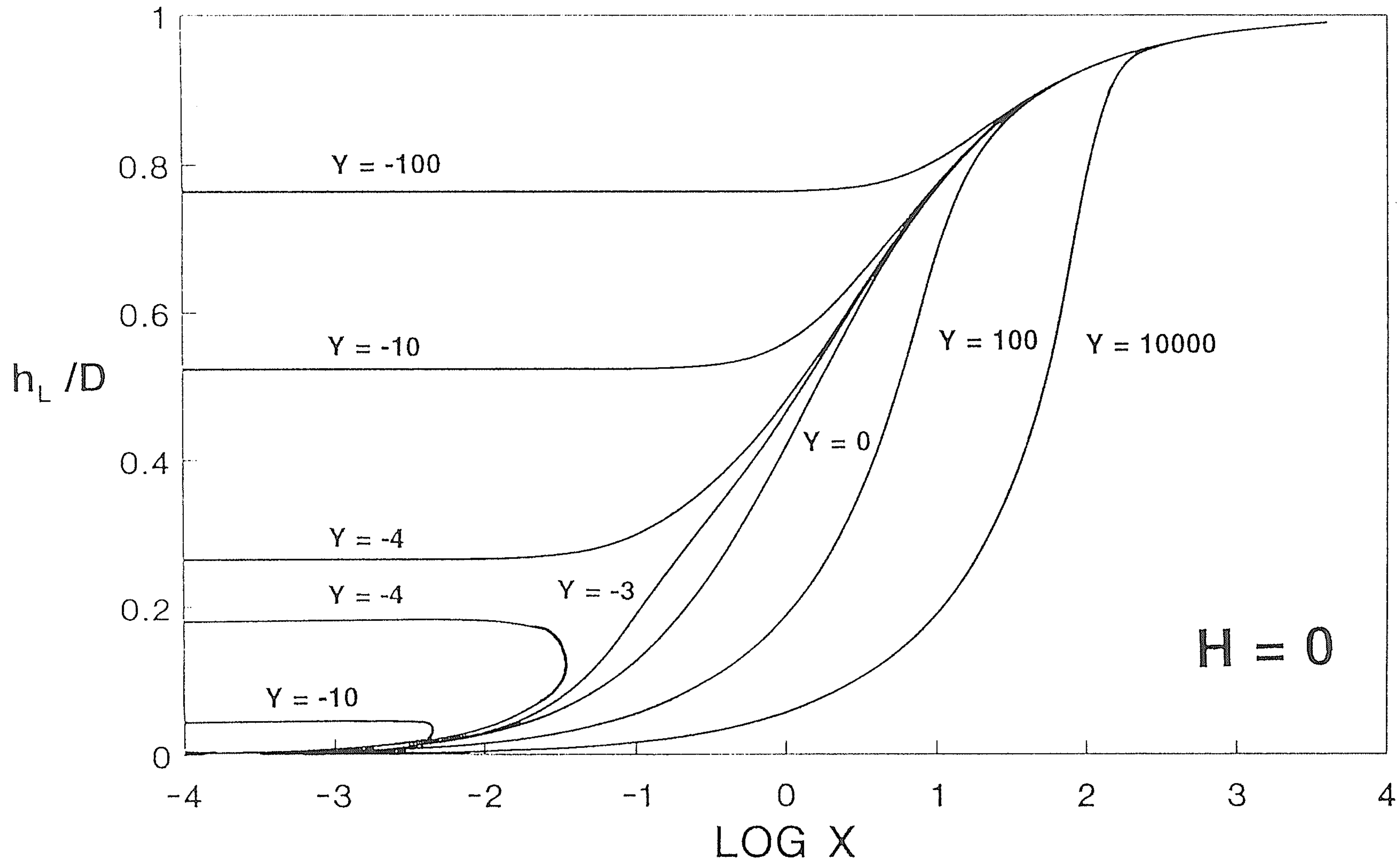

Figure 6.8 Equilibrium liquid level for H = 0.

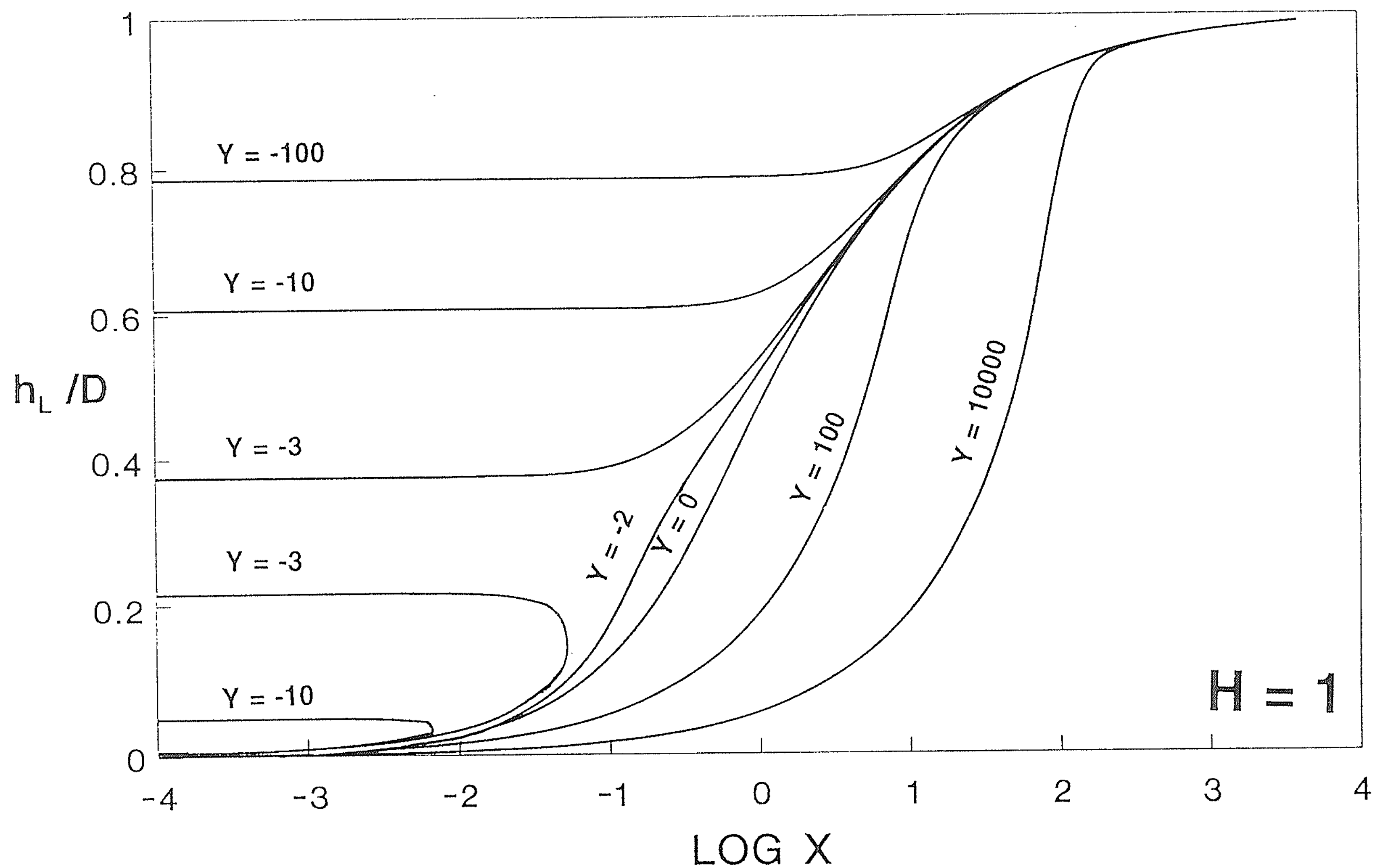

Figure 6.9 Equilibrium liquid level for H = 1.0

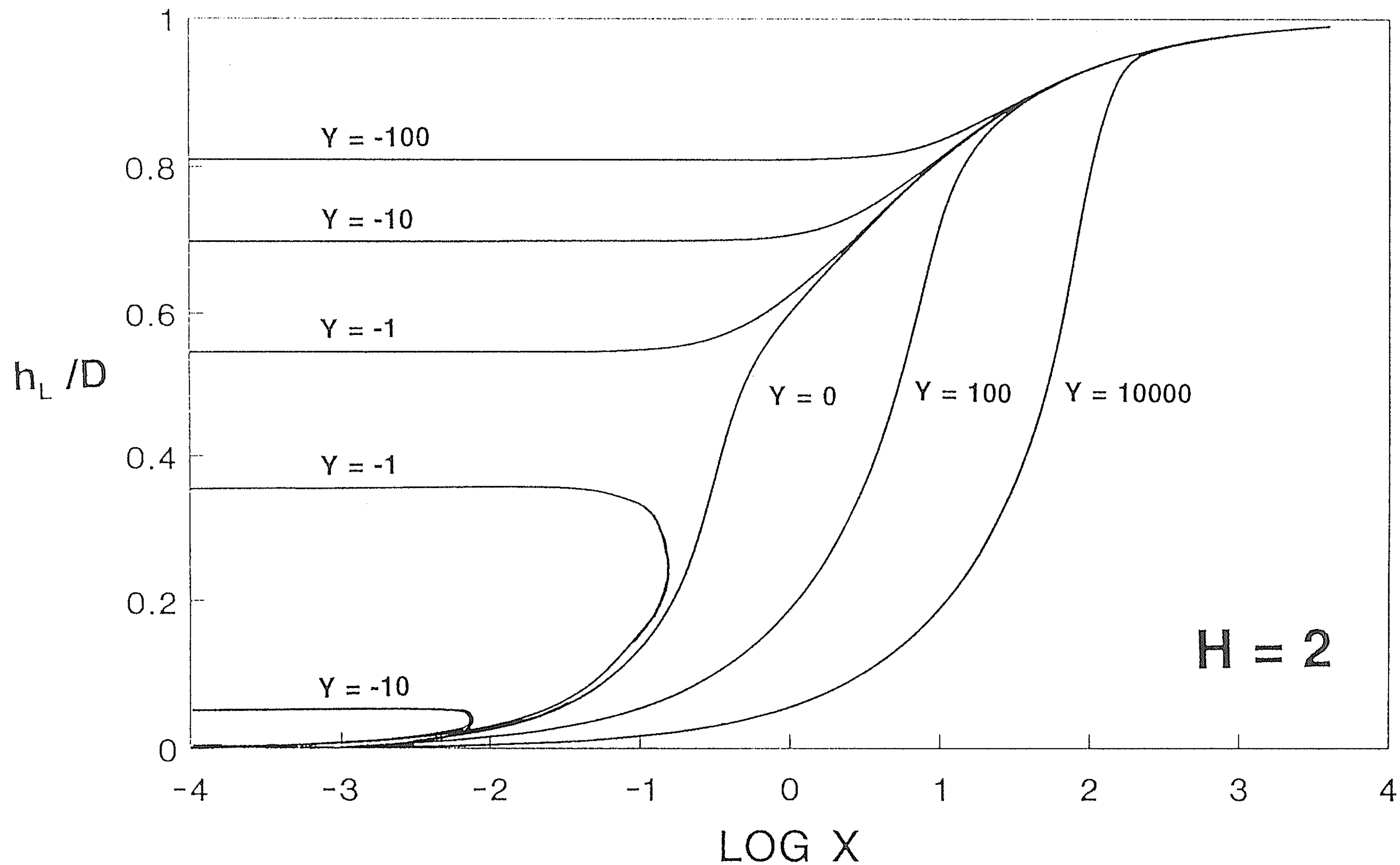

Figure 6.10 Equilibrium liquid level for H = 2.0

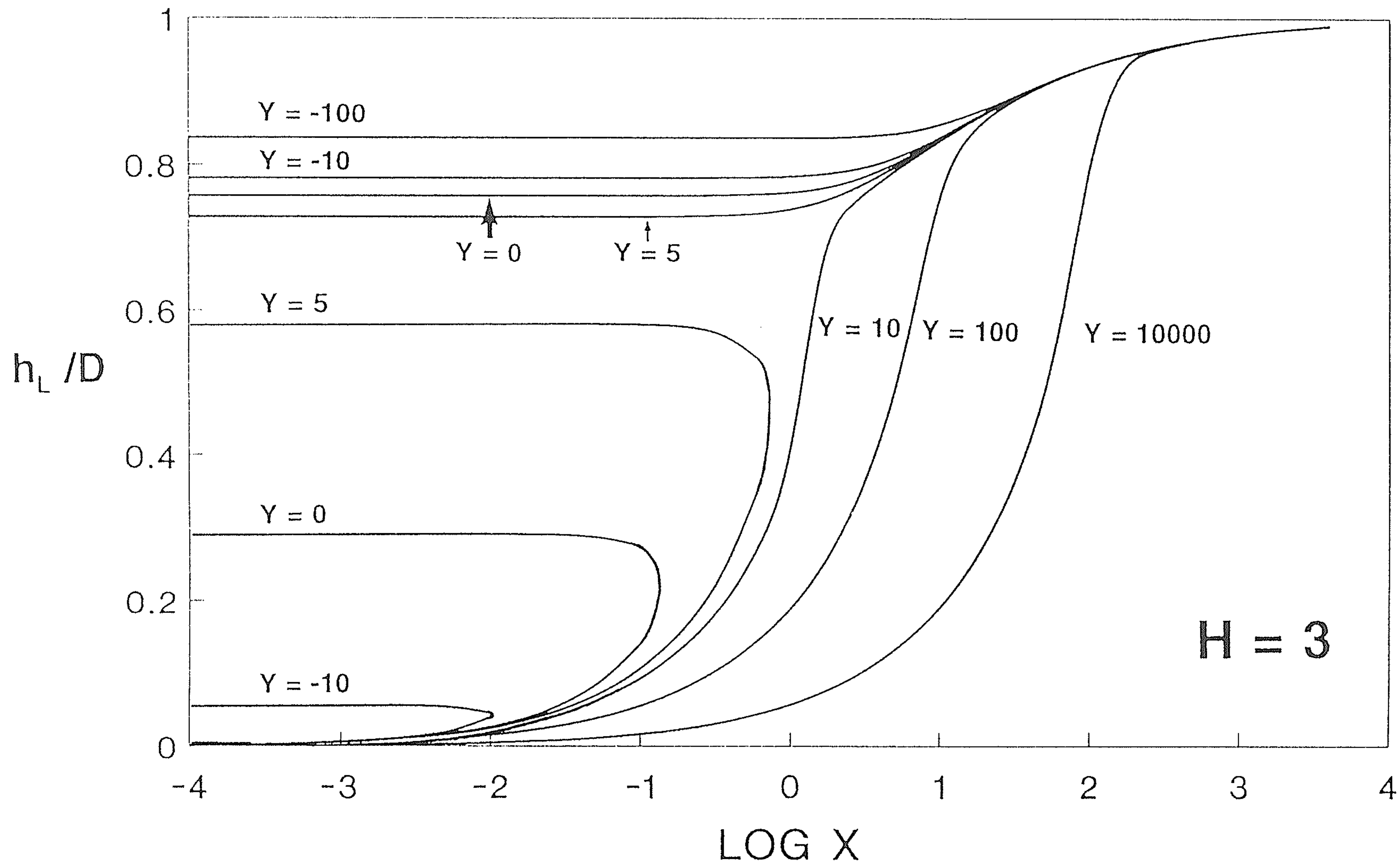

Figure 6.11 Equilibrium liquid level for H = 3.0

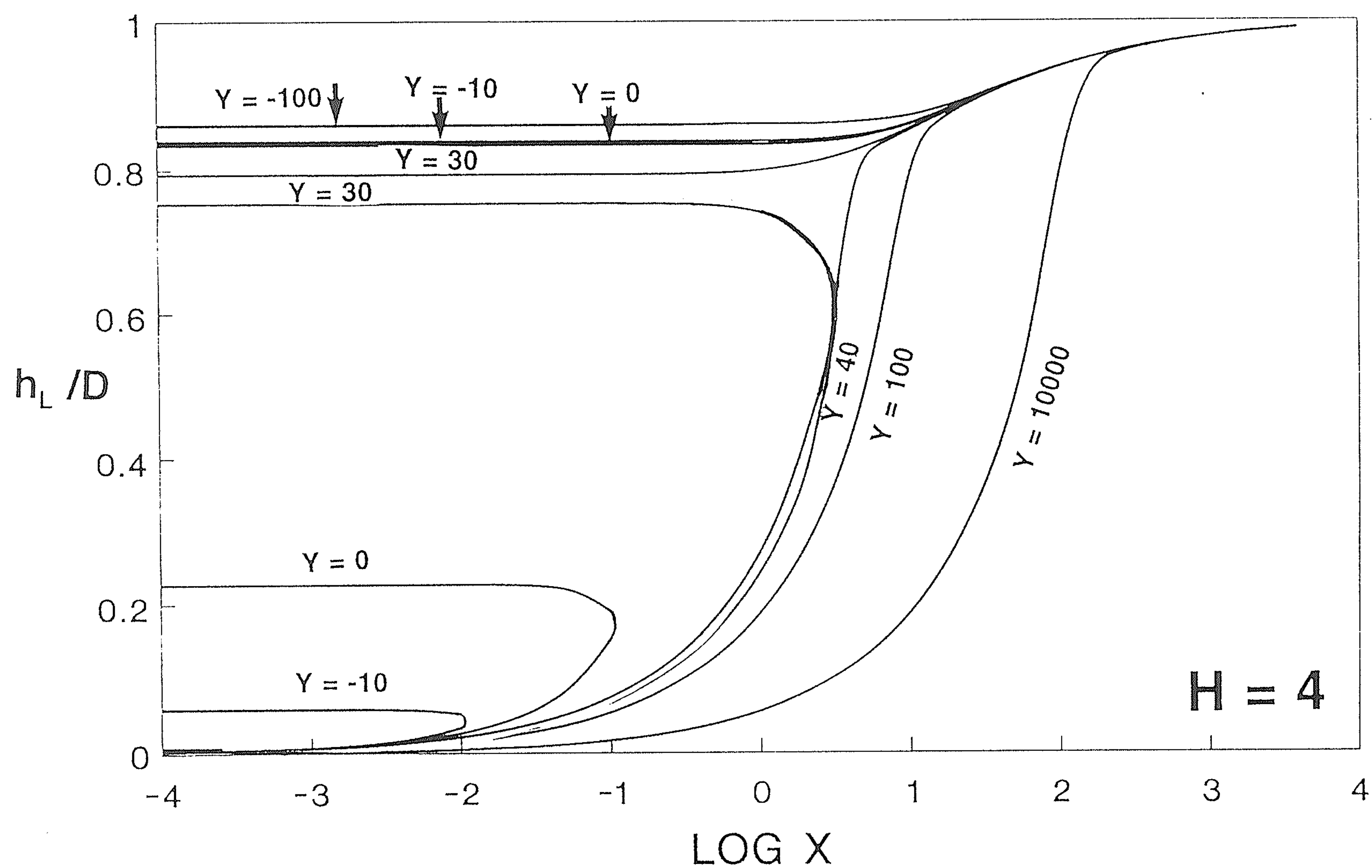

Figure 6.12 Equilibrium liquid level for H = 4.0

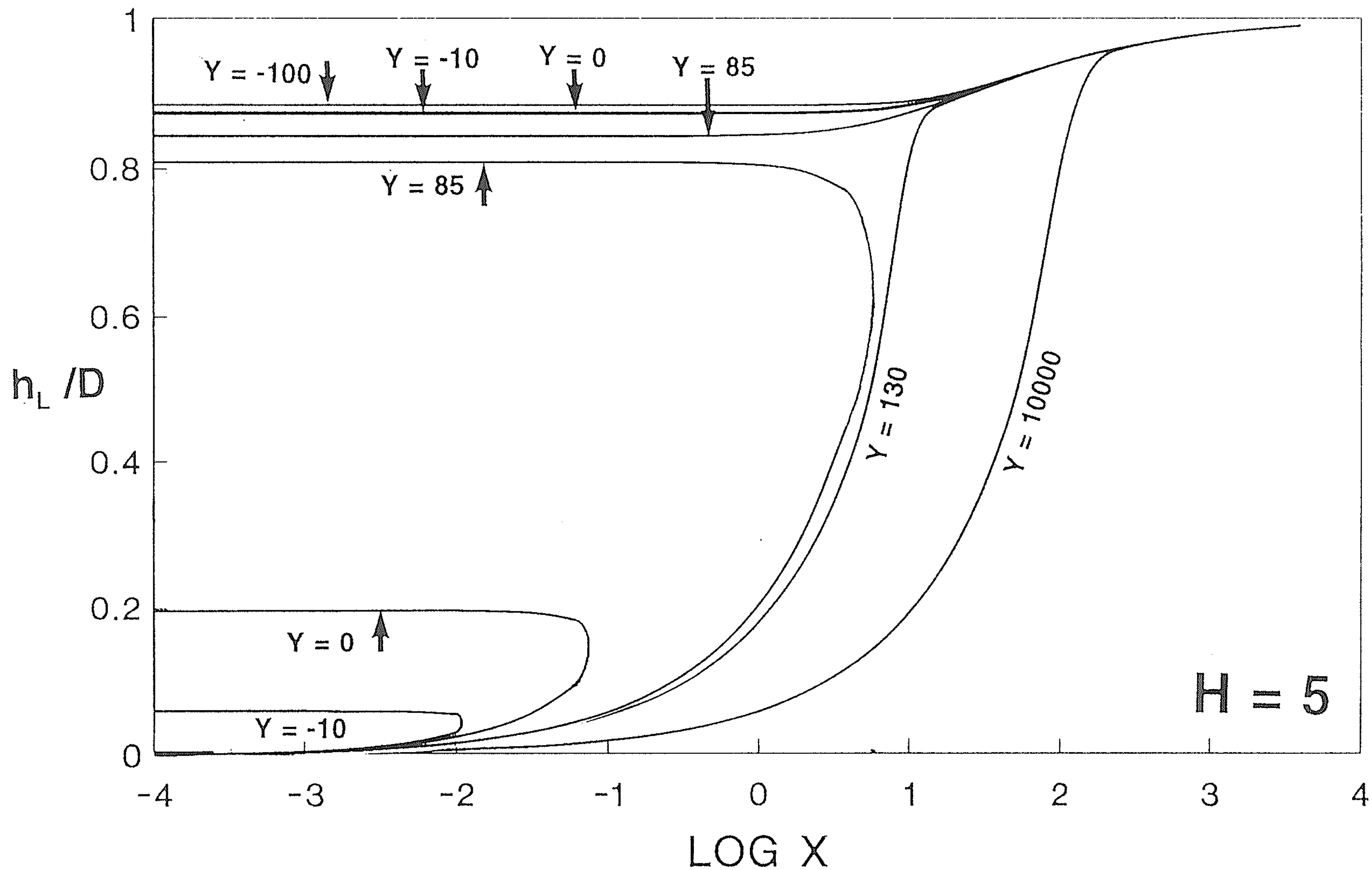

Figure 6.13 Equilibrium liquid level for H = 5.0

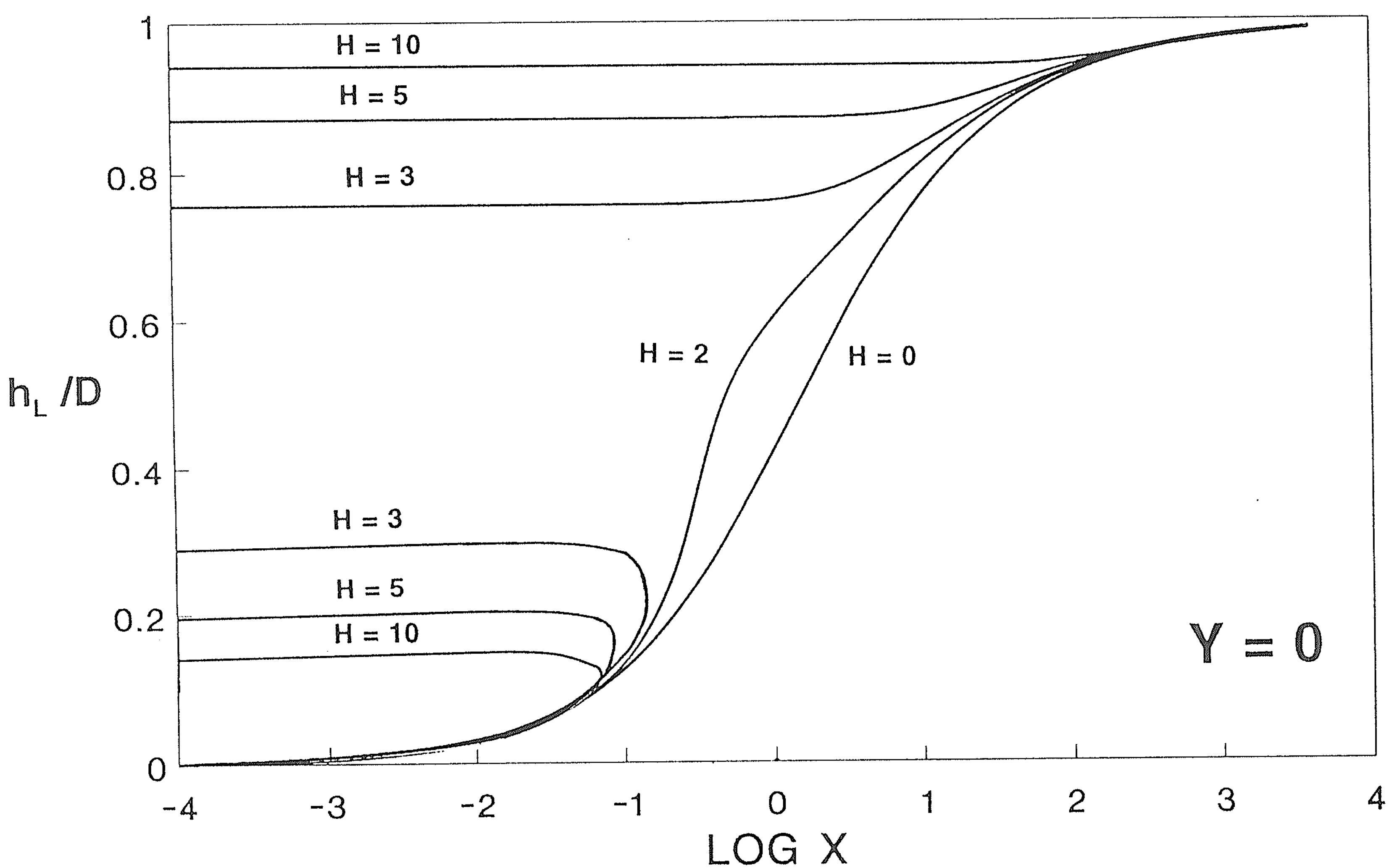

Figure 6.14 Equilibrium liquid level for Y = 0.

No attempt was made in this investigation to explain the physical meaning of having multiple values of h_L/D at the same flow parameters. It is possible that this mathematical behaviour is due to the assumed formulations of the wall and interfacial shear stresses, but does not have physical basis. This point was not explored further because the stratified-nonstratified boundary, which is the main objective of this analysis, was always found in the region where a unique solution existed.

6.3 Transition Criterion

The stratified-nonstratified transition criterion was applied by solving Equations (5.19), (5.20), (5.29), and (5.30) simultaneously. In order to demonstrate the trend in these results, the case of condensing steam [Figure 6.15] at a saturation temperature of 100°C in a tube with 25.4-mm I.D. using $\Delta T = 10°C$ is compared with the adiabatic case [Figure 6.16]. Both sets of results indicate that the stratified region shrinks in size as the upward inclination angle increases. This is consistent with the experimental results shown in Chapter 4, where the wavy flow regime was not observed in upward inclinations for $V_{LS} \geq 0.02$ m/s. Considering Figures 6.15 and 6.16 comparatively indicates that for large inclinations, e.g., $\theta = -5°$ and $-10°$, the transition line is not significantly influenced by condensation. However, at small inclinations [$-1° \leq \theta \leq 1°$], the deviation is obviously significant and it is consistent with the trend that condensation influences the transition line in a manner similar to the introduction of a small upward inclination in adiabatic flow.

6.4 Comparisons with Experimental Data

Comparisons were made between the present theory and the present flow-regime

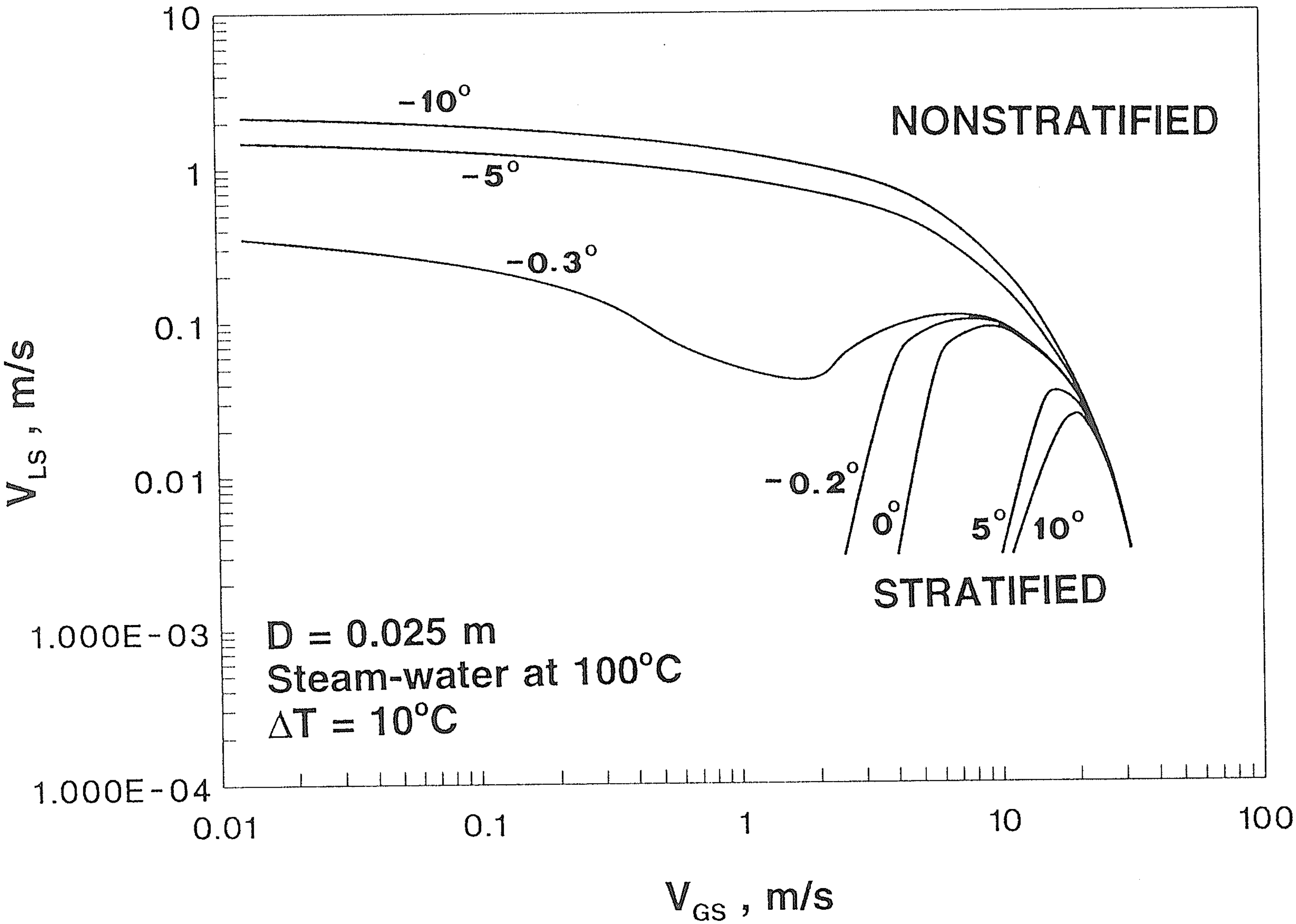

Figure 6.15 Effect of inclination on the transition line (condensation case).

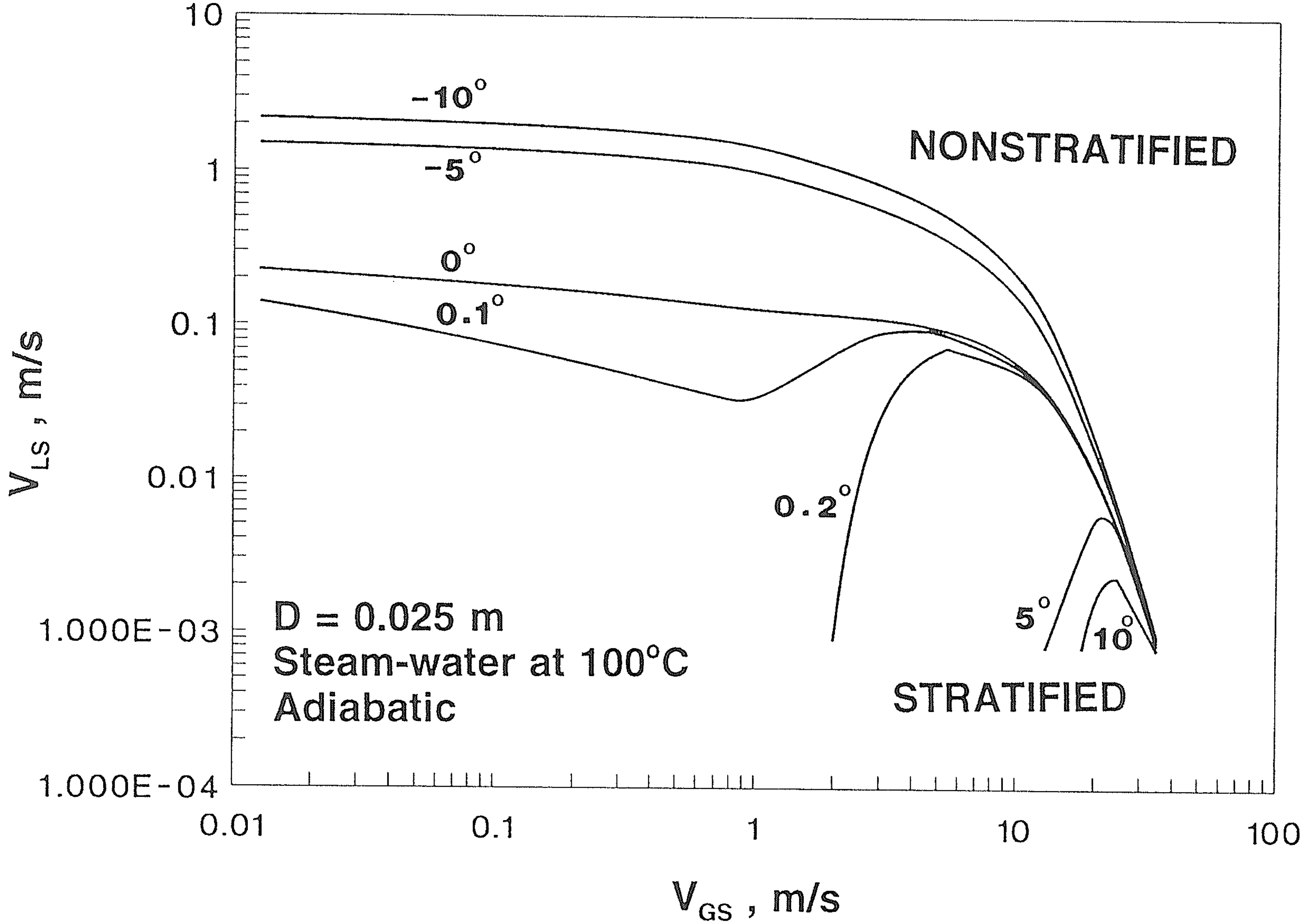

Figure 6.16 Effect of inclination on the transition line (adiabatic case).

data, as well as others available in the literature for condensation of different fluids inside tubes of different diameters. A sample of these results is shown in Figures 6.17 - 6.23 for horizontal and downward inclined tubes. For upward inclinations, the present data [which are the only available results] did not include wavy/stratified flow.

Figure 6.17 shows the comparison between the flow-regime data of Soliman and Azer (1974) for condensing R-12 inside a horizontal 12.7-mm I.D. condenser and the stratified- nonstratified transition line based on the present analysis. The calculations are made for a saturation temperature of 27.8°C and a saturation to wall temperature difference equal to 10°C. It is clear from the figure that the present theory predicts the boundary of the wavy-flow region very well, both at the annular-wavy and the wavy-slug transitions.

Figure 6.18 shows the comparison with the data for Rashwan (1987). In producing the transition line in this figure, the saturation to wall temperature difference was selected equal to 20°C. This is a reasonable value considering the saturation temperature of steam [100°C] and the average cooling water temperature [$\approx$ 50°C] used in Rashwan's experiment. After accounting for the thermal resistances of the cooling water and the tube wall, a reasonable estimate for ΔT was found to be about 20°C. The data correspond to a horizontal, 25.3-mm I.D. tube. Again, the stratified-nonstratified transition line predicts the data very well.

Figure 6.19 compares the data of Traviss and Rohsenow (1973) with the present analysis. These data were obtained with R-12 condensing at T_s = 27.8°C inside an 8-mm I.D. horizontal tube. The predictions are made with ΔT = 10°C. Traviss and Rohsenow

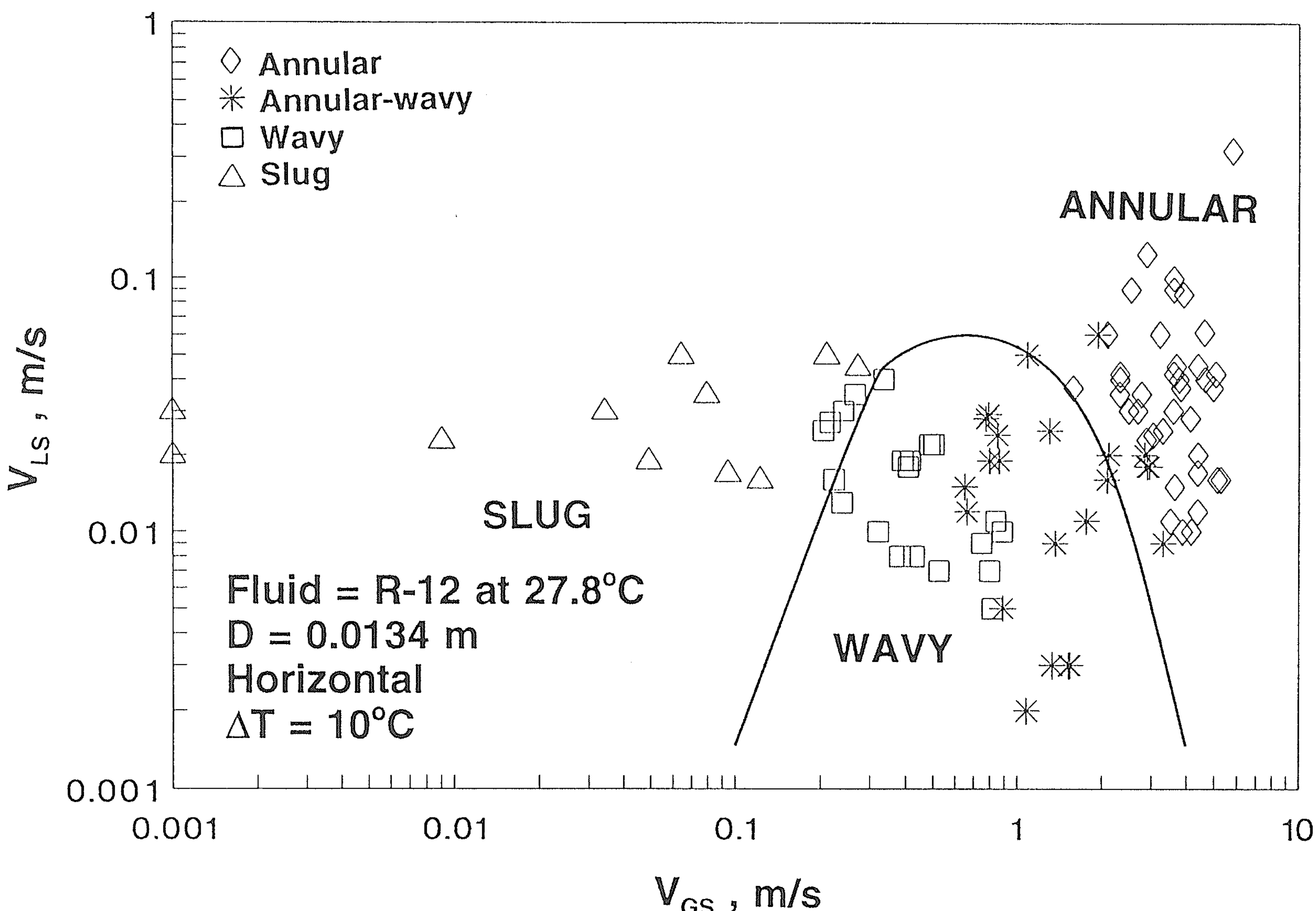

Figure 6.17 Comparison between the present theory and data of Soliman and Azer (1974) for refrigerant R-12.

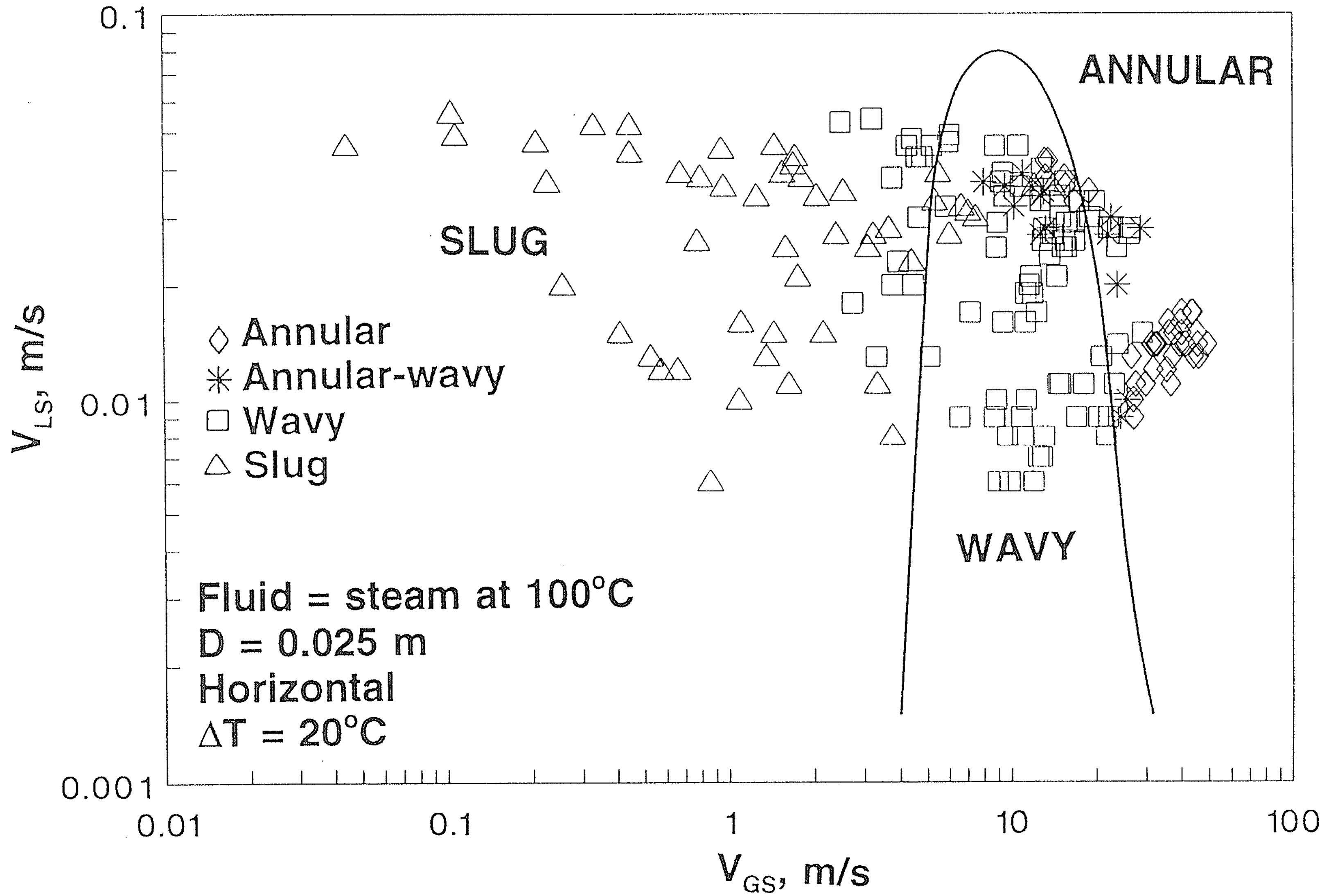

Figure 6.18 Comparisons between the present theory and data of Rashwan (1987).

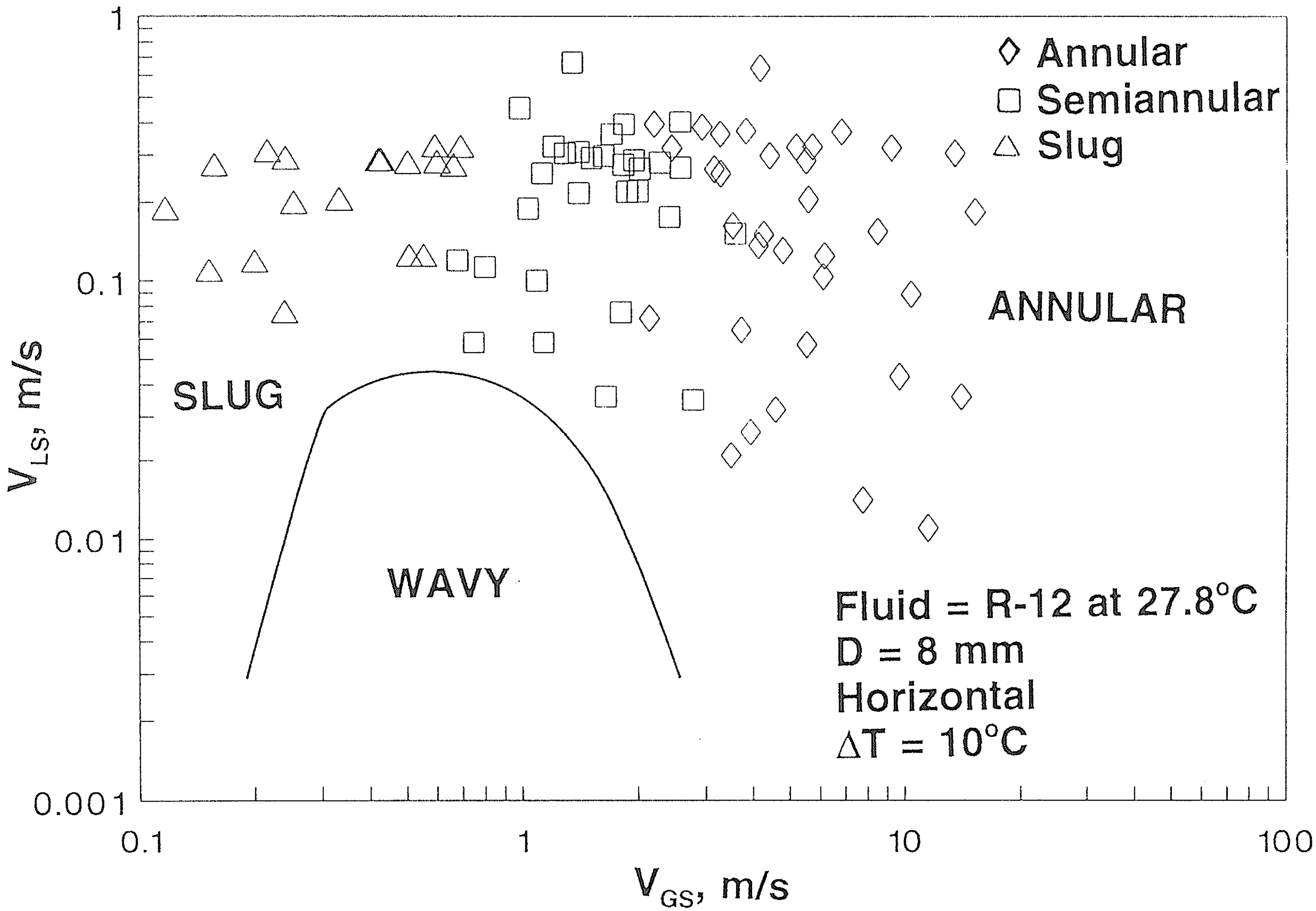

Figure 6.19 Comparisons between the present theory and data of Traviss and Rohsenow (1973).

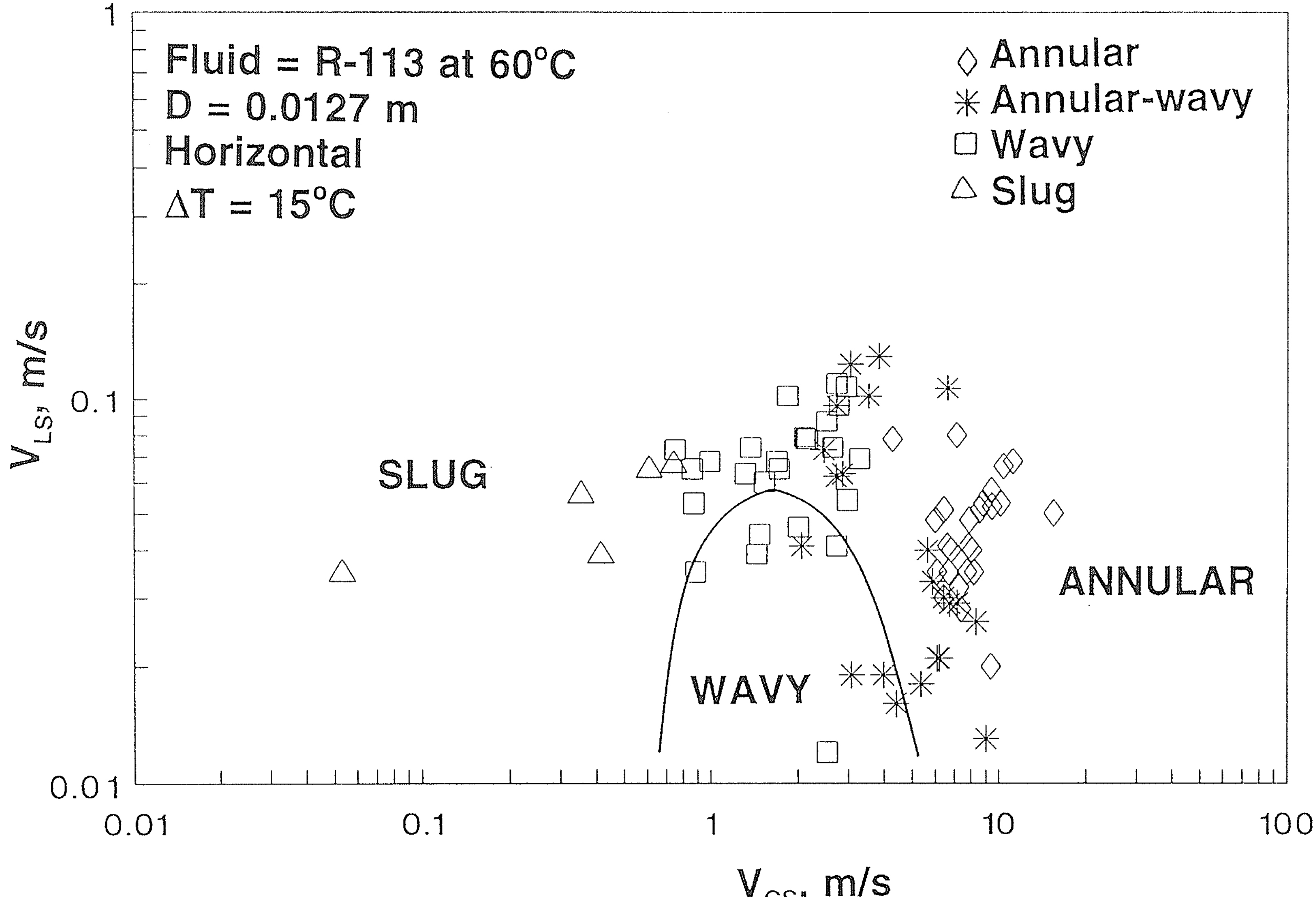

Figure 6.20 Comparison between the present theory and data of Soliman and Azer (1974).

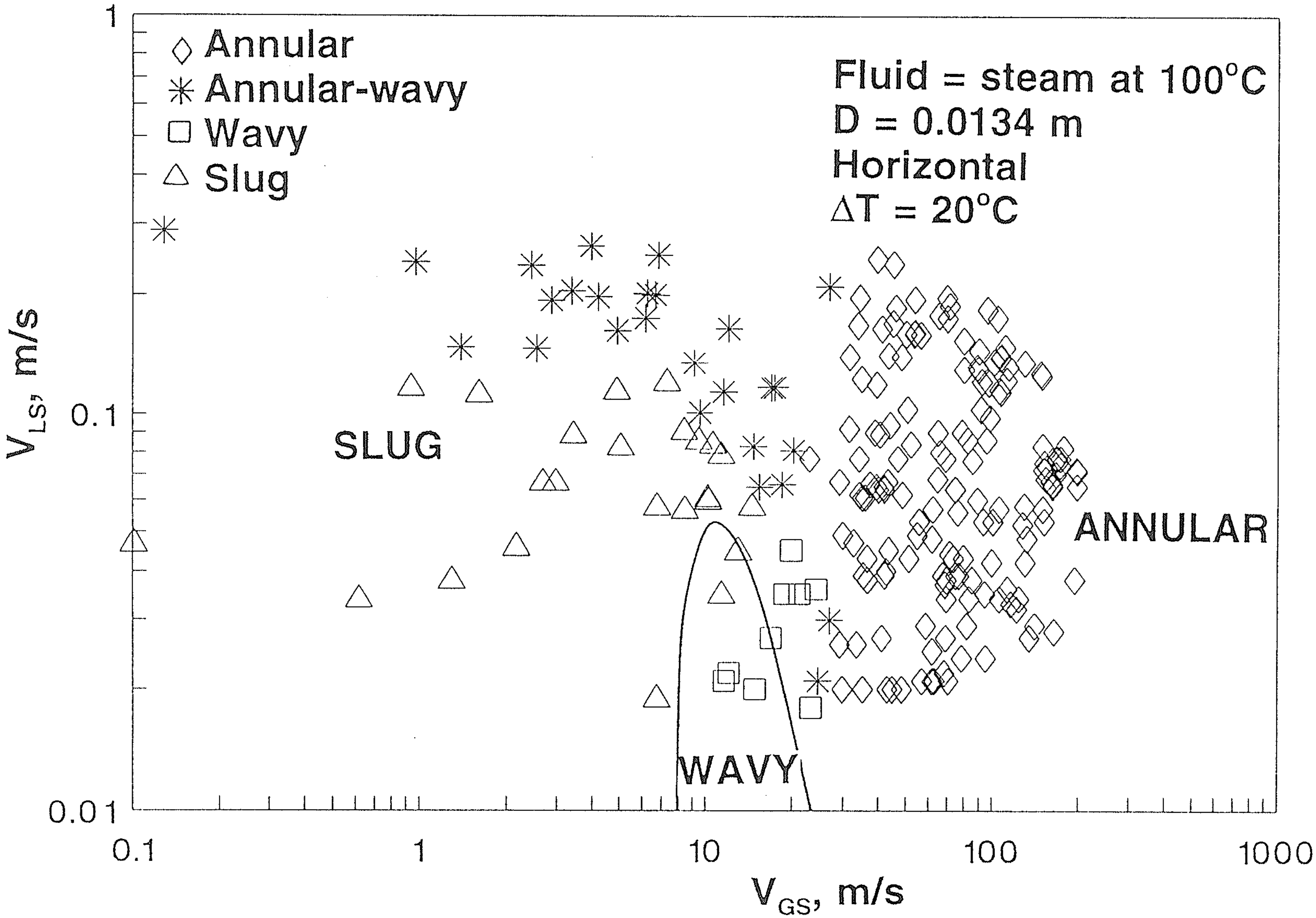

Figure 6.21 Comparison between the present theory and the present data of horizontal inclination.

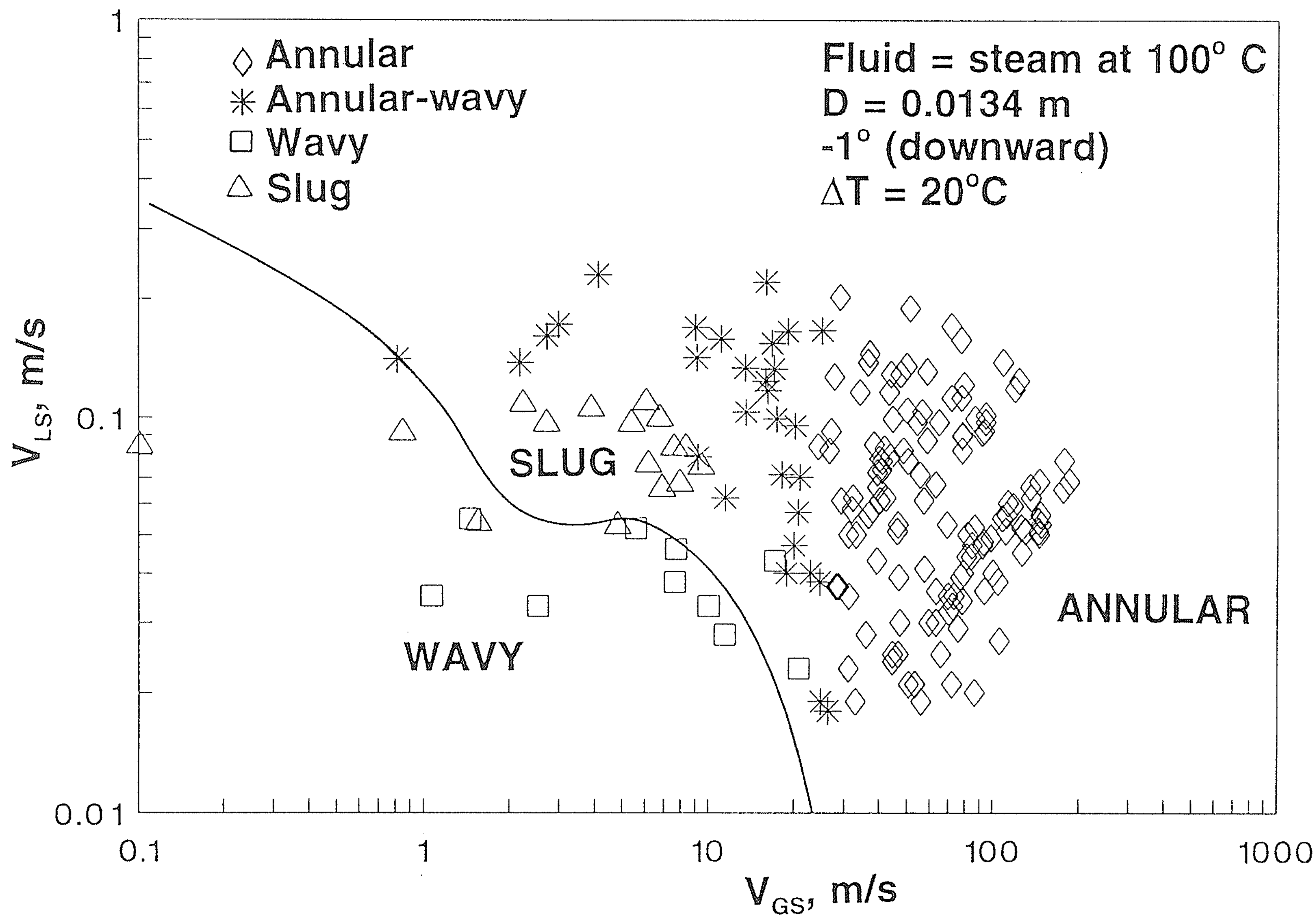

Figure 6.22 Comparison between the present theory and the present data of −1° [downward] inclination.

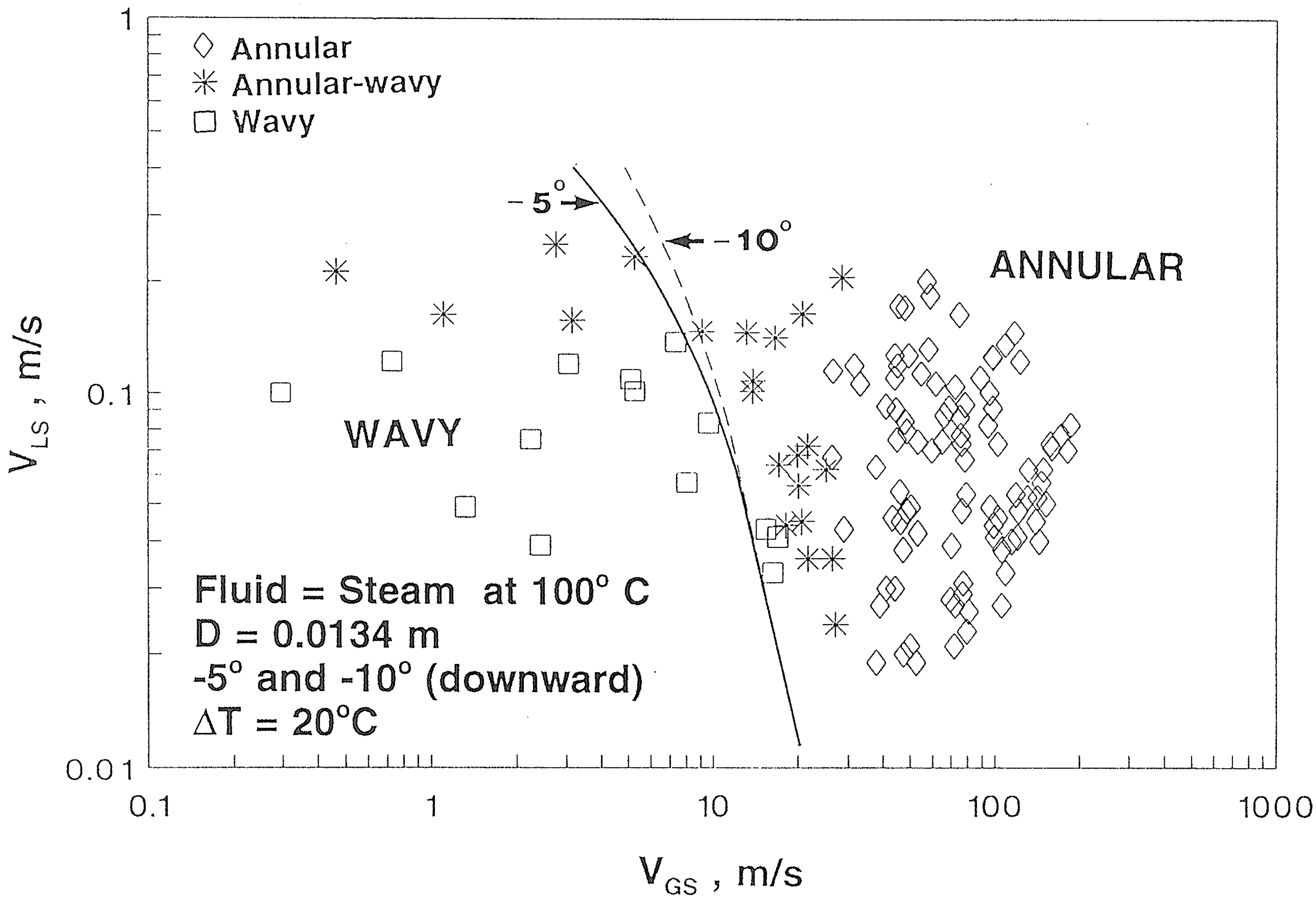

Figure 6.23 Comparison between the present theory and the present data of –5° and –10° [downward] inclination.

reported that wavy flow was not observed in their experiment and they only observed annular, semiannular, and slug flow. Figure 6.19 shows that the present theory is consistent with these observations.

Figure 6.20 compares the R-113 data of Soliman and Azer (1974) with the present analysis. In generating the transition line, a $\Delta T = 15°C$ was used. The data was obtained in a 12.7-mm I.D. horizontal tube. The transition is predicted reasonably well.

Figure 6.21 compares the present horizontal data and the transition line. A saturation to wall temperature difference equal to 20°C was used in the analysis. Although the transition line appears shifted to the left, the agreement is considered fair in view of the fact that the trend of the data is very well predicted. Figure 6.22 compares the present data at $-1°$ [downward] inclination with the analytical prediction. Although a few data points in the region $V_{GS} < 1$ m/s are inadequately predicted, the agreement is considered reasonably good. Excellent agreement is shown in Figure 6.23 between the present combined data of $-5°$ and $10°$ [downward] inclination and the analysis. The experimental data and theory are also in agreement with the trend whereby changing the inclination from $-5°$ and $10°$ does not significantly influence the stratified-flow boundary.

It is fair to conclude from the above comparisons that the present theory for predicting the stratified-nonstratified boundary is in fairly good agreement with a wide range of experimental data.

Chapter 7

CONCLUSIONS

An experimental investigation has been conducted in order to study the effect of inclination on the two-phase flow regimes of condensing flow inside a tube. The data correspond to steam at a mean saturation temperature of about 110°C condensing inside a 13.4-mm I. D. tube with inclination angles within ±10°. Inside this range of inclination angles, the annular flow regime boundary experiences very small [almost insignificant] shifts. On the other hand, small inclinations of only 1° [upward or downward] from the horizontal resulted in significant changes in the wavy and slug regions. Wavy flow is more prominent in downward inclinations and slug flow is more prominent in upward inclinations. The shifts in the transition boundaries due to changes in the inclination angle from 5° to 10° are found to be insignificant.

The existence of slug flow was found to coincide always with the full-tube condition at exit. If the tube was not running full at the end of the condensation path, i.e. stratified conditions at exit, slugging was not observed. Beyond a certain mass flux, which was found to be independent of inclination, slugging was not observed and the flow regime progressed from annular to annular-wavy to complete condensation with full tube. This upper bound on slugging during condensation was analyzed and the resulting simple correlation agreed well with the present data.

Comparisons with some of the available gas-liquid correlations suggested that for small inclinations [e.g., ±1°], the present results for a given angle are consistent in trend with those of gas-liquid flow with slight upward inclination added to the given angle. This is attributed to the increasing liquid height along the condenser. For larger angles [e.g., 5° and 10°], the present data agreed reasonably well in magnitude and trend with the gas-liquid correlation of Taitel and Dukler (1976).

A mechanistic model has been developed for the evaluation of the equilibrium liquid level during condensation inside horizontal and slightly inclined tubes. Basic conservation equations of mass, momentum, and energy have been applied on a differential control volume. Two possible formulations were developed; a complete and a simplified versions. The resulting values of h_L/D from the two versions were compared at different inclinations and mass flow rates. Very good agreement was obtained, particularly at large mass flow rates and large qualities for all inclinations tested. The location where transition took place was found to be in the region where there was excellent agreement between the two methods. Therefore, the simplified method was utilized in predicting the equilibrium liquid levels in this study.

Using the simplified method, equilibrium liquid levels for different values of the heat transfer parameter H were generated. These curves qualitatively show that inclining the tube upward in adiabatic gas-liquid flow [decreasing the parameter Y] is equivalent to increasing the heat transfer parameter H. This is consistent with the condensing flow experimental observations.

A stratified [wavy] to nonstratified regime transition criterion for condensing flows was developed using a force balance on a finite amplitude wave. The stratified [wavy] transition boundary predicted by the proposed model was compared with different data sets. It is shown that the present theory is capable of good agreement with experimental data in magnitude and trend.

REFERENCES

Baker, O., "Simultaneous Flow of Oil and Gas", Oil and Gas J., **53**, 185-195 (1954).

Barnea, D., "Transition From Annular and From Dispersed Bubble Flow - Unified Models for the Whole Range of Pipe Inclinations", Int. J. Multiphase Flow, **12**, 733-744 (1986).

Barnea, D., "A Unified Model for Predicting Flow-Pattern Transitions for the Whole Range of Pipe Inclinations", Int. J. Multiphase Flow, **13**, 1-12 (1987).

Barnea, D., O. Shoham and Y. Taitel, "Flow Pattern Transition for Downward Inclined Two Phase Flow; Horizontal to Vertical", Chem. Eng. Sci., **37**, 735-740 (1982).

Barnea, D., O. Shoham and Y. Taitel, "Gas-Liquid Flow in Inclined Tubes: Flow Pattern Transitions for Upward Flow", Chem. Eng. Sci., **40**, 131-136 (1985).

Barnea, D., and Y. Taitel, "Flow Pattern Transition in Two-Phase Gas-Liquid Flow", *Encyclopedia of Fluid Mechanics,* Chapter 16, 403-474 (1986).

Bell, K. J., J. Taborek and F. Fenoglio, "Interpretation of Horizontal In-Tube Condensation Heat Transfer Correlations with a Two-Phase Flow Regime Map", AIChE Symp. Ser. No. 102, **66,** 150-163 (1970).

Benjamin, T. B., "Gravity Currents and Related Phenomena", J. Fluid Mech., **31**, Part 2, 209-248 (1968).

Brauner, N., and D. M. Maron, "Analysis of Stratified/Nonstratified Transitional Boundaries in Horizontal Gas-Liquid Flows", Chem. Eng. Sci.,**46**, 1849-1859 (1991).

Breber, G., J. W. Palen and J. Taborek, "Prediction of Horizontal Tubeside Condensation of Pure Components Using Flow Regime Criteria", J. Heat Transfer, **102**, 471-476 (1980).

Chen, J. J. J., "A simple Explicit Formula for the Estimation of Pipe Friction Factor", Proc. Instn. Civil Engrs. Part 2, Technical Note 400, **77**, 49-55 (1984).

Collier, J. G., *"Convective Boiling and Condensation"*, 2nd Edition, McGraw-Hill, New York (1981).

Crawford, T. J., C. B. Weinberger and J. Weisman, "Two-Phase Flow Patterns and Void Fractions in Downward Flow, Part I: Steady-State Flow Patterns", Int. J. Multiphase Flow, **11**, 761-782 (1985).

Dukler, A. E., "Modelling Two Phase Flow and Heat Transfer", Proc. Sixth Int. Heat Transfer Conf., Vol. 6, Toronto, Canada, 541-557 (1978).

Ellis, S. R. M. and Gay, B., "The Parallel Flow of Two Fluid Streams: Interfacial Shear and Fluid-Fluid Interaction", Trans. Instn. Chem. Engrs., **37**, 206 (1959).

Fathi, A. M., "Analysis of Two-Phase Flow Patterns of Condensing Steam Inside a Horizontal Tube", M. Sc. thesis, University of Manitoba, Winnipeg, Canada (1980).

Fuji, T., H. Honda, T. Nagata, F. Fujii and S. Nozu, "Condensation of R-11 Inside a Horizontal Tube", Trans. JSME, **42**, 3541-3550 (1976).

Govier, G. W. and M. M. Omar, "The Horizontal Pipeline Flow of Air-Water Mixtures", Can. J. Chem. Eng., **40**, 93-104 (1962).

Gupta, C. P., H. K. Varma and T. N. Tandon, "Flow Regime Mapping for Condensation Inside Horizontal Tubes", *Handbook of Heat and Mass Transfer*, Chapter 22, 719-746 (1986).

Hancox, W. T. and W. B. Nicoll, "Prediction of Time-dependent Diabatic Two-phase Water Flows", *Progress in Heat and Mass Transfer* (edited by Hetsroni, G., Sideman, S. and Hartnett, J. P.), Vol. 6, 119-135, Pergamon Press, Oxford (1971).

Hoogendoorn, C. J., "Gas-Liquid Flow in Horizontal Pipes", Chem. Eng. Sci., **9**, 205-218 (1959).

Kokal, S. L. and J. F. Stanislav, "An Experimental Study of Two-Phase Flow in Slightly Inclined Pipes - I. Flow Patterns", Chem. Eng. Sci., **44**, 665-679 (1989).

Landman, M. J., "Non-Unique Holdup and Pressure Drop in Two-Phase Stratified Inclined Pipe Flow", Int. J. Multiphase Flow, **17**, 377-394 (1991).

Mandhane, J. M., G. A. Gregory and K. Aziz, "A Flow Pattern Map for Gas-Liquid Flow in Horizontal Pipes", Int. J. Multiphase Flow, **1**, 537-553 (1974).

Moffat, R. J., "Describing the Uncertainties in Experimental Results", Experimental Thermal and Fluid Science, **1**, 3-17 (1988).

Mukherjee, H. and J. P. Brill, "Empirical Equations to Predict Flow Patterns in Two-Phase Inclined Flow", Int. J. Multiphase Flow, **11**, 299-315 (1985).

Nitheanandan, T. , H. M. Soliman and R. E. Chant, "A Proposed Approach for Correlating Heat Transfer During Condensation Inside Tubes", ASHRAE Trans., **96, Part I,** 230-241 (1990).

Rahman, M. M., "Two-Phase Flow Patterns of Condensing Steam Inside a Horizontal Tube with Emphasis on the Wavy to Slug Transition", M. Sc. thesis, University of Manitoba, Winnipeg, Canada (1983).

Rahman, M. M., A. M. Fathi and H. M. Soliman,"Flow Pattern Prediction Boundaries During Condensation: New Experimental Data", Can. J. Chem. Eng., **63,** 547-552 (1985).

Rashwan, F. A., "Onset of Slugging During Horizontal Condensation: Experimental and Analytical Investigations", Ph. D. thesis, University of Manitoba, Winnipeg, Canada (1987).

Rashwan, F. A. and H. M. Soliman, "The Onset of Slugging in Horizontal Condensers", Can. J. Chem. Eng., **65**, 887-898 (1987).

Sardesai, R. G., R. G. Owen and D. J. Pulling, "Flow Regimes for Condensation of a Vapor Inside a Horizontal Tube", Chem. Eng. Sci., **36,** 1173-1180 (1981).

Soliman, H. M., "On the Annular-to-Wavy Flow Pattern Transition During Condensation Inside Horizontal Tubes", Can. J. Chem. Eng., **60**, 475-481 (1982).

Soliman, H. M., "Correlation of Mist-to-Annular Transition During Condensation", Can. J. Chem. Eng., **61**, 178-182 (1983).

Soliman, H. M., "Flow Pattern Transitions During Horizontal In-Tube Condensation", *Encyclopedia of Fluids Mechanics*, Chapter 22, 629-650 (1986).

Soliman, H. M. and N. Z. Azer, "Flow Patterns During Condensation Inside a Horizontal Tube", ASHRAE Trans., **77, Part I,** 210-224 (1971).

Soliman, H. M. and N. Z. Azer, "Visual Studies of Flow Patterns During Condensation Inside Horizontal Tubes", Proc. Fifth Int. Heat Transfer Conf., **Vol. 3,** Tokyo, Japan, 241 - 245 (1974).

Taitel, Y. and A. E. Dukler, "A Model for Predicting Flow Regime Transitions in Horizontal and Near Horizontal Gas-liquid Flow", AIChE J., **22,** 47-55 (1976).

Taitel, Y., D. Barnea and A. E. Dukler, "Modelling Flow Pattern Transitions for Steady Upward Gas-Liquid Flow in Vertical Tubes", AIChE J., **26**, 345-354 (1980).

Tandon, T. N., H. K. Varma and C. P. Gupta, "An Experimental Study of Flow Patterns During Condensation Inside a Horizontal Tube", ASHRAE Trans., **89, Part 2,** 471-482 (1983).

Traviss, D. P. and W. M. Rohsenow, "Flow Regimes in Horizontal Two-phase Flow with Condensation", ASHRAE Trans., **79, Part 2,** 31-39 (1973).

Wallis, G. B., "*One-Dimensional Two Phase Flow*", McGraw-Hill, New York (1969).

Wallis, G. B., C. J. Crawley and Y. Hagi, "Condition for a Pipe to Run Full When Discharging a Liquid into a Space Filled With Gas", J. Fluid Eng., **99**, 405-413 (1977).

Weisman, J., D. Duncan, J. Gibson and T. J. Crawford, "Effects of Liquid Properties and Pipe Diameter on Two-Phase Flow Patterns in Horizontal Lines", Int. J. of Multiphase Flow, **5**, 437-462 (1979).

Weisman, J. and S. Y. Kang, "Flow Pattern Transitions in Vertical and Upwardly Inclined Lines", Int. J. Multiphase Flow, **7**, 271-291 (1981).

Yadigaroglu, G. and R. T. Lahey, "On the Various Forms of the Conservation Equations in Two-phase Flow", Int. J. Multiphase Flow, **2**, 477-494 (1976).

Appendix A

OPERATING CONDITIONS AND HEAT BALANCE

This appendix lists the operating conditions for the seven data sets corresponding to the horizontal, and +1°, +5°, +10°, -1°, -5°, and -10° inclinations. For each test run, the values of the operating pressure P_{av}, corresponding saturation temperature $T_{s,\,av}$, total mass flux G, rate of heat lost by steam Q_S, rate of heat gained by cooling water Q_W, and the percentage heat balance error are listed. The percentage heat balance error is given by

$$Error\ \% = \frac{Q_S - Q_W}{Q_S} \times 100$$

TABLE A.1 Operating conditions for data in the horizontal position

Run number	P_{av} kPa	$T_{s,av}$ °C	G kg/s.m^2	Q_s kW	Q_w kW	Error %
1	124.6	105.9	123.86	43.42	41.58	4.2
2	124.6	105.9	123.86	43.35	42.70	1.5
3	138.1	108.9	158.84	54.59	52.02	4.7
4	170.2	115.2	225.14	79.03	76.09	3.7
5	170.2	115.2	254.60	90.62	87.31	3.7
6	131.4	107.5	134.91	49.51	49.82	-0.6
7	186.4	118.0	105.44	38.26	40.26	-5.2
8	134.7	108.2	186.47	66.25	62.58	5.5
9	106.6	101.5	86.72	31.36	32.14	-2.5
10	101.5	100.1	50.41	18.46	18.11	1.9
11	105.0	101.0	45.82	16.81	16.50	1.8
12	102.1	100.2	37.48	13.73	13.98	-1.9
13	105.5	101.2	43.32	15.89	16.18	-1.8
14	119.1	104.6	88.80	32.31	33.96	-5.1
15	104.7	100.9	55.42	20.28	20.03	1.2
16	104.7	100.9	44.99	16.48	16.60	-0.8
17	108.0	101.8	65.44	23.99	23.51	2.0
18	101.8	100.2	32.89	12.07	12.78	-5.9
19	101.8	100.2	34.97	12.80	12.81	-0.1
20	99.9	99.6	21.85	7.98	7.80	2.2
21	103.2	100.6	40.40	14.74	14.32	2.9
22	106.7	101.5	47.08	17.12	16.57	3.2
23	102.4	100.3	31.64	11.53	12.02	-4.3
24	104.1	100.8	49.16	17.87	16.81	6.0
25	102.4	100.3	44.99	16.37	15.73	3.9
26	107.5	101.7	63.77	23.12	22.49	2.7
27	107.5	101.7	59.59	21.60	22.51	-4.2
28	107.5	101.7	64.60	23.34	22.44	3.8
29	108.2	101.9	59.59	21.57	20.47	5.1
30	113.3	103.2	66.27	24.13	23.46	2.8
31	116.3	103.9	75.87	27.36	27.16	0.7
32	112.9	103.1	65.02	23.57	24.07	-2.1
33	116.3	103.9	72.53	26.27	27.20	-3.5
34	118.1	104.4	82.54	30.03	30.27	-0.8
35	117.5	104.2	82.96	30.07	28.91	3.8
36	119.2	104.6	84.63	30.45	28.46	6.5
37	117.5	104.2	89.22	32.08	29.63	7.6
38	117.5	104.2	88.80	32.32	30.85	4.5
39	109.0	102.1	90.71	32.70	31.30	4.3
40	111.1	102.6	81.50	29.62	30.58	-3.2
41	111.1	102.6	87.03	31.59	30.13	4.6
42	117.9	104.3	105.44	37.81	35.19	6.9
43	114.5	103.5	96.23	34.55	32.21	6.8
44	111.1	102.6	88.87	32.23	30.71	4.7
45	111.1	102.6	92.55	33.62	31.56	6.1
46	181.6	117.2	273.02	92.84	90.35	2.7
47	181.6	117.2	273.02	93.05	90.56	2.7
48	168.1	114.8	236.19	83.39	83.02	0.4
49	164.7	114.2	245.39	86.14	87.21	-1.2
50	140.6	109.5	190.15	67.21	67.68	-0.7
51	160.8	113.5	230.66	80.74	82.54	-2.2

TABLE A.1 Operating conditions for data in the horizontal position (cont'd.)

Run number	P_{av} kPa	$T_{s,av}$ °C	G kg/s.m^2	Q_s kW	Q_w kW	Error %
52	144.0	110.2	197.52	68.82	69.18	-0.5
53	157.5	112.9	217.77	74.87	74.47	0.5
54	147.1	110.8	215.93	76.01	75.96	0.1
55	143.7	110.1	197.52	69.21	71.91	-3.9
56	143.7	110.1	199.36	70.24	72.36	-3.0
57	153.9	112.2	226.98	80.45	82.19	-2.2
58	140.9	109.5	195.67	69.48	67.79	2.4
59	137.5	108.8	171.73	60.51	61.09	-0.9
60	127.4	106.6	166.21	59.12	54.89	7.2
61	120.6	105.0	116.49	41.98	39.43	6.1
62	120.6	105.0	120.17	43.14	41.14	4.6
63	138.4	109.0	191.99	67.73	63.89	5.7
64	124.9	106.0	134.91	48.02	47.46	1.2
65	124.9	106.0	142.27	50.72	49.51	2.4
66	118.1	104.4	109.13	39.03	37.93	2.8
67	118.1	104.4	112.81	40.12	39.30	2.0
68	119.3	104.7	112.81	40.19	40.55	-0.9
69	124.4	105.9	142.27	50.24	50.75	-1.0
70	102.8	100.4	27.16	10.07	10.40	-3.3
71	102.8	100.4	27.75	10.27	10.69	-4.1
72	102.8	100.4	28.34	10.54	10.75	-2.0
73	102.8	100.4	35.81	13.32	13.29	0.2

TABLE A.2 Operating conditions for data in -1^0 [downward] inclination

Run number	P_{av} kPa	$T_{s,av}$ °C	G kg/s.m^2	Q_s kW	Q_w kW	Error %
1	105.4	101.1	53.33	19.15	20.48	-6.9
2	105.4	101.1	53.33	18.98	18.34	3.3
3	106.9	101.5	51.67	18.42	18.17	1.3
4	106.9	101.5	50.41	18.02	17.89	0.7
5	106.9	101.5	51.67	18.50	17.84	3.6
6	106.9	101.5	49.16	17.67	17.85	-1.0
7	103.8	100.7	37.90	13.72	14.16	-3.3
8	103.8	100.7	41.23	14.94	15.35	-2.7
9	103.8	100.7	33.72	12.24	12.84	-4.9
10	102.1	100.2	32.89	11.91	12.47	-4.6
11	102.1	100.2	34.14	12.38	12.92	-4.4
12	102.1	100.2	34.14	12.41	12.48	-0.6
13	106.2	101.3	52.92	19.16	20.02	-4.5
14	106.2	101.3	53.33	19.28	19.89	-3.2
15	102.8	100.4	57.51	20.87	20.20	3.2
16	102.8	100.4	52.08	18.79	19.52	-3.9
17	116.4	104.0	68.77	24.87	25.37	-2.0
18	111.3	102.7	66.69	24.30	25.52	-5.0
19	113.0	103.1	70.03	25.32	25.27	0.2
20	113.0	103.1	67.94	24.58	25.02	-1.8
21	117.1	104.1	81.29	29.64	31.04	-4.7
22	118.8	104.6	81.71	29.72	30.94	-4.1
23	115.4	103.7	85.47	31.14	30.95	0.6
24	118.8	104.6	80.46	28.97	29.82	-2.9
25	112.6	103.0	76.29	27.87	28.60	-2.6
26	116.0	103.9	78.37	28.61	27.91	2.4
27	116.0	103.9	77.95	28.38	27.74	2.3
28	109.2	102.1	80.46	29.11	28.52	2.0
29	113.5	103.2	96.23	35.03	33.97	3.0
30	110.1	102.4	88.87	32.59	31.62	3.0
31	113.5	103.2	96.23	34.98	34.44	1.5
32	110.1	102.4	99.92	36.50	36.04	1.3
33	109.3	102.2	96.23	35.20	33.84	3.9
34	109.3	102.2	94.39	34.48	33.03	4.2
35	106.0	101.3	85.19	31.18	30.55	2.0
36	112.8	103.1	123.86	45.38	46.64	-2.8
37	116.1	103.9	129.38	46.91	47.55	-1.4
38	116.1	103.9	136.75	49.89	48.01	3.8
39	114.4	103.5	133.06	48.62	48.19	0.9
40	109.2	102.1	103.60	37.86	37.98	-0.3
41	109.2	102.1	105.44	38.33	37.42	2.4
42	112.6	103.0	105.44	38.26	37.94	0.8
43	109.2	102.1	105.44	38.43	38.86	-1.1
44	112.6	103.0	122.02	44.18	42.26	4.3
45	124.2	105.8	142.27	50.98	49.10	3.7
46	124.2	105.8	134.91	48.43	49.03	-1.2
47	120.8	105.0	138.59	49.87	49.89	0.0
48	120.8	105.0	140.43	50.48	49.10	2.7
49	127.6	106.6	158.84	57.00	55.46	2.7
50	125.9	106.2	158.84	57.22	57.27	-0.1
51	131.0	107.4	158.84	56.61	55.62	1.8

TABLE A.2 Operating conditions for data in -1^0 [downward] inclination (cont'd.)

Run number	P_{av} kPa	$T_{s,av}$ °C	G kg/s.m^2	Q_s kW	Q_w kW	Error %
52	127.6	106.6	155.16	55.55	55.58	-0.1
53	139.0	109.1	171.73	60.87	59.70	1.9
54	138.1	108.9	168.05	59.73	61.16	-2.4
55	132.2	107.7	166.21	59.22	59.61	-0.7
56	133.9	108.0	177.26	63.59	62.28	2.1
57	149.0	111.2	223.30	79.01	74.70	5.5
58	147.3	110.9	223.30	79.27	75.83	4.3
59	154.1	112.2	217.77	76.87	74.28	3.4
60	111.4	102.7	103.60	37.58	37.18	1.1
61	113.1	103.1	107.28	38.86	38.82	0.1
62	108.0	101.8	109.13	39.71	38.65	2.7
63	109.8	102.3	99.92	36.50	35.02	4.1

TABLE A.3 Operating conditions for data in -5^0 [downward] inclination

Run number	P_{av} kPa	$T_{s,av}$ °C	G kg/s.m^2	Q_s kW	Q_w kW	Error %
1	111.7	102.8	66.69	24.23	23.04	4.9
2	116.8	104.1	76.70	27.81	27.09	2.6
3	111.8	102.8	77.54	28.19	27.39	2.8
4	116.9	104.1	85.47	30.95	29.46	4.8
5	113.4	103.2	96.23	34.37	33.08	3.7
6	125.0	106.0	136.75	48.08	48.60	-1.1
7	125.0	106.0	136.75	48.76	51.52	-5.7
8	118.3	104.4	112.81	40.59	42.83	-5.5
9	121.6	105.2	116.49	41.39	42.38	-2.4
10	130.1	107.2	147.80	52.48	55.50	-5.8
11	126.7	106.4	153.32	54.63	54.69	-0.1
12	142.0	109.7	173.58	61.00	62.32	-2.2
13	133.5	107.9	173.58	61.62	62.58	-1.6
14	147.0	110.8	219.61	76.90	70.65	8.1
15	148.1	111.0	203.04	72.12	75.05	-4.1
16	148.1	111.0	203.04	72.09	74.75	-3.7
17	153.6	112.1	241.71	85.39	86.97	-1.9
18	156.2	112.6	226.98	80.09	80.26	-0.2
19	119.1	104.6	122.02	43.49	44.75	-2.9
20	117.3	104.2	116.49	41.45	41.96	-1.2
21	106.5	101.4	99.92	35.68	36.08	-1.1
22	111.0	102.6	72.11	26.22	27.87	-6.3
23	111.0	102.6	73.36	26.74	26.52	0.8
24	118.7	104.5	83.38	30.32	31.05	-2.4
25	122.1	105.3	82.54	30.00	30.99	-3.3
26	115.1	103.6	123.86	44.73	43.78	2.1
27	115.1	103.6	127.54	46.14	45.34	1.7
28	118.5	104.5	149.64	53.88	53.46	0.8
29	131.7	107.5	147.80	52.37	56.12	-7.2
30	123.9	105.8	157.00	56.11	57.10	-1.8
31	131.7	107.5	149.64	53.08	55.87	-5.3
32	111.5	102.7	105.44	38.26	40.94	-7.0
33	113.2	103.2	105.44	38.26	40.49	-5.8
34	113.2	103.2	107.28	38.93	40.08	-2.9
35	103.6	100.6	49.16	17.98	18.05	-0.4
36	108.7	102.0	60.01	21.99	22.56	-2.6
37	102.7	100.4	47.49	17.28	17.21	0.4
38	102.7	100.4	39.15	14.34	14.15	1.4
39	102.7	100.4	53.33	19.43	20.61	-6.0
40	102.7	100.4	55.42	20.19	21.26	-5.3
41	102.8	100.4	41.23	14.99	15.33	-2.2
42	102.8	100.4	50.00	18.11	18.67	-3.1
43	102.8	100.4	50.41	18.32	18.92	-3.3

TABLE A.4 Operating conditions for data in -10^0 [downward] inclination

Run number	P_{av} kPa	$T_{s,av}$ °C	G kg/s.m^2	Q_s kW	Q_w kW	Error %
1	121.2	105.1	98.08	35.85	36.99	-3.2
2	124.6	105.9	99.92	36.46	35.90	1.5
3	117.8	104.3	99.92	36.63	36.87	-0.6
4	117.8	104.3	99.92	36.59	37.17	-1.6
5	131.3	107.5	151.48	54.67	52.48	4.0
6	134.7	108.2	147.80	53.38	52.72	1.2
7	153.6	112.1	197.52	70.53	71.16	-0.9
8	150.2	111.4	206.72	73.12	75.04	-2.6
9	133.3	107.9	151.48	54.26	56.59	-4.3
10	140.1	109.4	166.21	58.72	59.79	-1.8
11	111.8	102.8	68.77	25.25	25.72	-1.9
12	111.8	102.8	57.09	21.00	21.35	-1.7
13	113.5	103.2	63.77	23.46	23.20	1.1
14	122.0	105.3	81.71	29.80	30.70	-3.0
15	122.0	105.3	84.63	31.14	30.27	2.8
16	107.8	101.8	81.50	30.00	31.00	-3.3
17	107.8	101.8	85.19	31.29	31.25	0.1
18	107.8	101.8	85.19	31.30	30.06	4.0
19	107.8	101.8	85.19	31.29	30.24	3.3
20	111.2	102.7	103.60	37.95	37.09	2.3
21	107.8	101.8	99.92	36.64	34.90	4.8
22	113.0	103.1	96.23	35.29	34.89	1.1
23	118.1	104.4	96.23	35.20	34.01	3.4
24	113.4	103.2	63.77	23.35	24.51	-5.0
25	108.3	101.9	32.47	11.97	12.27	-2.5
26	111.7	102.8	40.82	15.06	15.53	-3.1
27	111.7	102.8	52.92	19.48	20.15	-3.4
28	129.0	106.9	140.43	50.60	47.87	5.4
29	125.6	106.2	136.75	49.37	49.07	0.6
30	125.6	106.2	144.11	52.05	49.22	5.4
31	129.0	106.9	153.32	54.92	51.76	5.8
32	132.4	107.7	166.21	59.21	56.17	5.1
33	134.3	108.1	166.21	59.33	58.72	1.0
34	141.0	109.6	177.26	62.96	60.10	4.6
35	134.3	108.1	162.53	58.01	54.87	5.4
36	130.9	107.4	166.21	60.35	58.49	3.1
37	129.6	107.1	133.06	47.76	49.49	-3.6
38	126.2	106.3	134.91	48.85	49.86	-2.1
39	129.6	107.1	136.75	49.10	49.77	-1.4
40	122.9	105.5	136.75	50.04	49.17	1.7
41	128.1	106.7	144.11	52.97	54.86	-3.6
42	131.5	107.5	151.48	54.30	53.12	2.2
43	134.8	108.2	166.21	59.22	58.40	1.4
44	134.8	108.2	169.89	60.52	59.70	1.4
45	116.8	104.1	105.44	38.93	39.05	-0.3
46	116.8	104.1	98.08	36.22	36.21	0.0
47	111.7	102.8	70.45	26.21	25.44	2.9
48	115.2	103.7	63.77	23.68	24.71	-4.4
49	113.4	103.2	47.08	17.54	17.64	-0.6
50	115.2	103.7	51.25	19.10	18.87	1.2

TABLE A.5 Operating conditions for data in +1^{0} [upward] inclination

Run number	P_{av} kPa	$T_{s,av}$ °C	G kg/s.m^2	Q_S kW	Q_W kW	Error %
1	125.4	106.1	144.11	52.23	52.36	-0.2
2	125.4	106.1	147.80	53.49	53.36	0.2
3	128.7	106.9	144.11	52.47	52.56	-0.2
4	128.7	106.9	147.80	53.57	51.33	4.2
5	121.6	105.2	133.06	48.29	46.87	2.9
6	116.5	104.0	136.75	50.22	49.17	2.1
7	116.5	104.0	144.11	52.55	50.99	3.0
8	119.9	104.8	147.80	53.75	50.69	5.7
9	110.7	102.5	107.28	39.75	39.10	1.6
10	110.7	102.5	99.92	37.12	36.12	2.7
11	110.7	102.5	99.92	37.08	37.28	-0.5
12	110.7	102.5	99.92	36.82	35.81	2.7
13	110.7	102.5	99.92	37.10	36.95	0.4
14	106.3	101.4	85.19	31.49	30.69	2.5
15	106.3	101.4	88.87	33.02	32.08	2.8
16	106.3	101.4	92.55	34.30	32.73	4.6
17	106.3	101.4	92.55	34.34	32.61	5.1
18	109.7	102.3	88.87	32.78	32.14	2.0
19	106.5	101.4	60.43	22.58	22.24	1.5
20	106.5	101.4	57.51	21.48	20.97	2.4
21	106.5	101.4	57.51	21.42	21.17	1.2
22	106.5	101.4	57.51	21.41	21.74	-1.5
23	106.5	101.4	57.92	21.59	21.52	0.3
24	106.5	101.4	58.76	21.95	21.62	1.5
25	106.5	101.4	56.67	21.11	20.47	3.0
26	147.0	110.8	221.45	79.13	81.74	-3.3
27	153.7	112.1	228.82	81.56	85.24	-4.5
28	153.7	112.1	232.50	82.93	84.21	-1.5
29	153.7	112.1	225.14	80.49	83.06	-3.2
30	147.2	110.8	203.04	72.28	74.21	-2.7
31	143.8	110.1	199.36	71.23	73.26	-2.9
32	143.8	110.1	206.72	73.72	77.29	-4.8
33	143.8	110.1	203.04	72.38	73.58	-1.7
34	143.8	110.1	203.04	72.68	73.45	-1.1
35	140.4	109.4	197.52	70.78	71.97	-1.7
36	153.0	112.0	232.50	82.08	82.56	-0.6
37	156.4	112.6	239.87	84.67	83.45	1.4
38	153.0	112.0	228.82	81.08	82.17	-1.3
39	153.0	112.0	228.82	81.06	82.34	-1.6
40	153.0	112.0	226.98	80.69	80.63	0.1
41	159.8	113.3	239.87	85.02	84.27	0.9
42	121.7	105.2	147.80	53.30	51.27	3.8
43	121.7	105.2	136.75	49.28	50.75	-3.0
44	125.1	106.0	140.43	50.47	50.23	0.5
45	125.1	106.0	133.06	48.44	50.88	-5.0
46	101.6	100.1	25.39	9.42	9.77	-3.8
47	103.3	100.6	32.47	12.07	12.12	-0.4
48	103.3	100.6	33.31	12.40	11.95	3.6
49	103.3	100.6	32.05	11.95	12.40	-3.8
50	103.3	100.6	32.89	12.27	12.34	-0.6
51	103.3	100.6	42.07	15.68	16.25	-3.6

TABLE A.5 Operating conditions for data in +1^0 [upward] inclination (cont'd)

Run number	P_{av} kPa	$T_{s,av}$ °C	G kg/s.m^2	Q_s kW	Q_w kW	Error %
52	103.3	100.6	40.82	15.26	14.81	3.0
53	101.6	100.1	44.99	16.82	16.69	0.8
54	103.3	100.6	45.82	17.12	16.55	3.3
55	103.3	100.6	44.99	16.78	16.11	4.0
56	107.4	101.7	114.65	42.11	40.48	3.9
57	104.0	100.8	99.92	37.12	36.48	1.7
58	104.0	100.8	103.60	38.31	37.79	1.4
59	104.0	100.8	99.92	36.84	37.12	-0.7

TABLE A.6 Operating conditions for data in +5^0 [upward] inclination

Run number	P_{av} kPa	$T_{s,av}$ °C	G kg/s.m^2	Q_s kW	Q_w kW	Error %
1	101.8	100.2	44.99	16.81	16.40	2.4
2	106.9	101.5	62.10	23.13	23.10	0.1
3	106.9	101.5	65.02	24.23	23.11	4.6
4	103.5	100.6	46.24	17.33	17.14	1.1
5	103.5	100.6	63.77	23.79	23.38	1.7
6	103.5	100.6	60.85	22.74	21.83	4.0
7	106.4	101.4	96.23	35.72	36.28	-1.6
8	106.4	101.4	96.23	35.77	35.95	-0.5
9	106.4	101.4	98.08	36.54	36.98	-1.2
10	106.4	101.4	98.08	36.46	37.26	-2.2
11	106.4	101.4	92.55	34.38	33.35	3.0
12	106.4	101.4	96.23	35.74	36.06	-0.9
13	106.4	101.4	96.23	35.84	36.48	-1.8
14	112.3	102.9	136.75	50.06	51.63	-3.1
15	107.8	101.8	140.43	51.38	51.66	-0.5
16	107.8	101.8	136.75	50.22	51.20	-2.0
17	104.4	100.9	122.02	44.91	45.82	-2.0
18	107.8	101.8	140.43	51.20	51.31	-0.2
19	138.0	108.9	184.63	66.41	65.99	0.6
20	134.6	108.2	177.26	64.06	66.17	-3.3
21	141.4	109.6	191.99	68.62	68.16	0.7
22	138.0	108.9	184.63	67.37	68.07	-1.0
23	131.2	107.4	188.31	68.57	69.08	-0.7
24	131.2	107.4	188.31	68.21	69.00	-1.2
25	122.3	105.4	162.53	58.95	59.23	-0.5
26	118.9	104.6	151.48	55.05	57.94	-5.3
27	115.5	103.7	140.43	51.67	52.24	-1.1
28	115.5	103.7	144.11	52.83	54.48	-3.1
29	136.2	108.5	203.04	72.89	70.11	3.8
30	144.7	110.3	223.30	79.69	79.43	0.3
31	149.7	111.3	223.30	80.09	80.33	-0.3
32	146.3	110.7	221.45	79.39	79.14	0.3
33	103.0	100.5	22.44	8.36	8.53	-2.1
34	103.0	100.5	23.03	8.58	8.81	-2.7
35	103.0	100.5	23.91	8.91	8.82	1.0
36	103.0	100.5	23.62	8.79	9.08	-3.3
37	103.0	100.5	32.47	12.09	11.71	3.2
38	103.0	100.5	34.56	12.90	12.94	-0.3
39	103.0	100.5	38.73	14.48	14.01	3.2
40	102.7	100.4	36.64	13.73	13.39	2.5
41	102.7	100.4	38.73	14.53	14.49	0.2
42	102.7	100.4	42.90	16.09	15.77	2.0
43	102.7	100.4	43.74	16.41	16.49	-0.5
44	108.3	101.9	96.23	35.64	35.89	-0.7
45	104.9	101.0	81.50	30.41	29.24	3.8
46	104.9	101.0	88.87	33.14	31.99	3.5
47	104.9	101.0	88.87	33.19	31.73	4.4
48	104.9	101.0	74.14	27.64	26.54	4.0
49	104.9	101.0	61.68	23.14	23.48	-1.4
50	104.9	101.0	53.33	20.02	19.66	1.8
51	104.9	101.0	53.33	19.98	18.99	4.9

TABLE A.6 Operating conditions for data in +5^0 [upward] inclination (cont'd.)

Run number	P_{av} kPa	$T_{s,av}$ °C	G kg/s.m^2	Q_s kW	Q_w kW	Error %
52	158.4	113.0	269.33	96.35	91.21	5.3
53	161.8	113.7	276.70	98.76	94.09	4.7
54	165.1	114.3	276.70	98.77	93.50	5.3
55	161.8	113.7	269.33	96.29	91.92	4.5

TABLE A.7 Operating conditions for data in +10^0 [upward] inclination

Run number	P_{av} kPa	$T_{s,av}$ °C	G kg/s.m^2	Q_S kW	Q_W kW	Error %
1	106.3	101.4	47.08	17.65	17.03	3.5
2	106.3	101.4	50.83	19.06	18.56	2.7
3	111.4	102.7	63.35	23.59	24.09	-2.1
4	111.4	102.7	69.19	25.76	25.61	0.6
5	111.4	102.7	61.68	23.08	22.85	1.0
6	111.4	102.7	61.26	22.95	22.94	0.0
7	111.4	102.7	59.59	22.33	23.00	-3.0
8	111.4	102.7	65.44	24.46	23.25	5.0
9	114.0	103.4	74.20	27.67	26.69	3.5
10	114.0	103.4	71.28	26.54	26.33	0.8
11	114.0	103.4	75.45	28.02	27.88	0.5
12	114.0	103.4	77.12	28.72	29.25	-1.8
13	114.0	103.4	77.12	28.72	28.74	-0.1
14	116.0	103.9	129.38	47.83	49.33	-3.1
15	116.0	103.9	125.70	46.24	46.50	-0.6
16	116.0	103.9	125.70	46.13	47.79	-3.6
17	119.4	104.7	136.75	50.06	51.35	-2.6
18	119.4	104.7	136.75	50.21	50.47	-0.5
19	119.4	104.7	133.06	48.82	50.14	-2.7
20	119.4	104.7	133.06	48.83	49.44	-1.3
21	119.4	104.7	140.43	51.66	50.53	2.2
22	116.0	103.9	136.75	50.39	50.44	-0.1
23	140.3	109.4	203.04	73.18	72.90	0.4
24	140.3	109.4	203.04	73.11	73.36	-0.3
25	143.7	110.1	214.09	76.41	74.70	2.2
26	140.3	109.4	195.67	70.46	71.47	-1.4
27	140.3	109.4	195.67	70.70	71.91	-1.7
28	147.1	110.8	214.09	76.89	75.07	2.4
29	143.7	110.1	199.36	71.33	71.61	-0.4
30	143.7	110.1	203.04	71.85	72.83	-1.4
31	156.4	112.6	228.82	81.86	84.08	-2.7
32	153.0	112.0	228.82	81.52	83.55	-2.5
33	153.0	112.0	232.50	82.69	84.28	-1.9
34	156.4	112.6	232.50	82.53	83.75	-1.5
35	168.2	114.9	254.60	90.73	93.48	-3.0
36	164.8	114.2	258.28	91.87	93.14	-1.4
37	168.2	114.9	261.97	93.06	93.56	-0.5
38	164.8	114.2	261.97	93.03	93.56	-0.6
39	161.5	113.6	258.28	91.67	90.63	1.1
40	161.5	113.6	261.97	92.45	88.76	4.0
41	130.8	107.3	162.53	58.29	59.87	-2.7
42	134.2	108.1	166.21	59.34	61.84	-4.2
43	134.2	108.1	162.53	58.14	58.79	-1.1
44	130.8	107.3	158.84	56.56	58.04	-2.6
45	130.8	107.3	166.21	61.32	64.68	-5.5
46	127.4	106.6	166.21	60.43	63.51	-5.1
47	127.4	106.6	162.53	59.43	60.29	-1.4
48	124.1	105.8	162.53	59.44	61.06	-2.7
49	113.5	103.2	114.65	42.44	43.67	-2.9
50	113.5	103.2	114.65	42.43	41.99	1.0
51	113.5	103.2	114.65	42.30	43.14	-2.0
52	116.8	104.1	136.75	50.45	49.88	1.1

Appendix B

FLOW-REGIME PARAMETERS

The flow conditions corresponding to each visual observation [or data point] is tabulated in this Appendix. For each test run, the flow regimes observed in each visual section and the corresponding values of x, $T_{s,av}$, and G are provided. When the calculated value of the vapor quality [based on thermodynamic equilibrium] became negative [indicating subcooled conditions] a zero-value was entered and the data point was not used in plotting the flow-regime maps. The following abbreviations were used in listing the observed flow regimes.

ANNU	= Annular flow
ANWA	= Annular-wavy flow
WAVY	= Wavy flow
SLUG	= Slug flow
STRA	= Stratified flow
FULL	= Tube running full

TABLE B.1 Flow-regime parameters for data set in the horizontal position.

Run number	Visual observation section	x	$T_{s,av}$ °C	G $kg/m^2.s$	Observed flow regime
1	A	0.790	105.9	123.86	ANNU
	B	0.590			ANNU
	C	0.404			ANNU
	D	0.102			ANWA
	E	0.000			FULL
	F	0.000			FULL
2	A	0.792	105.9	123.86	ANNU
	B	0.589			ANNU
	C	0.386			ANNU
	D	0.099			ANWA
	E	0.000			FULL
	F	0.000			FULL
3	A	0.830	108.9	158.84	ANNU
	B	0.653			ANNU
	C	0.482			ANNU
	D	0.159			ANNU
	E	0.025			ANWA
	F	0.000			FULL
4	A	0.842	115.2	225.14	ANNU
	B	0.650			ANNU
	C	0.389			ANNU
	D	0.116			ANWA
	E	0.000			FULL
	F	0.000			FULL
5	A	0.758	115.2	254.60	ANNU
	B	0.498			ANNU
	C	0.266			ANNU
	D	0.015			ANWA
	E	0.000			FULL
	F	0.000			FULL
6	A	0.798	107.5	134.91	ANNU
	B	0.598			ANNU
	C	0.366			ANNU
	D	0.000			FULL
	E	0.000			FULL
	F	0.000			FULL

TABLE B.1 Flow-regime parameters for data set in the horizontal position (cont'd.)

Run number	Visual observation section	x	$T_{s,av}$ °C	G $kg/m^2.s$	Observed flow regime
7	A	0.696	118.0	105.44	ANNU
	B	0.418			ANNU
	C	0.096			ANWA
	D	0.000			FULL
	E	0.000			FULL
	F	0.000			FULL
8	A	0.633	108.2	186.47	ANNU
	B	0.335			ANNU
	C	0.142			ANNU
	D	0.012			ANWA
	E	0.000			FULL
	F	0.000			FULL
9	A	0.513	101.5	86.72	ANNU
	B	0.284			ANNU
	C	0.076			SLUG
	D	0.000			FULL
	E	0.000			FULL
	F	0.000			FULL
10	A	0.486	100.1	50.41	ANNU
	B	0.154			SLUG
	C	0.000			STRA
	D	0.000			FULL
	E	0.000			FULL
	F	0.000			FULL
11	A	0.451	101.0	45.82	ANNU
	B	0.029			SLUG
	C	0.000			STRA
	D	0.000			FULL
	E	0.000			FULL
	F	0.000			FULL
12	A	0.479	100.2	37.48	ANNU
	B	0.021			SLUG
	C	0.000			STRA
	D	0.000			FULL
	E	0.000			FULL
	F	0.000			FULL

TABLE B.1 Flow-regime parameters for data set in the horizontal position (cont'd.)

Run number	Visual observation section	x	$T_{s,av}$ °C	G $kg/m^2.s$	Observed flow regime
13	A	0.418	101.2	43.32	ANNU
	B	0.000			SLUG
	C	0.000			STRA
	D	0.000			FULL
	E	0.000			FULL
	F	0.000			FULL
14	A	0.743	104.6	88.80	ANNU
	B	0.483			ANNU
	C	0.000			SLUG
	D	0.000			FULL
	E	0.000			FULL
	F	0.000			FULL
15	A	0.632	100.9	55.42	ANNU
	B	0.220			WAVY
	C	0.000			FULL
	D	0.000			FULL
	E	0.000			FULL
	F	0.000			FULL
16	A	0.368	100.9	44.99	ANWA
	B	0.001			SLUG
	C	0.000			STRA
	D	0.000			FULL
	E	0.000			FULL
	F	0.000			FULL
17	A	0.290	101.8	65.44	ANNU
	B	0.026			SLUG
	C	0.000			FULL
	D	0.000			FULL
	E	0.000			FULL
	F	0.000			FULL
18	A	0.011	100.2	32.89	SLUG
	B	0.000			FULL
	C	0.000			STRA
	D	0.000			FULL
	E	0.000			FULL
	F	0.000			FULL

TABLE B.1 Flow-regime parameters for data set in the horizontal position (cont'd.)

Run number	Visual observation section	x	$T_{s,av}$ °C	G $kg/m^2.s$	Observed flow regime
19	A	0.421	100.2	34.97	ANWA
	B	0.000			FULL
	C	0.000			STRA
	D	0.000			FULL
	E	0.000			FULL
	F	0.000			FULL
20	A	0.182	99.6	21.85	SLUG
	B	0.000			STRA
	C	0.000			STRA
	D	0.000			FULL
	E	0.000			FULL
	F	0.000			STRA
21	A	0.530	100.6	40.40	ANNU
	B	0.170			SLUG
	C	0.000			STRA
	D	0.000			FULL
	E	0.000			FULL
	F	0.000			STRA
22	A	0.596	101.5	47.08	ANNU
	B	0.282			WAVY
	C	0.000			STRA
	D	0.000			FULL
	E	0.000			FULL
	F	0.000			STRA
23	A	0.442	100.3	31.64	WAVY
	B	0.000			SLUG
	C	0.000			STRA
	D	0.000			FULL
	E	0.000			FULL
	F	0.000			STRA
24	A	0.602	100.8	49.16	ANNU
	B	0.301			WAVY
	C	0.000			FULL
	D	0.000			FULL
	E	0.000			FULL
	F	0.000			STRA

TABLE B.1 Flow-regime parameters for data set in the horizontal position (cont'd.)

Run number	Visual observation section	x	$T_{s,av}$ °C	G kg/m^2.s	Observed flow regime
25	A	0.575	100.3	44.99	ANNU
	B	0.251			WAVY
	C	0.000			STRA
	D	0.000			FULL
	E	0.000			FULL
	F	0.000			STRA
26	A	0.674	101.7	63.77	ANNU
	B	0.415			ANNU
	C	0.101			SLUG
	D	0.000			FULL
	E	0.000			FULL
	F	0.000			STRA
27	A	0.667	101.7	59.59	ANNU
	B	0.387			ANNU
	C	0.072			SLUG
	D	0.000			FULL
	E	0.000			FULL
	F	0.000			STRA
28	A	0.687	101.7	64.60	ANNU
	B	0.415			ANNU
	C	0.142			SLUG
	D	0.000			FULL
	E	0.000			FULL
	F	0.000			STRA
29	A	0.658	101.9	59.59	ANNU
	B	0.376			ANNU
	C	0.090			SLUG
	D	0.000			FULL
	E	0.000			FULL
	F	0.000			STRA
30	A	0.587	103.2	66.27	ANNU
	B	0.327			ANNU
	C	0.030			SLUG
	D	0.000			FULL
	E	0.000			FULL
	F	0.000			FULL

TABLE B.1 Flow-regime parameters for data set in the horizontal position (cont'd.)

Run number	Visual observation section	x	$T_{s,av}$ °C	G $kg/m^2.s$	Observed flow regime
31	A	0.702	103.9	75.87	ANNU
	B	0.459			ANNU
	C	0.165			ANWA
	D	0.000			FULL
	E	0.000			FULL
	F	0.000			FULL
32	A	0.629	103.1	65.02	ANNU
	B	0.370			ANNU
	C	0.103			SLUG
	D	0.000			FULL
	E	0.000			FULL
	F	0.000			FULL
33	A	0.646	103.9	72.53	ANNU
	B	0.407			ANNU
	C	0.144			ANWA
	D	0.000			FULL
	E	0.000			FULL
	F	0.000			FULL
34	A	0.573	104.4	82.54	ANNU
	B	0.300			ANNU
	C	0.042			SLUG
	D	0.000			FULL
	E	0.000			FULL
	F	0.000			FULL
35	A	0.556	104.2	82.96	ANNU
	B	0.283			ANNU
	C	0.094			SLUG
	D	0.000			FULL
	E	0.000			FULL
	F	0.000			FULL
36	A	0.672	104.6	84.63	ANNU
	B	0.450			ANNU
	C	0.240			ANNU
	D	0.000			FULL
	E	0.000			FULL
	F	0.000			FULL

TABLE B.1 Flow-regime parameters for data set in the horizontal position (cont'd.)

Run number	Visual observation section	x	$T_{s,av}$ °C	G $kg/m^2.s$	Observed flow regime
37	A	0.640	104.2	89.22	ANNU
	B	0.428			ANNU
	C	0.176			ANNU
	D	0.000			FULL
	E	0.000			FULL
	F	0.000			FULL
38	A	0.578	104.2	88.80	ANNU
	B	0.309			ANNU
	C	0.073			SLUG
	D	0.000			FULL
	E	0.000			FULL
	F	0.000			FULL
39	A	0.599	102.1	90.71	ANNU
	B	0.342			ANNU
	C	0.142			ANWA
	D	0.000			FULL
	E	0.000			FULL
	F	0.000			FULL
40	A	0.553	102.6	81.50	ANNU
	B	0.280			ANNU
	C	0.000			SLUG
	D	0.000			FULL
	E	0.000			FULL
	F	0.000			FULL
41	A	0.573	102.6	87.03	ANNU
	B	0.279			ANNU
	C	0.026			SLUG
	D	0.000			FULL
	E	0.000			FULL
	F	0.000			FULL
42	A	0.691	104.3	105.44	ANNU
	B	0.495			ANNU
	C	0.306			ANNU
	D	0.000			FULL
	E	0.000			FULL
	F	0.000			FULL

TABLE B.1 Flow-regime parameters for data set in the horizontal position (cont'd.)

Run number	Visual observation section	x	$T_{s,av}$ °C	G $kg/m^2.s$	Observed flow regime
43	A	0.656	103.5	96.23	ANNU
	B	0.432			ANNU
	C	0.238			ANNU
	D	0.000			FULL
	E	0.000			FULL
	F	0.000			FULL
44	A	0.537	102.6	88.87	ANNU
	B	0.307			ANNU
	C	0.107			ANWA
	D	0.000			FULL
	E	0.000			FULL
	F	0.000			FULL
45	A	0.558	102.6	92.55	ANNU
	B	0.303			ANNU
	C	0.059			SLUG
	D	0.000			FULL
	E	0.000			FULL
	F	0.000			FULL
46	A	0.750	117.2	273.02	ANNU
	B	0.566			ANNU
	C	0.395			ANNU
	D	0.171			ANNU
	E	0.000			ANWA
	F	0.000			FULL
47	A	0.753	117.2	273.02	ANNU
	B	0.562			ANNU
	C	0.365			ANNU
	D	0.150			ANNU
	E	0.000			FULL
	F	0.000			FULL
48	A	0.692	114.8	236.19	ANNU
	B	0.439			ANNU
	C	0.219			ANNU
	D	0.000			FULL
	E	0.000			FULL
	F	0.000			FULL

TABLE B.1 Flow-regime parameters for data set in the horizontal position (cont'd.)

Run number	Visual observation section	x	$T_{s,av}$ °C	G $kg/m^2.s$	Observed flow regime
49	A	0.684	114.2	245.39	ANNU
	B	0.427			ANNU
	C	0.273			ANNU
	D	0.026			ANWA
	E	0.000			FULL
	F	0.000			FULL
50	A	0.660	109.5	190.15	ANNU
	B	0.394			ANNU
	C	0.176			ANNU
	D	0.000			ANWA
	E	0.000			FULL
	F	0.000			FULL
51	A	0.694	113.5	230.66	ANNU
	B	0.457			ANNU
	C	0.280			ANNU
	D	0.004			ANWA
	E	0.000			FULL
	F	0.000			FULL
52	A	0.687	110.2	197.52	ANNU
	B	0.452			ANNU
	C	0.237			ANNU
	D	0.026			ANWA
	E	0.000			FULL
	F	0.000			FULL
53	A	0.697	112.9	217.77	ANNU
	B	0.468			ANNU
	C	0.331			ANNU
	D	0.142			ANNU
	E	0.000			ANWA
	F	0.000			FULL
54	A	0.661	110.8	215.93	ANNU
	B	0.400			ANNU
	C	0.181			ANNU
	D	0.000			ANWA
	E	0.000			FULL
	F	0.000			FULL

TABLE B.1 Flow-regime parameters for data set in the horizontal position (cont'd.)

Run number	Visual observation section	x	$T_{s,av}$ °C	G $kg/m^2.s$	Observed flow regime
55	A	0.641	110.1	197.52	ANNU
	B	0.376			ANNU
	C	0.226			ANNU
	D	0.014			ANWA
	E	0.000			FULL
	F	0.000			FULL
56	A	0.650	110.1	199.36	ANNU
	B	0.370			ANNU
	C	0.187			ANNU
	D	0.000			ANWA
	E	0.000			FULL
	F	0.000			FULL
57	A	0.678	112.2	226.98	ANNU
	B	0.417			ANNU
	C	0.255			ANNU
	D	0.010			ANWA
	E	0.000			FULL
	F	0.000			FULL
58	A	0.680	109.5	195.67	ANNU
	B	0.441			ANNU
	C	0.222			ANNU
	D	0.028			ANWA
	E	0.000			FULL
	F	0.000			FULL
59	A	0.707	108.8	171.73	ANNU
	B	0.455			ANNU
	C	0.224			ANNU
	D	0.029			ANWA
	E	0.000			FULL
	F	0.000			FULL
60	A	0.671	106.6	166.21	ANNU
	B	0.407			ANNU
	C	0.193			ANNU
	D	0.054			ANWA
	E	0.000			FULL
	F	0.000			FULL

TABLE B.1 Flow-regime parameters for data set in the horizontal position (cont'd.)

Run number	Visual observation section	x	$T_{s,av}$ °C	G $kg/m^2.s$	Observed flow regime
61	A	0.737	105.0	116.49	ANNU
	B	0.563			ANNU
	C	0.314			ANNU
	D	0.070			ANWA
	E	0.000			FULL
	F	0.000			FULL
62	A	0.727	105.0	120.17	ANNU
	B	0.520			ANNU
	C	0.257			ANNU
	D	0.043			SLUG
	E	0.000			FULL
	F	0.000			FULL
63	A	0.669	109.0	191.99	ANNU
	B	0.406			ANNU
	C	0.209			ANNU
	D	0.017			ANWA
	E	0.000			FULL
	F	0.000			FULL
64	A	0.704	106.0	134.91	ANNU
	B	0.461			ANNU
	C	0.272			ANNU
	D	0.049			ANWA
	E	0.000			FULL
	F	0.000			FULL
65	A	0.678	106.0	142.27	ANNU
	B	0.420			ANNU
	C	0.201			ANNU
	D	0.013			ANWA
	E	0.000			FULL
	F	0.000			FULL
66	A	0.630	104.4	109.13	ANNU
	B	0.408			ANNU
	C	0.199			ANNU
	D	0.010			SLUG
	E	0.000			FULL
	F	0.000			FULL

TABLE B.1 Flow-regime parameters for data set in the horizontal position (cont'd.)

Run number	Visual observation section	x	$T_{s,av}$ °C	G $kg/m^2.s$	observed flow regime
67	A	0.691	104.4	112.81	ANNU
	B	0.457			ANNU
	C	0.237			ANNU
	D	0.006			SLUG
	E	0.000			FULL
	F	0.000			FULL
68	A	0.717	104.7	112.81	ANNU
	B	0.458			ANNU
	C	0.250			ANNU
	D	0.030			SLUG
	E	0.000			FULL
	F	0.000			FULL
69	A	0.652	105.9	142.27	ANNU
	B	0.400			ANNU
	C	0.178			ANNU
	D	0.007			ANWA
	E	0.000			FULL
	F	0.000			FULL
70	A	0.258	100.4	27.16	WAVY
	B	0.000			FULL
	C	0.000			FULL
	D	0.000			FULL
	E	0.000			FULL
	F	0.000			STRA
71	A	0.324	100.4	27.75	WAVY
	B	0.000			FULL
	C	0.000			FULL
	D	0.000			FULL
	E	0.000			FULL
	F	0.000			STRA
72	A	0.257	100.4	28.34	WAVY
	B	0.000			FULL
	C	0.000			FULL
	D	0.000			FULL
	E	0.000			FULL
	F	0.000			STRA

TABLE B.1 Flow-regime parameters for data set in the horizontal position (cont'd.)

Run number	Visual observation section	x	$T_{s,av}$ °C	G kg/m^2.s	Observed flow regime
73	A	0.285	100.4	35.81	WAVY
	B	0.000			FULL
	C	0.000			FULL
	D	0.000			FULL
	E	0.000			FULL
	F	0.000			STRA

TABLE B.2 Flow-regime parameters for data set in -1° [downward] inclination

Run number	Visual observation section	x	$T_{s,av}$ °C	G kg/m^2.s	Observed flow regime
1	A	0.621	101.1	53.33	ANNU
	B	0.327			ANNU
	C	0.056			SLUG
	D	0.000			FULL
	E	0.000			FULL
	F	0.000			STRA
2	A	0.619	101.1	53.33	ANNU
	B	0.333			ANNU
	C	0.017			WAVY
	D	0.000			STRA
	E	0.000			STRA
	F	0.000			STRA
3	A	0.615	101.5	51.67	ANNU
	B	0.299			ANWA
	C	0.000			FULL
	D	0.000			STRA
	E	0.000			STRA
	F	0.000			STRA
4	A	0.553	101.5	50.41	ANNU
	B	0.233			ANWA
	C	0.000			STRA
	D	0.000			STRA
	E	0.000			STRA
	F	0.000			STRA
5	A	0.540	101.5	51.67	ANNU
	B	0.207			WAVY
	C	0.000			STRA
	D	0.000			STRA
	E	0.000			STRA
	F	0.000			STRA
6	A	0.458	101.5	49.16	ANNU
	B	0.098			WAVY
	C	0.000			STRA
	D	0.000			STRA
	E	0.000			STRA
	F	0.000			STRA

TABLE B.2 Flow-regime parameters for data set in -1° [downward] inclination (cont'd.)

Run number	Visual observation section	x	$T_{s,av}$ °C	G $kg/m^2.s$	Observed flow regime
7	A	0.531	100.7	37.90	ANNU
	B	0.161			WAVY
	C	0.000			STRA
	D	0.000			STRA
	E	0.000			STRA
	F	0.000			STRA
8	A	0.460	100.7	41.23	ANNU
	B	0.113			WAVY
	C	0.000			STRA
	D	0.000			STRA
	E	0.000			STRA
	F	0.000			STRA
9	A	0.449	100.7	33.72	ANWA
	B	0.019			WAVY
	C	0.000			STRA
	D	0.000			STRA
	E	0.000			STRA
	F	0.000			STRA
10	A	0.481	100.2	32.89	ANWA
	B	0.046			WAVY
	C	0.000			STRA
	D	0.000			STRA
	E	0.000			STRA
	F	0.000			STRA
11	A	0.365	100.2	34.14	WAVY
	B	0.000			STRA
	C	0.000			STRA
	D	0.000			STRA
	E	0.000			STRA
	F	0.000			STRA
12	A	0.201	100.2	34.14	WAVY
	B	0.000			STRA
	C	0.000			STRA
	D	0.000			STRA
	E	0.000			STRA
	F	0.000			STRA

TABLE B.2 Flow-regime parameters for data set in -1° [downward] inclination (cont'd.)

Run number	Visual observation section	x	$T_{s,av}$ °C	G $kg/m^2.s$	Observed flow regime
13	A	0.626	101.3	52.92	ANNU
	B	0.330			ANNU
	C	0.018			SLUG
	D	0.000			STRA
	E	0.000			FULL
	F	0.000			STRA
14	A	0.655	101.3	53.33	ANNU
	B	0.364			ANNU
	C	0.065			WAVY
	D	0.000			STRA
	E	0.000			FULL
	F	0.000			STRA
15	A	0.496	100.4	57.51	ANNU
	B	0.209			ANWA
	C	0.000			WAVY
	D	0.000			STRA
	E	0.000			STRA
	F	0.000			STRA
16	A	0.540	100.4	52.08	ANNU
	B	0.264			ANWA
	C	0.000			FULL
	D	0.000			STRA
	E	0.000			STRA
	F	0.000			STRA
17	A	0.712	104.0	68.77	ANNU
	B	0.463			ANNU
	C	0.204			ANWA
	D	0.000			FULL
	E	0.000			FULL
	F	0.000			STRA
18	A	0.642	102.7	66.69	ANNU
	B	0.383			ANNU
	C	0.112			ANWA
	D	0.000			FULL
	E	0.000			FULL
	F	0.000			STRA

TABLE B.2 Flow-regime parameters for data set in -1° [downward] inclination (cont'd.)

Run number	Visual observation section	x	$T_{s,av}$ °C	G $kg/m^2.s$	Observed flow regime
19	A	0.597	103.1	70.03	ANNU
	B	0.312			ANNU
	C	0.075			SLUG
	D	0.000			FULL
	E	0.000			FULL
	F	0.000			STRA
20	A	0.580	103.1	67.94	ANNU
	B	0.303			ANNU
	C	0.067			SLUG
	D	0.000			FULL
	E	0.000			FULL
	F	0.000			STRA
21	A	0.587	104.1	81.29	ANNU
	B	0.271			ANNU
	C	0.001			SLUG
	D	0.000			FULL
	E	0.000			FULL
	F	0.000			FULL
22	A	0.613	104.6	81.71	ANNU
	B	0.321			ANNU
	C	0.078			ANWA
	D	0.000			FULL
	E	0.000			FULL
	F	0.000			FULL
23	A	0.617	103.7	85.47	ANNU
	B	0.317			ANNU
	C	0.060			SLUG
	D	0.000			FULL
	E	0.000			FULL
	F	0.000			FULL
24	A	0.652	104.6	80.46	ANNU
	B	0.398			ANNU
	C	0.155			ANWA
	D	0.000			FULL
	E	0.000			FULL
	F	0.000			STRA

TABLE B.2 Flow-regime parameters for data set in -1° [downward] inclination (cont'd.)

Run number	Visual observation section	x	$T_{s,av}$ °C	G $kg/m^2.s$	Observed flow regime
25	A	0.547	103.0	76.29	ANNU
	B	0.276			ANNU
	C	0.053			SLUG
	D	0.000			FULL
	E	0.000			FULL
	F	0.000			FULL
26	A	0.605	103.9	78.37	ANNU
	B	0.316			ANNU
	C	0.082			SLUG
	D	0.000			FULL
	E	0.000			FULL
	F	0.000			FULL
27	A	0.752	103.9	77.95	ANNU
	B	0.501			ANNU
	C	0.254			ANNU
	D	0.000			FULL
	E	0.000			FULL
	F	0.000			FULL
28	A	0.581	102.1	80.46	ANNU
	B	0.369			ANNU
	C	0.166			ANWA
	D	0.000			FULL
	E	0.000			FULL
	F	0.000			STRA
29	A	0.644	103.2	96.23	ANNU
	B	0.395			ANNU
	C	0.167			ANNU
	D	0.000			FULL
	E	0.000			FULL
	F	0.000			FULL
30	A	0.573	102.4	88.87	ANNU
	B	0.285			ANNU
	C	0.006			SLUG
	D	0.000			FULL
	E	0.000			FULL
	F	0.000			FULL

TABLE B.2 Flow-regime parameters for data set in -1° [downward] inclination (cont'd.)

Run number	Visual observation section	x	$T_{s,av}$ °C	G kg/m^2.s	Observed flow regime
31	A	0.728	103.2	96.23	ANNU
	B	0.477			ANNU
	C	0.183			ANNU
	D	0.000			FULL
	E	0.000			FULL
	F	0.000			FULL
32	A	0.546	102.4	99.92	ANNU
	B	0.264			ANNU
	C	0.044			SLUG
	D	0.000			FULL
	E	0.000			FULL
	F	0.000			FULL
33	A	0.559	102.2	96.23	ANNU
	B	0.272			ANNU
	C	0.036			SLUG
	D	0.000			FULL
	E	0.000			FULL
	F	0.000			FULL
34	A	0.549	102.2	94.39	ANNU
	B	0.267			ANNU
	C	0.018			SLUG
	D	0.000			FULL
	E	0.000			FULL
	F	0.000			FULL
35	A	0.563	101.3	85.19	ANNU
	B	0.307			ANNU
	C	0.061			SLUG
	D	0.000			FULL
	E	0.000			FULL
	F	0.000			FULL
36	A	0.574	103.1	123.86	ANNU
	B	0.237			ANNU
	C	0.000			ANWA
	D	0.000			FULL
	E	0.000			FULL
	F	0.000			FULL

TABLE B.2 Flow-regime parameters for data set in -1° [downward] inclination (cont'd.)

Run number	Visual observation section	x	$T_{s,av}$ °C	G kg/m^2.s	Observed flow regime
37	A	0.587	103.9	129.38	ANNU
	B	0.284			ANNU
	C	0.083			ANWA
	D	0.000			FULL
	E	0.000			FULL
	F	0.000			FULL
38	A	0.585	103.9	136.75	ANNU
	B	0.280			ANNU
	C	0.067			ANWA
	D	0.000			FULL
	E	0.000			FULL
	F	0.000			FULL
39	A	0.568	103.5	133.06	ANNU
	B	0.251			ANNU
	C	0.011			ANWA
	D	0.000			FULL
	E	0.000			FULL
	F	0.000			FULL
40	A	0.570	102.1	103.60	ANNU
	B	0.269			ANNU
	C	0.024			SLUG
	D	0.000			FULL
	E	0.000			FULL
	F	0.000			FULL
41	A	0.563	102.1	105.44	ANNU
	B	0.305			ANNU
	C	0.105			ANWA
	D	0.000			FULL
	E	0.000			FULL
	F	0.000			FULL
42	A	0.651	103.0	105.44	ANNU
	B	0.394			ANNU
	C	0.168			ANNU
	D	0.000			FULL
	E	0.000			FULL
	F	0.000			FULL

TABLE B.2 Flow-regime parameters for data set in -1° [downward] inclination (cont'd.)

Run number	Visual observation section	x	$T_{s,av}$ °C	G kg/m^2.s	Observed flow regime
43	A	0.525	102.1	105.44	ANNU
	B	0.232			ANNU
	C	0.014			SLUG
	D	0.000			FULL
	E	0.000			FULL
	F	0.000			FULL
44	A	0.600	103.0	122.02	ANNU
	B	0.317			ANNU
	C	0.087			ANWA
	D	0.000			FULL
	E	0.000			FULL
	F	0.000			FULL
45	A	0.659	105.8	142.27	ANNU
	B	0.398			ANNU
	C	0.220			ANNU
	D	0.046			ANWA
	E	0.000			FULL
	F	0.000			FULL
46	A	0.678	105.8	134.91	ANNU
	B	0.419			ANNU
	C	0.183			ANNU
	D	0.004			ANWA
	E	0.000			FULL
	F	0.000			FULL
47	A	0.639	105.0	138.59	ANNU
	B	0.329			ANNU
	C	0.086			ANWA
	D	0.000			FULL
	E	0.000			FULL
	F	0.000			FULL
48	A	0.654	105.0	140.43	ANNU
	B	0.392			ANNU
	C	0.139			ANNU
	D	0.000			FULL
	E	0.000			FULL
	F	0.000			FULL

TABLE B.2 Flow-regime parameters for data set in -1° [downward] inclination (cont'd.)

Run number	Visual observation section	x	$T_{s,av}$ °C	G kg/m^2.s	Observed flow regime
49	A	0.674	106.6	158.84	ANNU
	B	0.405			ANNU
	C	0.170			ANNU
	D	0.000			FULL
	E	0.000			FULL
	F	0.000			FULL
50	A	0.627	106.2	158.84	ANNU
	B	0.331			ANNU
	C	0.077			ANWA
	D	0.000			FULL
	E	0.000			FULL
	F	0.000			FULL
51	A	0.693	107.4	158.84	ANNU
	B	0.447			ANNU
	C	0.227			ANNU
	D	0.053			ANWA
	E	0.000			FULL
	F	0.000			FULL
52	A	0.695	106.6	155.16	ANNU
	B	0.439			ANNU
	C	0.210			ANNU
	D	0.013			ANWA
	E	0.000			FULL
	F	0.000			FULL
53	A	0.687	109.1	171.73	ANNU
	B	0.442			ANNU
	C	0.275			ANNU
	D	0.089			ANWA
	E	0.000			FULL
	F	0.000			FULL
54	A	0.701	108.9	168.05	ANNU
	B	0.449			ANNU
	C	0.237			ANNU
	D	0.043			ANWA
	E	0.000			FULL
	F	0.000			FULL

TABLE B.2 Flow-regime parameters for data set in -1° [downward] inclination (cont'd.)

Run number	Visual observation section	x	$T_{s,av}$ °C	G $kg/m^2.s$	Observed flow regime
55	A	0.624	107.7	166.21	ANNU
	B	0.359			ANNU
	C	0.170			ANNU
	D	0.014			ANWA
	E	0.000			FULL
	F	0.000			FULL
56	A	0.637	108.0	177.26	ANNU
	B	0.348			ANNU
	C	0.110			ANWA
	D	0.000			FULL
	E	0.000			FULL
	F	0.000			FULL
57	A	0.711	111.2	223.30	ANNU
	B	0.474			ANNU
	C	0.275			ANNU
	D	0.061			ANWA
	E	0.000			FULL
	F	0.000			FULL
58	A	0.674	110.9	223.30	ANNU
	B	0.413			ANNU
	C	0.195			ANNU
	D	0.016			ANWA
	E	0.000			FULL
	F	0.000			FULL
59	A	0.717	112.2	217.77	ANNU
	B	0.486			ANNU
	C	0.315			ANNU
	D	0.118			ANNU
	E	0.000			FULL
	F	0.000			FULL
60	A	0.630	102.7	103.60	ANNU
	B	0.349			ANNU
	C	0.126			ANWA
	D	0.000			FULL
	E	0.000			FULL
	F	0.000			FULL

TABLE B.2 Flow-regime parameters for data set in -1°
[downward] inclination (cont'd.)

Run number	Visual observation section	x	$T_{s,av}$ °C	G $kg/m^2.s$	Observed flow regime
61	A	0.572	103.1	107.28	ANNU
	B	0.257			ANNU
	C	0.083			ANWA
	D	0.000			FULL
	E	0.000			FULL
	F	0.000			FULL
62	A	0.572	101.8	109.13	ANNU
	B	0.281			ANNU
	C	0.035			SLUG
	D	0.000			FULL
	E	0.000			FULL
	F	0.000			FULL
63	A	0.525	102.3	99.92	ANNU
	B	0.257			ANNU
	C	0.043			SLUG
	D	0.000			FULL
	E	0.000			FULL
	F	0.000			FULL

TABLE B.3 Flow-regime parameters for data set in -5° [downward] inclination

Run number	Visual observation section	x	$T_{s,av}$ °C	G $kg/m^2.s$	Observed flow regime
1	A	0.704	102.8	66.69	ANNU
	B	0.461			ANNU
	C	0.197			ANWA
	D	0.000			STRA
	E	0.000			STRA
	F	0.000			STRA
2	A	0.707	104.1	76.70	ANNU
	B	0.472			ANNU
	C	0.222			ANWA
	D	0.000			STRA
	E	0.000			STRA
	F	0.000			STRA
3	A	0.648	102.8	77.54	ANNU
	B	0.408			ANNU
	C	0.168			ANWA
	D	0.000			FULL
	E	0.000			STRA
	F	0.000			STRA
4	A	0.559	104.1	85.47	ANNU
	B	0.300			ANNU
	C	0.076			WAVY
	D	0.000			STRA
	E	0.000			STRA
	F	0.000			STRA
5	A	0.728	103.2	96.23	ANNU
	B	0.525			ANNU
	C	0.319			ANNU
	D	0.002			WAVY
	E	0.000			STRA
	F	0.000			STRA
6	A	0.628	106.0	136.75	ANNU
	B	0.398			ANNU
	C	0.233			ANNU
	D	0.039			WAVY
	E	0.000			STRA
	F	0.000			STRA

TABLE B.3 Flow-regime parameters for data set in -5° [downward] inclination (cont'd.)

Run number	Visual observation section	x	$T_{s,av}$ °C	G kg/m^2.s	Observed flow regime
7	A	0.629	106.0	136.75	ANNU
	B	0.365			ANNU
	C	0.168			ANNU
	D	0.000			WAVY
	E	0.000			FULL
	F	0.000			STRA
8	A	0.586	104.4	112.81	ANNU
	B	0.292			ANNU
	C	0.084			ANWA
	D	0.000			STRA
	E	0.000			STRA
	F	0.000			STRA
9	A	0.622	105.2	116.49	ANNU
	B	0.395			ANNU
	C	0.248			ANNU
	D	0.004			WAVY
	E	0.000			STRA
	F	0.000			STRA
10	A	0.665	107.2	147.80	ANNU
	B	0.399			ANNU
	C	0.230			ANNU
	D	0.047			ANWA
	E	0.000			FULL
	F	0.000			STRA
11	A	0.679	106.4	153.32	ANNU
	B	0.419			ANNU
	C	0.211			ANNU
	D	0.015			ANWA
	E	0.000			FULL
	F	0.000			STRA
12	A	0.690	109.7	173.58	ANNU
	B	0.451			ANNU
	C	0.274			ANNU
	D	0.098			ANWA
	E	0.000			FULL
	F	0.000			STRA

TABLE B.3 Flow-regime parameters for data set in -5° [downward] inclination (cont'd.)

Run number	Visual observation section	x	$T_{s,av}$ °C	G $kg/m^2.s$	Observed flow regime
13	A	0.662	107.9	173.58	ANNU
	B	0.394			ANNU
	C	0.185			ANNU
	D	0.000			ANWA
	E	0.000			FULL
	F	0.000			FULL
14	A	0.699	110.8	219.61	ANNU
	B	0.473			ANNU
	C	0.288			ANNU
	D	0.110			ANWA
	E	0.000			FULL
	F	0.000			STRA
15	A	0.660	111.0	203.04	ANNU
	B	0.413			ANNU
	C	0.201			ANNU
	D	0.002			ANWA
	E	0.000			FULL
	F	0.000			FULL
16	A	0.669	111.0	203.04	ANNU
	B	0.410			ANNU
	C	0.191			ANNU
	D	0.000			ANWA
	E	0.000			FULL
	F	0.000			FULL
17	A	0.677	112.1	241.71	ANNU
	B	0.428			ANNU
	C	0.209			ANNU
	D	0.010			ANWA
	E	0.000			FULL
	F	0.000			FULL
18	A	0.680	112.6	226.98	ANNU
	B	0.430			ANNU
	C	0.233			ANNU
	D	0.021			ANWA
	E	0.000			FULL
	F	0.000			STRA

TABLE B.3 Flow-regime parameters for data set in -5° [downward] inclination (cont'd.)

Run number	Visual observation section	x	$T_{s,av}$ °C	G $kg/m^2.s$	Observed flow regime
19	A	0.683	104.6	122.02	ANNU
	B	0.432			ANNU
	C	0.207			ANNU
	D	0.000			WAVY
	E	0.000			STRA
	F	0.000			STRA
20	A	0.673	104.2	116.49	ANNU
	B	0.458			ANNU
	C	0.261			ANNU
	D	0.018			WAVY
	E	0.000			STRA
	F	0.000			STRA
21	A	0.680	101.4	99.92	ANNU
	B	0.493			ANNU
	C	0.279			ANNU
	D	0.033			WAVY
	E	0.000			STRA
	F	0.000			STRA
22	A	0.626	102.6	72.11	ANNU
	B	0.387			ANNU
	C	0.154			ANWA
	D	0.000			STRA
	E	0.000			STRA
	F	0.000			STRA
23	A	0.642	102.6	73.36	ANNU
	B	0.408			ANNU
	C	0.020			WAVY
	D	0.000			STRA
	E	0.000			STRA
	F	0.000			STRA
24	A	0.641	104.5	83.38	ANNU
	B	0.379			ANNU
	C	0.179			ANWA
	D	0.000			STRA
	E	0.000			STRA
	F	0.000			STRA

TABLE B.3 Flow-regime parameters for data set in -5° [downward] inclination (cont'd.)

Run number	Visual observation section	x	$T_{s,av}$ °C	G $kg/m^2.s$	Observed flow regime
25	A	0.696	105.3	82.54	ANNU
	B	0.433			ANNU
	C	0.226			ANNU
	D	0.000			STRA
	E	0.000			STRA
	F	0.000			STRA
26	A	0.685	103.6	123.86	ANNU
	B	0.409			ANNU
	C	0.179			ANNU
	D	0.000			STRA
	E	0.000			STRA
	F	0.000			STRA
27	A	0.637	103.6	127.54	ANNU
	B	0.347			ANNU
	C	0.140			ANNU
	D	0.000			STRA
	E	0.000			STRA
	F	0.000			STRA
28	A	0.605	104.5	149.64	ANNU
	B	0.334			ANNU
	C	0.117			ANNU
	D	0.000			STRA
	E	0.000			STRA
	F	0.000			STRA
29	A	0.742	107.5	147.80	ANNU
	B	0.527			ANNU
	C	0.319			ANNU
	D	0.086			ANWA
	E	0.000			FULL
	F	0.000			FULL
30	A	0.697	105.8	157.00	ANNU
	B	0.450			ANNU
	C	0.227			ANNU
	D	0.005			ANWA
	E	0.000			FULL
	F	0.000			FULL

TABLE B.3 Flow-regime parameters for data set in -5° [downward] inclination (cont'd.)

Run number	Visual observation section	x	$T_{s,av}$ °C	G $kg/m^2.s$	Observed flow regime
31	A	0.712	107.5	149.64	ANNU
	B	0.481			ANNU
	C	0.279			ANNU
	D	0.067			ANWA
	E	0.000			FULL
	F	0.000			STRA
32	A	0.652	102.7	105.44	ANNU
	B	0.368			ANNU
	C	0.133			ANNU
	D	0.000			STRA
	E	0.000			STRA
	F	0.000			STRA
33	A	0.625	103.2	105.44	ANNU
	B	0.333			ANNU
	C	0.086			ANWA
	D	0.000			STRA
	E	0.000			STRA
	F	0.000			STRA
34	A	0.609	103.2	107.28	ANNU
	B	0.299			ANNU
	C	0.031			WAVY
	D	0.000			STRA
	E	0.000			STRA
	F	0.000			STRA
35	A	0.481	100.6	49.16	ANNU
	B	0.209			WAVY
	C	0.000			STRA
	D	0.000			STRA
	E	0.000			STRA
	F	0.000			STRA
36	A	0.307	102.0	60.01	ANNU
	B	0.085			WAVY
	C	0.000			STRA
	D	0.000			STRA
	E	0.000			STRA
	F	0.000			STRA

TABLE B.3 Flow-regime parameters for data set in -5° [downward] inclination (cont'd.)

Run number	Visual observation section	x	$T_{s,av}$ °C	G $kg/m^2.s$	Observed flow regime
37	A	0.601	100.4	47.49	ANNU
	B	0.274			ANWA
	C	0.017			WAVY
	D	0.000			STRA
	E	0.000			STRA
	F	0.000			STRA
38	A	0.417	100.4	39.15	ANWA
	B	0.037			WAVY
	C	0.000			STRA
	D	0.000			STRA
	E	0.000			STRA
	F	0.000			STRA
39	A	0.463	100.4	53.33	ANNU
	B	0.204			ANWA
	C	0.000			STRA
	D	0.000			STRA
	E	0.000			STRA
	F	0.000			STRA
40	A	0.480	100.4	55.42	ANNU
	B	0.223			ANWA
	C	0.000			STRA
	D	0.000			STRA
	E	0.000			STRA
	F	0.000			STRA
41	A	0.554	100.4	41.23	ANNU
	B	0.239			WAVY
	C	0.000			STRA
	D	0.000			STRA
	E	0.000			STRA
	F	0.000			STRA
42	A	0.605	100.4	50.00	ANNU
	B	0.318			ANWA
	C	0.000			STRA
	D	0.000			STRA
	E	0.000			STRA
	F	0.000			STRA

TABLE B.3 Flow-regime parameters for data set in -5° [downward] inclination (cont'd.)

Run number	Visual observation section	x	$T_{s,av}$ °C	G $kg/m^2.s$	Observed flow regime
43	A	0.631	100.4	50.41	ANNU
	B	0.184			WAVY
	C	0.000			STRA
	D	0.000			STRA
	E	0.000			STRA
	F	0.000			STRA

TABLE B.4 Flow-regime parameters for data set in -10° [downward] inclination

Run number	Visual observation section	x	$T_{s,av}$ °C	G $kg/m^2.s$	Observed flow regime
1	A	0.651	105.1	98.08	ANNU
	B	0.405			ANNU
	C	0.219			ANNU
	D	0.000			STRA
	E	0.000			FULL
	F	0.000			STRA
2	A	0.772	105.9	99.92	ANNU
	B	0.556			ANNU
	C	0.337			ANNU
	D	0.000			STRA
	E	0.000			FULL
	F	0.000			STRA
3	A	0.581	104.3	99.92	ANNU
	B	0.219			ANNU
	C	0.000			STRA
	D	0.000			STRA
	E	0.000			STRA
	F	0.000			STRA
4	A	0.578	104.3	99.92	ANNU
	B	0.258			ANNU
	C	0.033			WAVY
	D	0.000			STRA
	E	0.000			STRA
	F	0.000			STRA
5	A	0.685	107.5	151.48	ANNU
	B	0.426			ANNU
	C	0.248			ANNU
	D	0.000			WAVY
	E	0.000			STRA
	F	0.000			STRA
6	A	0.680	108.2	147.80	ANNU
	B	0.438			ANNU
	C	0.262			ANNU
	D	0.000			WAVY
	E	0.000			STRA
	F	0.000			STRA

TABLE B.4 Flow-regime parameters for data set in -10° [downward] inclination (cont'd.)

Run number	Visual observation section	x	$T_{s,av}$ °C	G $kg/m^2.s$	Observed flow regime
7	A	0.673	112.1	197.52	ANNU
	B	0.441			ANNU
	C	0.252			ANNU
	D	0.013			ANWA
	E	0.000			FULL
	F	0.000			FULL
8	A	0.673	111.4	206.72	ANNU
	B	0.416			ANNU
	C	0.252			ANNU
	D	0.074			ANWA
	E	0.000			FULL
	F	0.000			FULL
9	A	0.613	107.9	151.48	ANNU
	B	0.381			ANNU
	C	0.180			ANNU
	D	0.000			ANWA
	E	0.000			STRA
	F	0.000			FULL
10	A	0.728	109.4	166.21	ANNU
	B	0.525			ANNU
	C	0.345			ANNU
	D	0.138			ANNU
	E	0.000			FULL
	F	0.000			FULL
11	A	0.702	102.8	68.77	ANNU
	B	0.441			ANNU
	C	0.120			WAVY
	D	0.000			STRA
	E	0.000			STRA
	F	0.000			STRA
12	A	0.635	102.8	57.09	ANNU
	B	0.339			ANNU
	C	0.000			WAVY
	D	0.000			STRA
	E	0.000			STRA
	F	0.000			STRA

TABLE B.4 Flow-regime parameters for data set in -10° [downward] inclination (cont'd.)

Run number	Visual observation section	x	$T_{s,av}$ °C	G $kg/m^2.s$	Observed flow regime
13	A	0.517	103.2	63.77	ANNU
	B	0.229			ANWA
	C	0.000			STRA
	D	0.000			STRA
	E	0.000			STRA
	F	0.000			STRA
14	A	0.617	105.3	81.71	ANNU
	B	0.381			ANNU
	C	0.117			ANWA
	D	0.000			STRA
	E	0.000			STRA
	F	0.000			STRA
15	A	0.410	105.3	84.63	ANNU
	B	0.189			ANNU
	C	0.000			WAVY
	D	0.000			STRA
	E	0.000			STRA
	F	0.000			STRA
16	A	0.545	101.8	81.50	ANNU
	B	0.224			ANNU
	C	0.000			WAVY
	D	0.000			STRA
	E	0.000			STRA
	F	0.000			STRA
17	A	0.619	101.8	85.19	ANNU
	B	0.334			ANNU
	C	0.082			WAVY
	D	0.000			STRA
	E	0.000			STRA
	F	0.000			STRA
18	A	0.676	101.8	85.19	ANNU
	B	0.394			ANNU
	C	0.129			ANWA
	D	0.000			STRA
	E	0.000			STRA
	F	0.000			STRA

TABLE B.4 Flow-regime parameters for data set in -10° [downward] inclination (cont'd.)

Run number	Visual observation section	x	$T_{s,av}$ °C	G $kg/m^2.s$	Observed flow regime
19	A	0.622	101.8	85.19	ANNU
	B	0.372			ANNU
	C	0.143			ANWA
	D	0.000			STRA
	E	0.000			STRA
	F	0.000			STRA
20	A	0.595	102.7	103.60	ANNU
	B	0.298			ANNU
	C	0.074			WAVY
	D	0.000			STRA
	E	0.000			STRA
	F	0.000			STRA
21	A	0.583	101.8	99.92	ANNU
	B	0.282			ANNU
	C	0.047			WAVY
	D	0.000			STRA
	E	0.000			STRA
	F	0.000			STRA
22	A	0.615	103.1	96.23	ANNU
	B	0.368			ANNU
	C	0.164			ANWA
	D	0.000			STRA
	E	0.000			STRA
	F	0.000			STRA
23	A	0.700	104.4	96.23	ANNU
	B	0.447			ANNU
	C	0.230			ANNU
	D	0.000			STRA
	E	0.000			STRA
	F	0.000			STRA
24	A	0.484	103.2	63.77	ANNU
	B	0.173			ANWA
	C	0.000			STRA
	D	0.000			STRA
	E	0.000			STRA
	F	0.000			STRA

TABLE B.4 Flow-regime parameters for data set in -10° [downward] inclination (cont'd.)

Run number	Visual observation section	x	$T_{s,av}$ °C	G $kg/m^2.s$	Observed flow regime
25	A	0.419	101.9	32.47	WAVY
	B	0.000			STRA
	C	0.000			STRA
	D	0.000			STRA
	E	0.000			STRA
	F	0.000			STRA
26	A	0.518	102.8	40.82	ANNU
	B	0.149			WAVY
	C	0.000			STRA
	D	0.000			STRA
	E	0.000			STRA
	F	0.000			STRA
27	A	0.609	102.8	52.92	ANNU
	B	0.289			ANWA
	C	0.000			STRA
	D	0.000			STRA
	E	0.000			STRA
	F	0.000			STRA
28	A	0.726	106.9	140.43	ANNU
	B	0.466			ANNU
	C	0.284			ANNU
	D	0.052			ANWA
	E	0.000			STRA
	F	0.000			FULL
29	A	0.676	106.2	136.75	ANNU
	B	0.405			ANNU
	C	0.188			ANNU
	D	0.000			ANWA
	E	0.000			STRA
	F	0.000			FULL
30	A	0.623	106.2	144.11	ANNU
	B	0.364			ANNU
	C	0.146			ANNU
	D	0.000			STRA
	E	0.000			STRA
	F	0.000			FULL

TABLE B.4 Flow-regime parameters for data set in -10° [downward] inclination (cont'd.)

Run number	Visual observation section	x	$T_{s,av}$ °C	G $kg/m^2.s$	Observed flow regime
31	A	0.642	106.9	153.32	ANNU
	B	0.370			ANNU
	C	0.175			ANNU
	D	0.001			WAVY
	E	0.000			STRA
	F	0.000			STRA
32	A	0.653	107.7	166.21	ANNU
	B	0.390			ANNU
	C	0.227			ANNU
	D	0.055			ANWA
	E	0.000			STRA
	F	0.000			STRA
33	A	0.607	108.1	166.21	ANNU
	B	0.323			ANNU
	C	0.135			ANNU
	D	0.000			WAVY
	E	0.000			FULL
	F	0.000			STRA
34	A	0.746	109.6	177.26	ANNU
	B	0.533			ANNU
	C	0.334			ANNU
	D	0.108			ANWA
	E	0.000			FULL
	F	0.000			STRA
35	A	0.675	108.1	162.53	ANNU
	B	0.416			ANNU
	C	0.193			ANNU
	D	0.025			ANWA
	E	0.000			FULL
	F	0.000			STRA
36	A	0.622	107.4	166.21	ANNU
	B	0.307			ANNU
	C	0.040			ANWA
	D	0.000			STRA
	E	0.000			STRA
	F	0.000			STRA

TABLE B.4 Flow-regime parameters for data set in -10° [downward] inclination (cont'd.)

Run number	Visual observation section	x	$T_{s,av}$ °C	G $kg/m^2.s$	Observed flow regime
37	A	0.661	107.1	133.06	ANNU
	B	0.387			ANNU
	C	0.232			ANNU
	D	0.000			ANWA
	E	0.000			STRA
	F	0.000			STRA
38	A	0.651	106.3	134.91	ANNU
	B	0.367			ANNU
	C	0.131			ANWA
	D	0.000			WAVY
	E	0.000			STRA
	F	0.000			STRA
39	A	0.672	107.1	136.75	ANNU
	B	0.391			ANNU
	C	0.199			ANNU
	D	0.000			ANWA
	E	0.000			STRA
	F	0.000			STRA
40	A	0.584	105.5	136.75	ANNU
	B	0.251			ANNU
	C	0.000			WAVY
	D	0.000			STRA
	E	0.000			STRA
	F	0.000			STRA
41	A	0.667	106.7	144.11	ANNU
	B	0.410			ANNU
	C	0.205			ANNU
	D	0.006			ANWA
	E	0.000			FULL
	F	0.000			FULL
42	A	0.683	107.5	151.48	ANNU
	B	0.448			ANNU
	C	0.237			ANNU
	D	0.026			ANWA
	E	0.000			STRA
	F	0.000			STRA

TABLE B.4 Flow-regime parameters for data set in -10° [downward] inclination (cont'd.)

Run number	Visual observation section	x	$T_{s,av}$ °C	G kg/m^2.s	Observed flow regime
43	A	0.680	108.2	166.21	ANNU
	B	0.438			ANNU
	C	0.225			ANNU
	D	0.007			ANWA
	E	0.000			STRA
	F	0.000			STRA
44	A	0.694	108.2	169.89	ANNU
	B	0.431			ANNU
	C	0.196			ANNU
	D	0.000			ANWA
	E	0.000			STRA
	F	0.000			FULL
45	A	0.506	104.1	105.44	ANNU
	B	0.203			ANNU
	C	0.005			WAVY
	D	0.000			STRA
	E	0.000			FULL
	F	0.000			STRA
46	A	0.544	104.1	98.08	ANNU
	B	0.251			ANNU
	C	0.030			WAVY
	D	0.000			STRA
	E	0.000			FULL
	F	0.000			STRA
47	A	0.360	102.8	70.45	ANNU
	B	0.071			WAVY
	C	0.000			STRA
	D	0.000			STRA
	E	0.000			STRA
	F	0.000			STRA
48	A	0.426	103.7	63.77	ANNU
	B	0.071			WAVY
	C	0.000			STRA
	D	0.000			STRA
	E	0.000			STRA
	F	0.000			STRA

TABLE B.4 Flow-regime parameters for data set in -10° [downward] inclination (cont'd.)

Run number	Visual observation section	x	$T_{s,av}$ °C	G $kg/m^2.s$	Observed flow regime
49	A	0.098	103.2	47.08	WAVY
	B	0.000			STRA
	C	0.000			STRA
	D	0.000			STRA
	E	0.000			STRA
	F	0.000			STRA
50	A	0.107	103.7	51.25	WAVY
	B	0.000			STRA
	C	0.000			STRA
	D	0.000			STRA
	E	0.000			STRA
	F	0.000			STRA

TABLE B.5 Flow-regime parameters for data set in +1° [upward] inclination

Run number	Visual observation section	x	$T_{s,av}$ °C	G $kg/m^2.s$	Observed flow regime
1	A	0.663	106.1	144.11	ANNU
	B	0.422			ANNU
	C	0.195			ANNU
	D	0.005			ANWA
	E	0.000			FULL
	F	0.000			FULL
2	A	0.704	106.1	147.80	ANNU
	B	0.452			ANNU
	C	0.254			ANNU
	D	0.057			ANWA
	E	0.000			FULL
	F	0.000			FULL
3	A	0.734	106.9	144.11	ANNU
	B	0.511			ANNU
	C	0.305			ANNU
	D	0.088			ANWA
	E	0.000			FULL
	F	0.000			FULL
4	A	0.750	106.9	147.80	ANNU
	B	0.568			ANNU
	C	0.398			ANNU
	D	0.201			ANNU
	E	0.000			FULL
	F	0.000			FULL
5	A	0.691	105.2	133.06	ANNU
	B	0.440			ANNU
	C	0.262			ANNU
	D	0.049			ANWA
	E	0.000			FULL
	F	0.000			FULL
6	A	0.569	104.0	136.75	ANNU
	B	0.258			ANNU
	C	0.014			SLUG
	D	0.000			FULL
	E	0.000			FULL
	F	0.000			FULL

TABLE B.5 Flow-regime parameters for data set in +1° [upward] inclination (cont'd.)

Run number	Visual observation section	x	$T_{s,av}$ °C	G $kg/m^2.s$	Observed flow regime
7	A	0.602	104.0	144.11	ANNU
	B	0.272			ANNU
	C	0.023			SLUG
	D	0.000			FULL
	E	0.000			FULL
	F	0.000			FULL
8	A	0.610	104.8	147.80	ANNU
	B	0.329			ANNU
	C	0.121			ANNU
	D	0.000			FULL
	E	0.000			FULL
	F	0.000			FULL
9	A	0.579	102.5	107.28	ANNU
	B	0.269			ANNU
	C	0.070			ANWA
	D	0.000			FULL
	E	0.000			FULL
	F	0.000			FULL
10	A	0.534	102.5	99.92	ANNU
	B	0.218			ANNU
	C	0.017			SLUG
	D	0.000			FULL
	E	0.000			FULL
	F	0.000			FULL
11	A	0.536	102.5	99.92	ANNU
	B	0.217			ANNU
	C	0.034			SLUG
	D	0.000			FULL
	E	0.000			FULL
	F	0.000			FULL
12	A	0.606	102.5	99.92	ANNU
	B	0.339			ANNU
	C	0.123			ANNU
	D	0.000			FULL
	E	0.000			FULL
	F	0.000			FULL

TABLE B.5 Flow-regime parameters for data set in +1° [upward] inclination (cont'd.)

Run number	Visual observation section	x	$T_{s,av}$ °C	G $kg/m^2.s$	Observed flow regime
13	A	0.511	102.5	99.92	ANNU
	B	0.229			ANNU
	C	0.038			SLUG
	D	0.000			FULL
	E	0.000			FULL
	F	0.000			FULL
14	A	0.545	101.4	85.19	ANNU
	B	0.242			ANNU
	C	0.047			SLUG
	D	0.000			FULL
	E	0.000			FULL
	F	0.000			FULL
15	A	0.564	101.4	88.87	ANNU
	B	0.274			ANNU
	C	0.049			SLUG
	D	0.000			FULL
	E	0.000			FULL
	F	0.000			FULL
16	A	0.580	101.4	92.55	ANNU
	B	0.297			ANNU
	C	0.040			SLUG
	D	0.000			FULL
	E	0.000			FULL
	F	0.000			FULL
17	A	0.504	101.4	92.55	ANNU
	B	0.279			ANNU
	C	0.072			SLUG
	D	0.000			FULL
	E	0.000			FULL
	F	0.000			FULL
18	A	0.564	102.3	88.87	ANNU
	B	0.331			ANNU
	C	0.127			ANWA
	D	0.000			FULL
	E	0.000			FULL
	F	0.000			FULL

TABLE B.5 Flow-regime parameters for data set in +1° [upward] inclination (cont'd.)

Run number	Visual observation section	x	$T_{s,av}$ °C	G kg/m^2.s	Observed flow regime
19	A	0.327	101.4	60.43	ANNU
	B	0.035			SLUG
	C	0.000			FULL
	D	0.000			FULL
	E	0.000			FULL
	F	0.000			FULL
20	A	0.353	101.4	57.51	ANNU
	B	0.053			SLUG
	C	0.000			FULL
	D	0.000			FULL
	E	0.000			FULL
	F	0.000			FULL
21	A	0.468	101.4	57.51	ANNU
	B	0.150			ANWA
	C	0.000			FULL
	D	0.000			FULL
	E	0.000			FULL
	F	0.000			FULL
22	A	0.652	101.4	57.51	ANNU
	B	0.310			ANNU
	C	0.000			FULL
	D	0.000			FULL
	E	0.000			FULL
	F	0.000			FULL
23	A	0.433	101.4	57.92	ANNU
	B	0.124			ANWA
	C	0.000			FULL
	D	0.000			FULL
	E	0.000			FULL
	F	0.000			FULL
24	A	0.334	101.4	58.76	ANNU
	B	0.045			SLUG
	C	0.000			FULL
	D	0.000			FULL
	E	0.000			FULL
	F	0.000			FULL

TABLE B.5 Flow-regime parameters for data set in +1° [upward] inclination (cont'd.)

Run number	Visual observation section	x	$T_{s,av}$ °C	G $kg/m^2.s$	Observed flow regime
25	A	0.535	101.4	56.67	ANNU
	B	0.205			ANWA
	C	0.000			FULL
	D	0.000			FULL
	E	0.000			FULL
	F	0.000			FULL
26	A	0.627	110.8	221.45	ANNU
	B	0.338			ANNU
	C	0.138			ANNU
	D	0.000			ANWA
	E	0.000			FULL
	F	0.000			FULL
27	A	0.635	112.1	228.82	ANNU
	B	0.378			ANNU
	C	0.173			ANNU
	D	0.000			ANWA
	E	0.000			FULL
	F	0.000			FULL
28	A	0.636	112.1	232.50	ANNU
	B	0.377			ANNU
	C	0.179			ANNU
	D	0.006			ANWA
	E	0.000			FULL
	F	0.000			FULL
29	A	0.678	112.1	225.14	ANNU
	B	0.404			ANNU
	C	0.196			ANNU
	D	0.002			ANWA
	E	0.000			FULL
	F	0.000			FULL
30	A	0.637	110.8	203.04	ANNU
	B	0.363			ANNU
	C	0.212			ANNU
	D	0.042			ANNU
	E	0.000			FULL
	F	0.000			FULL

TABLE B.5 Flow-regime parameters for data set in +1° [upward] inclination (cont'd.)

Run number	Visual observation section	x	$T_{s,av}$ °C	G $kg/m^2.s$	Observed flow regime
31	A	0.645	110.1	199.36	ANNU
	B	0.333			ANNU
	C	0.168			ANNU
	D	0.015			ANWA
	E	0.000			FULL
	F	0.000			FULL
32	A	0.660	110.1	206.72	ANNU
	B	0.359			ANNU
	C	0.138			ANNU
	D	0.000			ANWA
	E	0.000			FULL
	F	0.000			FULL
33	A	0.651	110.1	203.04	ANNU
	B	0.345			ANNU
	C	0.160			ANNU
	D	0.026			ANWA
	E	0.000			FULL
	F	0.000			FULL
34	A	0.655	110.1	203.04	ANNU
	B	0.349			ANNU
	C	0.140			ANNU
	D	0.008			ANWA
	E	0.000			FULL
	F	0.000			FULL
35	A	0.645	109.4	197.52	ANNU
	B	0.360			ANNU
	C	0.146			ANNU
	D	0.000			ANWA
	E	0.000			FULL
	F	0.000			FULL
36	A	0.658	112.0	232.50	ANNU
	B	0.396			ANNU
	C	0.243			ANNU
	D	0.044			ANNU
	E	0.000			FULL
	F	0.000			FULL

TABLE B.5 Flow-regime parameters for data set in +1° [upward] inclination (cont'd.)

Run number	Visual observation section	x	$T_{s,av}$ °C	G kg/m^2.s	Observed flow regime
37	A	0.666	112.6	239.87	ANNU
	B	0.412			ANNU
	C	0.245			ANNU
	D	0.048			ANNU
	E	0.000			FULL
	F	0.000			FULL
38	A	0.662	112.0	228.82	ANNU
	B	0.406			ANNU
	C	0.213			ANNU
	D	0.017			ANNU
	E	0.000			FULL
	F	0.000			FULL
39	A	0.664	112.0	228.82	ANNU
	B	0.410			ANNU
	C	0.197			ANNU
	D	0.009			ANWA
	E	0.000			FULL
	F	0.000			FULL
40	A	0.665	112.0	226.98	ANNU
	B	0.409			ANNU
	C	0.196			ANNU
	D	0.003			ANWA
	E	0.000			FULL
	F	0.000			FULL
41	A	0.675	113.3	239.87	ANNU
	B	0.430			ANNU
	C	0.225			ANNU
	D	0.014			ANWA
	E	0.000			FULL
	F	0.000			FULL
42	A	0.666	105.2	147.80	ANNU
	B	0.401			ANNU
	C	0.182			ANNU
	D	0.006			ANWA
	E	0.000			FULL
	F	0.000			FULL

TABLE B.5 Flow-regime parameters for data set in +1° [upward] inclination (cont'd.)

Run number	Visual observation section	x	$T_{s,av}$ °C	G kg/m^2.s	Observed flow regime
43	A	0.684	105.2	136.75	ANNU
	B	0.432			ANNU
	C	0.221			ANNU
	D	0.021			SLUG
	E	0.000			FULL
	F	0.000			FULL
44	A	0.711	106.0	140.43	ANNU
	B	0.467			ANNU
	C	0.264			ANNU
	D	0.080			ANWA
	E	0.000			FULL
	F	0.000			FULL
45	A	0.708	106.0	133.06	ANNU
	B	0.474			ANNU
	C	0.271			ANNU
	D	0.077			ANWA
	E	0.000			FULL
	F	0.000			FULL
46	A	0.276	100.1	25.39	SLUG
	B	0.000			FULL
	C	0.000			FULL
	D	0.000			FULL
	E	0.000			FULL
	F	0.000			FULL
47	A	0.424	100.6	32.47	ANWA
	B	0.000			FULL
	C	0.000			FULL
	D	0.000			FULL
	E	0.000			FULL
	F	0.000			FULL
48	A	0.282	100.6	33.31	ANWA
	B	0.000			FULL
	C	0.000			FULL
	D	0.000			FULL
	E	0.000			FULL
	F	0.000			FULL

TABLE B.5 Flow-regime parameters for data set in +1° [upward] inclination (cont'd.)

Run number	Visual observation section	x	$T_{s,av}$ °C	G $kg/m^2.s$	Observed flow regime
49	A	0.171	100.6	32.05	SLUG
	B	0.000			FULL
	C	0.000			FULL
	D	0.000			FULL
	E	0.000			FULL
	F	0.000			FULL
50	A	0.101	100.6	32.89	SLUG
	B	0.000			FULL
	C	0.000			FULL
	D	0.000			FULL
	E	0.000			FULL
	F	0.000			FULL
51	A	0.221	100.6	42.07	ANWA
	B	0.000			FULL
	C	0.000			FULL
	D	0.000			FULL
	E	0.000			FULL
	F	0.000			FULL
52	A	0.149	100.6	40.82	SLUG
	B	0.000			FULL
	C	0.000			FULL
	D	0.000			FULL
	E	0.000			FULL
	F	0.000			FULL
53	A	0.141	100.1	44.99	SLUG
	B	0.000			FULL
	C	0.000			FULL
	D	0.000			FULL
	E	0.000			FULL
	F	0.000			FULL
54	A	0.438	100.6	45.82	ANNU
	B	0.067			SLUG
	C	0.000			FULL
	D	0.000			FULL
	E	0.000			FULL
	F	0.000			FULL

TABLE B.5 Flow-regime parameters for data set in +1° [upward] inclination (cont'd.)

Run number	Visual observation section	x	$T_{s,av}$ °C	G $kg/m^2.s$	Observed flow regime
55	A	0.345	100.6	44.99	ANNU
	B	0.000			FULL
	C	0.000			FULL
	D	0.000			FULL
	E	0.000			FULL
	F	0.000			FULL
56	A	0.564	101.7	114.65	ANNU
	B	0.208			ANNU
	C	0.009			SLUG
	D	0.000			FULL
	E	0.000			FULL
	F	0.000			FULL
57	A	0.416	100.8	99.92	ANNU
	B	0.091			ANWA
	C	0.000			FULL
	D	0.000			FULL
	E	0.000			FULL
	F	0.000			FULL
58	A	0.424	100.8	103.60	ANNU
	B	0.143			ANNU
	C	0.000			FULL
	D	0.000			FULL
	E	0.000			FULL
	F	0.000			FULL
59	A	0.423	100.8	99.92	ANNU
	B	0.121			ANNU
	C	0.000			FULL
	D	0.000			FULL
	E	0.000			FULL
	F	0.000			FULL

TABLE B.6 Flow-regime parameters for data set in +5° [upward] inclination

Run number	Visual observation section	x	$T_{s,av}$ °C	G $kg/m^2.s$	Observed flow regime
1	A	0.495	100.2	44.99	ANNU
	B	0.129			SLUG
	C	0.000			FULL
	D	0.000			FULL
	E	0.000			FULL
	F	0.000			FULL
2	A	0.442	101.5	62.10	ANNU
	B	0.059			SLUG
	C	0.000			FULL
	D	0.000			FULL
	E	0.000			FULL
	F	0.000			FULL
3	A	0.344	101.5	65.02	ANNU
	B	0.103			SLUG
	C	0.000			FULL
	D	0.000			FULL
	E	0.000			FULL
	F	0.000			FULL
4	A	0.232	100.6	46.24	ANWA
	B	0.000			FULL
	C	0.000			FULL
	D	0.000			FULL
	E	0.000			FULL
	F	0.000			FULL
5	A	0.232	100.6	63.77	ANNU
	B	0.000			FULL
	C	0.000			FULL
	D	0.000			FULL
	E	0.000			FULL
	F	0.000			FULL
6	A	0.273	100.6	60.85	ANNU
	B	0.008			SLUG
	C	0.000			FULL
	D	0.000			FULL
	E	0.000			FULL
	F	0.000			FULL

TABLE B.6 Flow-regime parameters for data set in +5° [upward] inclination (cont'd.)

Run number	Visual observation section	x	$T_{s,av}$ °C	G kg/m^2.s	Observed flow regime
7	A	0.477	101.4	96.23	ANNU
	B	0.226			ANNU
	C	0.000			SLUG
	D	0.000			FULL
	E	0.000			FULL
	F	0.000			FULL
8	A	0.501	101.4	96.23	ANNU
	B	0.247			ANNU
	C	0.064			ANWA
	D	0.000			FULL
	E	0.000			FULL
	F	0.000			FULL
9	A	0.509	101.4	98.08	ANNU
	B	0.262			ANNU
	C	0.043			ANWA
	D	0.000			FULL
	E	0.000			FULL
	F	0.000			FULL
10	A	0.509	101.4	98.08	ANNU
	B	0.219			ANNU
	C	0.024			SLUG
	D	0.000			FULL
	E	0.000			FULL
	F	0.000			FULL
11	A	0.551	101.4	92.55	ANNU
	B	0.197			ANNU
	C	0.028			SLUG
	D	0.000			FULL
	E	0.000			FULL
	F	0.000			FULL
12	A	0.411	101.4	96.23	ANNU
	B	0.149			ANNU
	C	0.000			FULL
	D	0.000			FULL
	E	0.000			FULL
	F	0.000			FULL

TABLE B.6 Flow-regime parameters for data set in +5° [upward] inclination (cont'd.)

Run number	Visual observation section	x	$T_{s,av}$ °C	G $kg/m^2.s$	Observed flow regime
13	A	0.424	101.4	96.23	ANNU
	B	0.094			ANWA
	C	0.000			FULL
	D	0.000			FULL
	E	0.000			FULL
	F	0.000			FULL
14	A	0.585	102.9	136.75	ANNU
	B	0.239			ANNU
	C	0.000			ANWA
	D	0.000			FULL
	E	0.000			FULL
	F	0.000			FULL
15	A	0.555	101.8	140.43	ANNU
	B	0.209			ANNU
	C	0.003			SLUG
	D	0.000			FULL
	E	0.000			FULL
	F	0.000			FULL
16	A	0.536	101.8	136.75	ANNU
	B	0.228			ANNU
	C	0.011			SLUG
	D	0.000			FULL
	E	0.000			FULL
	F	0.000			FULL
17	A	0.533	100.9	122.02	ANNU
	B	0.225			ANNU
	C	0.004			SLUG
	D	0.000			FULL
	E	0.000			FULL
	F	0.000			FULL
18	A	0.582	101.8	140.43	ANNU
	B	0.281			ANNU
	C	0.055			ANWA
	D	0.000			FULL
	E	0.000			FULL
	F	0.000			FULL

TABLE B.6 Flow-regime parameters for data set in +5° [upward] inclination (cont'd.)

Run number	Visual observation section	x	$T_{s,av}$ °C	G $kg/m^2.s$	Observed flow regime
19	A	0.652	108.9	184.63	ANNU
	B	0.366			ANNU
	C	0.172			ANNU
	D	0.000			ANWA
	E	0.000			FULL
	F	0.000			FULL
20	A	0.637	108.2	177.26	ANNU
	B	0.375			ANNU
	C	0.177			ANNU
	D	0.000			ANWA
	E	0.000			FULL
	F	0.000			FULL
21	A	0.692	109.6	191.99	ANNU
	B	0.449			ANNU
	C	0.247			ANNU
	D	0.063			ANNU
	E	0.000			FULL
	F	0.000			FULL
22	A	0.691	108.9	184.63	ANNU
	B	0.426			ANNU
	C	0.201			ANNU
	D	0.009			ANWA
	E	0.000			FULL
	F	0.000			FULL
23	A	0.595	107.4	188.31	ANNU
	B	0.275			ANNU
	C	0.025			ANWA
	D	0.000			FULL
	E	0.000			FULL
	F	0.000			FULL
24	A	0.592	107.4	188.31	ANNU
	B	0.270			ANNU
	C	0.043			ANWA
	D	0.000			FULL
	E	0.000			FULL
	F	0.000			FULL

TABLE B.6 Flow-regime parameters for data set in +5° [upward] inclination (cont'd.)

Run number	Visual observation section	x	$T_{s,av}$ °C	G $kg/m^2.s$	Observed flow regime
25	A	0.582	105.4	162.53	ANNU
	B	0.283			ANNU
	C	0.078			ANNU
	D	0.000			FULL
	E	0.000			FULL
	F	0.000			FULL
26	A	0.565	104.6	151.48	ANNU
	B	0.253			ANNU
	C	0.046			ANWA
	D	0.000			FULL
	E	0.000			FULL
	F	0.000			FULL
27	A	0.528	103.7	140.43	ANNU
	B	0.229			ANNU
	C	0.032			ANWA
	D	0.000			FULL
	E	0.000			FULL
	F	0.000			FULL
28	A	0.553	103.7	144.11	ANNU
	B	0.232			ANNU
	C	0.001			SLUG
	D	0.000			FULL
	E	0.000			FULL
	F	0.000			FULL
29	A	0.647	108.5	203.04	ANNU
	B	0.353			ANNU
	C	0.145			ANNU
	D	0.001			ANWA
	E	0.000			FULL
	F	0.000			FULL
30	A	0.667	110.3	223.30	ANNU
	B	0.390			ANNU
	C	0.197			ANNU
	D	0.052			ANNU
	E	0.000			FULL
	F	0.000			FULL

TABLE B.6 Flow-regime parameters for data set in +5° [upward] inclination (cont'd.)

Run number	Visual observation section	x	$T_{s,av}$ °C	G $kg/m^2.s$	Observed flow regime
31	A	0.676	111.3	223.30	ANNU
	B	0.403			ANNU
	C	0.189			ANNU
	D	0.000			ANWA
	E	0.000			FULL
	F	0.000			FULL
32	A	0.666	110.7	221.45	ANNU
	B	0.390			ANNU
	C	0.191			ANNU
	D	0.026			ANWA
	E	0.000			FULL
	F	0.000			FULL
33	A	0.197	100.5	22.44	SLUG
	B	0.000			FULL
	C	0.000			FULL
	D	0.000			FULL
	E	0.000			FULL
	F	0.000			FULL
34	A	0.111	100.5	23.03	SLUG
	B	0.000			FULL
	C	0.000			FULL
	D	0.000			FULL
	E	0.000			FULL
	F	0.000			FULL
35	A	0.069	100.5	23.91	SLUG
	B	0.000			FULL
	C	0.000			FULL
	D	0.000			FULL
	E	0.000			FULL
	F	0.000			FULL
36	A	0.241	100.5	23.62	SLUG
	B	0.000			FULL
	C	0.000			FULL
	D	0.000			FULL
	E	0.000			FULL
	F	0.000			FULL

TABLE B.6 Flow-regime parameters for data set in +5° [upward] inclination (cont'd.)

Run number	Visual observation section	x	$T_{s,av}$ °C	G kg/m^2.s	Observed flow regime
37	A	0.397	100.5	32.47	ANWA
	B	0.000			FULL
	C	0.000			FULL
	D	0.000			FULL
	E	0.000			FULL
	F	0.000			FULL
38	A	0.354	100.5	34.56	ANWA
	B	0.000			FULL
	C	0.000			FULL
	D	0.000			FULL
	E	0.000			FULL
	F	0.000			FULL
39	A	0.280	100.5	38.73	ANWA
	B	0.000			FULL
	C	0.000			FULL
	D	0.000			FULL
	E	0.000			FULL
	F	0.000			FULL
40	A	0.436	100.4	36.64	ANNU
	B	0.000			FULL
	C	0.000			FULL
	D	0.000			FULL
	E	0.000			FULL
	F	0.000			FULL
41	A	0.340	100.4	38.73	ANWA
	B	0.000			FULL
	C	0.000			FULL
	D	0.000			FULL
	E	0.000			FULL
	F	0.000			FULL
42	A	0.286	100.4	42.90	ANWA
	B	0.000			FULL
	C	0.000			FULL
	D	0.000			FULL
	E	0.000			FULL
	F	0.000			FULL

TABLE B.6 Flow-regime parameters for data set in +5° [upward] inclination (cont'd.)

Run number	Visual observation section	x	$T_{s,av}$ °C	G $kg/m^2.s$	Observed flow regime
43	A	0.197	100.4	43.74	SLUG
	B	0.000			FULL
	C	0.000			FULL
	D	0.000			FULL
	E	0.000			FULL
	F	0.000			FULL
44	A	0.676	101.9	96.23	ANNU
	B	0.374			ANNU
	C	0.115			ANWA
	D	0.000			FULL
	E	0.000			FULL
	F	0.000			FULL
45	A	0.612	101.0	81.50	ANNU
	B	0.350			ANNU
	C	0.125			ANWA
	D	0.000			FULL
	E	0.000			FULL
	F	0.000			FULL
46	A	0.554	101.0	88.87	ANNU
	B	0.277			ANNU
	C	0.086			ANWA
	D	0.000			FULL
	E	0.000			FULL
	F	0.000			FULL
47	A	0.561	101.0	88.87	ANNU
	B	0.285			ANNU
	C	0.051			SLUG
	D	0.000			FULL
	E	0.000			FULL
	F	0.000			FULL
48	A	0.651	101.0	74.14	ANNU
	B	0.378			ANNU
	C	0.130			ANWA
	D	0.000			FULL
	E	0.000			FULL
	F	0.000			FULL

TABLE B.6 Flow-regime parameters for data set in +5° [upward] inclination (cont'd.)

Run number	Visual observation section	x	$T_{s,av}$ °C	G kg/m^2.s	Observed flow regime
49	A	0.639	101.0	61.68	ANNU
	B	0.347			ANNU
	C	0.062			SLUG
	D	0.000			FULL
	E	0.000			FULL
	F	0.000			FULL
50	A	0.493	101.0	53.33	ANNU
	B	0.157			ANWA
	C	0.000			FULL
	D	0.000			FULL
	E	0.000			FULL
	F	0.000			FULL
51	A	0.557	101.0	53.33	ANNU
	B	0.226			ANWA
	C	0.000			FULL
	D	0.000			FULL
	E	0.000			FULL
	F	0.000			FULL
52	A	0.673	113.0	269.33	ANNU
	B	0.405			ANNU
	C	0.200			ANNU
	D	0.038			ANWA
	E	0.000			FULL
	F	0.000			FULL
53	A	0.672	113.7	276.70	ANNU
	B	0.410			ANNU
	C	0.207			ANNU
	D	0.044			ANWA
	E	0.000			FULL
	F	0.000			FULL
54	A	0.670	114.3	276.70	ANNU
	B	0.404			ANNU
	C	0.223			ANNU
	D	0.058			ANNU
	E	0.000			FULL
	F	0.000			FULL

TABLE B.6 Flow-regime parameters for data set in +5° [upward] inclination (cont'd.)

Run number	Visual observation section	x	$T_{s,av}$ °C	G $kg/m^2.s$	Observed flow regime
55	A	0.654	113.7	269.33	ANNU
	B	0.415			ANNU
	C	0.223			ANNU
	D	0.052			ANNU
	E	0.000			FULL
	F	0.000			FULL

TABLE B.7 Flow-regime parameters for data set in +10° [upward] inclination

Run number	Visual observation section	x	$T_{s,av}$ °C	G $kg/m^2.s$	Observed flow regime
1	A	0.540	101.4	47.08	ANNU
	B	0.189			ANWA
	C	0.000			FULL
	D	0.000			FULL
	E	0.000			FULL
	F	0.000			FULL
2	A	0.449	101.4	50.83	ANNU
	B	0.119			SLUG
	C	0.000			FULL
	D	0.000			FULL
	E	0.000			FULL
	F	0.000			FULL
3	A	0.449	102.7	63.35	ANNU
	B	0.177			ANWA
	C	0.000			FULL
	D	0.000			FULL
	E	0.000			FULL
	F	0.000			FULL
4	A	0.401	102.7	69.19	ANNU
	B	0.145			ANWA
	C	0.000			FULL
	D	0.000			FULL
	E	0.000			FULL
	F	0.000			FULL
5	A	0.399	102.7	61.68	ANNU
	B	0.125			SLUG
	C	0.000			FULL
	D	0.000			FULL
	E	0.000			FULL
	F	0.000			FULL
6	A	0.277	102.7	61.26	ANNU
	B	0.013			SLUG
	C	0.000			FULL
	D	0.000			FULL
	E	0.000			FULL
	F	0.000			FULL

TABLE B.7 Flow-regime parameters for data set in +10° [upward] inclination (cont'd.)

Run number	Visual observation section	x	$T_{s,av}$ °C	G $kg/m^2.s$	Observed flow regime
7	A	0.261	102.7	59.59	ANNU
	B	0.000			FULL
	C	0.000			FULL
	D	0.000			FULL
	E	0.000			FULL
	F	0.000			FULL
8	A	0.537	102.7	65.44	ANNU
	B	0.209			ANNU
	C	0.000			FULL
	D	0.000			FULL
	E	0.000			FULL
	F	0.000			FULL
9	A	0.588	103.4	74.20	ANNU
	B	0.282			ANNU
	C	0.019			SLUG
	D	0.000			FULL
	E	0.000			FULL
	F	0.000			FULL
10	A	0.687	103.4	71.28	ANNU
	B	0.408			ANNU
	C	0.149			ANWA
	D	0.000			FULL
	E	0.000			FULL
	F	0.000			FULL
11	A	0.561	103.4	75.45	ANNU
	B	0.311			ANNU
	C	0.083			ANWA
	D	0.000			FULL
	E	0.000			FULL
	F	0.000			FULL
12	A	0.518	103.4	77.12	ANNU
	B	0.275			ANNU
	C	0.041			SLUG
	D	0.000			FULL
	E	0.000			FULL
	F	0.000			FULL

TABLE B.7 Flow-regime parameters for data set in +10° [upward] inclination (cont'd.)

Run number	Visual observation section	x	$T_{s,av}$ °C	G $kg/m^2.s$	Observed flow regime
13	A	0.562	103.4	77.12	ANNU
	B	0.304			ANNU
	C	0.068			SLUG
	D	0.000			FULL
	E	0.000			FULL
	F	0.000			FULL
14	A	0.560	103.9	129.38	ANNU
	B	0.224			ANNU
	C	0.000			SLUG
	D	0.000			FULL
	E	0.000			FULL
	F	0.000			FULL
15	A	0.532	103.9	125.70	ANNU
	B	0.217			ANNU
	C	0.000			SLUG
	D	0.000			FULL
	E	0.000			FULL
	F	0.000			FULL
16	A	0.590	103.9	125.70	ANNU
	B	0.289			ANNU
	C	0.049			ANWA
	D	0.000			FULL
	E	0.000			FULL
	F	0.000			FULL
17	A	0.615	104.7	136.75	ANNU
	B	0.281			ANNU
	C	0.063			ANWA
	D	0.000			FULL
	E	0.000			FULL
	F	0.000			FULL
18	A	0.614	104.7	136.75	ANNU
	B	0.276			ANNU
	C	0.076			ANNU
	D	0.000			FULL
	E	0.000			FULL
	F	0.000			FULL

TABLE B.7 Flow-regime parameters for data set in +10° [upward] inclination (cont'd.)

Run number	Visual observation section	x	$T_{s,av}$ °C	G $kg/m^2.s$	Observed flow regime
19	A	0.602	104.7	133.06	ANNU
	B	0.286			ANNU
	C	0.083			ANNU
	D	0.000			FULL
	E	0.000			FULL
	F	0.000			FULL
20	A	0.596	104.7	133.06	ANNU
	B	0.297			ANNU
	C	0.116			ANNU
	D	0.000			FULL
	E	0.000			FULL
	F	0.000			FULL
21	A	0.565	104.7	140.43	ANNU
	B	0.232			ANNU
	C	0.005			SLUG
	D	0.000			FULL
	E	0.000			FULL
	F	0.000			FULL
22	A	0.562	103.9	136.75	ANNU
	B	0.230			ANNU
	C	0.015			SLUG
	D	0.000			FULL
	E	0.000			FULL
	F	0.000			FULL
23	A	0.627	109.4	203.04	ANNU
	B	0.359			ANNU
	C	0.154			ANNU
	D	0.009			ANWA
	E	0.000			FULL
	F	0.000			FULL
24	A	0.622	109.4	203.04	ANNU
	B	0.347			ANNU
	C	0.187			ANNU
	D	0.036			ANWA
	E	0.000			FULL
	F	0.000			FULL

TABLE B.7 Flow-regime parameters for data set in +10° [upward] inclination (cont'd.)

Run number	Visual observation section	x	$T_{s,av}$ °C	G $kg/m^2.s$	Observed flow regime
25	A	0.622	110.1	214.09	ANNU
	B	0.377			ANNU
	C	0.218			ANNU
	D	0.069			ANNU
	E	0.000			FULL
	F	0.000			FULL
26	A	0.656	109.4	195.67	ANNU
	B	0.375			ANNU
	C	0.170			ANNU
	D	0.000			ANWA
	E	0.000			FULL
	F	0.000			FULL
27	A	0.646	109.4	195.67	ANNU
	B	0.388			ANNU
	C	0.178			ANNU
	D	0.000			ANWA
	E	0.000			FULL
	F	0.000			FULL
28	A	0.664	110.8	214.09	ANNU
	B	0.417			ANNU
	C	0.213			ANNU
	D	0.045			ANNU
	E	0.000			FULL
	F	0.000			FULL
29	A	0.641	110.1	199.36	ANNU
	B	0.391			ANNU
	C	0.201			ANNU
	D	0.050			ANNU
	E	0.000			FULL
	F	0.000			FULL
30	A	0.669	110.1	203.04	ANNU
	B	0.427			ANNU
	C	0.235			ANNU
	D	0.077			ANNU
	E	0.000			FULL
	F	0.000			FULL

TABLE B.7 Flow-regime parameters for data set in +10° [upward] inclination (cont'd.)

Run number	Visual observation section	x	$T_{s,av}$ °C	G $kg/m^2.s$	Observed flow regime
31	A	0.663	112.6	228.82	ANNU
	B	0.403			ANNU
	C	0.205			ANNU
	D	0.006			ANWA
	E	0.000			FULL
	F	0.000			FULL
32	A	0.666	112.0	228.82	ANNU
	B	0.405			ANNU
	C	0.203			ANNU
	D	0.034			ANWA
	E	0.000			FULL
	F	0.000			FULL
33	A	0.660	112.0	232.50	ANNU
	B	0.399			ANNU
	C	0.199			ANNU
	D	0.053			ANNU
	E	0.000			FULL
	F	0.000			FULL
34	A	0.663	112.6	232.50	ANNU
	B	0.397			ANNU
	C	0.215			ANNU
	D	0.067			ANNU
	E	0.000			FULL
	F	0.000			FULL
35	A	0.672	114.9	254.60	ANNU
	B	0.418			ANNU
	C	0.211			ANNU
	D	0.015			ANWA
	E	0.000			FULL
	F	0.000			FULL
36	A	0.668	114.2	258.28	ANNU
	B	0.402			ANNU
	C	0.178			ANNU
	D	0.001			ANWA
	E	0.000			FULL
	F	0.000			FULL

TABLE B.7 Flow-regime parameters for data set in +10° [upward] inclination (cont'd.)

Run number	Visual observation section	x	$T_{s,av}$ °C	G $kg/m^2.s$	Observed flow regime
37	A	0.668	114.9	261.97	ANNU
	B	0.401			ANNU
	C	0.178			ANNU
	D	0.015			ANWA
	E	0.000			FULL
	F	0.000			FULL
38	A	0.666	114.2	261.97	ANNU
	B	0.396			ANNU
	C	0.191			ANNU
	D	0.027			ANWA
	E	0.000			FULL
	F	0.000			FULL
39	A	0.661	113.6	258.28	ANNU
	B	0.386			ANNU
	C	0.195			ANNU
	D	0.045			ANNU
	E	0.000			FULL
	F	0.000			FULL
40	A	0.659	113.6	261.97	ANNU
	B	0.385			ANNU
	C	0.214			ANNU
	D	0.099			ANNU
	E	0.000			FULL
	F	0.000			FULL
41	A	0.633	107.3	162.53	ANNU
	B	0.370			ANNU
	C	0.159			ANNU
	D	0.000			ANWA
	E	0.000			FULL
	F	0.000			FULL
42	A	0.674	108.1	166.21	ANNU
	B	0.390			ANNU
	C	0.178			ANNU
	D	0.000			ANWA
	E	0.000			FULL
	F	0.000			FULL

TABLE B.7 Flow-regime parameters for data set in +10° [upward] inclination (cont'd.)

Run number	Visual observation section	x	$T_{s,av}$ °C	G kg/m^2.s	Observed flow regime
43	A	0.665	108.1	162.53	ANNU
	B	0.419			ANNU
	C	0.209			ANNU
	D	0.023			ANWA
	E	0.000			FULL
	F	0.000			FULL
44	A	0.678	107.3	158.84	ANNU
	B	0.440			ANNU
	C	0.223			ANNU
	D	0.029			ANWA
	E	0.000			FULL
	F	0.000			FULL
45	A	0.572	107.3	166.21	ANNU
	B	0.233			ANNU
	C	0.000			ANWA
	D	0.000			FULL
	E	0.000			FULL
	F	0.000			FULL
46	A	0.546	106.6	166.21	ANNU
	B	0.258			ANNU
	C	0.039			ANWA
	D	0.000			FULL
	E	0.000			FULL
	F	0.000			FULL
47	A	0.597	106.6	162.53	ANNU
	B	0.273			ANNU
	C	0.043			ANNU
	D	0.000			FULL
	E	0.000			FULL
	F	0.000			FULL
48	A	0.586	105.8	162.53	ANNU
	B	0.255			ANNU
	C	0.027			ANWA
	D	0.000			FULL
	E	0.000			FULL
	F	0.000			FULL

TABLE B.7 Flow-regime parameters for data set in +10° [upward] inclination (cont'd.)

Run number	Visual observation section	x	$T_{s,av}$ °C	G $kg/m^2.s$	Observed flow regime
49	A	0.558	103.2	114.65	ANNU
	B	0.242			ANNU
	C	0.012			SLUG
	D	0.000			FULL
	E	0.000			FULL
	F	0.000			FULL
50	A	0.522	103.2	114.65	ANNU
	B	0.209			ANNU
	C	0.007			SLUG
	D	0.000			FULL
	E	0.000			FULL
	F	0.000			FULL
51	A	0.559	103.2	114.65	ANNU
	B	0.242			ANNU
	C	0.028			SLUG
	D	0.000			FULL
	E	0.000			FULL
	F	0.000			FULL
52	A	0.556	104.1	136.75	ANNU
	B	0.234			ANNU
	C	0.022			SLUG
	D	0.000			FULL
	E	0.000			FULL
	F	0.000			FULL

Appendix C

ESTIMATION OF EXPERIMENTAL UNCERTAINTY

This appendix describes the procedure followed in estimating the experimental uncertainty of measured and calculated variables described in the experimental study.

The uncertainty in measured variables such as temperatures, static pressures and volume flow rates were obtained from calibration curves. All pressure gauges, thermocouples and flow meters were calibrated prior to the experiment. From the calibration data of an instrument a least sum of square curve fit was obtained. This least sum of square fit to the calibration data [of a given instrument] provided an estimate of the uncertainty in the observed value [using that instrument]. From the curve fit the uncertainties were estimated at a confidence level of 20:1 odds or 95% probability. The confidence level indicates that the odds are 20 to 1 against the uncertainty for a measurement χ_i being larger than $\pm\delta\chi_i$. In order to estimate the odds the standard deviation ($S_{(N)}$) of the calibration curve was obtained. The uncertainty in the measurement is estimated by

$$\delta\chi_i = \frac{\bar{t}\, S_{(N)}}{\sqrt{N}} \tag{C.1}$$

where $\bar{t}$ is the Student's $\bar{t}$ values appropriate for the number of samples N and the confidence level desired.

The uncertainties in calculated variables [such as such as mass flux (G), quality (x), superficial liquid velocity (V_{LS}) and superficial vapor velocity (V_{VS})] were estimated using the method suggested by Moffat(1988). If R is the calculated value from a set of measurements χ_1, χ_2, χ_3, etc. using a data interpretation program then

$$R = R(\chi_1, \chi_2, \chi_3, \ldots \chi_n) \tag{C.2}$$

The partial derivative of R with respect to χ_n is defined as the sensitivity coefficient for the result R with respect to measurement χ_n. When several independent measurements are used in the function R, the individual terms are combined by a root-sum-square method given below.

$$(\delta R)^2 = \sum_{i=1}^{N} \left(\frac{\partial R}{\partial \chi_i} \delta \chi_i \right)^2 \tag{C.3}$$

The relative error is the fraction δR/R. The uncertainties reported in the following pages are the relative errors given as percentage.

A computer code was used to reduce the experimental data. The estimated uncertainties in the measured variables were supplied to this computer program that converted the measured data [such as pressures, temperatures and flow rates] to the final form of reduced data [such as G, x and V_{VS} , and V_{LS}]. In order to calculate the superficial velocities the vapor quality and the mass flow rate are required. The vapor quality in each visual section was calculated by using the following relationship.

$$x_i = \frac{h_{in} - \frac{1}{\dot{m}_s} \sum_{i=1}^{6} [\, \dot{m}_{W,i}\, C_{PL}\, (T_{out,i} - T_{in,i})] - h_f}{h_{fg}} \tag{C.4}$$

where h_{in} is the enthalpy of steam at the inlet to the test section; $\mathring{m}_{W,i}$ is the mass flow rate of cooling water to i^{th} heat exchanger; C_{PL} is the average specific heat of liquid water; $\mathring{m}_S$ is the steam mass flow rate; h_f and h_{fg} are the enthalpy of liquid water and the latent heat of vaporization respectively at the saturation temperature; and $T_{OUT,i}$ and $T_{IN,i}$ are the temperature of cooling water leaving and temperature of cooling water entering respectively in the i^{th} heat exchanger. For any given test run the variables such as G, x, V_{LS} and V_{VS} were first calculated by the computer program using the observed values of the measured variables for that run. The resulting values of G, x, V_{LS} and V_{VS} were stored as base values for that run under consideration. Each of the measured variables used in the computer program [such as pressures, temperatures and flow rates] were perturbed sequentially by adding the uncertainty in the measurement [estimated from the calibration curves] to the respective observed value of the variable. The difference between the resulting value [after perturbation] and the base amount was then squared and summed as the measured variables were perturbed one by one. The root-sum-square of all differences was recorded as the uncertainty in the calculated variable. The relative uncertainty was obtained by dividing the uncertainty by the base value. This relative uncertainty is reported as a percentage.

TABLE C.1 Experimental uncertainty estimates in the horizontal data set

Run No.	Visual section	G %	x %	V_{GS} %	V_{LS} %
1	A	2.54	0.52	2.78	2.74
	B		0.95	3.08	2.38
	C		1.65	3.65	2.26
	D		8.46	10.14	2.19
	E		0.00	0.00	2.54
	F		0.00	0.00	2.54
2	A	2.54	0.52	2.77	2.75
	B		0.96	3.08	2.38
	C		1.78	3.76	2.25
	D		8.92	10.59	2.19
	E		0.00	0.00	2.54
	F		0.00	0.00	2.54
3	A	2.33	0.39	2.48	2.70
	B		0.67	2.64	2.33
	C		1.08	2.92	2.20
	D		4.39	5.79	2.14
	E		30.00	31.36	2.11
	F		0.00	0.00	2.33
4	A	2.16	0.34	2.26	2.66
	B		0.64	2.39	2.30
	C		1.49	2.89	2.18
	D		5.95	6.82	2.12
	E		0.00	0.00	2.16
	F		0.00	0.00	2.16
5	A	2.12	0.61	2.29	2.73
	B		1.24	2.62	2.32
	C		2.58	3.62	2.18
	D		48.06	48.63	2.10
	E		0.00	0.00	2.12
	F		0.00	0.00	2.12
6	A	2.46	0.52	2.67	2.79
	B		0.98	2.96	2.42
	C		2.08	3.82	2.29
	D		0.00	0.00	2.46
	E		0.00	0.00	2.46
	F		0.00	0.00	2.46
7	A	2.73	0.82	3.16	2.67
	B		2.06	4.15	2.43
	C		12.33	14.07	2.34
	D		0.00	0.00	2.73
	E		0.00	0.00	2.73
	F		0.00	0.00	2.73
8	A	2.24	1.23	2.73	2.90
	B		2.65	3.81	2.38
	C		6.18	7.12	2.22
	D		72.24	73.21	2.16
	E		0.00	0.00	2.24
	F		0.00	0.00	2.24
9	A	2.67	2.09	3.88	2.93
	B		4.05	5.70	2.52
	C		16.02	17.59	2.35
	D		0.00	0.00	2.67
	E		0.00	0.00	2.67
	F		0.00	0.00	2.67
10	A	3.66	2.69	5.61	3.20
	B		11.14	13.99	2.83
	C		0.00	0.00	3.66
	D		0.00	0.00	3.66
	E		0.00	0.00	3.66
	F		0.00	0.00	3.66
11	A	3.93	3.38	6.46	3.40
	B		72.96	77.06	2.96
	C		0.00	0.00	3.93
	D		0.00	0.00	3.93
	E		0.00	0.00	3.93
	F		0.00	0.00	3.93
12	A	4.60	3.22	7.18	3.52
	B		116.12	122.97	3.15
	C		0.00	0.00	4.60
	D		0.00	0.00	4.60
	E		0.00	0.00	4.60
	F		0.00	0.00	4.60
13	A	4.10	4.07	7.26	3.49
	B		0.00	0.00	4.10
	C		0.00	0.00	4.10
	D		0.00	0.00	4.10
	E		0.00	0.00	4.10
	F		0.00	0.00	4.10
14	A	2.64	0.76	2.99	2.90
	B		1.72	3.70	2.51
	C		0.00	0.00	2.64
	D		0.00	0.00	2.64
	E		0.00	0.00	2.64
	F		0.00	0.00	2.64
15	A	3.43	1.48	4.37	3.17
	B		6.95	9.51	2.77
	C		0.00	0.00	3.43
	D		0.00	0.00	3.43
	E		0.00	0.00	3.43
	F		0.00	0.00	3.43
16	A	3.98	4.83	7.83	3.41
	B		1428.31	1468.01	2.79
	C		0.00	0.00	3.98
	D		0.00	0.00	3.98
	E		0.00	0.00	3.98
	F		0.00	0.00	3.98
17	A	3.09	5.75	7.58	3.06
	B		67.71	70.03	2.67
	C		0.00	0.00	3.09
	D		0.00	0.00	3.09
	E		0.00	0.00	3.09
	F		0.00	0.00	3.09
18	A	5.13	274.16	285.28	3.64
	B		0.00	0.00	5.13
	C		0.00	0.00	5.13
	D		0.00	0.00	5.13
	E		0.00	0.00	5.13
	F		0.00	0.00	5.13
19	A	4.87	4.24	8.40	3.67
	B		0.00	0.00	4.87
	C		0.00	0.00	4.87
	D		0.00	0.00	4.87
	E		0.00	0.00	4.87
	F		0.00	0.00	4.87
20	A	7.40	18.94	25.95	4.87
	B		0.00	0.00	7.40
	C		0.00	0.00	7.40
	D		0.00	0.00	7.40
	E		0.00	0.00	7.40
	F		0.00	0.00	7.40
21	A	4.33	2.54	6.25	3.49
	B		11.46	15.14	3.12
	C		0.00	0.00	4.33
	D		0.00	0.00	4.33
	E		0.00	0.00	4.33
	F		0.00	0.00	4.33
22	A	3.85	1.79	5.09	3.29
	B		5.40	8.57	2.92
	C		0.00	0.00	3.85
	D		0.00	0.00	3.85
	E		0.00	0.00	3.85
	F		0.00	0.00	3.85
23	A	5.30	4.19	8.87	3.82
	B		0.00	0.00	4.95
	C		0.00	0.00	5.30
	D		0.00	0.00	5.30
	E		0.00	0.00	5.30
	F		0.00	0.00	5.30
24	A	3.73	1.73	4.89	3.30
	B		4.94	7.91	2.94
	C		0.00	0.00	2.75
	D		0.00	0.00	3.73
	E		0.00	0.00	3.73
	F		0.00	0.00	3.73
25	A	3.98	2.02	5.41	3.38
	B		6.63	9.88	3.01
	C		0.00	0.00	3.98
	D		0.00	0.00	3.98
	E		0.00	0.00	3.98
	F		0.00	0.00	3.98
26	A	3.14	1.14	3.80	3.05
	B		2.52	5.02	2.65
	C		13.53	15.90	2.49
	D		0.00	0.00	3.14
	E		0.00	0.00	3.14
	F		0.00	0.00	3.14

TABLE C.1 Experimental uncertainty estimates in the horizontal data set (cont'd.)

Run No.	Visual section	G %	x %	V_{TB} %	V_{LS} %
27	A	3.27	1.20	4.01	3.04
	B		2.92	5.58	2.65
	C		20.74	23.44	2.50
	D		0.00	0.00	3.27
	E		0.00	0.00	3.27
	F		0.00	0.00	3.27
28	A	3.11	1.06	3.72	3.02
	B		2.45	4.94	2.62
	C		8.99	11.35	2.48
	D		0.00	0.00	3.11
	E		0.00	0.00	3.11
	F		0.00	0.00	3.11
29	A	3.27	1.26	4.03	3.10
	B		3.05	5.65	2.71
	C		16.20	18.74	2.56
	D		0.00	0.00	3.27
	E		0.00	0.00	3.27
	F		0.00	0.00	3.27
30	A	3.07	1.65	4.05	3.04
	B		3.62	5.88	2.64
	C		48.33	50.94	2.47
	D		0.00	0.00	3.07
	E		0.00	0.00	3.07
	F		0.00	0.00	3.07
31	A	2.85	0.96	3.34	2.96
	B		1.99	4.19	2.57
	C		7.18	9.11	2.42
	D		0.00	0.00	2.85
	E		0.00	0.00	2.85
	F		0.00	0.00	2.85
32	A	3.10	1.41	3.93	3.04
	B		3.12	5.48	2.66
	C		13.87	16.10	2.51
	D		0.00	0.00	3.10
	E		0.00	0.00	3.10
	F		0.00	0.00	3.10
33	A	2.91	1.27	3.62	3.00
	B		2.59	4.76	2.62
	C		9.05	11.00	2.47
	D		0.00	0.00	2.91
	E		0.00	0.00	2.91
	F		0.00	0.00	2.91
34	A	2.73	1.72	3.67	3.01
	B		3.87	5.61	2.56
	C		31.38	33.07	2.39
	D		0.00	0.00	2.73
	E		0.00	0.00	2.73
	F		0.00	0.00	2.73
35	A	2.72	1.82	3.73	3.01
	B		4.08	5.79	2.54
	C		13.24	14.85	2.40
	D		0.00	0.00	2.72
	E		0.00	0.00	2.72
	F		0.00	0.00	2.72
36	A	2.70	1.06	3.21	2.91
	B		1.92	3.92	2.52
	C		4.18	6.00	2.38
	D		0.00	0.00	2.70
	E		0.00	0.00	2.70
	F		0.00	0.00	2.70
37	A	2.63	1.23	3.23	2.94
	B		2.10	3.97	2.53
	C		5.89	7.52	2.35
	D		0.00	0.00	2.63
	E		0.00	0.00	2.63
	F		0.00	0.00	2.63
38	A	2.64	1.64	3.49	2.97
	B		3.51	5.16	2.52
	C		16.36	17.84	2.36
	D		0.00	0.00	2.64
	E		0.00	0.00	2.64
	F		0.00	0.00	2.64
39	A	2.95	1.61	3.86	3.09
	B		3.33	5.44	2.62
	C		8.89	10.91	2.47
	D		0.00	0.00	2.95
	E		0.00	0.00	2.95
	F		0.00	0.00	2.95
40	A	3.14	2.02	4.40	3.14
	B		4.73	7.00	2.66
	C		0.00	0.00	2.39
	D		0.00	0.00	3.14
	E		0.00	0.00	3.14
	F		0.00	0.00	3.14
41	A	3.02	1.82	4.09	3.12
	B		4.50	6.60	2.63
	C		55.17	57.74	2.46
	D		0.00	0.00	3.02
	E		0.00	0.00	3.02
	F		0.00	0.00	3.02
42	A	2.73	0.99	3.21	2.95
	B		1.63	3.74	2.54
	C		3.01	5.00	2.38
	D		0.00	0.00	2.69
	E		0.00	0.00	2.73
	F		0.00	0.00	2.73
43	A	2.85	1.19	3.48	2.99
	B		2.16	4.33	2.57
	C		4.44	6.49	2.42
	D		0.00	0.00	2.85
	E		0.00	0.00	2.85
	F		0.00	0.00	2.85
44	A	2.98	2.11	4.25	3.14
	B		4.04	6.10	2.66
	C		12.50	14.53	2.49
	D		0.00	0.00	2.98
	E		0.00	0.00	2.98
	F		0.00	0.00	2.98
45	A	2.91	1.92	4.02	3.12
	B		3.94	5.93	2.62
	C		22.37	24.38	2.43
	D		0.00	0.00	2.91
	E		0.00	0.00	2.91
	F		0.00	0.00	2.91
46	A	2.10	0.60	2.27	2.66
	B		0.90	2.42	2.29
	C		1.37	2.71	2.16
	D		3.46	4.39	2.09
	E		0.00	0.00	2.10
	F		0.00	0.00	2.10
47	A	2.10	0.59	2.27	2.66
	B		0.91	2.42	2.28
	C		1.53	2.81	2.16
	D		4.00	4.87	2.09
	E		0.00	0.00	2.10
	F		0.00	0.00	2.10
48	A	2.14	0.94	2.45	2.88
	B		1.73	2.96	2.38
	C		3.61	4.53	2.21
	D		0.00	0.00	2.14
	E		0.00	0.00	2.14
	F		0.00	0.00	2.14
49	A	2.13	0.96	2.45	2.86
	B		1.78	2.97	2.37
	C		2.78	3.78	2.22
	D		29.79	30.35	2.12
	E		0.00	0.00	2.13
	F		0.00	0.00	2.13
50	A	2.23	1.13	2.66	2.94
	B		2.16	3.41	2.41
	C		4.96	5.94	2.23
	D		0.00	0.00	2.14
	E		0.00	0.00	2.23
	F		0.00	0.00	2.23
51	A	2.15	0.88	2.44	2.79
	B		1.53	2.85	2.35
	C		2.60	3.69	2.21
	D		202.10	203.15	2.12
	E		0.00	0.00	2.15
	F		0.00	0.00	2.15
52	A	2.21	0.96	2.55	2.88
	B		1.65	3.02	2.38
	C		3.28	4.39	2.21
	D		30.65	31.48	2.13
	E		0.00	0.00	2.21
	F		0.00	0.00	2.21

TABLE C.1 Experimental uncertainty estimates in the horizontal data set (cont'd.)

Run No.	Visual section	G %	x %	V_{TB} %	V_{LS} %
53	A	2.17	0.86	2.46	2.78
	B		1.44	2.82	2.34
	C		2.05	3.30	2.21
	D		4.95	5.89	2.13
	E		0.00	0.00	2.17
	F		0.00	0.00	2.17
54	A	2.17	1.14	2.58	2.96
	B		2.11	3.27	2.42
	C		4.72	5.59	2.22
	D		0.00	0.00	2.17
	E		0.00	0.00	2.17
	F		0.00	0.00	2.17
55	A	2.21	1.28	2.71	3.01
	B		2.40	3.56	2.44
	C		3.97	4.96	2.28
	D		64.19	65.00	2.17
	E		0.00	0.00	2.21
	F		0.00	0.00	2.21
56	A	2.21	1.23	2.68	3.01
	B		2.46	3.60	2.44
	C		4.86	5.77	2.26
	D		0.00	0.00	2.21
	E		0.00	0.00	2.21
	F		0.00	0.00	2.21
57	A	2.16	1.04	2.51	2.93
	B		1.95	3.13	2.41
	C		3.23	4.21	2.25
	D		90.43	91.13	2.15
	E		0.00	0.00	2.16
	F		0.00	0.00	2.16
58	A	2.22	1.05	2.59	2.97
	B		1.82	3.13	2.43
	C		3.75	4.79	2.24
	D		31.00	31.78	2.16
	E		0.00	0.00	2.22
	F		0.00	0.00	2.22
59	A	2.28	0.90	2.62	2.91
	B		1.69	3.16	2.41
	C		3.73	4.93	2.23
	D		30.74	31.74	2.16
	E		0.00	0.00	2.28
	F		0.00	0.00	2.28
60	A	2.30	1.14	2.75	3.05
	B		2.16	3.51	2.47
	C		4.66	5.78	2.27
	D		17.07	18.02	2.20
	E		0.00	0.00	2.30
	F		0.00	0.00	2.30
61	A	2.61	0.81	2.96	2.98
	B		1.28	3.32	2.56
	C		2.89	4.68	2.38
	D		15.58	17.12	2.30
	E		0.00	0.00	2.61
	F		0.00	0.00	2.61
62	A	2.57	0.85	2.94	2.98
	B		1.47	3.41	2.52
	C		3.66	5.34	2.34
	D		25.00	26.55	2.27
	E		0.00	0.00	2.57
	F		0.00	0.00	2.57
63	A	2.23	1.11	2.64	2.98
	B		2.07	3.33	2.43
	C		4.03	5.06	2.24
	D		48.19	49.04	2.15
	E		0.00	0.00	2.23
	F		0.00	0.00	2.23
64	A	2.46	0.95	2.86	2.96
	B		1.77	3.48	2.47
	C		3.27	4.81	2.31
	D		20.34	21.66	2.23
	E		0.00	0.00	2.46
	F		0.00	0.00	2.46
65	A	2.42	1.09	2.87	3.00
	B		2.09	3.64	2.47
	C		4.65	5.99	2.29
	D		76.13	77.67	2.21
	E		0.00	0.00	2.42
	F		0.00	0.00	2.42
66	A	2.68	1.40	3.38	3.08
	B		2.47	4.31	2.59
	C		5.61	7.28	2.41
	D		121.35	123.89	2.33
	E		0.00	0.00	2.68
	F		0.00	0.00	2.68
67	A	2.64	1.01	3.12	2.97
	B		1.88	3.82	2.51
	C		4.12	5.89	2.34
	D		194.32	197.86	2.26
	E		0.00	0.00	2.64
	F		0.00	0.00	2.64
68	A	2.64	0.90	3.06	2.97
	B		1.87	3.82	2.50
	C		3.89	5.69	2.34
	D		36.72	38.59	2.26
	E		0.00	0.00	2.64
	F		0.00	0.00	2.64
69	A	2.42	1.23	2.95	3.00
	B		2.26	3.78	2.46
	C		5.37	6.68	2.27
	D		140.12	142.15	2.20
	E		0.00	0.00	2.42
	F		0.00	0.00	2.42
70	A	6.06	12.55	17.27	4.83
	B		0.00	0.00	6.06
	C		0.00	0.00	6.06
	D		0.00	0.00	6.06
	E		0.00	0.00	6.06
	F		0.00	0.00	6.06
71	A	5.95	8.93	13.66	4.72
	B		0.00	0.00	5.95
	C		0.00	0.00	5.95
	D		0.00	0.00	5.95
	E		0.00	0.00	5.95
	F		0.00	0.00	5.95
72	A	5.84	12.21	16.69	4.70
	B		0.00	0.00	5.84
	C		0.00	0.00	5.84
	D		0.00	0.00	5.84
	E		0.00	0.00	5.84
	F		0.00	0.00	5.84
73	A	4.78	8.98	12.41	4.12
	B		0.00	0.00	4.78
	C		0.00	0.00	4.78
	D		0.00	0.00	4.78
	E		0.00	0.00	4.78
	F		0.00	0.00	4.78

TABLE C.2 Experimental uncertainty estimates in the -1° [downward] data set

Run No.	Visual section	G %	x %	V_{GJ} %	V_{LG} %
1	A	3.52	1.61	4.56	3.23
	B		4.42	7.15	2.88
	C		33.16	36.05	2.74
	D		0.00	0.00	3.52
	E		0.00	0.00	3.52
	F		0.00	0.00	3.52
2	A	3.52	1.63	4.54	3.31
	B		4.32	6.99	2.96
	C		113.55	117.46	2.81
	D		0.00	0.00	3.52
	E		0.00	0.00	3.52
	F		0.00	0.00	3.52
3	A	3.60	1.64	4.66	3.29
	B		5.00	7.77	2.93
	C		0.00	0.00	2.60
	D		0.00	0.00	3.60
	E		0.00	0.00	3.60
	F		0.00	0.00	3.60
4	A	3.66	2.19	5.14	3.37
	B		7.34	10.03	2.99
	C		0.00	0.00	3.66
	D		0.00	0.00	3.66
	E		0.00	0.00	3.66
	F		0.00	0.00	3.66
5	A	3.60	2.29	5.12	3.36
	B		8.37	10.94	2.98
	C		0.00	0.00	3.60
	D		0.00	0.00	3.60
	E		0.00	0.00	3.60
	F		0.00	0.00	3.60
6	A	3.73	3.28	6.10	3.40
	B		20.36	23.13	2.98
	C		0.00	0.00	3.73
	D		0.00	0.00	3.73
	E		0.00	0.00	3.73
	F		0.00	0.00	3.73
7	A	4.56	2.80	6.69	3.69
	B		14.35	18.09	3.36
	C		0.00	0.00	4.56
	D		0.00	0.00	4.56
	E		0.00	0.00	4.56
	F		0.00	0.00	4.56
8	A	4.26	3.72	7.08	3.69
	B		20.73	24.08	3.27
	C		0.00	0.00	4.26
	D		0.00	0.00	4.26
	E		0.00	0.00	4.26
	F		0.00	0.00	4.26
9	A	5.02	4.30	8.49	3.96
	B		155.50	163.15	3.60
	C		0.00	0.00	5.02
	D		0.00	0.00	5.02
	E		0.00	0.00	5.02
	F		0.00	0.00	5.02
10	A	5.13	3.82	8.19	3.99
	B		64.51	69.96	3.66
	C		0.00	0.00	5.13
	D		0.00	0.00	5.13
	E		0.00	0.00	5.13
	F		0.00	0.00	5.13
11	A	4.97	6.10	10.07	3.98
	B		0.00	0.00	4.73
	C		0.00	0.00	4.97
	D		0.00	0.00	4.97
	E		0.00	0.00	4.97
	F		0.00	0.00	4.97
12	A	4.97	14.54	18.12	4.16
	B		0.00	0.00	4.97
	C		0.00	0.00	4.97
	D		0.00	0.00	4.97
	E		0.00	0.00	4.97
	F		0.00	0.00	4.97
13	A	3.54	1.64	4.60	3.30
	B		4.49	7.22	2.90
	C		106.49	110.56	2.75
	D		0.00	0.00	3.54
	E		0.00	0.00	3.54
	F		0.00	0.00	3.54
14	A	3.52	1.45	4.43	3.31
	B		3.89	6.62	2.93
	C		28.94	31.68	2.78
	D		0.00	0.00	3.52
	E		0.00	0.00	3.52
	F		0.00	0.00	3.52
15	A	3.35	2.79	5.20	3.36
	B		8.07	10.30	2.91
	C		0.00	0.00	3.35
	D		0.00	0.00	3.35
	E		0.00	0.00	3.35
	F		0.00	0.00	3.35
16	A	3.58	2.39	5.20	3.37
	B		6.30	8.94	2.95
	C		0.00	0.00	3.58
	D		0.00	0.00	3.58
	E		0.00	0.00	3.58
	F		0.00	0.00	3.58
17	A	3.00	1.09	3.56	3.27
	B		2.50	4.68	2.89
	C		7.61	9.43	2.74
	D		0.00	0.00	3.00
	E		0.00	0.00	3.00
	F		0.00	0.00	3.00
18	A	3.06	1.48	3.89	3.25
	B		3.42	5.56	2.85
	C		15.09	16.95	2.70
	D		0.00	0.00	3.06
	E		0.00	0.00	3.06
	F		0.00	0.00	3.06
19	A	2.97	1.78	3.97	3.26
	B		4.54	6.42	2.84
	C		22.78	24.48	2.69
	D		0.00	0.00	2.97
	E		0.00	0.00	2.97
	F		0.00	0.00	2.97
20	A	3.02	1.93	4.14	3.27
	B		4.80	6.74	2.84
	C		25.91	27.72	2.69
	D		0.00	0.00	3.02
	E		0.00	0.00	3.02
	F		0.00	0.00	3.02
21	A	2.75	1.70	3.67	3.07
	B		4.72	6.39	2.61
	C		1459.11	1478.43	2.30
	D		0.00	0.00	2.75
	E		0.00	0.00	2.75
	F		0.00	0.00	2.75
22	A	2.74	1.50	3.53	3.04
	B		3.71	5.46	2.60
	C		17.82	19.39	2.45
	D		0.00	0.00	2.74
	E		0.00	0.00	2.74
	F		0.00	0.00	2.74
23	A	2.68	1.49	3.44	3.08
	B		3.70	5.36	2.60
	C		22.59	24.07	2.43
	D		0.00	0.00	2.68
	E		0.00	0.00	2.68
	F		0.00	0.00	2.68
24	A	2.76	1.27	3.41	3.04
	B		2.67	4.59	2.61
	C		8.19	9.87	2.45
	D		0.00	0.00	2.76
	E		0.00	0.00	2.76
	F		0.00	0.00	2.76
25	A	2.84	2.09	4.05	3.17
	B		4.98	6.70	2.71
	C		29.25	30.91	2.54
	D		0.00	0.00	2.84
	E		0.00	0.00	2.84
	F		0.00	0.00	2.84
26	A	2.80	1.60	3.65	3.13
	B		3.93	5.70	2.67
	C		17.73	19.30	2.52
	D		0.00	0.00	2.80
	E		0.00	0.00	2.80
	F		0.00	0.00	2.80

TABLE C.2 Experimental uncertainty estimates in the -1° [downward] data set (cont'd.)

Run No.	Visual section	G %	x %	V_{SG} %	V_{SL} %
27	A	2.81	0.85	3.20	3.20
	B		2.02	4.05	2.81
	C		5.26	6.94	2.66
	D		0.00	0.00	2.81
	E		0.00	0.00	2.81
	F		0.00	0.00	2.81
28	A	2.76	1.88	3.78	3.24
	B		3.46	5.15	2.81
	C		8.86	10.33	2.64
	D		0.00	0.00	2.76
	E		0.00	0.00	2.76
	F		0.00	0.00	2.76
29	A	2.85	1.39	3.58	3.17
	B		2.90	4.86	2.72
	C		8.14	9.86	2.56
	D		0.00	0.00	2.85
	E		0.00	0.00	2.85
	F		0.00	0.00	2.85
30	A	2.98	1.97	4.11	3.27
	B		4.92	6.82	2.77
	C		271.54	275.71	2.59
	D		0.00	0.00	2.98
	E		0.00	0.00.	2.98
	F		0.00	0.00	2.98
31	A	2.85	0.93	3.31	3.11
	B		2.03	4.18	2.68
	C		7.03	8.84	2.51
	D		0.00	0.00	2.85
	E		0.00	0.00	2.85
	F		0.00	0.00	2.85
32	A	2.80	2.14	4.02	3.22
	B		5.08	6.75	2.67
	C		33.55	35.24	2.49
	D		0.00	0.00	2.80
	E		0.00	0.00	2.80
	F		0.00	0.00	2.80
33	A	2.85	2.10	4.04	3.30
	B		5.18	6.87	2.75
	C		44.54	46.26	2.58
	D		0.00	0.00	2.85
	E		0.00	0.00	2.85
	F		0.00	0.00	2.85
34	A	2.88	2.23	4.17	3.34
	B		5.42	7.12	2.78
	C		89.21	91.31	2.59
	D		0.00	0.00	2.88
	E		0.00	0.00	2.88
	F		0.00	0.00	2.88
35	A	3.05	2.07	4.28	3.28
	B		4.50	6.54	2.79
	C		26.50	28.51	2.61
	D		0.00	0.00	3.05
	E		0.00	0.00	3.05
	F		0.00	0.00	3.05
36	A	2.54	1.88	3.51	3.19
	B		5.50	6.78	2.59
	C		0.00	0.00	2.54
	D		0.00	0.00	2.54
	E		0.00	0.00	2.54
	F		0.00	0.00	2.54
37	A	2.50	1.71	3.34	3.10
	B		3.99	5.36	2.51
	C		14.23	15.45	2.34
	D		0.00	0.00	2.50
	E		0.00	0.00	2.50
	F		0.00	0.00	2.50
38	A	2.45	1.76	3.30	3.15
	B		4.15	5.40	2.54
	C		18.11	19.17	2.35
	D		0.00	0.00	2.45
	E		0.00	0.00	2.45
	F		0.00	0.00	2.45
39	A	2.47	1.96	3.46	3.23
	B		4.95	6.16	2.57
	C		117.71	119.20	2.36
	D		0.00	0.00	2.47
	E		0.00	0.00	2.47
	F		0.00	0.00	2.47
40	A	2.75	1.93	3.81	3.19
	B		4.84	6.48	2.64
	C		60.26	62.09	2.45
	D		0.00	0.00	2.75
	E		0.00	0.00	2.75
	F		0.00	0.00	2.75
41	A	2.73	2.00	3.82	3.22
	B		4.14	5.78	2.67
	C		13.07	14.56	2.49
	D		0.00	0.00	2.73
	E		0.00	0.00	2.73
	F		0.00	0.00	2.73
42	A	2.73	1.27	3.37	3.05
	B		2.62	4.51	2.58
	C		7.06	8.75	2.42
	D		0.00	0.00	2.73
	E		0.00	0.00	2.73
	F		0.00	0.00	2.73
43	A	2.73	2.23	4.02	3.13
	B		5.70	7.27	2.59
	C		104.45	106.63	2.42
	D		0.00	0.00	2.73
	E		0.00	0.00	2.73
	F		0.00	0.00	2.73
44	A	2.56	1.61	3.35	3.10
	B		3.47	4.98	2.54
	C		13.63	14.94	2.36
	D		0.00	0.00	2.56
	E		0.00	0.00	2.56
	F		0.00	0.00	2.56
45	A	2.42	1.17	2.91	2.98
	B		2.26	3.77	2.46
	C		4.33	5.66	2.31
	D		22.01	23.18	2.24
	E		0.00	0.00	2.42
	F		0.00	0.00	2.42
46	A	2.46	1.06	2.92	2.96
	B		2.11	3.73	2.47
	C		5.45	6.82	2.30
	D		248.29	251.09	2.24
	E		0.00	0.00	2.46
	F		0.00	0.00	2.46
47	A	2.44	1.31	3.02	3.03
	B		3.11	4.51	2.48
	C		12.77	13.91	2.30
	D		0.00	0.00	2.44
	E		0.00	0.00	2.44
	F		0.00	0.00	2.44
48	A	2.43	1.21	2.95	3.00
	B		2.37	3.87	2.48
	C		7.40	8.61	2.30
	D		0.00	0.00	2.43
	E		0.00	0.00	2.43
	F		0.00	0.00	2.43
49	A	2.33	1.09	2.77	2.97
	B		2.14	3.56	2.44
	C		5.47	6.61	2.26
	D		0.00	0.00	2.33
	E		0.00	0.00	2.33
	F		0.00	0.00	2.33
50	A	2.33	1.39	2.93	3.03
	B		3.00	4.25	2.45
	C		13.49	14.45	2.26
	D		0.00	0.00	2.33
	E		0.00	0.00	2.33
	F		0.00	0.00	2.33
51	A	2.33	0.95	2.70	2.89
	B		1.74	3.27	2.41
	C		3.71	5.01	2.25
	D		16.95	18.03	2.18
	E		0.00	0.00	2.33
	F		0.00	0.00	2.33
52	A	2.35	0.95	2.72	2.90
	B		1.81	3.35	2.41
	C		4.16	5.45	2.25
	D		72.39	73.75	2.18
	E		0.00	0.00	2.35
	F		0.00	0.00	2.35

TABLE C.2 Experimental uncertainty estimates in the -1° [downward] data set (cont'd.)

Run No.	Visual section	G %	x %	V_{TB} %	V_{LS} %
53	A	2.28	0.94	2.64	2.83
	B		1.69	3.17	2.37
	C		2.83	4.14	2.24
	D		9.34	10.38	2.16
	E		0.00	0.00	2.28
	F		0.00	0.00	2.28
54	A	2.30	0.88	2.63	2.83
	B		1.67	3.18	2.38
	C		3.44	4.71	2.23
	D		20.48	21.49	2.16
	E		0.00	0.00	2.30
	F		0.00	0.00	2.30
55	A	2.30	1.32	2.86	2.93
	B		2.52	3.82	2.41
	C		5.42	6.51	2.25
	D		68.77	69.91	2.18
	E		0.00	0.00	2.30
	F		0.00	0.00	2.30
56	A	2.27	1.28	2.78	2.97
	B		2.64	3.85	2.42
	C		8.58	9.48	2.23
	D		0.00	0.00	2.27
	E		0.00	0.00	2.27
	F		0.00	0.00	2.27
57	A	2.16	0.80	2.42	2.79
	B		1.41	2.79	2.34
	C		2.54	3.67	2.19
	D		11.90	12.64	2.12
	E		0.00	0.00	2.16
	F		0.00	0.00	2.16
58	A	2.16	1.02	2.51	2.89
	B		1.88	3.09	2.37
	C		4.05	4.97	2.20
	D		50.26	50.95	2.13
	E		0.00	0.00	2.16
	F		0.00	0.00	2.16
59	A	2.17	0.77	2.42	2.77
	B		1.34	2.76	2.34
	C		2.16	3.39	2.20
	D		6.15	7.03	2.13
	E		0.00	0.00	2.17
	F		0.00	0.00	2.17
60	A	2.75	1.42	3.49	3.09
	B		3.21	5.04	2.60
	C		10.08	11.72	2.44
	D		0.00	0.00	2.75
	E		0.00	0.00	2.75
	F		0.00	0.00	2.75
61	A	2.70	1.84	3.70	3.12
	B		4.88	6.48	2.57
	C		15.97	17.49	2.43
	D		0.00	0.00	2.70
	E		0.00	0.00	2.70
	F		0.00	0.00	2.70
62	A	2.68	1.87	3.68	3.15
	B		4.29	5.90	2.58
	C		36.99	38.62	2.38
	D		0.00	0.00	2.68
	E		0.00	0.00	2.68
	F		0.00	0.00	2.68
63	A	2.80	2.24	4.11	3.15
	B		5.16	6.83	2.65
	C		33.26	34.95	2.48
	D		0.00	0.00	2.80
	E		0.00	0.00	2.80
	F		0.00	0.00	2.80

TABLE C.3 Experimental uncertainty estimates in the -5° [downward] data set

Run No.	Visual section	G %	x %	V_{SG} %	V_{LG} %
1	A	3.06	1.07	3.62	3.20
	B		2.34	4.65	2.81
	C		7.23	9.23	2.66
	D		0.00	0.00	3.06
	E		0.00	0.00	3.06
	F		0.00	0.00	3.06
2	A	2.83	0.99	3.32	3.06
	B		2.02	4.14	2.66
	C		5.45	7.29	2.51
	D		0.00	0.00	2.83
	E		0.00	0.00	2.83
	F		0.00	0.00	2.83
3	A	2.81	1.30	3.49	3.07
	B		2.58	4.57	2.64
	C		7.49	9.25	2.48
	D		0.00	0.00	2.81
	E		0.00	0.00	2.81
	F		0.00	0.00	2.81
4	A	2.68	1.86	3.69	3.06
	B		3.90	5.54	2.59
	C		16.73	18.22	2.41
	D		0.00	0.00	2.68
	E		0.00	0.00	2.68
	F		0.00	0.00	2.68
5	A	2.85	0.89	3.30	3.05
	B		1.57	3.86	2.61
	C		3.10	5.24	2.44
	D		592.98	603.47	2.31
	E		0.00	0.00	2.85
	F		0.00	0.00	2.85
6	A	2.45	1.37	3.08	3.02
	B		2.32	3.88	2.48
	C		4.07	5.50	2.31
	D		25.59	26.92	2.22
	E		0.00	0.00	2.45
	F		0.00	0.00	2.45
7	A	2.45	1.38	3.08	3.03
	B		2.70	4.19	2.48
	C		6.17	7.47	2.30
	D		0.00	0.00	2.45
	E		0.00	0.00	2.45
	F		0.00	0.00	2.45
8	A	2.64	1.77	3.57	3.15
	B		4.09	5.67	2.56
	C		14.92	16.41	2.37
	D		0.00	0.00	2.64
	E		0.00	0.00	2.64
	F		0.00	0.00	2.64
9	A	2.61	1.44	3.32	3.04
	B		2.51	4.26	2.54
	C		4.20	5.85	2.39
	D		262.62	266.42	2.27
	E		0.00	0.00	2.61
	F		0.00	0.00	2.61
10	A	2.39	1.15	2.87	2.98
	B		2.25	3.74	2.45
	C		4.08	5.41	2.29
	D		21.38	22.54	2.21
	E		0.00	0.00	2.39
	F		0.00	0.00	2.39
11	A	2.36	1.08	2.79	3.00
	B		2.06	3.54	2.45
	C		4.32	5.58	2.27
	D		63.74	65.04	2.19
	E		0.00	0.00	2.36
	F		0.00	0.00	2.36
12	A	2.28	0.96	2.64	2.88
	B		1.69	3.16	2.39
	C		2.90	4.19	2.24
	D		8.54	9.57	2.17
	E		0.00	0.00	2.28
	F		0.00	0.00	2.28
13	A	2.28	1.17	2.74	3.00
	B		2.24	3.55	2.44
	C		4.90	5.97	2.25
	D		0.00	0.00	2.28
	E		0.00	0.00	2.28
	F		0.00	0.00	2.28
14	A	2.17	0.96	2.49	2.96
	B		1.56	2.87	2.41
	C		2.56	3.67	2.23
	D		6.68	7.51	2.14
	E		0.00	0.00	2.17
	F		0.00	0.00	2.17
15	A	2.20	1.19	2.65	3.02
	B		2.12	3.32	2.46
	C		4.47	5.40	2.26
	D		432.36	434.50	2.13
	E		0.00	0.00	2.20
	F		0.00	0.00	2.20
16	A	2.20	1.16	2.63	3.04
	B		2.15	3.34	2.46
	C		4.73	5.64	2.26
	D		0.00	0.00	2.20
	E		0.00	0.00	2.20
	F		0.00	0.00	2.20
17	A	2.13	1.06	2.50	2.97
	B		1.94	3.08	2.44
	C		4.03	4.87	2.23
	D		83.48	84.10	2.14
	E		0.00	0.00	2.13
	F		0.00	0.00	2.13
18	A	2.16	1.03	2.51	2.93
	B		1.87	3.07	2.42
	C		3.51	4.46	2.23
	D		39.85	40.48	2.14
	E		0.00	0.00	2.16
	F		0.00	0.00	2.16
19	A	2.56	1.11	3.06	3.06
	B		2.16	3.90	2.54
	C		5.10	6.62	2.35
	D		0.00	0.00	2.56
	E		0.00	0.00	2.56
	F		0.00	0.00	2.56
20	A	2.61	1.13	3.14	3.01
	B		1.95	3.81	2.54
	C		3.87	5.55	2.37
	D		64.96	66.87	2.28
	E		0.00	0.00	2.61
	F		0.00	0.00	2.61
21	A	2.80	1.15	3.38	3.09
	B		1.85	3.99	2.63
	C		3.84	5.81	2.44
	D		38.74	40.81	2.35
	E		0.00	0.00	2.80
	F		0.00	0.00	2.80
22	A	2.92	1.51	3.76	3.15
	B		3.09	5.14	2.72
	C		9.37	11.20	2.56
	D		0.00	0.00	2.92
	E		0.00	0.00	2.92
	F		0.00	0.00	2.92
23	A	2.90	1.42	3.65	3.18
	B		2.86	4.87	2.76
	C		82.16	84.29	2.57
	D		0.00	0.00	2.90
	E		0.00	0.00	2.90
	F		0.00	0.00	2.90
24	A	2.72	1.37	3.41	3.10
	B		2.99	4.76	2.66
	C		7.34	8.88	2.52
	D		0.00	0.00	2.72
	E		0.00	0.00	2.72
	F		0.00	0.00	2.72
25	A	2.73	1.06	3.24	3.07
	B		2.40	4.29	2.66
	C		5.49	7.14	2.51
	D		0.00	0.00	2.73
	E		0.00	0.00	2.73
	F		0.00	0.00	2.73
26	A	2.54	1.15	3.05	3.16
	B		2.46	4.08	2.59
	C		6.30	7.68	2.40
	D		0.00	0.00	2.54
	E		0.00	0.00	2.54
	F		0.00	0.00	2.54

TABLE C.3 Experimental uncertainty estimates in the -5°[downward] data set (cont'd.)

Run No.	Visual section	G %	x %	V_{sg} %	V_{sl} %
27	A	2.51	1.44	3.18	3.18
	B		3.17	4.63	2.58
	C		8.41	9.67	2.39
	D		0.00	0.00	2.51
	E		0.00	0.00	2.51
	F		0.00	0.00	2.51
28	A	2.38	1.57	3.09	3.09
	B		3.20	4.46	2.53
	C		9.50	10.52	2.33
	D		0.00	0.00	2.38
	E		0.00	0.00	2.38
	F		0.00	0.00	2.38
29	A	2.39	0.72	2.67	2.81
	B		1.28	3.05	2.40
	C		2.46	4.03	2.25
	D		10.63	11.88	2.18
	E		0.00	0.00	2.39
	F		0.00	0.00	2.39
30	A	2.34	0.95	2.72	2.92
	B		1.78	3.31	2.43
	C		3.88	5.16	2.26
	D		187.61	189.58	2.18
	E		0.00	0.00	2.34
	F		0.00	0.00	2.34
31	A	2.38	0.85	2.72	2.86
	B		1.55	3.22	2.41
	C		2.98	4.44	2.26
	D		13.80	15.00	2.19
	E		0.00	0.00	2.38
	F		0.00	0.00	2.38
32	A	2.73	1.27	3.38	3.03
	B		2.94	4.80	2.56
	C		9.41	11.07	2.40
	D		0.00	0.00	2.73
	E		0.00	0.00	2.73
	F		0.00	0.00	2.73
33	A	2.73	1.44	3.48	3.05
	B		3.43	5.22	2.57
	C		15.24	16.85	2.40
	D		0.00	0.00	2.73
	E		0.00	0.00	2.73
	F		0.00	0.00	2.73
34	A	2.70	1.54	3.51	3.06
	B		3.98	5.67	2.57
	C		43.17	44.87	2.39
	D		0.00	0.00	2.70
	E		0.00	0.00	2.70
	F		0.00	0.00	2.70
35	A	3.73	3.11	5.94	3.46
	B		9.00	11.68	3.07
	C		0.00	0.00	3.73
	D		0.00	0.00	3.73
	E		0.00	0.00	3.73
	F		0.00	0.00	3.73
36	A	3.26	6.47	8.32	3.45
	B		24.21	26.13	2.97
	C		0.00	0.00	3.26
	D		0.00	0.00	3.26
	E		0.00	0.00	3.26
	F		0.00	0.00	3.26
37	A	3.83	2.15	5.19	3.77
	B		7.30	9.92	3.39
	C		152.45	156.49	3.27
	D		0.00	0.00	3.83
	E		0.00	0.00	3.83
	F		0.00	0.00	3.83
38	A	4.44	5.20	8.37	4.21
	B		82.47	86.24	3.77
	C		0.00	0.00	4.44
	D		0.00	0.00	4.44
	E		0.00	0.00	4.44
	F		0.00	0.00	4.44
39	A	3.52	3.43	5.93	3.50
	B		9.65	11.95	3.12
	C		0.00	0.00	3.52
	D		0.00	0.00	3.52
	E		0.00	0.00	3.52
	F		0.00	0.00	3.52
40	A	3.43	3.17	5.60	3.47
	B		8.42	10.64	3.08
	C		0.00	0.00	3.43
	D		0.00	0.00	3.43
	E		0.00	0.00	3.43
	F		0.00	0.00	3.43
41	A	4.26	2.66	6.13	3.82
	B		9.25	12.38	3.50
	C		0.00	0.00	4.26
	D		0.00	0.00	4.26
	E		0.00	0.00	4.26
	F		0.00	0.00	4.26
42	A	3.69	1.89	4.91	3.46
	B		5.26	7.99	3.12
	C		0.00	0.00	2.81
	D		0.00	0.00	3.69
	E		0.00	0.00	3.69
	F		0.00	0.00	3.69
43	A	3.66	1.69	4.74	3.44
	B		10.77	13.29	3.10
	C		0.00	0.00	3.66
	D		0.00	0.00	3.66
	E		0.00	0.00	3.66
	F		0.00	0.00	3.66

TABLE C.4 Experimental uncertainty estimates in the -10° [downward] data set

Run No.	Visual section	G %	x %	V_{GS} %	V_{LS} %
1	A	2.83	1.26	3.49	3.02
	B		2.63	4.65	2.62
	C		5.67	7.51	2.50
	D		0.00	0.00	2.83
	E		0.00	0.00	2.83
	F		0.00	0.00	2.83
2	A	2.80	0.69	3.13	3.01
	B		1.43	3.67	2.64
	C		3.10	5.09	2.51
	D		0.00	0.00	2.80
	E		0.00	0.00	2.80
	F		0.00	0.00	2.80
3	A	2.80	1.74	3.76	3.08
	B		6.17	7.83	2.60
	C		0.00	0.00	2.60
	D		0.00	0.00	2.80
	E		0.00	0.00	2.80
	F		0.00	0.00	2.80
4	A	2.80	1.74	3.77	3.06
	B		4.99	6.72	2.60
	C		44.32	46.14	2.46
	D		0.00	0.00	2.80
	E		0.00	0.00	2.80
	F		0.00	0.00	2.80
5	A	2.37	0.97	2.75	2.87
	B		1.92	3.45	2.42
	C		3.58	4.90	2.29
	D		0.00	0.00	2.37
	E		0.00	0.00	2.37
	F		0.00	0.00	2.37
6	A	2.39	0.99	2.79	2.86
	B		1.85	3.43	2.43
	C		3.39	4.77	2.30
	D		0.00	0.00	2.39
	E		0.00	0.00	2.39
	F		0.00	0.00	2.39
7	A	2.21	0.97	2.56	2.79
	B		1.67	3.04	2.36
	C		3.07	4.21	2.22
	D		65.06	65.96	2.14
	E		0.00	0.00	2.21
	F		0.00	0.00	2.21
8	A	2.19	1.00	2.55	2.83
	B		1.83	3.12	2.35
	C		3.08	4.18	2.22
	D		10.86	11.66	2.14
	E		0.00	0.00	2.19
	F		0.00	0.00	2.19
9	A	2.37	1.42	3.00	2.96
	B		2.47	3.87	2.47
	C		5.51	6.69	2.29
	D		0.00	0.00	2.37
	E		0.00	0.00	2.37
	F		0.00	0.00	2.37
10	A	2.30	0.74	2.58	2.76
	B		1.21	2.89	2.37
	C		2.05	3.55	2.23
	D		5.79	6.99	2.17
	E		0.00	0.00	2.30
	F		0.00	0.00	2.30
11	A	3.00	1.01	3.56	3.02
	B		2.34	4.66	2.66
	C		11.83	13.84	2.52
	D		0.00	0.00	3.00
	E		0.00	0.00	3.00
	F		0.00	0.00	3.00
12	A	3.37	1.46	4.28	3.16
	B		4.03	6.59	2.82
	C		0.00	0.00	2.70
	D		0.00	0.00	3.37
	E		0.00	0.00	3.37
	F		0.00	0.00	3.37
13	A	3.14	2.28	4.60	3.11
	B		6.42	8.53	2.73
	C		0.00	0.00	3.14
	D		0.00	0.00	3.14
	E		0.00	0.00	3.14
	F		0.00	0.00	3.14
14	A	2.74	1.36	3.47	2.91
	B		2.69	4.61	2.54
	C		10.61	12.30	2.40
	D		0.00	0.00	2.74
	E		0.00	0.00	2.74
	F		0.00	0.00	2.74
15	A	2.70	3.39	4.91	3.06
	B		7.56	8.95	2.64
	C		0.00	0.00	2.70
	D		0.00	0.00	2.70
	E		0.00	0.00	2.70
	F		0.00	0.00	2.70
16	A	3.14	2.17	4.49	3.20
	B		6.78	8.87	2.74
	C		0.00	0.00	3.14
	D		0.00	0.00	3.14
	E		0.00	0.00	3.14
	F		0.00	0.00	3.14
17	A	3.05	1.54	3.94	3.14
	B		3.81	5.98	2.72
	C		18.89	20.93	2.57
	D		0.00	0.00	3.05
	E		0.00	0.00	3.05
	F		0.00	0.00	3.05
18	A	3.05	1.20	3.71	3.14
	B		2.94	5.19	2.74
	C		11.45	13.45	2.60
	D		0.00	0.00	3.05
	E		0.00	0.00	3.05
	F		0.00	0.00	3.05
19	A	3.05	1.53	3.93	3.16
	B		3.27	5.46	2.75
	C		10.25	12.25	2.61
	D		0.00	0.00	3.05
	E		0.00	0.00	3.05
	F		0.00	0.00	3.05
20	A	2.75	1.62	3.62	3.06
	B		4.00	5.74	2.59
	C		18.07	19.67	2.44
	D		0.00	0.00	2.75
	E		0.00	0.00	2.75
	F		0.00	0.00	2.75
21	A	2.80	1.73	3.75	3.10
	B		4.43	6.18	2.62
	C		29.69	31.38	2.47
	D		0.00	0.00	2.80
	E		0.00	0.00	2.80
	F		0.00	0.00	2.80
22	A	2.85	1.53	3.69	3.11
	B		3.16	5.11	2.68
	C		8.21	9.97	2.53
	D		0.00	0.00	2.85
	E		0.00	0.00	2.85
	F		0.00	0.00	2.85
23	A	2.85	1.00	3.37	3.02
	B		2.19	4.32	2.63
	C		5.20	7.11	2.50
	D		0.00	0.00	2.85
	E		0.00	0.00	2.85
	F		0.00	0.00	2.85
24	A	3.14	2.81	4.98	3.26
	B		10.25	12.11	2.89
	C		0.00	0.00	3.14
	D		0.00	0.00	3.14
	E		0.00	0.00	3.14
	F		0.00	0.00	3.14
25	A	5.19	5.69	9.65	4.55
	B		0.00	0.00	5.19
	C		0.00	0.00	5.19
	D		0.00	0.00	5.19
	E		0.00	0.00	5.19
	F		0.00	0.00	5.19
26	A	4.30	3.24	6.60	3.96
	B		17.85	20.79	3.67
	C		0.00	0.00	4.30
	D		0.00	0.00	4.30
	E		0.00	0.00	4.30
	F		0.00	0.00	4.30

TABLE C.4 Experimental uncertainty estimates in the -10°[downward] data set (cont'd.)

Run No.	Visual section	G %	x %	V_{GS} %	V_{LS} %
27	A	3.54	1.88	4.72	3.48
	B		6.19	8.60	3.16
	C		0.00	0.00	3.54
	D		0.00	0.00	3.54
	E		0.00	0.00	3.54
	F		0.00	0.00	3.54
28	A	2.43	0.80	2.75	2.87
	B		1.63	3.33	2.42
	C		2.95	4.47	2.29
	D		18.58	19.82	2.22
	E		0.00	0.00	2.43
	F		0.00	0.00	2.43
29	A	2.45	1.04	2.90	2.90
	B		2.14	3.75	2.43
	C		5.05	6.44	2.28
	D		0.00	0.00	2.45
	E		0.00	0.00	2.45
	F		0.00	0.00	2.45
30	A	2.40	1.32	2.99	2.93
	B		2.54	3.98	2.45
	C		6.67	7.88	2.28
	D		0.00	0.00	2.40
	E		0.00	0.00	2.40
	F		0.00	0.00	2.40
31	A	2.36	1.21	2.87	2.92
	B		2.38	3.79	2.42
	C		5.25	6.44	2.26
	D		703.12	709.40	2.15
	E		0.00	0.00	2.36
	F		0.00	0.00	2.36
32	A	2.30	1.11	2.75	2.87
	B		2.10	3.50	2.38
	C		3.71	4.94	2.25
	D		15.94	16.94	2.18
	E		0.00	0.00	2.30
	F		0.00	0.00	2.30
33	A	2.30	1.40	2.90	2.92
	B		2.90	4.13	2.40
	C		7.05	8.06	2.25
	D		0.00	0.00	2.30
	E		0.00	0.00	2.30
	F		0.00	0.00	2.30
34	A	2.27	0.67	2.50	2.76
	B		1.14	2.79	2.35
	C		2.04	3.48	2.22
	D		7.13	8.20	2.15
	E		0.00	0.00	2.27
	F		0.00	0.00	2.27
35	A	2.32	0.99	2.71	2.84
	B		1.90	3.37	2.38
	C		4.39	5.60	2.23
	D		36.06	37.15	2.17
	E		0.00	0.00	2.32
	F		0.00	0.00	2.32
36	A	2.30	1.37	2.88	2.98
	B		3.19	4.36	2.42
	C		25.16	26.05	2.23
	D		0.00	0.00	2.30
	E		0.00	0.00	2.30
	F		0.00	0.00	2.30
37	A	2.47	1.09	2.96	2.86
	B		2.31	3.94	2.43
	C		4.15	5.62	2.31
	D		0.00	0.00	2.47
	E		0.00	0.00	2.47
	F		0.00	0.00	2.47
38	A	2.46	1.16	2.98	2.90
	B		2.53	4.09	2.43
	C		7.90	9.20	2.28
	D		0.00	0.00	2.46
	E		0.00	0.00	2.46
	F		0.00	0.00	2.46
39	A	2.45	1.03	2.90	2.86
	B		2.24	3.84	2.42
	C		4.81	6.21	2.29
	D		0.00	0.00	2.45
	E		0.00	0.00	2.45
	F		0.00	0.00	2.45
40	A	2.45	1.64	3.24	3.01
	B		4.48	5.74	2.47
	C		0.00	0.00	2.45
	D		0.00	0.00	2.45
	E		0.00	0.00	2.45
	F		0.00	0.00	2.45
41	A	2.40	1.08	2.86	2.89
	B		2.10	3.65	2.43
	C		4.60	5.93	2.28
	D		162.21	164.23	2.21
	E		0.00	0.00	2.40
	F		0.00	0.00	2.40
42	A	2.37	0.97	2.76	2.86
	B		1.71	3.31	2.40
	C		3.53	4.91	2.25
	D		34.91	36.13	2.18
	E		0.00	0.00	2.37
	F		0.00	0.00	2.37
43	A	2.30	0.98	2.68	2.84
	B		1.73	3.23	2.38
	C		3.62	4.88	2.23
	D		121.10	122.63	2.15
	E		0.00	0.00	2.30
	F		0.00	0.00	2.30
44	A	2.29	0.91	2.63	2.84
	B		1.76	3.23	2.37
	C		4.18	5.37	2.21
	D		0.00	0.00	2.15
	E		0.00	0.00	2.29
	F		0.00	0.00	2.29
45	A	2.73	2.38	4.13	3.11
	B		6.91	8.40	2.62
	C		330.76	334.50	2.46
	D		0.00	0.00	2.73
	E		0.00	0.00	2.73
	F		0.00	0.00	2.73
46	A	2.83	2.03	4.00	3.09
	B		5.44	7.13	2.67
	C		51.60	53.40	2.53
	D		0.00	0.00	2.83
	E		0.00	0.00	2.83
	F		0.00	0.00	2.83
47	A	3.44	5.06	7.25	3.45
	B		30.21	32.38	3.05
	C		0.00	0.00	3.44
	D		0.00	0.00	3.44
	E		0.00	0.00	3.44
	F		0.00	0.00	3.44
48	A	3.14	3.65	5.66	3.30
	B		28.86	30.63	2.92
	C		0.00	0.00	3.14
	D		0.00	0.00	3.14
	E		0.00	0.00	3.14
	F		0.00	0.00	3.14
49	A	3.85	33.43	35.38	4.11
	B		0.00	0.00	3.85
	C		0.00	0.00	3.85
	D		0.00	0.00	3.85
	E		0.00	0.00	3.85
	F		0.00	0.00	3.85
50	A	3.62	28.66	30.38	3.96
	B		0.00	0.00	3.62
	C		0.00	0.00	3.62
	D		0.00	0.00	3.62
	E		0.00	0.00	3.62
	F		0.00	0.00	3.62

TABLE C.5 Experimental uncertainty estimates in the +1° [upward] data set

Run No.	Visual section	G %	x %	V_{GS} %	V_{LS} %
1	A	2.40	1.08	2.87	2.86
	B		2.00	3.57	2.43
	C		4.81	6.13	2.28
	D		186.40	188.57	2.21
	E		0.00	0.00	2.40
	F		0.00	0.00	2.40
2	A	2.39	0.88	2.74	2.85
	B		1.72	3.34	2.41
	C		3.40	4.81	2.27
	D		16.95	18.11	2.21
	E		0.00	0.00	2.39
	F		0.00	0.00	2.39
3	A	2.40	0.75	2.70	2.82
	B		1.37	3.13	2.41
	C		2.66	4.20	2.27
	D		10.63	11.86	2.21
	E		0.00	0.00	2.40
	F		0.00	0.00	2.40
4	A	2.39	0.67	2.65	2.79
	B		1.06	2.91	2.40
	C		1.72	3.42	2.27
	D		3.94	5.38	2.20
	E		0.00	0.00	2.39
	F		0.00	0.00	2.39
5	A	2.47	0.96	2.89	2.88
	B		1.88	3.58	2.45
	C		3.50	5.02	2.32
	D		21.56	22.86	2.25
	E		0.00	0.00	2.47
	F		0.00	0.00	2.47
6	A	2.45	1.85	3.37	3.12
	B		4.57	5.79	2.52
	C		87.00	88.31	2.34
	D		0.00	0.00	2.45
	E		0.00	0.00	2.45
	F		0.00	0.00	2.45
7	A	2.40	1.54	3.12	3.03
	B		4.00	5.23	2.47
	C		48.82	49.94	2.29
	D		0.00	0.00	2.40
	E		0.00	0.00	2.40
	F		0.00	0.00	2.40
8	A	2.39	1.45	3.04	3.00
	B		3.01	4.33	2.46
	C		8.58	9.67	2.30
	D		0.00	0.00	2.39
	E		0.00	0.00	2.39
	F		0.00	0.00	2.39
9	A	2.70	1.74	3.64	3.07
	B		4.64	6.24	2.59
	C		19.70	21.16	2.46
	D		0.00	0.00	2.70
	E		0.00	0.00	2.70
	F		0.00	0.00	2.70
10	A	2.80	2.15	4.04	3.13
	B		6.37	7.98	2.65
	C		91.20	93.25	2.51
	D		0.00	0.00	2.80
	E		0.00	0.00	2.80
	F		0.00	0.00	2.80
11	A	2.80	2.12	4.03	3.11
	B		6.36	8.00	2.62
	C		44.58	46.32	2.50
	D		0.00	0.00	2.80
	E		0.00	0.00	2.80
	F		0.00	0.00	2.80
12	A	2.80	1.58	3.65	3.09
	B		3.53	5.35	2.66
	C		11.29	12.90	2.52
	D		0.00	0.00	2.80
	E		0.00	0.00	2.80
	F		0.00	0.00	2.80
13	A	2.80	2.36	4.21	3.13
	B		6.08	7.71	2.65
	C		40.10	41.78	2.51
	D		0.00	0.00	2.80
	E		0.00	0.00	2.80
	F		0.00	0.00	2.80
14	A	3.05	2.07	4.32	3.14
	B		5.87	7.88	2.71
	C		33.98	36.08	2.59
	D		0.00	0.00	3.05
	E		0.00	0.00	3.05
	F		0.00	0.00	3.05
15	A	2.98	1.91	4.11	3.13
	B		4.88	6.85	2.69
	C		31.45	33.44	2.55
	D		0.00	0.00	2.98
	E		0.00	0.00	2.98
	F		0.00	0.00	2.98
16	A	2.91	1.78	3.93	3.13
	B		4.29	6.21	2.67
	C		37.61	39.54	2.52
	D		0.00	0.00	2.91
	E		0.00	0.00	2.91
	F		0.00	0.00	2.91
17	A	2.91	2.40	4.39	3.12
	B		4.85	6.69	2.72
	C		20.92	22.68	2.56
	D		0.00	0.00	2.91
	E		0.00	0.00	2.91
	F		0.00	0.00	2.91
18	A	2.98	1.88	4.10	3.10
	B		3.81	5.86	2.71
	C		11.38	13.28	2.57
	D		0.00	0.00	2.98
	E		0.00	0.00	2.98
	F		0.00	0.00	2.98
19	A	3.24	5.78	7.66	3.42
	B		61.92	63.99	3.00
	C		0.00	0.00	3.24
	D		0.00	0.00	3.24
	E		0.00	0.00	3.24
	F		0.00	0.00	3.24
20	A	3.35	5.20	7.25	3.45
	B		41.46	43.52	3.05
	C		0.00	0.00	3.35
	D		0.00	0.00	3.35
	E		0.00	0.00	3.35
	F		0.00	0.00	3.35
21	A	3.35	3.16	5.50	3.39
	B		13.03	15.07	3.02
	C		0.00	0.00	3.35
	D		0.00	0.00	3.35
	E		0.00	0.00	3.35
	F		0.00	0.00	3.35
22	A	3.35	1.47	4.23	3.33
	B		5.08	7.40	2.98
	C		0.00	0.00	3.35
	D		0.00	0.00	3.35
	E		0.00	0.00	3.35
	F		0.00	0.00	3.35
23	A	3.33	3.62	5.88	3.37
	B		16.01	18.03	2.98
	C		0.00	0.00	3.33
	D		0.00	0.00	3.33
	E		0.00	0.00	3.33
	F		0.00	0.00	3.33
24	A	3.30	5.52	7.51	3.39
	B		47.99	50.09	2.99
	C		0.00	0.00	3.30
	D		0.00	0.00	3.30
	E		0.00	0.00	3.30
	F		0.00	0.00	3.30
25	A	3.38	2.56	5.01	3.53
	B		9.64	11.66	3.17
	C		0.00	0.00	3.38
	D		0.00	0.00	3.38
	E		0.00	0.00	3.38
	F		0.00	0.00	3.38
26	A	2.16	1.26	2.65	2.88
	B		2.60	3.65	2.37
	C		6.36	7.13	2.21
	D		0.00	0.00	2.16
	E		0.00	0.00	2.16
	F		0.00	0.00	2.16

TABLE C.5 Experimental uncertainty estimates in the +1° [upward] data set (cont'd.)

Run No.	Visual section	G %	x %	$V_{2\phi}$ %	$V_{1\phi}$ %
27	A	2.15	1.20	2.60	2.86
	B		2.19	3.31	2.37
	C		4.84	5.68	2.21
	D		0.00	0.00	2.15
	E		0.00	0.00	2.15
	F		0.00	0.00	2.15
28	A	2.15	1.19	2.59	2.86
	B		2.17	3.29	2.36
	C		4.58	5.42	2.20
	D		137.99	138.80	2.13
	E		0.00	0.00	2.15
	F		0.00	0.00	2.15
29	A	2.16	0.96	2.49	2.80
	B		1.89	3.11	2.34
	C		4.04	4.96	2.20
	D		335.21	336.70	2.12
	E		0.00	0.00	2.16
	F		0.00	0.00	2.16
30	A	2.20	1.19	2.66	2.86
	B		2.31	3.49	2.36
	C		3.97	4.96	2.23
	D		20.40	21.14	2.15
	E		0.00	0.00	2.20
	F		0.00	0.00	2.20
31	A	2.21	1.15	2.65	2.86
	B		2.65	3.77	2.36
	C		5.24	6.15	2.23
	D		58.86	59.67	2.16
	E		0.00	0.00	2.21
	F		0.00	0.00	2.21
32	A	2.19	1.07	2.58	2.85
	B		2.35	3.51	2.36
	C		6.23	7.09	2.20
	D		0.00	0.00	2.09
	E		0.00	0.00	2.19
	F		0.00	0.00	2.19
33	A	2.20	1.13	2.62	2.87
	B		2.50	3.63	2.36
	C		5.40	6.29	2.21
	D		33.78	34.52	2.15
	E		0.00	0.00	2.20
	F		0.00	0.00	2.20
34	A	2.20	1.10	2.61	2.86
	B		2.44	3.59	2.36
	C		6.17	7.03	2.20
	D		108.14	109.09	2.15
	E		0.00	0.00	2.20
	F		0.00	0.00	2.20
35	A	2.21	1.16	2.66	2.88
	B		2.37	3.56	2.37
	C		5.97	6.87	2.21
	D		0.00	0.00	2.19
	E		0.00	0.00	2.21
	F		0.00	0.00	2.21
36	A	2.15	1.03	2.51	2.78
	B		1.89	3.09	2.32
	C		3.07	4.09	2.20
	D		17.06	17.71	2.12
	E		0.00	0.00	2.15
	F		0.00	0.00	2.15
37	A	2.14	0.99	2.47	2.78
	B		1.76	2.98	2.32
	C		2.96	3.97	2.19
	D		15.23	15.87	2.11
	E		0.00	0.00	2.14
	F		0.00	0.00	2.14
38	A	2.15	1.02	2.51	2.79
	B		1.84	3.07	2.33
	C		3.56	4.53	2.19
	D		44.70	45.38	2.12
	E		0.00	0.00	2.15
	F		0.00	0.00	2.15
39	A	2.15	1.01	2.50	2.79
	B		1.81	3.04	2.33
	C		3.87	4.81	2.18
	D		83.88	84.65	2.11
	E		0.00	0.00	2.15
	F		0.00	0.00	2.15

Run No.	Visual section	G %	x %	$V_{2\phi}$ %	$V_{1\phi}$ %
40	A	2.16	1.01	2.50	2.80
	B		1.82	3.06	2.33
	C		3.90	4.84	2.18
	D		263.86	265.15	2.11
	E		0.00	0.00	2.16
	F		0.00	0.00	2.16
41	A	2.14	0.95	2.45	2.77
	B		1.65	2.90	2.32
	C		3.24	4.21	2.18
	D		54.83	55.48	2.11
	E		0.00	0.00	2.14
	F		0.00	0.00	2.14
42	A	2.39	1.06	2.83	2.87
	B		2.07	3.61	2.40
	C		4.91	6.22	2.25
	D		147.78	149.73	2.19
	E		0.00	0.00	2.39
	F		0.00	0.00	2.39
43	A	2.45	0.98	2.87	2.86
	B		1.88	3.57	2.41
	C		4.08	5.56	2.27
	D		47.54	49.04	2.20
	E		0.00	0.00	2.45
	F		0.00	0.00	2.45
44	A	2.43	0.84	2.78	2.83
	B		1.59	3.32	2.40
	C		3.15	4.69	2.26
	D		11.49	12.81	2.20
	E		0.00	0.00	2.43
	F		0.00	0.00	2.43
45	A	2.47	0.85	2.84	2.81
	B		1.58	3.40	2.40
	C		3.16	4.78	2.27
	D		12.54	13.95	2.21
	E		0.00	0.00	2.47
	F		0.00	0.00	2.47
46	A	6.44	12.80	17.72	5.30
	B		0.00	0.00	6.44
	C		0.00	0.00	6.44
	D		0.00	0.00	6.44
	E		0.00	0.00	6.44
	F		0.00	0.00	6.44
47	A	5.19	5.59	9.55	4.58
	B		0.00	0.00	5.19
	C		0.00	0.00	5.19
	D		0.00	0.00	5.19
	E		0.00	0.00	5.19
	F		0.00	0.00	5.19
48	A	5.08	10.47	13.93	4.63
	B		0.00	0.00	5.08
	C		0.00	0.00	5.08
	D		0.00	0.00	5.08
	E		0.00	0.00	5.08
	F		0.00	0.00	5.08
49	A	5.24	19.66	23.36	4.50
	B		0.00	0.00	5.24
	C		0.00	0.00	5.24
	D		0.00	0.00	5.24
	E		0.00	0.00	5.24
	F		0.00	0.00	5.24
50	A	5.13	36.43	39.95	4.58
	B		0.00	0.00	5.13
	C		0.00	0.00	5.13
	D		0.00	0.00	5.13
	E		0.00	0.00	5.13
	F		0.00	0.00	5.13
51	A	4.19	12.07	14.73	3.91
	B		0.00	0.00	4.19
	C		0.00	0.00	4.19
	D		0.00	0.00	4.19
	E		0.00	0.00	4.19
	F		0.00	0.00	4.19
52	A	4.30	20.62	23.16	4.14
	B		0.00	0.00	4.30
	C		0.00	0.00	4.30
	D		0.00	0.00	4.30
	E		0.00	0.00	4.30
	F		0.00	0.00	4.30

TABLE C.5 Experimental uncertainty estimates in the +1° [upward] data set (cont'd.)

Run No.	Visual section	G %	x %	V_{GS} %	V_{LS} %
53	A	3.98	20.86	23.08	3.96
	B		0.00	0.00	3.98
	C		0.00	0.00	3.98
	D		0.00	0.00	3.98
	E		0.00	0.00	3.98
	F		0.00	0.00	3.98
54	A	3.93	4.21	6.99	3.83
	B		39.88	42.49	3.49
	C		0.00	0.00	3.93
	D		0.00	0.00	3.93
	E		0.00	0.00	3.93
	F		0.00	0.00	3.93
55	A	3.98	6.33	8.94	3.89
	B		0.00	0.00	3.01
	C		0.00	0.00	3.98
	D		0.00	0.00	3.98
	E		0.00	0.00	3.98
	F		0.00	0.00	3.98
56	A	2.62	1.85	3.61	3.09
	B		6.20	7.59	2.55
	C		149.15	151.23	2.42
	D		0.00	0.00	2.62
	E		0.00	0.00	2.62
	F		0.00	0.00	2.62
57	A	2.80	3.56	5.17	3.20
	B		17.37	18.82	2.62
	C		0.00	0.00	2.80
	D		0.00	0.00	2.80
	E		0.00	0.00	2.80
	F		0.00	0.00	2.80
58	A	2.75	3.39	4.96	3.16
	B		10.50	11.92	2.62
	C		0.00	0.00	2.75
	D		0.00	0.00	2.75
	E		0.00	0.00	2.75
	F		0.00	0.00	2.75
59	A	2.80	3.47	5.09	3.19
	B		12.83	14.31	2.63
	C		0.00	0.00	2.80
	D		0.00	0.00	2.80
	E		0.00	0.00	2.80
	F		0.00	0.00	2.80

TABLE C.6 Experimental uncertainty estimates in the +5° [upward] data set

Run No.	Visual section	G %	x %	V_{SG} %	V_{LS} %
1	A	3.98	3.19	6.24	3.69
	B		18.51	21.21	3.39
	C		0.00	0.00	3.98
	D		0.00	0.00	3.98
	E		0.00	0.00	3.98
	F		0.00	0.00	3.98
2	A	3.19	3.30	5.45	3.25
	B		32.85	34.83	2.84
	C		0.00	0.00	3.19
	D		0.00	0.00	3.19
	E		0.00	0.00	3.19
	F		0.00	0.00	3.19
3	A	3.10	4.88	6.72	3.23
	B		18.30	20.00	2.89
	C		0.00	0.00	3.10
	D		0.00	0.00	3.10
	E		0.00	0.00	3.10
	F		0.00	0.00	3.10
4	A	3.90	10.45	12.85	3.72
	B		0.00	0.00	3.90
	C		0.00	0.00	3.90
	D		0.00	0.00	3.90
	E		0.00	0.00	3.90
	F		0.00	0.00	3.90
5	A	3.14	8.99	10.59	3.34
	B		0.00	0.00	2.57
	C		0.00	0.00	3.14
	D		0.00	0.00	3.14
	E		0.00	0.00	3.14
	F		0.00	0.00	3.14
6	A	3.23	7.28	9.05	3.37
	B		260.57	264.33	2.94
	C		0.00	0.00	3.23
	D		0.00	0.00	3.23
	E		0.00	0.00	3.23
	F		0.00	0.00	3.23
7	A	2.85	2.71	4.56	3.13
	B		6.57	8.21	2.72
	C		4653.74	4712.95	2.37
	D		0.00	0.00	2.85
	E		0.00	0.00	2.85
	F		0.00	0.00	2.85
8	A	2.85	2.45	4.36	3.12
	B		5.73	7.43	2.70
	C		24.55	26.19	2.56
	D		0.00	0.00	2.85
	E		0.00	0.00	2.85
	F		0.00	0.00	2.85
9	A	2.83	2.35	4.25	3.10
	B		5.23	6.94	2.68
	C		35.88	37.57	2.53
	D		0.00	0.00	2.83
	E		0.00	0.00	2.83
	F		0.00	0.00	2.83
10	A	2.83	2.34	4.24	3.09
	B		6.46	8.12	2.65
	C		64.68	66.60	2.52
	D		0.00	0.00	2.83
	E		0.00	0.00	2.83
	F		0.00	0.00	2.83
11	A	2.91	2.05	4.11	3.17
	B		7.54	9.25	2.69
	C		57.37	59.32	2.58
	D		0.00	0.00	2.91
	E		0.00	0.00	2.91
	F		0.00	0.00	2.91
12	A	2.85	3.59	5.28	3.16
	B		10.78	12.31	2.71
	C		0.00	0.00	2.85
	D		0.00	0.00	2.85
	E		0.00	0.00	2.85
	F		0.00	0.00	2.85
13	A	2.85	3.38	5.11	3.15
	B		17.45	18.98	2.65
	C		0.00	0.00	2.85
	D		0.00	0.00	2.85
	E		0.00	0.00	2.85
	F		0.00	0.00	2.85
14	A	2.45	1.61	3.24	2.98
	B		4.61	5.90	2.42
	C		0.00	0.00	2.45
	D		0.00	0.00	2.45
	E		0.00	0.00	2.45
	F		0.00	0.00	2.45
15	A	2.43	1.87	3.38	3.03
	B		5.57	6.74	2.44
	C		372.25	375.52	2.24
	D		0.00	0.00	2.43
	E		0.00	0.00	2.43
	F		0.00	0.00	2.43
16	A	2.45	2.03	3.52	3.04
	B		5.15	6.37	2.47
	C		110.27	111.81	2.30
	D		0.00	0.00	2.45
	E		0.00	0.00	2.45
	F		0.00	0.00	2.45
17	A	2.56	2.09	3.70	3.06
	B		5.44	6.81	2.50
	C		279.12	282.23	2.32
	D		0.00	0.00	2.56
	E		0.00	0.00	2.56
	F		0.00	0.00	2.56
18	A	2.43	1.64	3.22	3.00
	B		3.80	5.10	2.45
	C		20.25	21.37	2.28
	D		0.00	0.00	2.43
	E		0.00	0.00	2.43
	F		0.00	0.00	2.43
19	A	2.25	1.08	2.66	2.81
	B		2.24	3.52	2.35
	C		4.92	5.95	2.21
	D		0.00	0.00	2.08
	E		0.00	0.00	2.25
	F		0.00	0.00	2.25
20	A	2.27	1.16	2.74	2.82
	B		2.21	3.53	2.36
	C		4.91	5.98	2.22
	D		0.00	0.00	2.19
	E		0.00	0.00	2.27
	F		0.00	0.00	2.27
21	A	2.23	0.87	2.53	2.75
	B		1.55	2.99	2.33
	C		3.02	4.21	2.20
	D		12.61	13.49	2.14
	E		0.00	0.00	2.23
	F		0.00	0.00	2.23
22	A	2.25	0.89	2.57	2.78
	B		1.73	3.15	2.34
	C		3.99	5.11	2.20
	D		100.63	101.79	2.14
	E		0.00	0.00	2.25
	F		0.00	0.00	2.25
23	A	2.24	1.53	2.89	2.98
	B		3.68	4.68	2.41
	C		40.38	41.10	2.23
	D		0.00	0.00	2.24
	E		0.00	0.00	2.24
	F		0.00	0.00	2.24
24	A	2.24	1.56	2.91	2.99
	B		3.79	4.78	2.41
	C		23.87	24.58	2.23
	D		0.00	0.00	2.24
	E		0.00	0.00	2.24
	F		0.00	0.00	2.24
25	A	2.32	1.63	3.07	2.99
	B		3.67	4.80	2.43
	C		13.66	14.56	2.27
	D		0.00	0.00	2.32
	E		0.00	0.00	2.32
	F		0.00	0.00	2.32
26	A	2.37	1.79	3.24	3.03
	B		4.42	5.57	2.45
	C		24.94	25.90	2.29
	D		0.00	0.00	2.37
	E		0.00	0.00	2.37
	F		0.00	0.00	2.37

TABLE C.6 Experimental uncertainty estimates in the +5° [upward] data set (cont'd.)

Run No.	Visual section	G %	x %	V_{GS} %	V_{LS} %
27	A	2.43	2.14	3.55	3.08
	B		5.26	6.40	2.50
	C		39.03	40.09	2.34
	D		0.00	0.00	2.43
	E		0.00	0.00	2.43
	F		0.00	0.00	2.43
28	A	2.40	1.90	3.36	3.04
	B		5.03	6.18	2.47
	C		1095.31	1104.26	2.19
	D		0.00	0.00	2.40
	E		0.00	0.00	2.40
	F		0.00	0.00	2.40
29	A	2.20	1.11	2.61	2.82
	B		2.33	3.51	2.34
	C		5.78	6.67	2.20
	D		1002.46	1008.16	2.09
	E		0.00	0.00	2.20
	F		0.00	0.00	2.20
30	A	2.16	0.97	2.50	2.76
	B		1.92	3.14	2.32
	C		3.89	4.84	2.18
	D		15.09	15.78	2.13
	E		0.00	0.00	2.16
	F		0.00	0.00	2.16
31	A	2.16	0.93	2.48	2.76
	B		1.83	3.07	2.32
	C		4.08	5.01	2.18
	D		0.00	0.00	2.05
	E		0.00	0.00	2.16
	F		0.00	0.00	2.16
32	A	2.16	0.97	2.50	2.75
	B		1.93	3.15	2.32
	C		4.04	4.99	2.18
	D		30.92	31.60	2.13
	E		0.00	0.00	2.16
	F		0.00	0.00	2.16
33	A	7.22	19.34	25.52	5.23
	B		0.00	0.00	7.22
	C		0.00	0.00	7.22
	D		0.00	0.00	7.22
	E		0.00	0.00	7.22
	F		0.00	0.00	7.22
34	A	7.05	36.68	43.15	5.05
	B		0.00	0.00	7.05
	C		0.00	0.00	7.05
	D		0.00	0.00	7.05
	E		0.00	0.00	7.05
	F		0.00	0.00	7.05
35	A	6.81	60.01	66.66	5.02
	B		0.00	0.00	6.81
	C		0.00	0.00	6.81
	D		0.00	0.00	6.81
	E		0.00	0.00	6.81
	F		0.00	0.00	6.81
36	A	6.88	14.08	19.95	4.96
	B		0.00	0.00	6.88
	C		0.00	0.00	6.88
	D		0.00	0.00	6.88
	E		0.00	0.00	6.88
	F		0.00	0.00	6.88
37	A	5.19	5.41	9.61	4.15
	B		0.00	0.00	5.19
	C		0.00	0.00	5.19
	D		0.00	0.00	5.19
	E		0.00	0.00	5.19
	F		0.00	0.00	5.19
38	A	4.92	6.16	10.07	3.92
	B		0.00	0.00	4.92
	C		0.00	0.00	4.92
	D		0.00	0.00	4.92
	E		0.00	0.00	4.92
	F		0.00	0.00	4.92
39	A	4.48	8.21	11.47	3.79
	B		0.00	0.00	4.48
	C		0.00	0.00	4.48
	D		0.00	0.00	4.48
	E		0.00	0.00	4.48
	F		0.00	0.00	4.48
40	A	4.69	4.54	8.18	4.05
	B		0.00	0.00	4.03
	C		0.00	0.00	4.69
	D		0.00	0.00	4.69
	E		0.00	0.00	4.69
	F		0.00	0.00	4.69
41	A	4.48	6.52	9.80	3.90
	B		0.00	0.00	4.48
	C		0.00	0.00	4.48
	D		0.00	0.00	4.48
	E		0.00	0.00	4.48
	F		0.00	0.00	4.48
42	A	4.13	7.89	10.69	3.74
	B		0.00	0.00	4.13
	C		0.00	0.00	4.13
	D		0.00	0.00	4.13
	E		0.00	0.00	4.13
	F		0.00	0.00	4.13
43	A	4.07	12.69	15.31	3.68
	B		0.00	0.00	4.07
	C		0.00	0.00	4.07
	D		0.00	0.00	4.07
	E		0.00	0.00	4.07
	F		0.00	0.00	4.07
44	A	2.85	1.09	3.44	2.95
	B		2.86	4.92	2.58
	C		11.49	13.30	2.46
	D		0.00	0.00	2.85
	E		0.00	0.00	2.85
	F		0.00	0.00	2.85
45	A	3.14	1.54	4.05	3.10
	B		3.60	5.88	2.76
	C		12.31	14.40	2.64
	D		0.00	0.00	3.14
	E		0.00	0.00	3.14
	F		0.00	0.00	3.14
46	A	2.98	1.89	4.12	3.04
	B		4.73	6.73	2.67
	C		17.50	19.39	2.56
	D		0.00	0.00	2.98
	E		0.00	0.00	2.98
	F		0.00	0.00	2.98
47	A	2.98	1.84	4.08	3.05
	B		4.56	6.56	2.68
	C		30.22	32.19	2.55
	D		0.00	0.00	2.98
	E		0.00	0.00	2.98
	F		0.00	0.00	2.98
48	A	3.33	1.37	4.16	3.19
	B		3.41	5.94	2.86
	C		12.73	15.04	2.75
	D		0.00	0.00	3.33
	E		0.00	0.00	3.33
	F		0.00	0.00	3.33
49	A	3.20	1.44	4.06	3.17
	B		3.99	6.27	2.86
	C		29.55	31.65	2.76
	D		0.00	0.00	3.20
	E		0.00	0.00	3.20
	F		0.00	0.00	3.20
50	A	3.52	2.87	5.49	3.40
	B		12.67	14.94	3.08
	C		0.00	0.00	3.52
	D		0.00	0.00	3.52
	E		0.00	0.00	3.52
	F		0.00	0.00	3.52
51	A	3.52	2.23	4.96	3.42
	B		8.24	10.55	3.13
	C		0.00	0.00	3.52
	D		0.00	0.00	3.52
	E		0.00	0.00	3.52
	F		0.00	0.00	3.52
52	A	2.10	0.93	2.40	2.75
	B		1.75	2.92	2.30
	C		3.60	4.45	2.17
	D		19.04	19.56	2.11
	E		0.00	0.00	2.10
	F		0.00	0.00	2.10

TABLE C.6 Experimental uncertainty estimates in the +5° [upward] data set (cont'd.)

Run No.	Visual section	G %	x %	V_{TB} %	V_{LS} %
53	A	2.10	0.92	2.39	2.72
	B		1.70	2.87	2.29
	C		3.41	4.27	2.16
	D		15.85	16.37	2.10
	E		0.00	0.00	2.10
	F		0.00	0.00	2.10
54	A	2.10	0.93	2.39	2.73
	B		1.74	2.90	2.29
	C		3.16	4.05	2.17
	D		12.11	12.65	2.11
	E		0.00	0.00	2.10
	F		0.00	0.00	2.10
55	A	2.10	1.01	2.44	2.74
	B		1.70	2.88	2.31
	C		3.19	4.10	2.17
	D		13.68	14.23	2.11
	E		0.00	0.00	2.10
	F		0.00	0.00	2.10

TABLE C.7 Experimental uncertainty estimates in the +10° [upward] data set

Run No.	Visual section	G %	x %	V_{TB} %	V_{LS} %
1	A	3.85	2.74	5.67	3.77
	B		12.26	14.68	3.50
	C		0.00	0.00	3.85
	D		0.00	0.00	3.85
	E		0.00	0.00	3.85
	F		0.00	0.00	3.85
2	A	3.64	3.71	6.27	3.61
	B		19.62	21.82	3.32
	C		0.00	0.00	3.64
	D		0.00	0.00	3.64
	E		0.00	0.00	3.64
	F		0.00	0.00	3.64
3	A	3.15	3.19	5.32	3.23
	B		10.13	11.98	2.92
	C		0.00	0.00	3.15
	D		0.00	0.00	3.15
	E		0.00	0.00	3.15
	F		0.00	0.00	3.15
4	A	2.99	3.75	5.59	3.18
	B		12.21	13.82	2.85
	C		0.00	0.00	2.99
	D		0.00	0.00	2.99
	E		0.00	0.00	2.99
	F		0.00	0.00	2.99
5	A	3.20	4.01	6.06	3.30
	B		15.72	17.52	2.99
	C		0.00	0.00	3.20
	D		0.00	0.00	3.20
	E		0.00	0.00	3.20
	F		0.00	0.00	3.20
6	A	3.22	7.01	8.82	3.32
	B		167.27	170.10	2.99
	C		0.00	0.00	3.22
	D		0.00	0.00	3.22
	E		0.00	0.00	3.22
	F		0.00	0.00	3.22
7	A	3.27	7.71	9.56	3.33
	B		0.00	0.00	2.84
	C		0.00	0.00	3.27
	D		0.00	0.00	3.27
	E		0.00	0.00	3.27
	F		0.00	0.00	3.27
8	A	3.09	2.27	4.47	3.28
	B		8.26	10.03	2.95
	C		0.00	0.00	3.09
	D		0.00	0.00	3.09
	E		0.00	0.00	3.09
	F		0.00	0.00	3.09
9	A	2.88	1.64	3.80	3.05
	B		4.74	6.54	2.71
	C		89.26	91.32	2.60
	D		0.00	0.00	2.88
	E		0.00	0.00	2.88
	F		0.00	0.00	2.88
10	A	2.94	1.09	3.52	3.06
	B		2.80	4.90	2.74
	C		10.05	11.81	2.64
	D		0.00	0.00	2.94
	E		0.00	0.00	2.94
	F		0.00	0.00	2.94
11	A	2.85	1.79	3.89	3.00
	B		4.04	5.88	2.67
	C		18.02	19.66	2.55
	D		0.00	0.00	2.85
	E		0.00	0.00	2.85
	F		0.00	0.00	2.85
12	A	2.82	2.13	4.10	2.99
	B		4.82	6.55	2.67
	C		38.61	40.29	2.54
	D		0.00	0.00	2.82
	E		0.00	0.00	2.82
	F		0.00	0.00	2.82
13	A	2.82	1.80	3.85	3.01
	B		4.18	5.96	2.67
	C		22.45	24.03	2.55
	D		0.00	0.00	2.82
	E		0.00	0.00	2.82
	F		0.00	0.00	2.82
14	A	2.50	1.76	3.41	2.95
	B		5.21	6.52	2.46
	C		0.00	0.00	2.25
	D		0.00	0.00	2.50
	E		0.00	0.00	2.50
	F		0.00	0.00	2.50
15	A	2.53	1.97	3.59	2.96
	B		5.53	6.85	2.48
	C		0.00	0.00	2.22
	D		0.00	0.00	2.53
	E		0.00	0.00	2.53
	F		0.00	0.00	2.53
16	A	2.53	1.55	3.31	2.94
	B		3.77	5.25	2.47
	C		24.70	26.00	2.32
	D		0.00	0.00	2.53
	E		0.00	0.00	2.53
	F		0.00	0.00	2.53
17	A	2.45	1.36	3.08	2.90
	B		3.73	5.10	2.43
	C		18.01	19.17	2.29
	D		0.00	0.00	2.45
	E		0.00	0.00	2.45
	F		0.00	0.00	2.45
18	A	2.45	1.37	3.09	2.91
	B		3.80	5.15	2.43
	C		14.77	15.92	2.30
	D		0.00	0.00	2.45
	E		0.00	0.00	2.45
	F		0.00	0.00	2.45
19	A	2.47	1.44	3.17	2.91
	B		3.69	5.10	2.44
	C		13.79	14.99	2.31
	D		0.00	0.00	2.47
	E		0.00	0.00	2.47
	F		0.00	0.00	2.47
20	A	2.47	1.48	3.19	2.91
	B		3.52	4.94	2.45
	C		9.65	10.88	2.32
	D		0.00	0.00	2.47
	E		0.00	0.00	2.47
	F		0.00	0.00	2.47
21	A	2.43	1.68	3.25	2.93
	B		4.74	5.97	2.43
	C		214.15	216.15	2.29
	D		0.00	0.00	2.43
	E		0.00	0.00	2.43
	F		0.00	0.00	2.43
22	A	2.45	1.74	3.32	2.95
	B		4.91	6.16	2.44
	C		79.16	80.53	2.30
	D		0.00	0.00	2.45
	E		0.00	0.00	2.45
	F		0.00	0.00	2.45
23	A	2.20	1.20	2.66	2.81
	B		2.30	3.49	2.35
	C		5.48	6.38	2.20
	D		96.95	97.85	2.15
	E		0.00	0.00	2.20
	F		0.00	0.00	2.20
24	A	2.20	1.23	2.68	2.81
	B		2.42	3.58	2.34
	C		4.51	5.46	2.22
	D		23.83	24.55	2.16
	E		0.00	0.00	2.20
	F		0.00	0.00	2.20
25	A	2.18	1.20	2.63	2.77
	B		2.09	3.29	2.34
	C		3.64	4.63	2.21
	D		11.73	12.46	2.15
	E		0.00	0.00	2.18
	F		0.00	0.00	2.18
26	A	2.22	1.04	2.51	2.79
	B		2.13	3.39	2.34
	C		4.34	5.91	2.21
	D		0.00	0.00	2.22
	E		0.00	0.00	2.22
	F		0.00	0.00	2.22

TABLE C.7 Experimental uncertainty estimates in the +10° [upward] data set (cont'd.)

Run No.	Visual section	G %	x %	V_{GS} %	V_{LS} %
27	A	2.22	1.08	2.63	2.77
	B		2.03	3.31	2.34
	C		4.66	5.66	2.21
	D		0.00	0.00	2.09
	E		0.00	0.00	2.22
	F		0.00	0.00	2.22
28	A	2.18	0.98	2.52	2.75
	B		1.74	3.04	2.33
	C		3.55	4.57	2.19
	D		17.43	18.15	2.13
	E		0.00	0.00	2.18
	F		0.00	0.00	2.18
29	A	2.21	1.11	2.63	2.78
	B		1.99	3.27	2.34
	C		4.00	5.03	2.21
	D		16.70	17.48	2.15
	E		0.00	0.00	2.21
	F		0.00	0.00	2.21
30	A	2.20	0.93	2.53	2.71
	B		1.65	3.02	2.32
	C		3.18	4.29	2.19
	D		10.18	11.02	2.14
	E		0.00	0.00	2.20
	F		0.00	0.00	2.20
31	A	2.15	0.97	2.49	2.73
	B		1.82	3.06	2.32
	C		3.73	4.68	2.18
	D		140.26	141.15	2.12
	E		0.00	0.00	2.15
	F		0.00	0.00	2.15
32	A	2.15	0.96	2.48	2.74
	B		1.81	3.05	2.32
	C		3.73	4.68	2.18
	D		22.94	23.59	2.12
	E		0.00	0.00	2.15
	F		0.00	0.00	2.15
33	A	2.15	0.98	2.49	2.72
	B		1.83	3.06	2.31
	C		3.78	4.71	2.18
	D		14.41	15.07	2.12
	E		0.00	0.00	2.15
	F		0.00	0.00	2.15
34	A	2.15	0.98	2.48	2.74
	B		1.85	3.07	2.31
	C		3.49	4.45	2.18
	D		11.35	12.04	2.13
	E		0.00	0.00	2.15
	F		0.00	0.00	2.15
35	A	2.12	0.90	2.41	2.69
	B		1.65	2.88	2.29
	C		3.39	4.32	2.16
	D		49.95	50.54	2.10
	E		0.00	0.00	2.12
	F		0.00	0.00	2.12
36	A	2.12	0.94	2.42	2.72
	B		1.79	2.97	2.30
	C		4.17	5.00	2.16
	D		485.77	487.56	2.08
	E		0.00	0.00	2.12
	F		0.00	0.00	2.12
37	A	2.11	0.94	2.42	2.72
	B		1.79	2.96	2.30
	C		4.14	4.96	2.16
	D		47.56	48.10	2.10
	E		0.00	0.00	2.11
	F		0.00	0.00	2.11
38	A	2.11	0.95	2.42	2.72
	B		1.82	2.98	2.30
	C		3.82	4.67	2.16
	D		26.66	27.19	2.11
	E		0.00	0.00	2.11
	F		0.00	0.00	2.11
39	A	2.12	0.99	2.44	2.75
	B		1.92	3.06	2.31
	C		3.80	4.66	2.17
	D		16.28	16.84	2.11
	E		0.00	0.00	2.12
	F		0.00	0.00	2.12
40	A	2.11	0.98	2.44	2.73
	B		1.89	3.03	2.30
	C		3.34	4.24	2.17
	D		7.17	7.85	2.12
	E		0.00	0.00	2.11
	F		0.00	0.00	2.11
41	A	2.32	1.18	2.81	2.80
	B		2.26	3.66	2.36
	C		5.55	6.71	2.22
	D		0.00	0.00	2.32
	E		0.00	0.00	2.32
	F		0.00	0.00	2.32
42	A	2.30	0.96	2.68	2.77
	B		2.01	3.46	2.33
	C		4.71	5.91	2.20
	D		0.00	0.00	2.09
	E		0.00	0.00	2.30
	F		0.00	0.00	2.30
43	A	2.32	1.00	2.72	2.77
	B		1.82	3.33	2.35
	C		3.92	5.20	2.22
	D		38.32	39.48	2.16
	E		0.00	0.00	2.32
	F		0.00	0.00	2.32
44	A	2.33	0.94	2.71	2.77
	B		1.69	3.26	2.36
	C		3.65	4.98	2.22
	D		30.68	31.84	2.16
	E		0.00	0.00	2.33
	F		0.00	0.00	2.33
45	A	2.30	1.67	3.08	2.96
	B		4.70	5.72	2.42
	C		0.00	0.00	2.30
	D		0.00	0.00	2.30
	E		0.00	0.00	2.30
	F		0.00	0.00	2.30
46	A	2.30	1.89	3.23	2.99
	B		4.23	5.28	2.44
	C		28.71	29.54	2.27
	D		0.00	0.00	2.30
	E		0.00	0.00	2.30
	F		0.00	0.00	2.30
47	A	2.32	1.50	2.99	2.95
	B		3.77	4.90	2.42
	C		24.82	25.71	2.26
	D		0.00	0.00	2.32
	E		0.00	0.00	2.32
	F		0.00	0.00	2.32
48	A	2.32	1.54	3.02	2.92
	B		4.05	5.16	2.40
	C		39.70	40.64	2.24
	D		0.00	0.00	2.32
	E		0.00	0.00	2.32
	F		0.00	0.00	2.32
49	A	2.62	1.79	3.59	2.96
	B		4.96	6.48	2.50
	C		110.01	112.03	2.36
	D		0.00	0.00	2.62
	E		0.00	0.00	2.62
	F		0.00	0.00	2.62
50	A	2.62	2.09	3.80	2.99
	B		5.99	7.43	2.52
	C		180.40	182.85	2.38
	D		0.00	0.00	2.62
	E		0.00	0.00	2.62
	F		0.00	0.00	2.62
51	A	2.62	1.78	3.59	2.96
	B		4.94	6.46	2.50
	C		46.28	47.85	2.37
	D		0.00	0.00	2.62
	E		0.00	0.00	2.62
	F		0.00	0.00	2.62
52	A	2.45	1.77	3.34	2.95
	B		4.76	6.02	2.44
	C		52.77	54.02	2.30
	D		0.00	0.00	2.45
	E		0.00	0.00	2.45
	F		0.00	0.00	2.45

Appendix D

THE ANALYSIS OF STRATIFIED-NONSTRATIFIED TRANSITION DURING CONDENSATION BY WAVE THEORY

The one dimensional, co-current stratified flow configuration in an inclined condenser tube is shown in Figure 5.1. Considering this flow configuration and applying the one dimensional two-fluid transient conservation laws, the resulting continuity and momentum equations are,

$$\rho_L \frac{\partial}{\partial t}\langle 1 - \alpha\rangle + \rho_L \frac{\partial}{\partial Z}(\langle 1 - \alpha\rangle\langle u_L\rangle_L) = \dot{W}_i \,, \tag{D.1}$$

$$\rho_G \frac{\partial}{\partial t}\langle \alpha\rangle + \rho_G \frac{\partial}{\partial Z}(\langle \alpha\rangle\langle u_G\rangle_G) = -\dot{W}_i \,, \tag{D.2}$$

$$\begin{aligned}
&\rho_L \frac{\partial}{\partial t}\langle u_L\rangle_L + \frac{\rho_L\langle u_L\rangle_L}{\langle 1 - \alpha\rangle}\frac{\partial}{\partial t}\langle 1 - \alpha\rangle + \frac{C_{3L}\langle u_L\rangle_L}{\langle 1 - \alpha\rangle}\dot{W}_i \\
&- \frac{C_{3L}\rho_L\langle u_L\rangle_L}{\langle 1 - \alpha\rangle}\frac{\partial}{\partial t}\langle 1 - \alpha\rangle + C_{3L}\rho_L\langle u_L\rangle_L\frac{\partial}{\partial Z}\langle u_L\rangle_L \\
&+ \frac{\tau_L S_L}{A\langle 1 - \alpha\rangle} - \frac{\tau_i S_i}{A\langle 1 - \alpha\rangle} + \rho_L g\sin\theta + \frac{\partial P_{iL}}{\partial Z} + \rho_L g\cos\theta\frac{\partial h_L}{\partial Z} \\
&- \frac{\dot{W}_i}{\langle 1 - \alpha\rangle}[\eta\langle u_L\rangle_L + (1 - \eta)\langle u_G\rangle_G] = 0 \,,
\end{aligned} \tag{D.3}$$

and

$$\rho_G \frac{\partial}{\partial t}<u_G> + \frac{\rho_G <u_G>_G}{<\alpha>} \frac{\partial}{\partial t}<1 - \alpha> - \frac{C_{3G}<u_G>_G}{\alpha} \dot{W}_i$$

$$- \frac{C_{3G}\rho_G <u_G>_G}{\alpha} \frac{\partial}{\partial t}<\alpha> + C_{3G}\rho_G <u_G>_G \frac{\partial}{\partial Z}<u_G>_G$$

$$+ \frac{\tau_G S_G}{A<\alpha>} + \frac{\tau_i S_i}{A<\alpha>} + \rho_G g \sin\theta + \frac{\partial P_{iG}}{\partial Z} + \rho_G g \cos\theta \frac{\partial h_L}{\partial Z}$$

$$+ \frac{\dot{W}_i}{<\alpha>}\left[\eta <u_L>_L + (1 - \eta)<u_G>_G\right] = 0 \,, \qquad \textbf{(D.4)}$$

where P_{iL} is the interfacial pressure experienced by the liquid, P_{iG} is the interfacial pressure on the vapor and t is time. All the other variables were defined in Chapter 6.

Substituting Equations (D.1) and (D.2) into Equations (D.3) and (D.4) respectively to eliminate $\partial/\partial t(<\rho_G <\alpha>)$ and $\partial/\partial t(<\rho_L <1 - \alpha>)$ and subtracting Equation (D.3) from (D.4),

$$\left[\rho_L(1 - C_{3L})\frac{<u_L>_L}{A_L} + \rho_G(1 - C_{3G})\frac{<u_G>_G}{A_G}\right]\frac{dA_L}{dh_L}\frac{\partial h_L}{\partial t}$$

$$+ (\rho_L - \rho_G) g \cos\theta \frac{\partial h_L}{\partial Z} + \frac{(\partial P_{iL} - \partial P_{iG})}{\partial Z} + \rho_L \frac{\partial <u_L>_L}{\partial t}$$

$$\rho_L <u_L>_L C_{3L} \frac{\partial <u_L>_L}{\partial Z} - \rho_G \frac{\partial <u_G>_G}{\partial t} - \rho_G <u_G>_G C_{3G} \frac{\partial <u_G>_G}{\partial Z} = \Delta f_{ab} \,, \qquad \textbf{(D.5)}$$

where

$$\Delta f_{ab} = -\frac{\tau_L S_L}{A_L} + \tau_i S_i\left[\frac{1}{A_L} + \frac{1}{A_G}\right] + \frac{\tau_G S_G}{A_G} - (\rho_L - \rho_G) g \sin\theta$$

$$\left\{\left(\eta\left[\frac{1}{A_G} + \frac{1}{A_L}\right] - \frac{C_{3G}}{A_L}\right)u_L + \left((1-\eta)\left[\frac{1}{A_G} + \frac{1}{A_L}\right] - \frac{C_{3G}}{A_G}\right)u_G\right\}\frac{\dot{W}_I}{A} \ . \qquad \textbf{(D.5a)}$$

The effect of surface tension, σ is assumed to cause a difference in the interfacial pressures ($P_{iL} \neq P_{iG}$) experienced by the two phases where

$$\frac{(\partial P_{iL} - \partial P_{iG})}{\partial Z} = -\frac{\partial}{\partial Z}\left[\sigma \frac{\dfrac{\partial^2 h_L}{\partial Z^2}}{\left[1 + \left(\dfrac{\partial h_L}{\partial Z}\right)^2\right]^{3/2}}\right] \ . \qquad \textbf{(D.5b)}$$

The analysis of instability and the transitional criteria are obtained by linearizing Equations (D.1), (D.2) and (D.5) around a smooth fully-developed stratified flow pattern (H_L, U_L,U_G) where the instantaneous phase averaged velocities are perturbed using the following:

$$\begin{aligned} &\langle u_L \rangle_L = U_L + u_L^{\star} \ , \\ &\langle u_G \rangle_G = U_G + u_G^{\star} \ , \\ &h_L = H_L + h_L^{\star} \ , \ and \\ &\Delta F_{ab}(H, U_L, U_G) = 0 \ . \end{aligned} \qquad \textbf{(D.6)}$$

The parameters H_L, U_L, U_G, and ΔF_{ab} are obtained by solving the steady stratified flow equation for a given flow rate. The steady flow equations obtained from the present analysis are exactly the same equations as in Chapter 5. Substituting the terms given in Equation (D.6) into Equations (D.1), (D.2) and (D.5) and performing the required differentiations two set of equations are obtained. One set describes the equilibrium steady stratified flow and the other set describing the perturbed unsteady flow. The perturbed set of equations are linearized by neglecting terms such as

$$h_L^{\star}/H_L \ll 1\ ,$$
$$u_L^{\star}/U_L \ll 1\ , \tag{D.7}$$
$$u_G^{\star}/U_G \ll 1\ ,$$

and the time variation of the steady state parameters for small perturbations. These parameters are small and do not provide any significant contributions to the resulting equations. Hence they are neglected.

The equilibrium condition in the flow field is described by,

$$\left(K\frac{\partial}{\partial Z}\right)\phi = I \tag{D.8}$$

where

$$K = \begin{bmatrix} \dfrac{dA_L}{dh_L}U_L & A_L & 0 \\ A_L U_G & 0 & -A_G \\ (\rho_L - \rho_G)g\cos\theta - \sigma\dfrac{\partial^2}{\partial Z^2} & \rho_L U_L C_{3L} & -\rho_G U_G C_{3G} \end{bmatrix}, \tag{D.8a}$$

$$
I = \begin{bmatrix} \dfrac{\dot{W}_i}{A\rho_L} \\ \\ \dfrac{\dot{W}_i}{A\rho_G} \\ \\ \Delta F_{ab} \end{bmatrix} , \tag{D.8b}
$$

and

$$
\phi = \begin{bmatrix} H \\ \\ U_L \\ \\ U_G \end{bmatrix} . \tag{D.8c}
$$

The linerized forms of the perturbed equations are given by

$$
\left(T\frac{\partial}{\partial t} + \bar{R}\frac{\partial}{\partial Z} \right) B = \hat{F}B \tag{D.9}
$$

where

$$
T = \begin{bmatrix} \dfrac{dA_L}{dh_L} & 0 & 0 \\ \\ \dfrac{dA_L}{dh_L} & 0 & 0 \\ \\ N & \rho_L & -\rho_G \end{bmatrix} , \tag{D.9a}
$$

$$\bar{R} = \begin{bmatrix} \frac{dA_L}{dh_L}U_L & A_L & 0 \\ \frac{dA_L}{dh_L}U_G & 0 & -A_G \\ \bar{G} & \rho_L C_{3L} U_L & -\rho_G C_{3G} U_G \end{bmatrix}, \tag{D.9b}$$

$$\hat{F} = \begin{bmatrix} \left(\frac{\partial \dot{W}_i}{\partial H_L}\right)\frac{1}{A\rho_L} & 0 & 0 \\ \left(\frac{\partial \dot{W}_i}{\partial H_L}\right)\frac{1}{A\rho_G} & 0 & 0 \\ \frac{\partial \Delta F_{ab}}{\partial H_L} & \frac{\partial \Delta F_{ab}}{\partial U_L} & \frac{\partial \Delta F_{ab}}{\partial U_G} \end{bmatrix}, \tag{D.9c}$$

$$B = \begin{bmatrix} h_L^{\star} \\ u_L^{\star} \\ u_G^{\star} \end{bmatrix}, \tag{D.9d}$$

$$\bar{G} = (\rho_L - \rho_G)g\cos\theta - \sigma\frac{\partial^2}{\partial Z^2}, \tag{D.10a}$$

$$N = \left[\rho_L(1 - C_{3L})\frac{U_L}{A_L} + \rho_G(1 - C_{3G})\frac{U_G}{A_G}\right]\frac{dA_L}{dh_L}, \tag{D.10b}$$

$$\frac{\partial \Delta F_{ab}}{\partial H_L} = \left.\frac{\partial \Delta f_{ab}}{\partial h_L}\right|_{h_L = H_L}, \tag{D.10c}$$

and

$$\frac{\partial \Delta F_{ab}}{\partial U_j} = \left.\frac{\partial \Delta f_{ab}}{\partial u_j}\right|_{u_j = U_j}, \quad j = L, G. \tag{D.10d}$$

The stability analysis is performed by substituting a standard form of perturbation into the linearized perturbed equation, i.e Equation(D.9)

$$\begin{aligned} h_L^{\star} &= \hat{h}_L e^{i(kZ - \omega t)}, \\ u_L^{\star} &= \hat{u}_L e^{i(kZ - \omega t)}, \text{ and} \\ u_G^{\star} &= \hat{u}_G e^{i(kZ - \omega t)} \end{aligned} \tag{D.11}$$

where k is the real wave number, ω is the complex angular velocity, i is $\sqrt{-1}$, and $\hat{h}$, $\hat{u}_L$, and $\hat{u}_G$ are complex amplitudes of the perturbation. When these terms are substituted Equation (D.9) becomes,

$$M\,\hat{B} = 0 \tag{D.12}$$

where

$$\hat{B} = \begin{bmatrix} \hat{h}_L \\ \hat{u}_L \\ \hat{u}_G \end{bmatrix}, \tag{D.12a}$$

$$M = \begin{bmatrix} \dfrac{dA_L}{dh_L}\dfrac{1}{A_L}\left[-\dfrac{\omega}{k} + U_L + \left(\dfrac{\partial \dot{W}_i}{\partial H_L}\right)\left(\dfrac{dh_L}{dA_L}\right)\dfrac{i}{k\rho_L A}\right] & 1 & 0 \\ \dfrac{dA_L}{dh_L}\dfrac{1}{A_G}\left[\dfrac{\omega}{k} - U_G - \left(\dfrac{\partial \dot{W}_i}{\partial H_L}\right)\left(\dfrac{dh_L}{dA_L}\right)\dfrac{i}{k\rho_G A}\right] & 0 & 1 \\ M_1 & M_2 & M_3 \end{bmatrix}, \tag{D.12b}$$

$$M_1 = -\frac{N\omega}{k} + (\rho_L - \rho_G)g\cos\theta + \sigma k^2 + \frac{i}{k}\frac{\partial \Delta F_{ab}}{\partial H_L}, \tag{D.13a}$$

$$M_2 = -\frac{\rho_L\omega}{k} + \rho_L U_L C_{3L} + \frac{i}{k}\frac{\partial \Delta F_{ab}}{\partial U_L}, \tag{D.13b}$$

and

$$M_3 = \frac{\rho_G\omega}{k} - \rho_G U_G C_{3G} + \frac{i}{k}\frac{\partial \Delta F_{ab}}{\partial U_G}. \tag{D.13c}$$

For non-trivial solutions det **M** = 0 from where the dispersion equation is obtained. The dispersion equation is given by,

$$aC^2 - 2(b_1 + ib_2)C + d_1 + id_2 = 0 \tag{D.14}$$

where

$$C = \frac{\omega}{k}, \tag{D.14a}$$

$$a = \frac{dA_L}{dh_L}\frac{\rho_L}{A_L} + \frac{dA_L}{dh_L}\frac{\rho_G}{A_G}, \tag{D.14b}$$

$$b_1 = \rho_L\frac{dA_L}{dh_L}\left(1 + \frac{(C_{3L} - 1)}{2}\right)\frac{U_L}{A_L} + \rho_G\frac{dA_L}{dh_L}\left(1 + \frac{(C_{3G} - 1)}{2}\right)\frac{U_G}{A_G} - \frac{1}{2}N, \tag{D.14c}$$

$$b_2 = \frac{1}{2k}\left(\frac{dA_L}{dh_L}\frac{1}{A_L}\frac{\partial\Delta F_{ab}}{\partial U_L} - \frac{dA_L}{dh_L}\frac{1}{A_G}\frac{\partial\Delta F_{ab}}{\partial U_G} + \left[\frac{1}{A_G} + \frac{1}{A_L}\right]\frac{\partial\dot{W}_i}{\partial H_L}\frac{1}{A}\right), \qquad \textbf{(D.14d)}$$

$$d_1 = \frac{\rho_L C_{3L} U_L^2}{A_L}\frac{dA_L}{dh_L} + \frac{\rho_G C_{3G} U_G^2}{A_G}\frac{dA_L}{dh_L}$$
$$- \left\{(\rho_L - \rho_G) g \cos\theta + \sigma k^2\right\}$$
$$+ \left(\frac{\partial\dot{W}_i}{\partial H_L}\right)\frac{1}{Ak^2}\left\{\frac{1}{\rho_G A_G}\frac{\partial\Delta F_{ab}}{\partial U_G} - \frac{1}{\rho_L A_L}\frac{\partial\Delta F_{ab}}{\partial U_L}\right\}, \qquad \textbf{(D.14e)}$$

and

$$d_2 = \frac{1}{k}\left(\frac{dA_L}{dh_L}\frac{U_L}{A_L}\frac{\partial\Delta F_{ab}}{\partial U_L} - \frac{dA_L}{dh_L}\frac{U_G}{A_G}\frac{\partial\Delta F_{ab}}{\partial U_G} - \frac{\partial\Delta F_{ab}}{\partial H_L} + \frac{1}{A}\left(\frac{\partial\dot{W}_i}{\partial H_L}\right)\left\{\frac{U_G C_{3G}}{A_G} + \frac{U_L C_{3L}}{A_L}\right\}\right). \qquad (D.14f)$$

The neutral stability condition is obtained when the imaginary quantities in Equation (D.14) become equal to zero. Then

$$C_m = \frac{d_2}{2b_2}\,. \qquad \textbf{(D.15)}$$

Substituting the values of d_2 and b_2,

$$C_m = \frac{\frac{dA_L}{dh_L}\frac{U_L}{A_L}\frac{\partial\Delta F_{ab}}{\partial U_L} - \frac{dA_L}{dh_L}\frac{U_G}{A_G}\frac{\partial\Delta F_{ab}}{\partial U_G} - \frac{\partial F_{ab}}{\partial H_L} + \frac{1}{A}\left(\frac{\partial\dot{W}_i}{\partial H_L}\right)\left\{\frac{U_G C_{3G}}{A_G} + \frac{U_L C_{3L}}{A_L}\right\}}{\frac{1}{A_L}\frac{dA_L}{dh_L}\frac{\partial\Delta F_{ab}}{\partial U_L} - \frac{1}{A_G}\frac{dA_L}{dh_L}\frac{\partial\Delta F_{ab}}{\partial U_G} + \frac{1}{A}\left[\frac{1}{A_G} + \frac{1}{A_L}\right]\left(\frac{\partial\dot{W}_i}{\partial H}\right)}. \qquad \textbf{(D.15a)}$$

Substituting the value of C_m in Equation (D.14) the equation of stable equilibrium is obtained.

$$\left(\frac{\rho_L}{A_L}\frac{dA_L}{dh_L} + \frac{\rho_G}{A_G}\frac{dA_L}{dh_L}\right)C_m^2 - 2\left(\frac{\rho_L C_{3L} U_L}{A_L}\frac{dA_L}{dh_L} + \frac{\rho_G C_{3G} U_G}{A_G}\frac{dA_L}{dh_L}\right)C_m$$

$$+ \frac{\rho_L C_{3L} U_L^2}{A_L}\frac{dA_L}{dh_L} + \frac{\rho_G C_{3G} U_G^2}{A_G}\frac{dA_L}{dh_L} - \left\{(\rho_L - \rho_G)g\cos\theta + \sigma k_n^2\right\}$$

$$+ \frac{1}{Ak_n^2}\left(\frac{\partial \dot{W}_i}{\partial H_L}\right)\left\{\frac{1}{\rho_G A_G}\frac{\partial \Delta F_{ab}}{\partial U_G} - \frac{1}{\rho_L A_L}\frac{\partial \Delta F_{ab}}{\partial U_L}\right\} = 0 \ . \qquad \textbf{(D.16)}$$

This dimensionless form of this equation is,

$$\frac{\pi^2}{16gD\cos\theta}\left\{\frac{\rho_G \tilde{U}_{GS}^2}{\rho_L \tilde{A}_G^3}\left(\frac{d\tilde{A}_L}{d\tilde{h}_L}\right)\left[\left(\frac{C_m}{U_G} - 1\right)^2 + (C_{3G} - 1)\left(1 - 2\frac{C_m}{U_G}\right)\right]\right\}$$

$$\left\{+ \frac{\tilde{U}_{LS}^2}{\tilde{A}_L^3}\left(\frac{d\tilde{A}_L}{d\tilde{h}_L}\right)\left[\left(\frac{C_m}{U_L} - 1\right)^2 + (C_{3L} - 1)\left(1 - \frac{2C_m}{U_L}\right)\right]\right\}$$

$$-\left[\frac{(\rho_L - \rho_G)}{\rho_L} + \frac{\sigma k_n^2}{\rho_L g\cos\theta} - \frac{\partial \dot{W}_i/\partial H_L}{D^2 k_n^2 A\rho_L g\cos\theta}\left\{\frac{1}{\rho_G \tilde{A}_G}\frac{\partial \Delta F_{ab}}{\partial U_G} - \frac{1}{\rho_L \tilde{A}_L}\frac{\partial \Delta F_{ab}}{\partial U_L}\right\}\right] = 0.(D.17)$$

The last term in Equation (D.17) is the contribution due to condensation during the flow. If the last term in Equation (D.17) becomes zero (adiabatic) then the analysis must yield the gas-liquid transition boundary given by Brauner and Maron(1991). The results obtained with the properties of air and water under adiabatic conditions are given in Figure D.1. These are exactly the same as reported by Brauner and Maron(1991). In Figure D.2 the predictions of Equation (D.17) are compared (diabatic flow) with horizontal

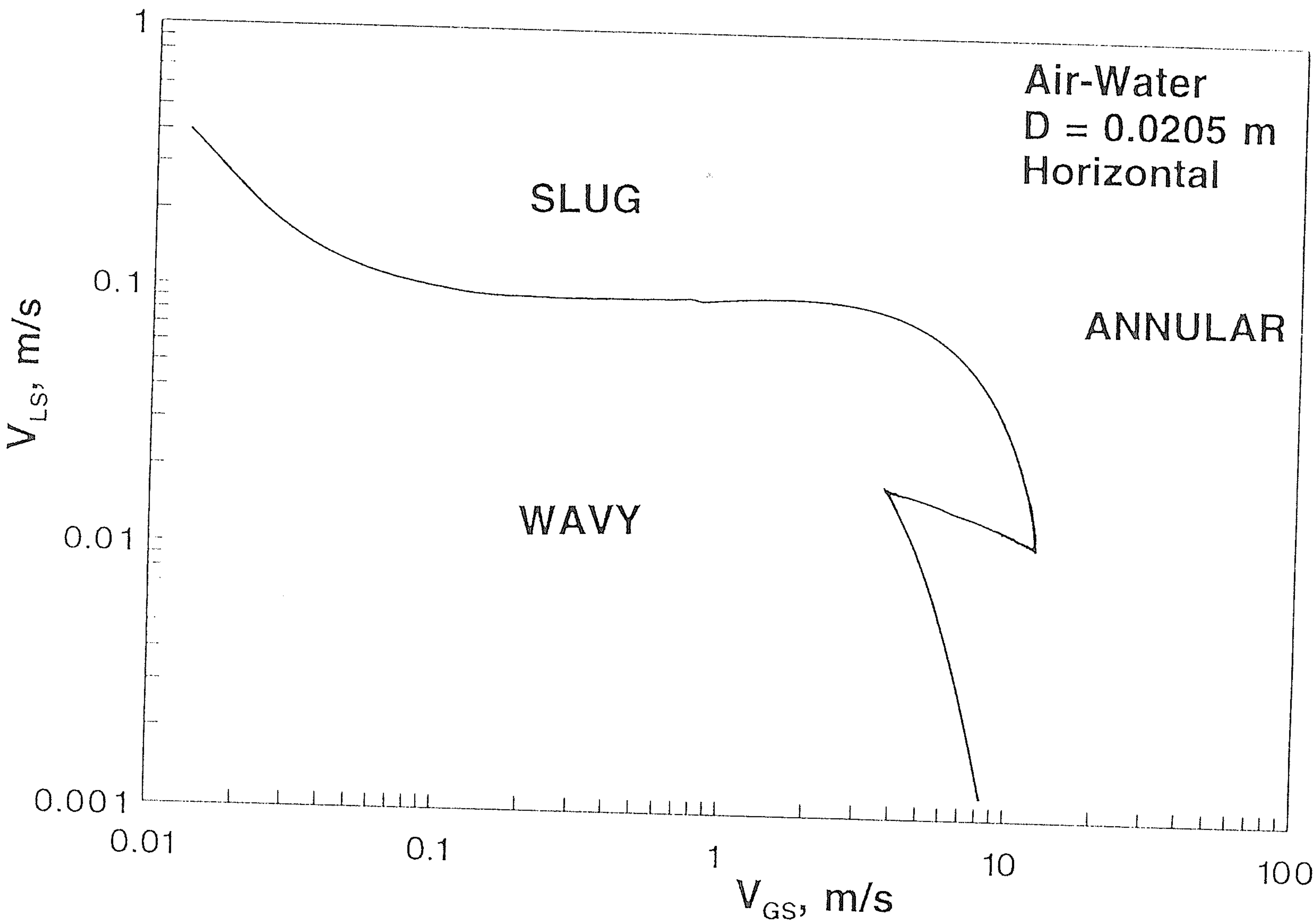

Figure D.1 Prediction of Equation (D.17) in the absence of condensation.

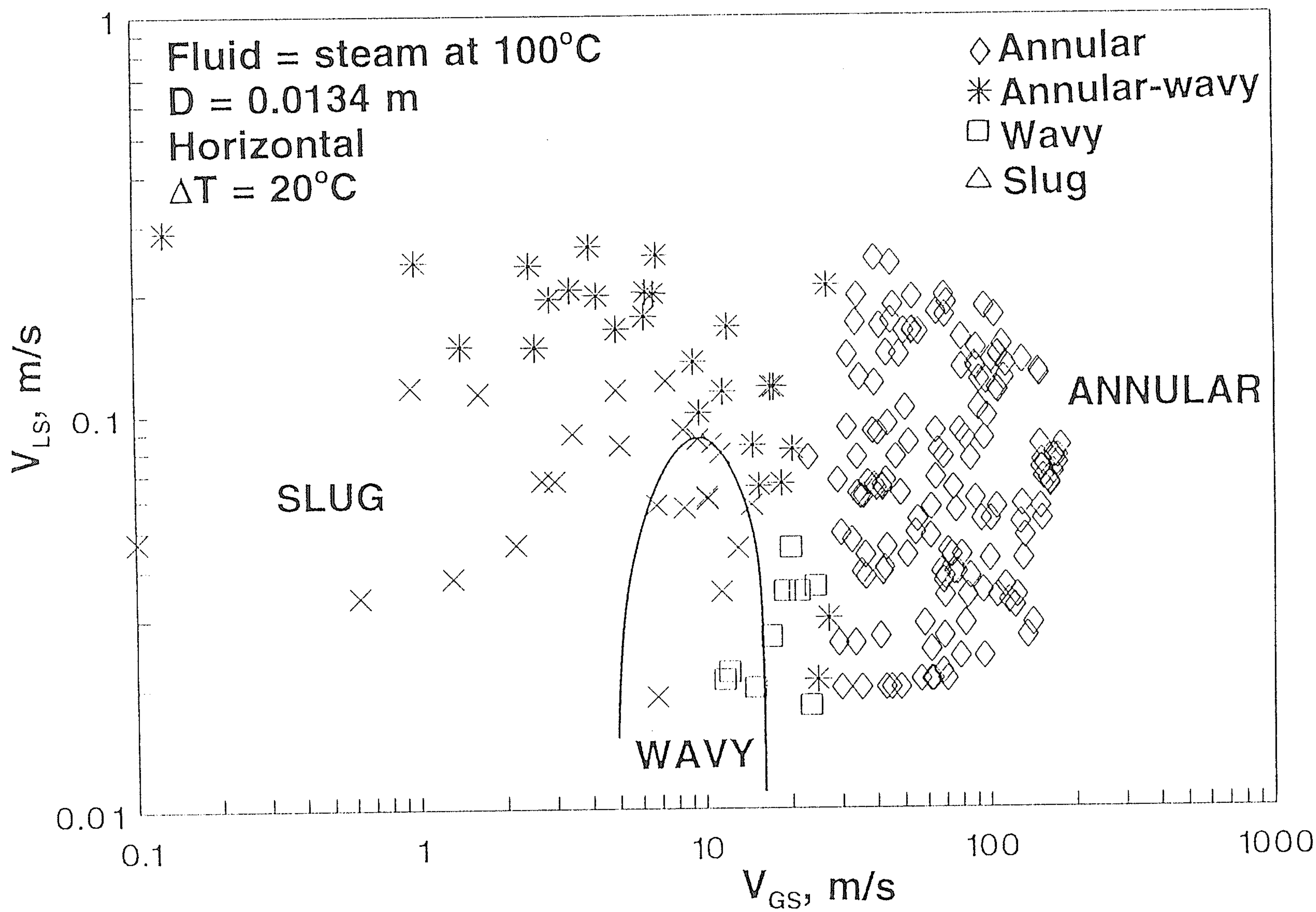

Figure D.2 Comparison of Equation (D.17) with the present data for the horizontal position.

steam-water data of 0.0134m I. D. tube. The predictions show similar trends as the mechanistic model described in Chapter 5.